ACADÉMIE DE MONTPELLIER

UNIVERSITÉ MONTPELLIER II

- SCIENCES ET TECHNIQUES DU LANGUEDOC -

THÈSE

pour obtenir le grade de

DOCTEUR DE L'UNIVERSITÉ MONTPELLIER II

Discipline : Génie Informatique, Automatique et Traitement du Signal
Formation Doctorale : Systèmes Automatiques et Microélectronique
École Doctorale : Information, Structures et Systèmes

présentée et soutenue publiquement

par

Xianbo XIANG

le 24 Février 2011

Titre :

Coordinated motion control of underactuated autonomous underwater vehicles

JURY :

Mr. Massimo CACCIA	Senior Researcher, CNR - ISSIA	Rapporteur
Mr. Luc JAULIN	Professeur, ENSTA - Bretagne	Rapporteur
Mr. René ZAPATA	Professeur, Université Montpellier II	Examinateur
Mr. Marco BIBULLI	Researcher, CNR - ISSIA	Examinateur
Mr. Lionel LAPIERRE	Maître de conférences, Université Montpellier II	Co-Directeur de thése
Mr. Bruno JOUVENCEL	Professeur, Université Montpellier II	Directeur de thése

CONTENTS

FIGURES

TABLES

Chapter 1

Introduction

1.1 Overview of underwater vehicles

With more and more concerns about the abounding and valuable ocean resources, these years have witnessed a remarkable growth in the wide range of underwater commercial activities for offshore oil and gas exploration, ocean survey especially focusing on undersea exploration and exploitation, and even extensively for salvage operations related to disastrous accidents occurred undersea. There are three main types of vehicles used in underwater activities, named as MUVs, ROVs and AUVs.

MUVs The human-occupied submersibles, or called Manned Underwater Vehicles (MUVs) with good abilities of directly manoeuvring and in-situ observation, have been widely utilized in commercial activity and scientific research, and reached the zenith in the late 1960s and early 1970s. In Figure 1.1, it shows one of the world's first manned deep-ocean submersibles *Alvin*, which has made more than 4,400 dives since it was built in 1964. However, these manned submersibles are equipped with complex handling systems, and they significantly cost many extra efforts in order to guarantee the critical vital safety of crew aboard.

ROVs Remotely Operated Vehicles (ROVs) physically connected via an umbilical cable to receive power and data, still with human operator in the loop but not inside the vehicle, are successful substitutes being low-cost vehicles designed to reach deep water greater than 1000ft. ROVs have impressive work capability for teleoperated subsea intervention during underwater installation, manipulation and inspection. Today, ROV becomes a well-established technology frequently used in the offshore industry, most notably in the commercial offshore oil and gas, pipeline and cable industries. The first ROV system used by the oil and gas industry, and extensively used by ocean researchers later, is the ROV *Jason* shown in Figure 1.2(a). The hybrid ROV and crawler *Roving Bat* developed by ECA company, France, illustrated

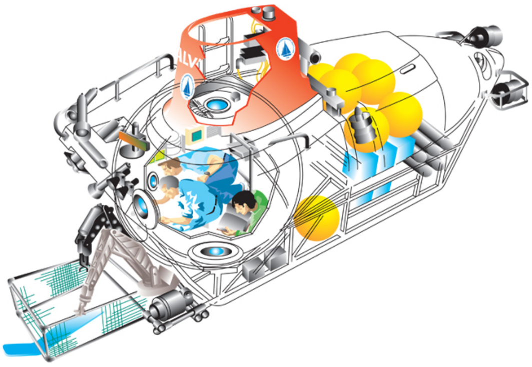

(a) *Alvin* carries two scientists and a pilot

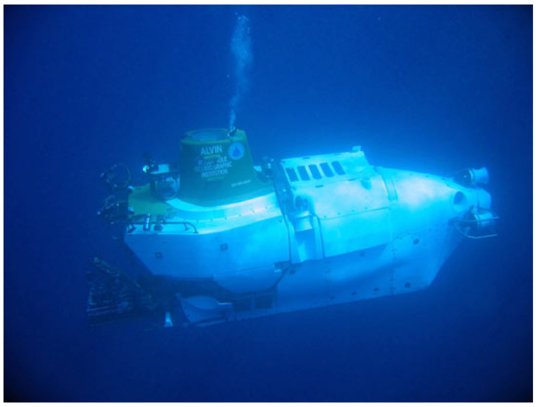

(b) *Alvin* dives underwater

Figure 1.1 – MUV *Alvin*, courtesy of the Woods Hole Oceanographic Institution(WHOI)

in Figure 1.2(b). *Roving Bat* is capable of reaching a target in free-flying mode and sticking to any vertical surface, such that it is quite suitable for hull inspection of immersed structures.

Nevertheless, the long umbilical cable, linked with the mother ship, greatly inhibits the speed and the moving range of the ROV, requiring the mother ship being equipped with deck gear capable of winding up this cable, and significantly restricting ship movement while deployed.

(a) The *Jason* ROV , courtesy of the WHOI

(b) The *Roving Bat* ROV, courtesy of the ECA

Figure 1.2 – Photos of two typical ROVs

AUVs More recently, with the development of advanced underwater technology, Autonomous Underwater Vehicles (AUVs) without human's occupation are steadily becoming the next significative step in ocean exploration, due to their freedom of full free-swimming, relieved from the constraints of an umbilical cable. Hence, these vehicles are also called Untethered Underwater Vehicles (UUVs). Such vehicles carry their own energy supplies and operate completely autonomously, as limited underwater acoustic communications only support intermittent human interaction and mainly work for vehicle emergencies. Nowadays there has been gradually growth in the AUV industry worldwide which would be on an unprecedented scale and AUVs will carry out interventions in undersea structures in the future [Whitcomb, 2000]. With further research results and technological advances, AUVs have the potential for supplementing or even substituting ROVs for deep water operations, and AUVs in a team hold considerable potential for challenging scientific and commercial missions at sea. In Figure 1.3(a), there is a low-cost and light weight AUV (30kg) *Taipan* developed at LIRMM, which can be easily launched from shore and accomplish coastal hydrographic survey. In Figure 1.3(b), one of the leading heavy AUV *Remus6000* (862kg) developed by Hydroid LLC., is launched for larger area search/survey and vulnerable deep-sea exploration up to 6000 meters.

(a) The *Taipan* AUV, courtesy : LIRMM

(b) The *Remus6000* AUV, courtesy : Hydroid

Figure 1.3 – Photos of two typical AUVs

Other than three main types of vehicles mentioned above, there are some other types of vehicles activated in marine society, such as towed vehicles, underwater gliders and autonomous surface vehicles(ASVs). Moreover, recent applications using Intervention Autonomous Underwater Vehicles (IAUVs), have demonstrated the feasibility of autonomous underwater manipulations, controlled via acoustic links, thus removing the disturbing effects of the umbilical cable (http ://www.freesubnet.eu).

To avoid confusion in discussing vehicle issues, we include the Autonomous Surface Vehicle (ASV) or called an Unmanned Surface Vehicle (USV), and the Autonomous Underwater Vehicle (AUV) or called an Unmanned Underwater Vehicle (UUV) as members of a broader class called Autonomous Marine Vehicle (AMV), as an AMV could be classified as " a vessel not under command" at all times in [Curtin et al., 2005].

On the other hand, as a group of coordinated multiple vehicles dealing with tasks provides flexibility, robustness and efficiency beyond what is possible with single robot, there is one attractive scenario for underwater activities–the AUV team concept, which could be a mix of several low-cost specific purpose AUVs, guided and controlled by one or two higher cost AUVs. The employment of multiple AUVs has significant advantages for both military and commercial applications. A team of underwater vehicles could survey large ocean areas more rapidly and cost-effectively than that could be accomplished with a single AUV or ship [McDowell et al., 2002].

1.2 Applications of autonomous underwater vehicles

AUVs are underwater "robots" that can be used for many different underwater applications, such as underwater exploration and documentation, recoveries, inspections, search and rescue, trenching, cable burial and much more.

Recent technological advances have stimulated a broad interest in autonomous vehicles. The development of powerful control techniques for single vehicles, the explosion in computation and communication capabilities have raised interest in multi-vehicle system which can cooperate each other and perform new capabilities. The types of applications of both single vehicle and multiple vehicles envisioned are numerous. Global expenditure on Autonomous Underwater Vehicles (AUVs) will total $\$2.3$ billion over the next decade $(2010-2019)$ according to business analysts, Douglas-Westwood, who also predicts that around 1,400 AUVs will be required over the next decade. Military, oil and gas, and research sectors are the main reasons for the increased demand in the key AUV market[Douglas-Westwood, 2009], as shown in Figure 1.4.

1.2.1 Applications of single AUV

The applications of autonomous underwater vehicle are very wide and cover all kinds of underwater activities. The following part gives some representative examples among inexhaustible practical AUV applications.

- **Underwater survey**

  Presently, AUVs are mostly used for survey mission, such as gathering environmental data for scientific application, and searching for hazards such as mines in military task. AUV surveying is also established as the most accurate and efficient method for pipeline routing and site surveying. For the oil and gas industry, the

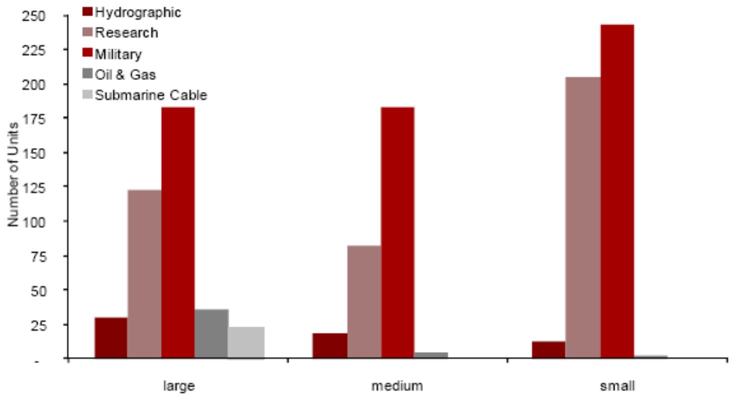

Figure 1.4 – Prospects of AUVs application market, courtesy of the Douglas-Wstwood

cost reduction of a survey performed with an AUVs instead of a towed vehicle is up to 30% and the data quality is generally higher [Antonelli et al., 2008].
In the early start of 1997, the AUV HUGIN I was used for the surveying of Statoil's Aasgaard pipeline route sketched in Figure 1.5(a), and then the AUV HUGIN II was also engaged to do seabed surveying in the Ormen Lange gas field in the Norwegian Sea in 2002. Ormen Lange is a significant gas province located in an area with water depths around 1000 metres, and parts of the area contain very rough terrain with significant slide areas. The HUGIN AUVs have proven their legitimacy through excellent survey data quality and high level of details as shown in Figure 1.5(b). The detailed information unveiled by the survey contributed significantly to the work of planning and selecting the most optimal site and route for the production and pipeline installations.

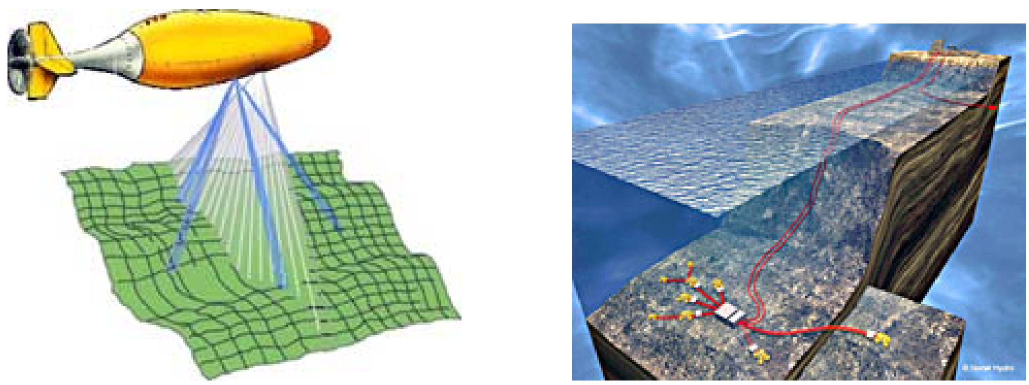

(a) Hugin *AUV* gas route survey (b) The Ormen Lange gas field

Figure 1.5 – Seabed gas route surveying using the AUV *Hugin*, courtesy of KONGSBERG(left) and Hydro(right)

- **Underwater intervention**

Although ROV are widely involved in interventions tasks such as opening or closing of a faulty valve, checking for hydrocarbon leaks or light maintenance repair, they can be enormously costly due to the main heavy expense of the tethered supporting vessel. The Autonomous Light Intervention Vehicle (ALIVE) with two manipulators, was devoted to broaden the scope of tasks carried out by AUVs as opposed to ROVs, economically carrying out light intervention tasks on standard, un-modified underwater structures. Sea trials of ALIVE have been successfully performed and coped well with difficult sea conditions, docking onto a subsea structure and carrying out pre-programmed operations, including opening and closing valves with its hydraulic arm, as the illustrative scheme shown in Figure 1.6(a). In Figure 1.6(b), a semi-autonomous underwater vehicle with a 7 degree of freedom (DOF) robotic manipulator for intervention missions, is operated by University of Hawaii. Additional intervention applications being envisaged include

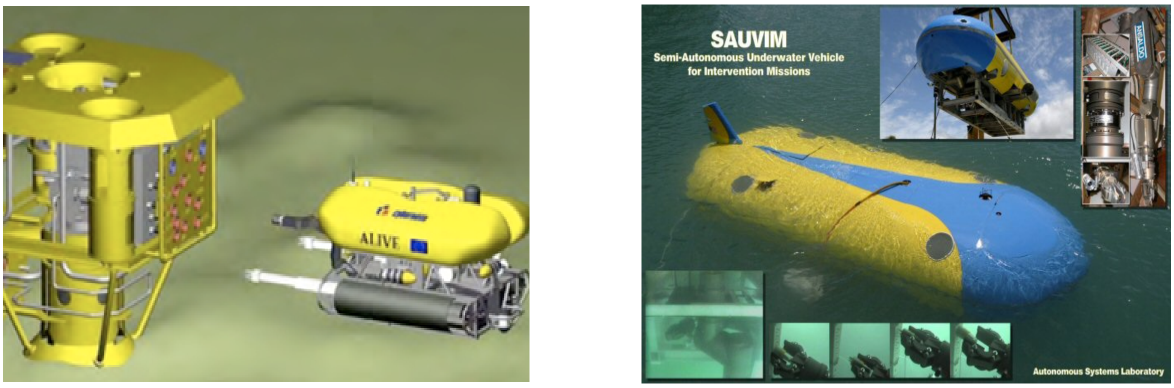

(a) Intervention AUV *ALIVE*, Cybernetics

(b) Intervention AUV *SAUVIM*, Univ. of Hawaii

Figure 1.6 – Underwater intervention of AUVs

assistance in rescue operations, archaeological missions, hazardous materials collection where a light vehicle, cost-effective and easy to mobilize, is promising to replace a ROV.

- **Underwater volcano observation**

  The Autonomous Benthic Explorer (ABE) was used to explore the active underwater Brothers Volcano roughly 537 kilometers northeast of New Zealand in 2007, and scientists from the Woods Hole Oceanographic Institution (WHOI) turned the sonar data collected by ABE into a richly textured three-dimensional seascape of the Brothers Volcano. In Figure 1.7, this view looks from the south into the crater at the summit of the volcano, the site of recent eruptions and ongoing hydrothermal venting, and sonar images reveals there are two volcanic cones with intense hydrothermal systems after its summit. In order to get sonar data of the volcano, ABE adopts 3-phased approach to ocean volcano exploration. First, guided by the chemical signals from a volcano using in-situ sensors. Second, flying closer to the seafloor and intercepting the hydrothermal plumes rising up above the seafloor. Finally, using obstacle avoidance techniques to stop it crashing into the rocky terrain while taking sonar data of what it has found : hydrothermal venting of the volcano [WHOI, 2007].

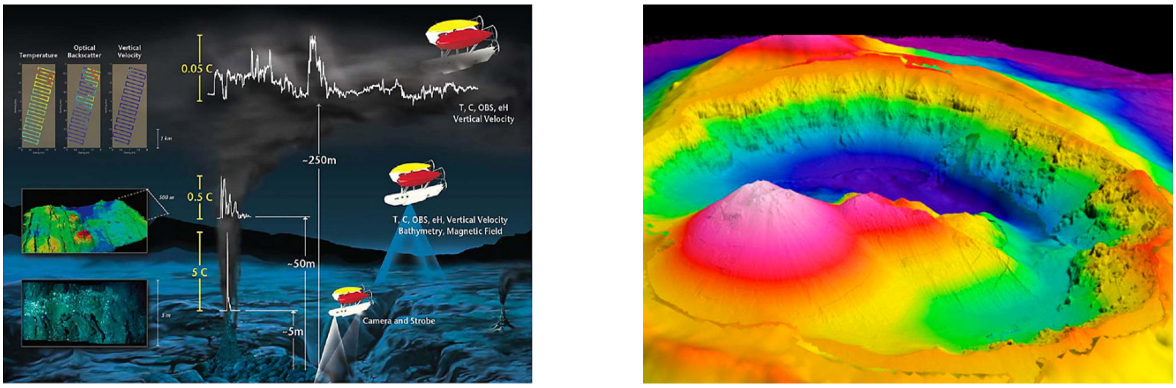

(a) 3-phased approach to volcano exploration (b) Observed paints map of deep-sea volcano

Figure 1.7 – AUV *ABE* exploration and observation of underwater volcano, courtesy of Christopher German(left), and the National Oceanic and Atmospheric Administration(NOAA)(right).

1.2.2 Applications of multiple AUVs

Recently, there has been much research activity focusing on coordinated control of multiple autonomous vehicles. Applications of multi-vehicle systems cover the whole world, in space, in the air, on land and at sea. Examples include satellite, spacecraft and aircraft formation flying control, cooperative control of mobile robots, coordinated control of marine (surface and underwater) vehicles, and even the whole collaboration for land, air, sea, and space vehicles [Murray, 2007]. Multiple vehicles in one team dealing with tasks could provide flexibility, robustness and efficiency beyond what is possible with single vehicle. Multi-vehicle systems enable enhanced and advanced operation through coordinated and cooperative teamwork in civilian, industrial and military fields, such as space-based interferometers, intelligent surveillance and reconnaissance, patrolling in hazardous environment, undersea oil pipeline inspection, and even hi-tech unmanned combat.

- Fast acoustic coverage

  One typical coordinated scenario of multiple underwater vehicles can be envisioned : A fleet of AUVs is required to get fast acoustic coverage of the seabed shown in Figure 1.8. In this valuable mission, vehicles are requested to fly above the seabed at the same depths along parallel paths, and map the seabed using same suites of acoustic sensors, for examples, side-scan sonar and sub-bottom profile. While following parallel paths in the manner of synchronization as a whole, multiple AUVs are able to build the acoustic 3D coverage overlap along the seabed, such that large areas can be completely covered in a short time. An Autonomous Surface Craft (ASC) in the high layer or another AUV in the medium layer that will operate in close cooperation with AUVs in the lower layer, as a mobile relay for fast communications. In the scenarios considered, the ASC will be equipped with a differential GPS receiver, an ultra short baseline unit (USBL), a radio link, and a high data rate communication link with the AUV that will be optimized for the vertical channel. By properly maneuvering the ASC to always remain in the vicinity of a vertical line with the AUV, a fast communication link can be established to transmit navigational data from the DGPS and USBL units to the AUV and ocean data from the AUV to the ASC, and subsequently to an end-user located on board a support ship or on shore via an aerial radio link.

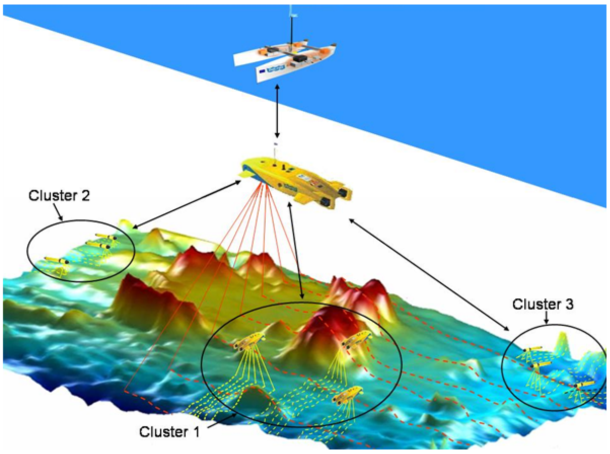

Figure 1.8 – Coordinated ASC and AUVs

- Cooperative underwater intervention

In Figure 1.9, the project Trident develops new forms of cooperation between an Autonomous Surface Craft and an Intervention Autonomous Underwater Vehicle, going beyond present-day methods which are typically based on manned and/or purpose-built systems [Sanz et al., 2010].

Firstly, the Intervention AUV performs a path following survey, where it gathers optical and/or acoustic data from the seafloor, whilst the ASC provides geo-referenced navigation data and communications with the end user. The motion of the ASC will be coordinated with that of the IAUV for precise Ultra Short Base

Line positioning and reliable acoustic communications. After the survey, the IAUV docks with the ASC and sends the data back to a ground station where a map is set up and a target object is identified by the end user. Secondly, the ASC navigates towards a waypoint near the intervention area to search for the object. When the target object has been found, the IAUV switches to free floating navigation mode. The manipulation of the object takes place through a dextrous hand attached to a redundant robot arm and assisted with proper perception. Particular emphasis will be put on the research of the vehicle's intelligent control architecture to provide the embedded knowledge representation framework and the high level reasoning agents required to enable a high degree of autonomy and on-board decision making of the platform.
This new methodology for multipurpose underwater intervention tasks with diverse potential applications like underwater archaeology, oceanography and offshore industries.

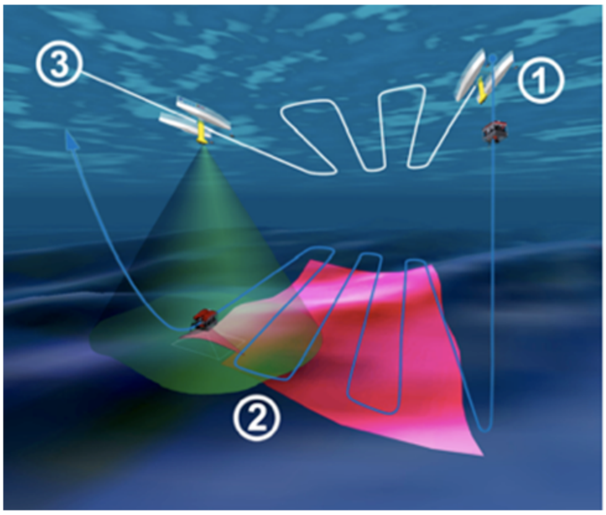

Figure 1.9 – Cooperative underwater intervention of ASC and AUV

- AUV team searching for hydrothermal vents
  Underwater hydrothermal vents produce methane that does not dissolve quickly in the water. A fleet of underwater vehicles, each equipped with a methane sensor, can detect the source of a vent by computing on-line and following the gradient of methane concentration, as illustrated in Figure 1.10.

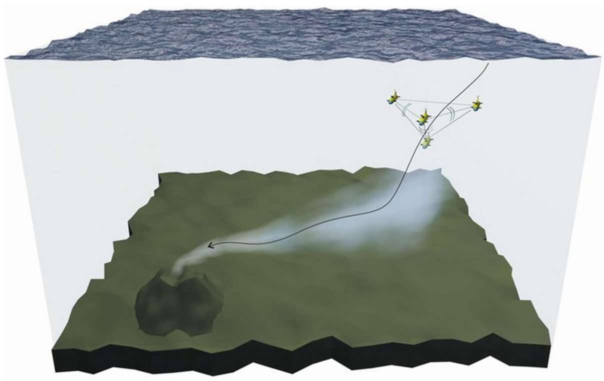

Figure 1.10 – AUVs formation searching for thermal vents

1.3 Motion control of autonomous vehicles

In order to implement varied types of practical applications, motion control of autonomous vehicles is one of the essential problem to achieve the exciting objectives, and the standard closed loop control structure is also applicable to autonomous vehicles.

1.3.1 Closed-loop marine control system

For a typical autonomous marine vehicle, the overall closed-loop control system can be constructed by four interconnected blocks called the plant, the navigation, guidance and control (NGC) sub-systems [Fossen, 1994], as illustrated in Figure 1.11. A description of the main components of a marine vehicle control system is as follows :

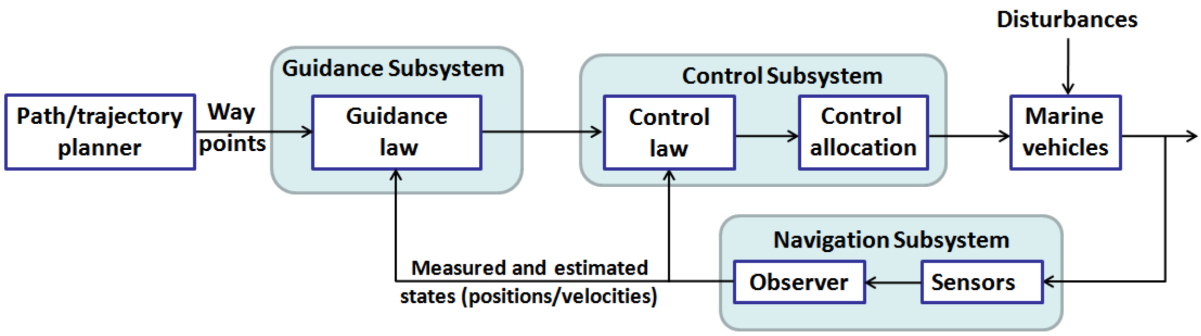

Figure 1.11 – Navigation, guidance and control for an autonomous marine vehicle

- **Plant** : the physical subsystem, i.e., the marine vehicle in this thesis, to be controlled, usually represented by the system model to describe its dynamic behavior during the control design.

- **Navigation** : the sensor subsystem measure some physical states of the plant, including position, course and distance traveled, or even the velocity and acceleration as well. It also includes filters and observers used to continuously estimate states that are not directly measured.
- **Guidance** : the reference subsystem using the guidance law, continuously computes the desired position, velocity and acceleration for the subsequent control subsystem, based on the target location, operator commands (if any), external data, obstacle information, and the output states from the navigation subsystem.
- **Control** : the kinematic or dynamic feedback control law, that determines the appropriate forces and moments in order to satisfy a certain control objective. It is necessary to optimally allocate the generalized forces τ to the actuators with physical limitations in terms of control input u.

In *marine surface vehicle* application, a Global Navigation Satellite System (GNSS) combined with an Inertial Navigation System (INS) usually constitutes the navigation system. The GNSS positioning system with specified constellations GPS or GALILEO, provides the absolute position and translational velocity. The INS measures linear acceleration by onboard accelerometers and orientation angles by onboard gyroscompasses. However, in *underwater vehicle* application, GPS are not available as the electromagnetic signals do not penetrate below the sea surface, hence Dead-reckoning (DR) is needed to fill gaps in GPS-denied coverage. Suffered from the accumulated error from DR which using INS sensing of the vehicle's self motion to deduce the vehicle's position, the underwater vehicle must periodically surface for GPS position fix. Another alternative way is that an acoustic beacon navigation for underwater vehicle positioning can be used, such as Long Baseline (LBL) or Ultra-short Baseline (USBL) Systems, to constrain DR/INS drift without the need for resurfacing.

1.3.2 Motion control design

Although all the three NGC subsystems in the whole closed-loop marine control system are important, the control subsystem is the key element. In this thesis, the main concern is dealing with the motion control design to build the control subsystem. In the following subsections, several main types of motion control tasks are briefly described, and the advantages and disadvantages are exposed, which inspire the new intentions of motion control strategy proposed in this thesis.

1.3.2.1 Conventional strategies

Conventionally, the motion control problem addressed in the literature can be classified into three basic categories : point stabilization , trajectory tracking and path following [Laumond, 1998]. However, some modified control strategies are introduced in order to improve the control performance, such as the maneuvering modified trajectory tracking [Hauser and Hindman, 1995], which motivates a new control problem statement called the maneuvering problem [Skjetne, 2005].

- **Point stabilization**
  the vehicle is stabilized at a desired goal posture (position and orientation), from a given initial configuration.
  Point stabilization of vehicles with nonholonomic constraints presents a true challenge to control system designers, since there is no smooth (or even continuous) constant state-feedback law to achieve the goal, as pointed out by the well-known Brockett's theorem in [Brockett, 1983]. To overcome this theoretical obstruction, three main approaches have been proposed among the numerous literatures, i.e., smooth time-varying control laws, discontinuous feedback laws and hybrid discrete/continuous control laws. In [Kolmanovsky and McClamroch, 1995], there is a comprehensive survey of the feedback control techniques elaborated for this control problem.
- **Trajectory tracking**
  the vehicle is required to track a time parameterized trajectory, i.e., a geometric path with an associated timing specification. Therefore, the trajectory tracking control objective can be considered to implement a time$\times$space task, that is the intersection set of spatial task and temporal task.
  The *trajectory tracking* (TT) problem for fully actuated systems is by now well understood, and satisfactory solutions can be found in standard nonlinear control textbooks [Khalil, 1996]. However, in the case of underactuated vehicles, that is, when the vehicle has less actuators than state variables to be tracked, the problem is still a very active topic of research. Feedback linearization methods [Walsh et al., 1994] and Lyapunov based control designs [Jiang and Nijmeijer, 1997] have been proposed, and applications to underactuated ships and autonomous underwater vehicles can be found in [Pettersen and Nijmeijer, 2001] and in [Do et al., 2004a] respectively.
- **Path following**
  the vehicle is required to converge to and follow a desired geometric path, without any temporal specifications. Therefore, the path following control objective can be

considered to implement a pure spatial task.

Path following (PF) control has received relatively less attention than the other two problems. The pioneering work in this field can be referred to the work of Samson [Samson, 1992, Micaelli and Samson, 1993]. Later, path following algorithms for marine vehicles have been reported in [Encarnacao and Pascoal, 2000], and the improved path following control of autonomous underwater vehicles was stated in [Lapierre et al., 2003] by introducing a collaborative virtual target moving along the path to overcome stringent initial condition in previous path following strategy.

The underlying assumption in path following control is that the vehicle's forward speed tracks a desired speed profile, while the controller only acts on the vehicle orientation to steer it to the path.

1.3.2.2 Advantages and disadvantages

Actually, in many practical applications, such as underwater route surveying or pipeline inspection, motion control of steering an autonomous vehicle to follow a predefined path or track a desired trajectory, is far more frequently adopted than stabilizing the vehicle in a fixed posture. Hence, the path following and trajectory tracking control attract more concerns in this thesis. It is useful to compare them and show the advantages and disadvantages, in order to give the guidance how to choose the suitable control method according to different tasks. The comparison is based on following two aspects :

- Spatial convergence

  As the path following control only focuses on the geometric task without any temporal restriction, the vehicle is not obliged to adjust its speed according to the path reference which has no time constraints, and only need to follow the predefined speed profile. Hence, there is no actuator saturation occurring in the path following control. Whereas in the case of trajectory tracking, the vehicle is forced to catch up the evolving reference on the trajectory, due to the strict time constraints coming from the time-parameterized trajectory. Therefore, the path following control has the advantage to achieve smoother convergence to a path when compared to the aggressive maneuvers requested by the trajectory tracking controller, and the control signals in path following control are less likely pushed to saturation as analyzed in [Hindman and Hauser, 1996].

- Temporal convergence

  On the other hand, as there is no temporal specification in the path following task, there is no temporal convergence which can be guaranteed by path following controller. Conversely, the trajectory tracking controller fulfills both the spatial and temporal requirements, such that it has the advantage to implement some time-critical assignments.

In order to clarify the above mentioned differences, a simulation example including trajectory tracking and path following is given as follows.

By using the trajectory tracking controller proposed in (4.4) and the path following controller proposed in [Lapierre et al., 2003], the simulation is performed to straightforwardly show the characteristics of path following and trajectory tracking strategies. The reference path to be followed was set as $x(\gamma) = 0, y(\gamma) = -6 + 6cos(0.04\pi\gamma)$ with $\dot{\gamma}(t) = 1.0m/s$.The initial vehicle surge and angular speeds are $u(0) = 1.0ms^{-1}, r(0) = 0rads^{-1}$, and the initial posture is set as $x(0) = 4m, y(0) = -8m, \psi(0) = \pi/2$.

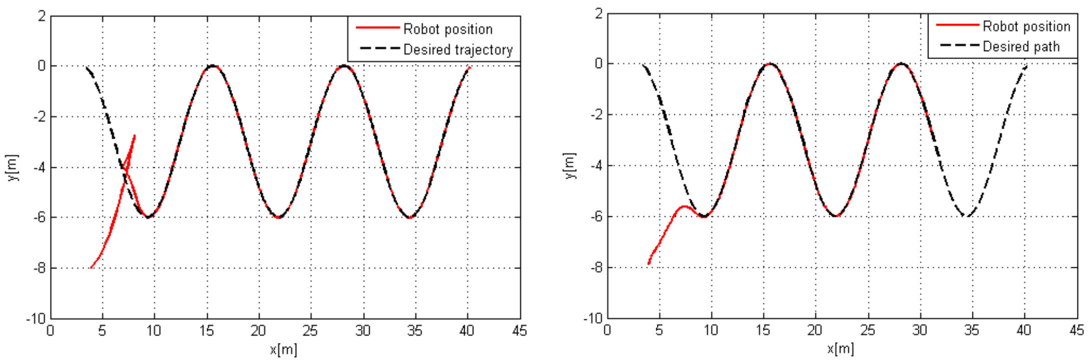

(a) Spatial convergence of trajectory tracking (b) Spatial convergence of path following

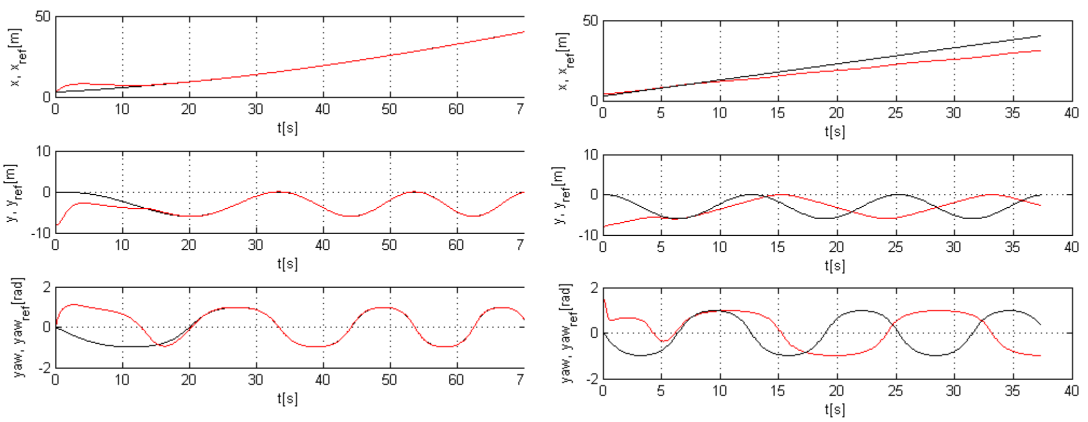

(c) Temporal convergence of trajectory tracking (d) Temporal convergence of path following

Figure 1.12 – Trajectory tracking versus path following : spatial and temporal convergence

In terms of spatial performance, Figure 1.12(a) refers to the pure trajectory tracking case, and from the $x - y$ trajectory depicted in this Figure, one can clearly see that the vehicle aggressively approach to the trajectory, and turns back in its attempt to be at the given reference point at the prescribed time. In the pure path following case, the convergence to the path is very smooth as depicted in Figure 1.12(b).

In terms of temporal performance, Figure 1.12(c) shows the time errors (by comparing relative posture of the vehicle and the reference point) quickly converge to zero driving by the trajectory tracking controller. However, Figure 1.12(d) shows that the time errors do not converge to zero and the vehicle always stays behind of the reference trajectory, as the path following primarily concerns the spatial convergence and does not need to respect the time specification, such that the vehicle only steers the orientation, but keeps the same surge speed and do not follow the time-varying speed of the reference point on the trajectory.

1.3.2.3 Modified strategies

From the simulation results shown in Figure 1.12, it illustrates that there are some spatial and temporal trade-offs between trajectory tracking and path following. Subsequently, one may expect that one controller could balance and benefit from both the path following and trajectory tracking performance. Then, the new concept of ***maneuver modified trajectory tracking*** came up, which was proposed by Hauser and Hinder [Hauser and Hindman, 1995] and was applied to autonomous underwater vehicles in [Encarnacao and Pascoal, 2001] later.

- **Maneuver modified trajectory tracking** (MMTT)

In [Hauser and Hindman, 1995], the authors assume that a trajectory tracking controller for a given system is available and that a Lyapunov function is known that yields asymptotic stability of the resulting control system about a desired trajectory. In order to execute a path following maneuver, the vehicle should "look at the closest point on the path" and adopt the posture of a virtual vehicle moving along the path at the closest point as a reference to which it should converge.

In fact, the MMTT strategy shows how to blend into a single control law trajectory tracking and path following behaviors, thus achieving smooth spatial convergence to the trajectory as well as time convergence. This is accomplished by modifying the projection function through the addition of a time dependent penalty term to obtain the projection.

However, two constraints in MMTT should be figured out :

(a) Complex projection algorithm

In order to modify the trajectory tracking controller by injecting path following behavior, the not-trivial projection mapping of the current vehicle states to the trajectory is required to get the closest reference point in terms of relative distance and time difference criterions. Obviously, the procedure of minimization should be done online to search the projection mapping point, which results in the control complexity and computation burden.

(b) Path limitations and local stability

There are some technical conditions on the path shapes and path parameterizations [Hindman and Hauser, 1996] in order to avoid the singularities for the projection algorithm, which is locally well defined with the "no sharp corners" and "non-intersecting" assumptions of the desired path, such that only local stability is achieved in the MMTT control design.

- **Maneuvering problem**

Inspired by the MMTT strategy, Skjetne formally defined ***the maneuvering problem*** in [Skjetne et al., 2004, Skjetne et al., 2005], where the temporal and spatial tasks are separated into two-folder tasks, i.e., a geometric task and a dynamic task. The geometric task, can be taken as path following, steering the vehicle to converge and stay on the path, while the dynamic task normally forces the vehicle to reach the desired speed assignment. An extra degree of freedom from a deliberate path parameter, is used to bridge the two separated tasks in the whole control design. The dynamic gradient minimization algorithm embedded in the maneuvering design, relaxes the restrictions imposed on the desired paths resulted by the projection algorithm in the MMTT design.

Although the dynamic task can be defined as a time assignment other than the speed or acceleration assignment in the maneuvering problem, the maneuver controller will be directly degenerated into a pure trajectory tracking controller in this case. This is the basic difference from MMTT control where trajectory tracking and path following are blended in a single control, achieving both the smooth spatial convergence to the trajectory and time convergence together.

- **Comparison among different strategies**

Now, we can make a conclusion about two conventional motion control strategies of trajectory tracking (TT) and path following (PF), and two modified strategies of modified maneuver trajectory tracking (MMTT) and the maneuvering strategy. The result is shown in Table 1.1.

By checking the comparison result in Table 1.1, if the time specification should be respected and smooth spatial convergence is simultaneously expected, it motivates a good intention to find another way and design a new type of modified trajectory tracking controller, in order to relieve the singularity and achieve global convergence, and decrease computational complexity as well.

Table 1.1 – Comparison of four motion control methods

Controller	TT	PF	MMTT	Maneuvering
Temporal convergence	guaranteed	not guaranteed	guaranteed	guaranteed [a]
Spatial convergence	aggressive	smooth	smooth	smooth
Extra DOF	no	yes	no	yes
Singularity	no	no [b]	yes	no
Complexity	low	low	high	medium

[a] If the time assignment is required to be guaranteed, the maneuvering problem is degenerated into pure trajectory tracking (Refer to page 35 in [Skjetne, 2005]).

[b] The singularity of path following control can be relieved by the proposed control design in [Soetanto et al., 2003, Lapierre et al., 2003].

1.3.2.4 New strategy : path tracking

Opposite to the MMTT strategy which goes from trajectory tracking to path following, a new strategy is proposed in the thesis to blend the trajectory tracking and path following in a single controller, by designing the controller to go from **path** following to trajectory **tracking**, named **path tracking** in abbreviative notation. Rather that, it can be considered as maneuver modified path following (MMPF) being analogous to the counterpart MMTT strategy.

In MMTT strategy, a trajectory tacking controller is assumed to be available. In order to execute a path following maneuver, the vehicle find a closest point on the path as a reference by means of projection mapping. And then, the path following is well merged into trajectory tracking controller, through modifying the projection function with a time dependent penalty term.

Actually, the path tracking strategy proposed in this thesis, is based on the nonsingular path following controller in [Lapierre et al., 2003, Soetanto et al., 2003], where a virtual target that is not coincident with the projection of the real target on the path is introduced, and an extra degree of freedom from the virtual target is instrumental for controller design. With the available path following controller, the next step is how to blend the trajectory tracking behaviors into the path following control, thus achieving smooth spatial convergence to the desired trajectory as well as time convergence. This is accomplished by modifying the path following Lyapunov function through the addition of a time dependent penalty term $(\tau - \tau_d)$, where τ_d is the time related parameter for the desired trajectory and τ is the virtual time related parameter with extra degree of freedom in order to achieve path following behavior. This concludes the path tracking control design which goes from path tracking to trajectory tracking. Therefore, the path tracking control objective can be considered to implement a time+space task, that is the union set of spatial task and temporal task, to primary achieve spatial convergence while approaching to the temporal specification in the end.

The virtual time parameter (corresponding to a virtual target on the path) plays an important role in path tracking strategy. When the vehicle is far away from the real target, the virtual target will adjust its speed (or even move backwards) and help the vehicle smoothly converge to the path ; when the vehicle is close to the target, it will increase its speed and lead the vehicle to catch the real target and achieve the time assignment in the sense of trajectory tracking. Thus, smooth but not aggressive spatial convergence is achieved with the time convergence as well, and it is also less likely pushed into actuation saturation.

Difference from existing strategies

In [Hindman and Hauser, 1996], the projection mapping of the current vehicle states onto the path was employed to determine the closest reference on the trajectory. However, no projection is required to find a reference in path tracking control design, and an instrumental virtual target moving along the path with extra degree of freedom is taken as a reference. Actually, this difference is basically reflected by the fact that MMTT goes from trajectory tracking and path tracking goes from path following to trajectory tracking. In addition, feedback linerization method was used for the MMTT control design, and the nonlinear control design method is adopted in path tracking.

Moreover, the restricted assumptions of "no sharp corners" and "non-intersecting", imposed on the desired paths for the maneuver modified trajectory tracking design in [Hindman and Hauser, 1996], and later followed by the combined trajectory tracking and path following design in [Encarnacao and Pascoal, 2001], is relaxed in path tracking design and global tracking is achieved, by using the extra degree of freedom of the virtual target acting as a tracking reference on the path.

In [Skjetne et al., 2004, Skjetne et al., 2005], the geometric task (path following behavior embedded) and the dynamic task (speed, acceleration assignment) is separated in the maneuvering problem, where the design of following the path and the desired motion along the path can be approached individually. However, these two tasks are merged into a single controller in path tracking strategy.

On the other hand, the dynamic task in maneuvering control is usually defined as a speed assignment but not an exact time assignment, such that the time convergence is not strictly guaranteed. If the dynamic task is defined as a time assignment, the maneuver controller will be directly degenerated into a pure trajectory tracking controller as mentioned before. This is the basic difference from path tracking control, where the time convergence is reached and smooth spatial convergence to the trajectory is achieved as well.

1.3.2.5 Further step : coordinated formation control

After addressing the problem of motion control for the single vehicle, it makes sense to go one step further, to address the problem of coordinated motion control for multiple vehicles. In this thesis, two main streams are followed for coordinated formation control of multi-vehicle system. One is the coordinated path following (CPF), and the other is coordinated path tracking (CPT).

As coordinated path following is popular used for cooperative multi-vehicle survey in marine engineering, it attracts a lot of attentions in CPF control design. Compared with conventional CPF controller proposed in [Encarnacao and Pascoal, 2001, Ghabcheloo et al., 2006a, Almeida et al., 2007a], etc., a coordinated path following controller based on geometric formulation, is proposed in this thesis, which emphasizes the important role of the virtual target introduced for single path following control, and utilizes this advantage for coordination.

If time specification is required for cooperative tasks, the coordinated control problem can be addressed based on the path tracking control design. Actually, the path-tracking based coordination of multiple vehicles is more straightforward than CPF, as there is a simple way to find the coordination variables which are identical to the path parameterization variables used in the formulation of path tracking problem, while the coordination variables in the path following control, are not directly associated with the geometric relationship of rigid formation shape.

On the other hand, the field of multi-vehicle control system have received a lot of attention with applications towards mechanical systems, aircrafts, satellites, ships and underwater vehicles. However, the stringent limitation introduced by inter-vehicle communication constraints related to limited bandwidth and range of communications, is especially challenging for underwater vehicles as described in Table 1.2 in [Schoenwald, 2000].

All-to-all communications cause heavy data flow which is not suitable for underwater vehicles due to the limited bandwidth of acoustic modems. Therefore, the topology of the communications network must be addressed explicitly, which is also possibly constrained by the range of communication. Tools from algebraic graph theory are used to explicitly deal with communication topology constraints in this thesis. Moreover, communication variables used for the vehicles exchanging motion-related information for coordination, should be kept minimum to compliant to the bandwidth limitation. This is also a practical issue to be taken into account during the coordinated control design.

Table 1.2 – Characteristics of autonomous vehicles

Property/Type	Ground	Aerial	Space	Underwater
Size	1cm-10m	10cm-10m	1m-10m	10cm-100m
Autonomy	full/tethered /teleoperated	full/teleoperated	full/attached to mother vehicle	full/tethered
Dynamics	simple to complex	standard	standard	*complex*
Environment	easy to difficult	moderate	difficult	severe
Communicaiton	numerous	numerous	limited	very restrictive

1.4 Contributions and organization of thesis

In this section, a brief description is given to illustrate the contributions and structure of the thesis.

According to the detailed analysis in section 1.3, the main contribution of this thesis are summarize as follows :

(1) The trajectory tracking and path following control problems are posed firstly, and the advantages/disadvantages of control performances are revealed. Then, a new control strategy, path tracking, is proposed in order to achieve smooth spatial convergence and tight temporal performance as well.

(2) Motion control design is addressed for nonholonomic unicycle-type wheeled vehicle, and then is extended to the underactuated autonomous underwater vehicles (AUVs), based on the similarity between two kinds of vehicles. However, different guidance strategies : approaching angle and Line-of-Sight heading guidance, are adopted for wheeled and underwater vehicles respectively, and the resulted difficulty from the side-slip angle in underactuated AUVs is solved, where stern-dominancy property is emphasized for well-posed control computation. Smooth transitions of path following and path tracking control from underactuated to fully actuated AUVs are also proposed.

(3) Coordinated motion control under formation constraint are addressed for multiple nonholonomic and underactuated autonomous vehicles, in both coordinated paths following and coordinated paths tracking manners, where the control of virtual targets moving along the path is the fundmental issue. Two approaches, the leader-follower method based on geometric formulation of formation pattern and the virtual structure with formation feedback, are employed to implement centralized control design of coordinated formation motion, and then the decentralized control design is achieved by resorting to the algebraic graph theory, which is used

to represent the communication topology of multi-vehicle system and provide a theoretical way to rigorously prove the proposed coordination laws. The flexibility of path parameter in path tracking renders the easily implementation of coordinated paths tracking, to avoid complex mathematical formulation in coordinated paths following.

An overview of the relations between the chapters is presented in Figure 1.13. The arrows represent the relations between the chapters, and indicate how the chapters are divided to solve the motion control problems of nonholonomic underactuated autonomous mobile and underwater vehicles, where the path following and path tracking control are the two main objectives and trajectory tracking is the minor interest shown as a comparative case in the thesis.

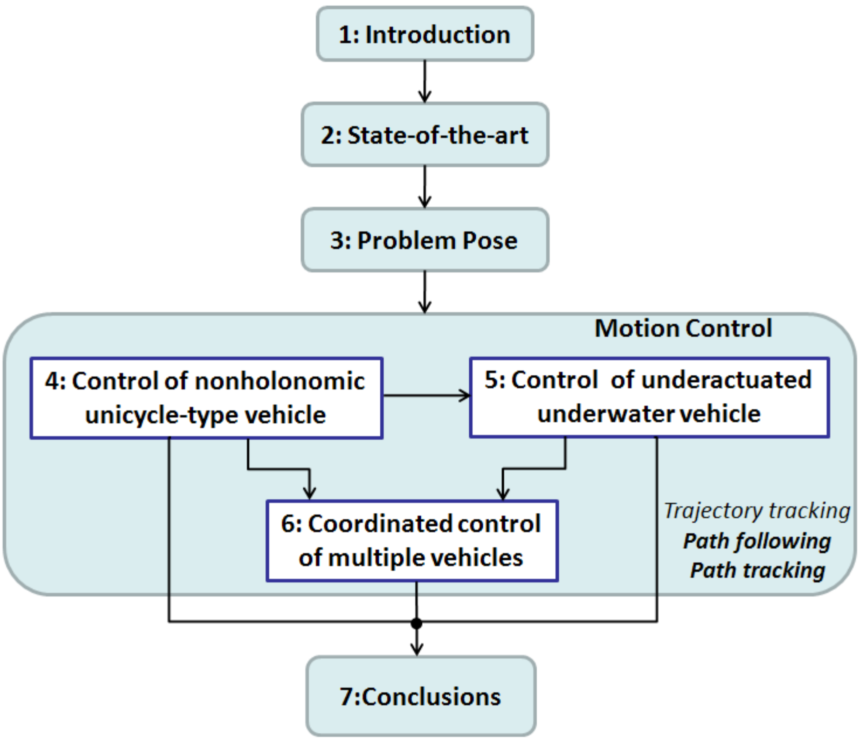

Figure 1.13 – Road map for the chapters

The chapters are organized as follows :

Chapter 2 contains the state-of-the-art of the motion control strategies.

Chapter 3 describes the problems of motion control of underactuated and nonholonomic system.

Chapter 4 derives kinematic and dynamic control laws for the motion control of the nonholonomic unicycle-type mobile robot.

Chapter 5 extends the results in chapter 4 to the path following and path tracking control of the underactuated AUV system.

Chapter 6 addresses the problem of coordinated path following and coordinated path tracking for multiple underactuated vehicles, based on centralized and decentralized control strategies.

Chapter 7 summarizes the results obtained and suggests the directions of further investigation.

Chapter 2

State-of-the-art of motion control of autonomous vehicles

Numerous applications related to autonomous vehicles, including air, land and marine vehicles, are presently operational in industrial, scientific and military fields and more ambitious applications are in engineering development. To meet various goals of different applications, vehicles must be equipped with control systems to steer them to achieve various motion tasks, and considerable interest in the development of advance methods for motion control problems. Namely, point stabilization, trajectory tracking and path following control.

Point stabilization is a point-to-point motion, stabilizing the system at a desired target point from a initial point. According to the viewpoint of Walsh [Walsh et al., 1994], the objective of *trajectory tracking* controller is to stabilize a system about a trajectory instead of a fixed point, such that the stabilized solution is explicitly time-varying. Hence, trajectory tracking can be taken as a generalized case of point stabilization, and has more broad and extensive applications. As the problem of *path following* control is to stabilize a system about a path without temporal specification, path following can be considered as a relaxed case of trajectory tracking in terms of stabilizing the distance to zero between the control system and the path without any time requirement [Morin and Samson, 2009]. Furthermore, the problem of *coordinated formation control* of multiple vehicles, is based on the tracking or following motion pattern of single vehicle, while the inter-vehicle geometric formation constraints is imposed on the whole multiple vehicle team. Hence, there is an inherent link between the control problem of point stabilization, trajectory tracking, path following and coordinated formation control. In the following part, the state of art of these motion control problems will be reviewed subsequently.

2.1 Stat-of-the-art of individual motion control

In this part, literature review in different approaches to point stabilization, trajectory tracking, path following and path tracking control for a single autonomous vehicle is presented.

2.1.1 Point stabilization

It is well known that nonholonomic systems pose considerable challenges to closed-loop feedback stabilization about a given equilibrium point. As pointed out in the famous Brockett theorem of necessary conditions for smooth feedback stabilizability [Brockett, 1983], there is no continuously differentiable, time invariant and static state feedback control laws for point stabilization applied in nonholonomic system. It is also shown that there is no continuous time-invariant state feedback in [Zabczyk, 1989]. These resulted limitations from Brockett theorem motivates a lot of research activities devoting to find novel solutions to the point stabilization problem. The proposed approaches to overcome the limitation are continuous smooth time-varying control laws, discontinuous or piecewise time-invariant smooth control laws, and hybrid discrete/-continuous controllers [M'Closkey and Murray, 1997].

The time varying feedback approach is first proposed for nonholonomic wheeled mobile robot in [Samson, 1992], and a generalized constructive approach know as Pomet's method generates smooth time-periodic feedback laws in [Pomet, 1992]. However, smooth time-varying controllers has slow convergence and cannot achieve exponential convergence as stated in [M'Closkey and Murray, 1994]. To overcome this difficulty, discontinuous control strategy is derived to solve the problem, by using the state scaling originated from the σ process, and get a fast transient response and usually an exponential stabilization is achieved [Astolfi, 1996], but the consequence is discontinuity in the control input. Another approach to address the feedback stabilization problem of nonholonomic system is a two-fold hybrid control, one discrete-time part that practically stabilizes a subset of the system states, and another piecewise continuous-time part that steers the remaining state-components to an arbitrary small neighborhood of the origin [Canudes de Wit et al., 1994]. In [Hespanha et al., 1999], a simple logic-based hybrid controller is proposed to get global exponential stabilization of the nonholonomic integrator.

In the case of underactuated marine vehicles, by using Brockett theorem, it can be shown there is no consinuous time-invariant feedback law such that the equilibrium is asymptotically stable [Pettersen, 1996], and it can not even be stabilized by discontinuous time-invariant feedback when the Filippov solutions of the closed-loop system are considered [Coron and Rosier, 1994]. Furthermore, as observed in [Pettersen, 1996], the underactuated marine system is not transformable into a standard drift-less chained system, such that existing control schemes developed for chained systems [Canudes de Wit et al., 1994, Astolfi, 1996, Hespanha et al., 1999] can not be applied directly. In [Leonard, 1995], a pioneering work in this field is reported to re-position and re-orient underactuated AUVs by a open loop small-amplitude periodic time-varying control laws. In [Pettersen and Egeland, 1996], a continuous periodic feedback control law that asymptotically stabilizes an underactuated AUV and yields exponential convergence to the origin is described. In [Astolfi et al., 2002], asymptotic stabilization of an underactuated AUV is achieved where the control design exploits the Hamiltonian nature of the system to be controlled and it is based on the so-called interconnection and damping assignment (IDA) procedure. A novel switched seesaw unstable/stable control law for stabilization of underactuated AUV is adopted in [Aguiar et al., 2005a].

For the ship, marine surface vehicle, or underwater vehicle, *Dynamic positioning* (DP) problem and some homing/docking tasks can be categorized into the problem of point stabilization. Although dynamic positioning is mostly limited to fully actuated vessels, a time-varying feedback control law including integral action is developed and proved to exponentially stabilizes the posture of the underactuated ship by experimental results in [Pettersen and Fossen, 2000]. A nonlinear adaptive dynamic positioning controller is proposed for an underactuated AUV in the presence of constant unknown ocean currents and parametric modeling uncertainty in [Aguiar and Pascoal, 2007b]. Depending on the obtained time differences of arrival (TDOA) measured by the ultrashort baseline sensor, an underactuated AUV is driven toward a fixed target in three dimensions by homing integrated guidance and control laws, and global asymptotic stability is achieved even under constant known ocean currents in [Batista et al., 2009].

2.1.2 Trajectory tracking

The trajectory tracking problem of nonholonomic mobile robot systems is very interesting from an engineering perspective, yet it is suffering from a non-directly controlled cross-track error due to the lateral zero-speed constraints. This is the point to bring more challenges for trajectory tracking control of nonholonomic systems than well understood holonomic or fully actuated systems with satisfactory solutions in standard control textbooks [Khalil, 1996]. There are two main methods to address the nonholonomic trajectory tracking problems. The first one is based on linearization method, and the second one relies on the Lyapunov's direct method.

By using Taylor linearization of the corresponding error model, a continuous feedback tracking control law with local asymptotic stability is achieved via Lyapunov's indirect method in [Kanayama et al., 1990], and a local exponential stability result is obtained in [Murray et al., 1992] using a linearized kinematic model similarly to [Kanayama et al., 1990]. Through linearization a chained form system around the reference trajectory, a linear time-varying feedback controller of nonholonomic trajectory tracking is achieved by stabilizing the resulting linear time-varying system in [Walsh et al., 1994]. In [Canudas de Wit, 1998], a dynamic feedback linearization approach is proposed in and local posture tracking with exponential convergence for restricted mobile robot. In [Oelen and van Amerongen, 1994], asymptotic stabilization is obtained using input/output linearization. Alternative approaches are developed including the linearization of the vehicle error dynamics around trajectories which lead to a time-invariant linear system, and various controllers are then designed based on the gain-scheduling technique and/or linear parameter varying methodologies to yield some local stability result about the trimming trajectories [Shamma and Cloutier, 1993, Kaminer et al., 1998, Silvestre et al., 2002].

Nonlinear Lyapunov's direct method based designs can overcome the basic limitation of linearization where the stability is only locally guaranteed in a neighborhood of the selected operating points, and get nonlinear control design for trajectory tracking in a global tracking sense. Combined with integrator backstepping technique, uniformly asymptotically stability of nonlinear feedback controller is achieved in [Fierro and Lewis, 1997] for both a kinematic and dynamic model, and a time-varying state feedback is obtained global results in the tracking problem [Jiang and Nijmeijer, 1997]. In the presence of input saturation for a class of unicycle-modeled nonholonomic mobile robots, a global tracking result is achieved by using the backstepping technique and invoking the LaSalle's invariance principle [Lee et al., 2001].

For underactuated marine vehicles, there is no actuators in the sway axis of underactuated ships, while in the case of underactuated underwater vehicles, there are no actuators in the sway and heave directions. This kind of configuration is by far most common among the marine vehicles [Fossen, 2002], while resulting in additional difficulties to track a reference trajectory. Recently, the position and orientation tracking of underactuated marine vehicles has been studied extensively.

An application of the recursive technique for the standard chain form systems is extended to the underactuated surface ships and yields a high gain based local exponential experimental tracking result [Pettersen and Nijmeijer, 2001]. A high gain based global practical tracking controller is developed in [Behal et al., 2002], based on a transformation of the ship tracking system into a skew-symmetric form. While the closed-loop system dynamics is increased due to the controller designed to make the states of the transformed system track the auxiliary signals generated by some oscillator.

In [Lefeber et al., 2003], a global k-exponential tracking result is obtained to solve the trajectory tracking problem for an underacuated surface vessel with only two propellers, where a cascaded approach is applied to reduce the problem of stabilizing the nonlinear tracking-error dynamics to two separate problems of stabilizing linear systems. The stability analysis relies on the stability theory of linear time varying systems. Based on Lyapunov's direct method and passivity approach, two constructive tracking solutions are proposed in [Jiang, 2002], by exploiting the inherent cascade interconnected structure of the underactuated ship dynamics and generating explicit Lyapunov functions. It is noted that in [Pettersen and Nijmeijer, 2001, Jiang, 2002, Lefeber et al., 2003], the nonzero yaw velocity is required to satisfy persistently excitation (PE) condition, which also appears in the tracking control of a nonholonomic mobile robot [Dixon et al., 2000]. This restrictive PE condition implies that the reference trajectory must be curved (e.g., a circle trajectory, sinusoidal trajectory, etc.), and a straight line is excluded to be tracked indeed. In [Do et al., 2002a], the chained form is not used and the tracking errors are projected on the body-fixed frame, such that a solution to the problem of trajectory tracking without imposing the yaw velocity to be nonzero is obtained. Other solutions to the tracking of both straight line and curved trajectories are presented in [Zhang et al., 2000, Encarnacao and Pascoal, 2001, Pettersen and Nijmeijer, 2002].

In [Aguiar and Hespanha, 2007], the problem of trajectory tracking control design is addressed for underactuated autonomous vehicles in the presence of possibly large modeling parametric uncertainty, where the desired trajectory did not need to be of a particular type (e.g., trimming trajectories) and could be any sufficiently smooth bounded curve parameterized by time. Some related work with different control strategies includes trajectory planning approach in [Sira-Ramfrez, 1999], local H-infinite optimal tracking control and output redefinition in [Toussaint et al., 2000], and a linear algebra approach to minimize the tracking error in [Rosales et al., 2009].

While the stabilization and tracking problems are typically studied as two separate problems, it is worth to solve the problem *simultaneously stabilization and trajectory tracking* (SSTT) as figured out in [Jiang, 2011]. Some preliminary results have been obtained in [Lee et al., 2001, Do et al., 2002b, Do et al., 2004a]. A time varying velocity feedback controller is proposed to achieve both stabilization and tracking of unicycle mobile robots at the kinematic level in [Lee et al., 2001], but it is difficult to be directly extended to the case of underactuated marine system due to the nonintegrable second-order constraint. In [Do et al., 2002b], a single universal controller is proposed to solve SSTT problem for underactuated surface ships with only surge force and yaw moment, based on Lyapunov's direct method and backstepping technique. In [Do et al., 2004a], a global output-feedback controller is designed to simultaneously solves SSTT problems for an underactuated omnidirectional spherical underwater vehicle by using the interconnected structure of the vehicle dynamics.

2.1.3 Path following

The past few decades have witnessed an increased effort in the area of motion control of autonomous vehicles, where trajectory tracking is a typical problem to accomplish non-static motion task. However, as pointed out in [Hindman and Hauser, 1996, Encarnacao and Pascoal, 2001, Al-Hiddabi and McClamroch, 2001, Al-Hiddabi and McClamroch, 2002], aggressive dynamic behavior is prone to be happened during the trajectory tracking motion operation, naturally introducing possible saturation of actuation as the controller always forces the system output to catch up the time-parameterized desired output as closely as possible. In practice, the requirement that the vehicle follows a given time parameterized trajectory, can be relaxed to require that the vehicle follows a desired path in space without constraint of being at a specific point on the path at a specific instant of time. That means path following strategy can be sometimes used to replace trajectory tracking strategy in engineering practice, such as way-point navigation, reconnaissance, and surveillance where the vehicle is not required to be on a given point of the trajectory at a give time instant. Actually, smoother convergence to the path is achieved in path following and the control signals are less likely pushed into saturation when compared with trajectory tracking. Moreover, there is an essential difference between path-following and standard trajectory-tracking for nonminimum phase system, by demonstrating that performance limitations on trajectory tracking due to unstable zero-dynamics can be relieved in the path-following problem [Aguiar et al., 2005b, Aguiar et al., 2008]. Thus, the path following problem has received some attentions from the control community over the last decade.

To the best knowledge of the author, the concept of path following and corresponding control design are firstly proposed for nonholonomic mobile robots in kinematics level by Samson in [Samson, 1992], and reported later in [Micaelli and Samson, 1993, Canudas de Wit, 1993]. Extended research work in dynamics level is reported in [Jiang and Nijmeijer, 1997, Soetanto et al., 2003].

Other studies on path following have been devoted to aerospace vehicles in [Al-Hiddabi and McClamroch, 2001, Rysdyk, 2003], and devoted to underwater vehicles in [Encarnacao and Pascoal, 2000, Lapierre et al., 2003]. In [Samson, 1995], path following problem is addressed for a car pulling several trailers, and this problem is more formally presented for a n-trailers vehicle that provides local asymptotic stability for a path of nonconstant curvature in [Altafini, 2002]. A path following control problem of fully actuated underactuated surface vessel can be formulated in [Almeida et al., 2007b], and a nonlinear adaptive path following controller is designed to yield convergence of the trajectories of the closed loop system to the path, in the presence of parametric model uncertainty and constant unknown ocean currents without the need for direct measurements of its velocity. However, in most cases, the planar three-degree-of-freedom problem is reduced to control the yaw angle and surge velocity. Recent development in nonlinear control and control of underactuated systems, has offered new tools and promising solutions to deal with all three degrees of freedom using two independent controls [Encarnacao and Pascoal, 2000, Lapierre et al., 2003, Do et al., 2004b, Aguiar and Hespanha, 2007, Oh and Sun, 2010]. Nevertheless, among the different solutions to the problem of path following control, the underlying questions to be solved concern the following issues.

2.1.3.1 Path parameterization

Any $\mathcal{C}^1$ path, such as straight line, circle, sinusoid curve, etc., can be regularly parameterized. Classic geometrical description can be used to parameterize the path which facilitates the path following control design. One of the conventional parameterization considers that there is a virtual target moving along the path and the along-path distance s is the path variable to parameterize the predefined path. The along-path distance s is also called the curvilinear abscissa of the virtual target point [Micaelli and Samson, 1993, Diaz del Rio et al., 2001, Skjetne and Fossen, 2001, Lapierre et al., 2003]. Hence, the path following is identified with the progress of the descriptor parameter. The derivative of the path parameter is used as an additional control to allow the vehicle to follow a desired path with arbitrary curvature.

An alternative way to parameterize a path is through a generalized variable τ related to the time instant t, either the recorded time for previous memorized trajectories or the real time when the path following is in progress and the virtual target on the path is moving [Diaz del Rio et al., 2001]. In this case, note that the time dependence of path parameter τ is not directly relevant to the speed of the vehicle, but only relevant to the movement of virtual target on the path such that the path can be represented as $p(\tau(t)) = [x_d(\tau(t)), y_d(\tau(t))]$. $\dot{\tau}(t)$ can be used as an additional effort to control the movement of the virtual target along the path, which is also called the *timing law* of the virtual target proposed for path following control in [Skjetne et al., 2005, Aguiar and Hespanha, 2007]. It is indicated that the generalized path variable τ can be designated as the path length (along-path distance) if required as shown in [Ihle et al., 2004], so that the linear speed of the virtual target on the path will be the same as the tangential speed along the path which can be easily expressed as $\dot{s}$.

2.1.3.2 Choice of the coordinate frame

In [Aicardi et al., 1995], *polar coordinate frame* is used to localize the vehicle requiring a nonsingular transformation in the original error space, and a path following controller for mobile robot is designed with hard switch control on the virtual target motion. Inspired by this solution, a path following controller is proposed in [Aicardi et al., 2001] by using a polar-like kinematic model for underactuated planar vehicles. It highlighted that knowledge of the path curvature and its derivative with respect to the curvilinear abscissa are not necessary in the controller. However, it is a "tube" controller adopting a set of polar-like variables, and only bounded path following error below an adjustable upper threshold is guaranteed. By using a polar coordinate transformation to interpret the path following error dynamics in a triangular form and a line-of-sight algorithm, a robust adaptive path-following controller for underactuated ships without off-diagonal dynamics terms is proposed in [Do et al., 2004b].

In [Micaelli and Samson, 1993], path following problem is formulated based on the moving *Frenet-Serret reference frame* attached to the virtual target on the path. Kinematic controller is derived by elaborating heading guidance design to shape the transient maneuvers, and LaSalle's invariance principle is recalled to simplify the nonlinear path following control law introduced in [Soetanto et al., 2003]. Integrator backstepping technique is recruited to deal with vehicle dynamics. The same circle of ideas is explored for marine vehicles, a fourth order ship model in Frenet-Serret frame is used in [Encarnacao et al., 2000] to develop a control strategy to track both straight line and circumference under the constant and known ocean-current disturbance. The underwater vehicle model in terms of Frenet-Serret frame is formulated in [Encarnacao and Pascoal, 2000], and later reported in [Lapierre et al., 2003, Lapierre and Soetanto, 2007]. A four-degree-of-freedom nonlinear surface vessel model, together with the Serret-Frenet equations, is introduced to describe the ship dynamics and path following error dynamics in [Li et al., 2009a]. The path-following errors is interpreted in a Frenet-Serret frame attached to the path in [Do and Pan, 2006], to design a new global controller forcing an underactuated ship to follow a reference path under disturbances induced by wave, wind and ocean-current.

In [Almeida et al., 2007b], the position error between the vehicle and the path is defined in the *body-fixed frame*, and a nonlinear adaptive controller is designed to yield the convegence of the closed loop system to the path in the presence of constant unknown ocean currents and parametric model uncertainty, for a fully actuated surface vehicle. In [Aguiar and Hespanha, 2007], the global diffeomorphic coordinate transformation expressing the path following error of an underactuated AUV in the body-fixed frame, and an adaptive controller is designed to solve the problem of global boundedness and convergence to neighborhoods of the origin by appropriate choice of the control parameters. In [Skjetne et al., 2005], the error variables are also decomposed in the body-fixed frame, to achieve the geometric path following task in the maneuvering problem.

2.1.3.3 Choice of the virtual target point

The virtual target point on the path and its moving speed are critical for path following control. The target point is defined as the orthogonal projection of the current vehicle position on the path in [Samson, 1992, Micaelli and Samson, 1993] for mobile robot system as illustrated in Figure 2.1(a), and later used in [Encarnacao et al., 2000, Encarnacao and Pascoal, 2000] for underwater vehicle system. That means the target point is the closest point of the path relative to the vehicle. This allows a simplified control design as the along track error is already zero, and it also brings a rapid convergence to the path due to the minimal distance to the path. Unfortunately, this orthogonal projection method induces a conservative condition on the vehicle's initial position. If the vehicle is located at the center of the osculating circle (i.e., an associated circle with radius of curvature [Skjetne and Fossen, 2001]), the position of the virtual target is not well defined on the path and singularity occurs in the control design. Consequently, it requires the initial position of the vehicle relative to the path under range of the smallest radius of curvature present on the path, and only local convergence to the path is guaranteed in the control law as pointed out in [Soetanto et al., 2003, Lapierre et al., 2003].

In order to relax this constrained initial condition, an additional control degree of freedom is introduced to the virtual target in [Soetanto et al., 2003, Lapierre et al., 2003], so that the virtual target is not "fixed" by the orthogonal projection any more as illustrated in Figure 2.1(b), but moves on the path with its own speed control laws to get a collaborative movement relative to the vehicle : when the vehicle is behind, the virtual target will slow down and wait for the actual vehicle ; when the vehicle is advance, the virtual target will accelerate. This implies the virtual

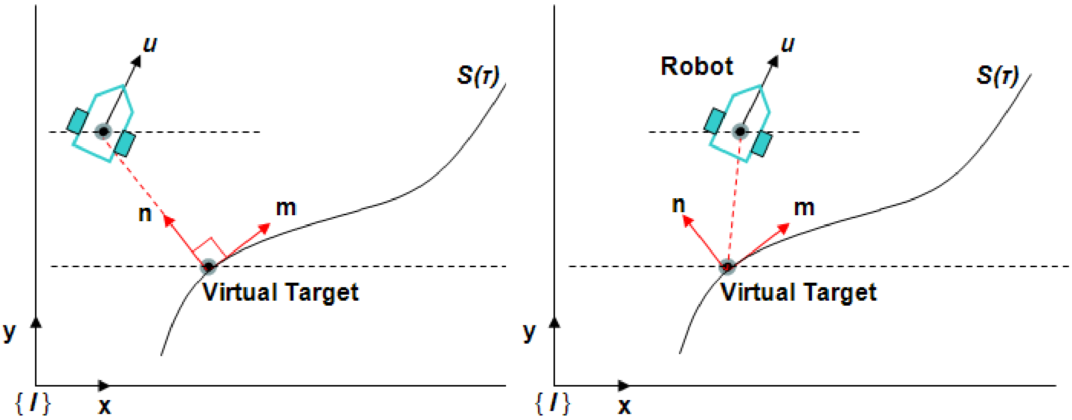

(a) Orthogonal projected virtual target (b) Freely moving virtual target

Figure 2.1 – Choice of the virtual target point

target will converge to the closest point and help the vehicle to converge to and follow the path with desired vehicle speed, while the target point is now well defined and the initial position of the vehicle could be anywhere far away from the path. This feature is suitable in practice because it avoids the use of a high gain control effort to generate large control signals. The running speed of the virtual target is explicitly controlled by modeling the kinematic equations of motion with respect to the vehicle's speed and along-path error in the Frenet-Serret frame.

The idea of virtual target is implicitly embedded in other research works. In [Aicardi et al., 1995], the motion control of a virtual target along a path is proposed for wheeled robots in polar coordinate. The speed of the virtual target is a continuous radial function centered on certain ellipsoidal domain, which attains its maximum value when the vehicle state is inside or on the surface of the ellipse, and attains a null minimum value when the vehicle state is outside. The similar idea is extended to the control of marine craft in [Aicardi et al., 2001]. In [Diaz del Rio et al., 2002], the concept of "error adaptive tracking" is introduced. By selecting the speed of the virtual target as a function of the tracking error, the movement of the virtual target is controlled and adapted to the tracking error (the target speed tends to 1 if errors are small, while tends to 0 if they are large), such that the singularity of the closest path point in [Micaelli and Samson, 1993, Encarnacao and Pascoal, 2000, Skjetne and Fossen, 2001] is avoided. A virtual vehicle concept is also proposed in [Egerstedt et al., 2001] to bypass the singularity, whose control law ensures global stability by determining the dynamics of the parameterized reference point. The motion of the virtual vehicle on the desired path is governed by a differential equation containing error feedback. However, not only the speed of the virtual target but also that of vehicle have to be adjusted simultaneously. This disobeys the underlying assumption in path following control that the vehicle's forward speed tracks a desired speed profile while the controller steers its orientation to drive it towards the path.

2.1.3.4 Choice of heading guidance

As the path following controller should steer the orientation of the vehicle to drive it to the path, the heading guidance specifying how to steer the orientation affects the path following performance. In [Micaelli and Samson, 1993], an approaching angle is generally chosen as $\delta(y_e, u) = -sign(u)\tanh(y_e)$ where u is the forward velocity of the wheeled robot and y_e is the cross-track error between the vehicle and the target. This choice is natural and an adequate reference sign definition is provided in the approaching angle in order to drive the vehicle to the path, i.e., turning right when the vehicle is on the left side of the path and turning left in the opposite situation. A larger positive lateral error distance leads to the desired relative heading between vehicle/path to be $\pi/2$ and the approach angle decreases as the vehicle approaches the path and y_e diminishes [Lapierre et al., 2007]. Hence, this approaching angle can be taken as a heading guidance which is instrumental in shaping the transient maneuvers during the path approach phase. However, it raises some mathematical difficulties because $\delta(y_e, u)$ is not differentiable with respect to u at $u = 0$.

Another choice is proposed in [Lapierre et al., 2006] and let the approaching angle be $\delta(y_e, u) = -\tanh(y_e u)$. However, this choice make the complicated computation of control derivation, and reduces the system performance in terms of convergence time. In [Lapierre et al., 2007], this problematic situation is avoided by imposing a forward velocity $u_d > 0$ which is justified to be able to escape from the "corner situation" in the case of obstacle avoidance. It is also reasonable for controllability reasons in the case of an torpedo-like AUV [Lapierre and Jouvencel, 2008]. In [Bibuli et al., 2009], for the problem of path following of underactuated unmanned surface vehicles using approaching angle, some heuristic methods are proposed to face the problem of speed of advance adaptation based on path curvature measurement and steering action prediction while approaching a curve or when tricky maneuvers are needed .

Line-of-sight (LOS) is an attractive method for path control, which is proposed for autonomous ocean vehicles in [Papoulias, 1991, Papoulias, 1992]. Now, it is a popular heading guidance applied to marine vehicles due to its clear physical meaning. LOS directs the orientation of the vehicle to aim at a point lying $\Delta > 0$ meters ahead of the vehicle projection onto the path, and parameter Δ is usually called a lookahead distance. This suggests the limitation of minimum turning radius of marine vehicles, can be easily incorporated into the LOS guidance by setting the lookahead distance beyond the minimum turning radius, such that LOS implies another physical meaning as a heading guidance.

In [Fossen, 2002], a LOS vector from the vehicle to the next way-point or point on the path between two waypoints can be computed for heading control. LOS based on path following control for marine surface vessels has been adopted in [Fossen et al., 2003] where a 3 degrees-of-freedom nonlinear controller for path following of marine craft is derived using only two controls. In this case the path following is achieved by a geometric assignment based on a LOS projection algorithm for minimization of the cross-track error to the path and the desired speed along the path can be specified independently. An improved approach concerning the calculation of a dynamic LOS vector norm is presented in [Moreira et al., 2007], in order to improve the speed of convergence of the LOS algorithm as it is important to minimize the cross track error, i.e., the shortest distance between the vehicle and the straight line [Pettersen and Lefeber, 2001]. The traditional LOS heading guidance is built in the inertial frame [Pettersen and Lefeber, 2001, Fossen, 2002, Fossen et al., 2003] to track straight-line path generated by given way-points during maneuvering. It is adapted and built in a moving Frenet-Serret frame, for underwater vehicles following both straight-line and curved path in [Xiang et al., 2009a]. Traditional LOS guidance has the drawback of being susceptible to environmental disturbances. In [Børhaug et al., 2008], a modified LOS guidance law with integral action is proposed to counteract environmental disturbances. Paired with a set of adaptive feedback controllers, it shows that this approach guarantees global asymptotic path following of straight-line paths in the presence constant and irrotational ocean currents.

In [Pavlov et al., 2009], an underactuated vessel is controlled to follow a straight line path using a LOS guidance, and a time-varying lookahead distance as a parameter of the LOS guidance law, is updated with a model predictive control (MPC) algorithm. It demonstrates that the performance of the system (fast convergence to the path with minimal overshoot) is improved compared to what can be achieved with a constant lookahead distance. In [Oh and Sun, 2010], a MPC strategy is adopted for a way-point tracking of underactuated surface vessels with input constraints, and a LOS decision variable is incorporated into the MPC design to improve the path following performance.

2.1.3.5 Control methods

Most of the research activity on this topic has focused on feedback linearization and backstepping methods. However, other control approaches such as model predictive control(MPC), sliding mode control and neural network techniques methods have also been developed.

Following the work of tracking trimming trajectories for autonomous vehicles in [Kaminer et al., 1998, Silvestre et al., 2002], the problem of path following control of wheeled robots is solved by using a simple algorithm where some local results are obtained by using linearization techniques and gain scheduling control theory for trimmed paths in [Ghabcheloo et al., 2006b]. In [Encarnacao et al., 2000, Lapierre et al., 2003, Aguiar et al., 2005b], a kinematic controller for underactuated underwater vehicles is first derived using nonlinear Lyapunov based method to get global convergence to the path, and extended to cope with vehicle dynamics by resorting to backstepping techniques. In [Lapierre and Jouvencel, 2008], a robust nonlinear path following controller is developed and robustness to vehicle parameter uncertainty is addressed by incorporating a hybrid parameter adaptation scheme. In [Do et al., 2004b], a nonlinear robust adaptive control strategy to force a underactuated underwater vehicle to follow a predefined path in the presence of both environmental disturbances induced by wave, wind and ocean-current and vehicle's unknown physical parameters. The proposed controller is designed using Lyapunov's direct method, the popular backstepping and parameter projection techniques. This method is later extended to robust path-following of underactuated ships by several nonlinear coordinate transformation and utilizing the ship dynamic structure in [Do and Pan, 2006]. In case of robust nonlinear parameter and state estimation, it can be guaranteed by using interval analysis for both the mobile robot [Jaulin et al., 2002] and underwater robots [Jaulin, 2009b].

Recently, some control methods, include MPC control, sliding mode control and neural network techniques, also have been applied to path following control . The advantage of MPC over other control strategies is that input and system constraints are able to be handled straightforwardly in the optimization problem so that the robot can travel safely with a high velocity. In [Bak et al., 2001], the path considered consists of straight lines intersected with given angles, and a fast realtime MPC controller which anticipates the intersections and smoothly controls the nonholonomic mobile robot through the turnings while fulfilling the velocity constraints. In [Kanjanawanishkul and Zell, 2009], model predictive control is employed to design the path following control law for an omnidirectional mobile robot. The nonlinear MPC is adopted for path following control of a nonholonomic mobile robot in [Faulwasser and Findeisen, 2009], which also allows to take constraints on states and inputs into account. Combining nonlinear model prediction control and the core idea of path-following leads to additional degrees of freedom in the controller design. These can be utilized to guarantee stability and to achieve better performance. In contrast to other works on path-following [Encarnacao et al., 2000, Lapierre et al., 2003, Aguiar et al., 2005b], which apply back-stepping techniques to construct output-feedback controllers, the results in [Faulwasser and Findeisen, 2009] are based on state-feedback. In [Li et al., 2009b], the problem of path following for marine surface vessels with rudder and roll constraints is addressed with an MPC method based on a linearized model for computational and implementation considerations. In [Rizzi et al., 2002], a path-following system implemented with two different types of neural networks to learn the path described as a sequence of selected points, that enables an autonomous mobile robot to return along a previously learned path in a dynamic environment. In [Skjetne and Teel, 2004], a sliding-mode control law is proposed to ensure rapid convergence of all states in finite time to the subset of the state space, where the geometric path following and dynamic speed assignment tasks are solved for the nominal part of the closed-loop system.

2.1.4 Path tracking

It has been shown that path following is more suitable for many engineering applications due to the smoother convergence and less likely pushing actuator into saturation, as the illustrative example shows in section 1.3.2.2. However, keeping time performance from trajectory tracking is also important in situations where temporal deterministic requirement is critical. Hence, one further appealing objective is, to gain the benefits of path following when errors are large but preserving time requirement at the end. Path tracking is named under this desirable aim to achieve both the smooth spatial convergence and time convergence as well.

In [Hauser and Hindman, 1995, Hindman and Hauser, 1996], the pioneering idea of maneuver modified trajectory tracking is proposed by Hauser and Hindman to solve this kind of problem. It showed how to blend trajectory tracking and path following into a single control law, and a general approach has been developed for feedback linearizable nonlinear control system, where a projection mapping of current vehicle states onto the path enables the composite controller to go from a trajectory tracking to path following behavior. Based on this work, an alternative nonlinear control design approach for the nonlinear non-minimum phase aircraft model is proposed in [Al-Hiddabi and McClamroch, 2002]. Following the original method proposed by Hauser and Hindman, the combined trajectory tracking and path following through a weighted factor is designed for marine vehicles in [Encarnacao and Pascoal, 2001], by using backstepping technique to deal with vehicle dynamics. However, there is a limitation on the path when the projection mapping is executed, such that "no sharp corners" and "non-intersecting" paths are required. In [Diaz del Rio et al., 2002], a different tracking method is introduced where the time t is directly injected into the "error adaptive tracking" term in the path following behaviors, in order to preserve time determinism of trajectory tracking.

From an inverse way, the path tracking control proposed in this thesis, is devoted to solve the same problem by going from path following to trajectory tracking control, and the complexity of the composite control design will be reduced and the strict limitation on path shapes is relaxed. Actually, the original idea of introducing path tracking is trigged by the work of Lapierre [Lapierre and Soetanto, 2003], where two marine vehicles are requested to follow two identical paths in different depths. The leader vehicle has its own desired speed and the follower adjusts its speed to catch up the leader depending on the relative along-path distance. Assuming two vehicles are put on the same path (let the depth difference be zero), this problem formulation degenerates into the path tracking problem of one vehicle tracking one path, where the leader vehicle can be taken as a desired target (i.e., evolving path parameter in path tracking) traveling with speed profile $\dot{\tau}_d(t)$, and the follower tracks the virtual target evolving with speed profile $\dot{\tau}(t)$. In this way, the implicit advantage of path tracking is that, the path following control is performed firstly in order to reach and follow the path, and temporal deterministic requirement of trajectory tracking is also realized, by going from path following to target tracking behavior. Moreover, the projection mapping is not required as the path following behavior is already existing, so that the path limitation imposed by orthogonal projection mapping is relaxed. By adding a time dependent penalty term during the control design, the resulted controller is simplified in terms of control computation. These properties will be shown in detail in the section 4.4.2.

Another similar work which is also inspired by the idea of Hauser and Hindman, is the maneuvering problem addressed in [Skjetne, 2005, Skjetne et al., 2005], where the spatial convergence and temporal convergence task are separated, denoted as geometric task (reach and follow a desired path) and dynamic task (speed assignment of the vehicle) respectively. An output maneuvering controller is designed for a class of strict feedback nonlinear processes and applied to fully actuated ships. However, the maneuvering solution do not consider both the spatial and strict temporal convergence together. Although the dynamic task can be designated as a pure time assignment, the maneuver controller will be directly degenerated into a pure trajectory tracking controller according to the control design therein.

2.2 Stat-of-the-art of coordinated motion control

Multiple autonomous vehicles dealing with tasks could provide flexibility, robustness, effectiveness and efficiency beyond what is possible with a single vehicle. Nowadays, there has been considerable interest due to the increasing important roles of multiple vehicles for scientific, commercial, civil and military purposes. Coordination and cooperation of multiple autonomous vehicles result in a wide variety of applications, such as space-based interferometers, intelligent surveillance and reconnaissance (ISR), patrolling in hazardous environment, undersea oil pipeline inspection, and even hi-tech unmanned combat, as they can be operated at sea, on land, in the air, in space, and even the whole collaboration for land, air, sea, and space vehicles [Murray, 2007].

During the early stage research, coordinated control algorithms are widely studied for multi-agent system [Jadbabaie et al., 2003, Fax and Murray, 2004], where the agent has simple kinematics or dynamics. Variants of the algorithms are applied to consensus [Wei and Beard, 2005, Olfati-Saber et al., 2007], synchronization [Wu, 2001, Ren, 2008b], flocking [Olfati-Saber, 2006, Tanner et al., 2007], swarming [Gazi and Passino, 2003, Dimarogonas and Kyriakopoulos, 2008b], and formation control [Lawton et al., 2003, Porfiri et al., 2007]. There are numerous works using single-integrator to model the agent kinematics in [Jadbabaie et al., 2003, Olfati-Saber and Murray, 2004, Lin et al., 2004, Ren et al., 2008, Dimarogonas and Kyriakopoulos, 2008a], to name a few. Some works extends the single-integrator kinematics to double-integrator dynamics in [Tanner et al., 2007, Ren, 2008a, Zhang and Tian, 2010]. Even for physical mechanical systems, some research works try to simplify the system dynamics. In [Fiorelli et al., 2006, Leonard et al., 2007], the planar unit speed unicycle-type vehicle is used to represent underwater gliders, and in [Klein et al., 2008, Klein et al., 2010], Kuramoto oscillator model is used to align heading angles of multiple fin-actuated autonomous robotic fishes.

However, inherent kinematics and dynamics play a key role in the coordinated mechanical systems, and it is more appealing for coordinated autonomous vehicles with complex dynamics which must be taken into account. For example, a larger number of works deal with coordinated formation control of nonholonomic unicycles [Lin et al., 2005, Ghommam et al., 2008], formation flying of spacecrafts with rigid body attitude dynamics [Beard et al., 2001a, Ren et al., 2004], nonlinear formation of fully actuated surface vessels [Skjetne et al., 2002, Ihle et al., 2004] and underwater vehicles [Ghabcheloo et al., 2006a, Erfu and Dongbing, 2007]. In this thesis, the nonholonomic and underactuated vehicle systems are studied in coordinated formation control respectively. In the literature, there have been roughly four approaches applied to coordinated formation control of multiple vehicles : leader-follower, behavioral, virtual structure and artificial potentials. Each approach has its own advantages and disadvantages, as discussed in the following part.

2.2.1 Leader-follower approach

In the leader-follower approach, some vehicles are considered as leaders while the others in the team act as followers. Note that leader/follower has also been referred to as chief/deputy, master/slave in some literatures. The basic idea is that the leaders track predefined reference trajectories, and the followers track transformed versions of the states of the leaders according to predefined schemes (e.g., assigned formation configuration with the leader) [Wang, 1991]. In [Desai et al., 2001], the leader-follower based formation control is applied to multiple mobile vehicles where a feedback linearization method is used. Two different controllers are proposed for the followers depending on the information of relative angles/distances between the followers and the leader, defined as $l-\psi$(separation-bearing) and $l-l$ (separation-separation) control respectively. As shown in Figure 2.2, the aim of $l-\psi$ control is to maintain a desired length l_{ij}^d and a desired relative angle φ_{ij}^d between the two robots, while the aim of $l-l$ control is to keep the desired lengths l_{ij}^d and l_{ik}^d of the third robot (denoted as R_i) from its two leaders (R_j, R_k). In [Dierks and Jagannathan, 2007], A multi-layer neural network (NN) is introduced with robust integral of the sign of the error (RISE) feedback to approximate the dynamics of the followers as well as its leader using online weight tuning. It shows that the errors for the whole formation team are asymptotically stable and the NN weights are bounded. In order to remove the need for measurement or estimation of the absolute velocity of the leader, a second-order sliding mode formation controller only based on the relative motion states is used, which combines a first-order sliding mode controller to asymptotically stabilize the vehicles to a time-varying desired formation [Defoort et al., 2008].

Apparently, Leader-follower approach leads to a broadcast-only communication structure (single-source, unidirectional) from the leader to followers. This is desirable in marine robotics due to limited underwater communication and low bandwidth. Hence, plenty of the formation control applications in the marine control community, seem to have been performed within a leader-follower framework. In [Encarnacao and Pascoal, 2001], an AUV tracks the planar projection of a surface craft onto its nominal path, while the surface craft follows its own path at sea. In [Lapierre et al., 2003], this method is proposed for two AUVs following two shifted

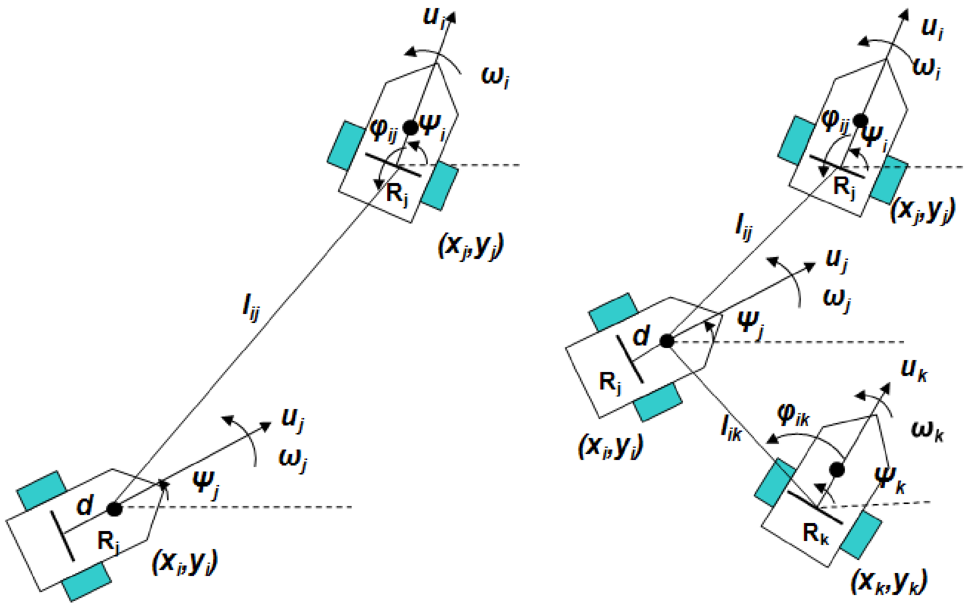

(a) Illustration of l-ψ control (b) Illustration of l-l control

Figure 2.2 – Leader-follower approach : l-ψ and l-l control

paths, the coordination is achieved by augmenting a speed adaptation algorithm to the controller of the follower vehicle. In [Kyrkjebø et al., 2007], surface vessels are synchronized through a leader-follower synchronization output feedback control scheme to implement a replenishment problem. In [Breivik et al., 2008], within a leader-follower framework, a so-called guided formation control scheme is developed for fully actuated ships by means of a modular design procedure inspired by concepts from integrator backstepping and cascade theory. In [Cui et al., 2010], leader-follower formation control of underactuated AUVs is proposed, where the follower tracks a reference trajectory based on the leader position and predetermined formation without the information of the leader's velocity and dynamics.

- Advantage :

An advantage of the leader-follower approach is that it is easy to understand and implement, since the coordinated team members only need maneuver according to the leader's motion, and the internal formation stability only depends on the control laws of individual vehicles. The leader's motion directs the whole group behavior so that a simple single-source and uni-direction way to broadcast the necessary information of the leader to other followers simplifies the communication network. In addition, the formation can still be maintained even if the leader is perturbed by some disturbances.

- Disadvantage :

However, a disadvantage is that there is no explicit feedback to the formation, that is, no explicit feedback from the followers to the leader in this case. It means that the formation cannot be maintained if the follower is perturbed. Consequently, the leader will not slow down to wait for the followers resulting the collapse of the formation, if some followers get saturated or disturbed and cannot keep up to the pace of the leader. Conversely, if the leader is in trouble, the followers will lost the guidance which means the failure of one vehicle (i.e. the leader) leads to the failures of the whole formation team.

2.2.2 Behavioral approach

In the behavioral approach, a number of desired behaviors such as formation keeping, trajectory and neighbor tacking, collision/obstacle avoidance and goal/target seeking, are prescribed for each vehicle and the formation control is calculated by using a weighting sum of the relative importance of each behavior output. The behavioral architecture combines the outputs of multiple controllers designed for achieving different and possibly competing behaviors.

In [Balch and Arkin, 1998], behavior based approach for a mobile robotic team is reported, where move-to-goal, avoid-static obstacle, avoid-robot and formation maintenance behaviors, are integrated through suitable weight coefficients in terms of relative priorities of behaviors. A motor scheme implementation enables a robot to move to a goal location while avoiding obstacles, collisions with other robots and keeping formation at the same time.

In [Anderson and Robbins, 1998], it provides a clear example of a behavioral approach for formation flight. They consider velocity-commanded aircraft with collision-avoidance, obstacle-avoidance, move-to-goal and maintain-formation behaviors. Each of the behaviors has an associated velocity vector and weighting, and the velocity of each aircraft is set to the weighted sum of its behavioral velocities.

In [Arrichiello et al., 2006], the null-space-based (NSB) behavioral control of a fleet of marine surface vessels is presented. A hierarchy of desired behaviors, or constraint functions, are defined and the control inputs are determined by sequentially projecting the behaviors onto the null space of the higher priority behavior. This approach allows for elegant inclusion of important behaviors such as collision avoidance, but the overall behavior of the system is hard to predict.

- Advantage :

The advantage of this approach is that it is natural to derive control strategies when vehicles have multiple competing objectives, and an explicit formation feedback is included through communication between neighbors by coupling the weights of the actions. Behavior-based approaches also give the system the autonomy to operate in an unknown or dynamically changing environment, by defining and integrating different behaviors dedicated to specified sub-tasks.

- Disadvantage :

The disadvantage is that the group behavior cannot be explicitly defined, and it is difficult to analyze the approach mathematically. Consequently, the convergence of the formation to a desired configuration cannot be guaranteed, and the group stability can not be provided in a rigorous way.

2.2.3 Virtual structure approach

In the virtual structure approach, the entire formation is treated as a single virtual structure acting as a single rigid body. When the virtual structure moves, it traces out desired trajectories for each vehicle in the team to track. In other words, each member in the formation team tracks a virtual target using individual vehicle controllers, while the trajectory of the virtual target is specified by a formation function that determines the desired geometry of the overall virtual structure. Some similar ideas are given based on the perceptive reference frame [Kang and Yeh, 2002], the virtual leader generating a virtual rigid body [Egerstedt and Xiaoming, 2001], and the formation reference point [Skjetne et al., 2002] respectively. The overall motions of the virtual structure include rotation, translation, contractions and expansions.

In [Lewis and Tan, 1997], a group of mobile robots achieve high precision formation control where each member in the formation is taken as a particles embedded in a rigid geometric structure and no leader selection is required. In [Do and Pan, 2007], a specific form of formation feedback is introduced in the virtual structure based control. Hence, the virtual structure will slow down and stop once the robots get out of the formation, and it moves towards its final goal if the robots are maintaining formation. In [Egerstedt and Xiaoming, 2001], a nonphysical, so-called virtual leader tracks its desired reference trajectory, and all nonholonomic robots in the formation team have to track their respective reference points which are constrained by a rigid body constraint function related to the moving virtual leader. In this way, formation constrained multi-robot control is achieved via a virtual structure. In [Ren et al., 2004], following a decentralized coordination architecture via the virtual structure approach, decentralized formation control scheme for spacecraft formation flying is presented, which are appropriate when a large number of spacecraft are involved and/or stringent inter-spacecraft communication limitations are exerted.

In case of formation control of marine vehicles, some research works also adopt the virtual structure method. In [Skjetne et al., 2002], the objective of flexible formation control for multiple maneuvering marine craft systems, is that each craft is to maintain its position in the formation while a virtual formation reference point (FRP) tracks a predefined path. A dynamic guidance system with feedback from the states of all crafts ensures that all crafts have the same priority (no leader) when moving along the path, which also yields a robust scheme with dynamic adjustment to the actuator saturation in the formation. In [Ihle et al., 2005], the control laws for formation control of marine craft is rooted in analytical mechanics for multi-body dynamics, facilitating a flexible and robust formation control scheme where the geometric constraints of a virtual structure are enforced by feedback control.

- Advantage :

The main advantage of the virtual structure approach is that it is fairly easy to prescribe the coordinated behavior for the whole formation group, and add a type of robustness to formation through the use of formation feedback. The formation can be maintained very well while manoeuvring, that means the virtual structure can evolve as a whole in a given direction with some given orientation and maintain a rigid geometric relationship among multiple vehicles.

- Disadvantage :

The disadvantage is that requiring the formation to act as a rigid virtual structure limits the class of potential applications. If the formation geometric pattern is time-varying or needs to be frequently reconfigured, this approach may not be the optimal choice, and obstacle avoidance is also a problem. The virtual structure approach is not suitable for controlling a large group of vehicles, because the constraint relationships among vehicles become more complicated as the numbers of the vehicles in the group increase.

2.2.4 Artificial potential approach

In the artificial potential approach, each member in the formation structures is influenced by its neighborhood through additional artificial potentials, which define interaction forces between neighboring vehicles. Each members can move freely and the group formation is maintained by the attractive forces to distant neighbors up to a maximum distance, and repulsive forces from neighbors too close. Therefore, the formation constrained by the artificial potentials is in a loose pattern but not a rigid geometric shape. Potential functions are widely used in designing a formation control system for multiple vehicles because stability of the controllers system can be mathematically analyzed.

In [Leonard and Fiorelli, 2001], artificial potentials generate interaction forces between neighboring vehicles, which are designed to enforce a desired inter-vehicle spacing. A virtual leader or virtual beacon is introduced to manipulate the group formation geometry and direct the motion of the whole group. In [Ogren et al., 2004], an application of cooperative AUVs which build a mobile underwater network of sensors is proposed. A formation controller based on the potential field method and Lyapunov's direct method, is used to climb the gradient of an environmental field, efficiently searching the densest source of a spatially distributed chemical signals. In [Ge and Fua, 2005], the formation structure is presented by queues and artificial potential trenches, of which the explicit representation of every single node is not required and the scalability of the formation is improved when the team size changes. This original scheme is extended to improve the performance of the scheme when only local communication is present, and resulted in a weakly connected network [Fua et al., 2007]. In [Olfati-Saber, 2006], artificial potentials is used to avoid obstacles and guarantee collision free between vehicles, to split and merge subgroups, and to perform squeezing maneuver for a large number of agents group. In [Cheah et al., 2009], a region-based controller for a swarm of fully actuated mobile robots is proposed by using potential energy functions. The global objective of the controller is to keep the positions of the robots inside a moving region as a group, and the local objective is to maintain a minimum distance from each other.

- Advantage :

The artificial potential approach is suitable to control a large group of vehicles in a loose formation pattern, and it has inborn ability to deal with obstacle avoidance and inter-vehicle collision. It is convenient to analyze the approach in a formal mathematical way. The framework also allows for a homogeneous group with no ordering of vehicles, which adds robustness of the group to a single vehicle failure.

- Disadvantage :

The local minimum is a well known problem in the applications of artificial potentials. One may need to examine the role of undesirable formations that are possible local minima for the designed potentials. It is difficult to build a desired rigid shape for the multi-vehicle system, if the vehicles are only controlled to maintain a minimum distance among themselves and stay close together as a group by means of artificial potential forces.

2.2.5 Summary of different approaches

In fact, all these four approaches to the coordinated formation control can be divided into two main categories : the analytic and the algorithmic [Breivik et al., 2008]. The analytic category represents those approaches that are most readily analyzed by mathematical tools, and include leader-follower, virtual structure and artificial potentials schemes. Conversely, the algorithmic category represents those approaches that are not easily analyzed in a rigorous mathematical way, but have to be numerically simulated by means of a computer in order to investigate their emergent behaviors. The behavior-based approach belong to this category. However, as discussed above, each approach for coordinated formation control of multiple vehicles has its own features. According to the different applications and situations, one can choose a suitable approach for the control design, or choose a mixed method combined with several approaches together as reported in [Beard et al., 2001a], where a coordination architecture for multiple spacecraft formation control, is introduced to incorporate the leader-follower, behavioral, and virtual structure approaches to the address the coordination problem. In [Ren, 2007], it also shows that many existing leader-follower, behavioral and virtual structure or virtual leader formation control approaches can be unified in the general framework of consensus building, for a multiple micro air vehicle formation flying.

A non-exhaustive list of other approaches to solve formation control problems includes : optimization based approach, cyclic approach, navigation based approach and so on. One way to address the formation control problem is to formulate it as an optimization problem. Receding horizon control, or model predictive control, is an effective control strategy in which the current control action is computed by solving a finite horizon optimal control problem online. In [Dunbar and Murray, 2006], a distributed implementation of receding horizon control is presented where each subsystem is assigned with its own optimal control problem, optimized only for its own control at each update, and exchanges most recent optimal control trajectory only with neighboring subsystems. The asymptotic stability of a multi-vehicle formation system is guaranteed by requiring that each distributed optimal control does not deviate too far from the previous optimal control. In [Fahimi, 2007], non-linear model predictive formation control (NMPC) is designed for controlling multiple autonomous underactuated surface vessels in arbitrary formations in environments containing obstacles. The real-time optimization abilities of the NMPC method has been used to improve the response of the unactuated DOF of the vessels and to directly incorporate the local obstacle avoidance into the formation control eliminating the need for an external local obstacle avoidance algorithm. This leads to more effective obstacle avoidance decisions based on the unactuated dynamics of the vehicle. In [De Gennaro and Jadbabaie, 2006], a navigation function formalism is proposed to obtain decentralized formation control in a given workspace for a group of mobile agents, where the navigation function is used to drive each agent of a group toward a desired final configuration which is expressed in terms of distances between the connected agents. The formation can be reached anywhere in the space and with any orientation, and the control law is designed as the gradient of a suitably-defined navigation function whose minimum corresponds to the desired configuration. In [Yang et al., 2005], the successive galerkin approximation (SGA) approach is applied to the nonlinear optimal and robust formation control of multiple AUVs. It shows that the formation-keeping performance is improved by solving the associated Hamilton-Jacobi-Isaacs (HJI) equation with the SGA algorithm.

Finally, the two dedicated workshop proceedings on coordination and cooperative control in [Kumar et al., 2005] and[Pettersen et al., 2006], and two special issues on networked control system in [Antsaklis and Baillieul, 2007] and [Bullo et al., 2009], report a broad number of formation control scenarios, and related issues such as the characterization of convergence speeds, the design of algorithms that tolerate delays, noisy measurements, and packet drops, and the study of the controllability of graph structures and the influence of the interconnection topology in the control design, etc.

2.2.6 Coordinated path following control

During recent years, the marine control community has focused considerably on concepts of formation control. Although there are many kinds of methods to achieve coordinated formation control of multiple vehicles, the problem of ***coordinated path following control (CPF)*** has only recently come to the front, and become one of the main topic in coordination and cooperation due to the practical application, such as simultaneous localization and mapping of multiple vehicles, cooperative lawn mowing with high efficient, fast acoustic coverage of wide seabed.

The initial idea for coordinated path following can be traced back to the ASIMOV project sponsored by European Commission that aims at the coordination of one Autonomous Surface Craft (ASC) and one autonomous underwater vehicle [Pascoal et al., 2000]. The foundational work in coordinated path following control of multiple surface and underwater vehicles is illustrated in [Encarnacao and Pascoal, 2001], where the AUV is forced to track the projection of the ASC onto the 2D nominal path. However, it requires a large amount of kinematics and dynamics information, be exchanged between the leader (ASC) and the follower (AUV), besides complex computation of trajectory tracking controllers as a complement of path following controller.

In [Lapierre and Soetanto, 2003], a leader-follower approach is also adopted for coordinated control of following two spatially shifted paths, and an important idea of almost decoupling the spatial assignment (predefined path) and dynamic assignment (desired speed) is proposed to relieve the problem of heavy information exchange. Both the leader and follower execute the same path following algorithm, and the leader travels along its assigned path at a desired speed profile, while the speed of the follower is adapted according to the "generalized along-path distance" $\Delta_S = s_L - s_F$ between two virtual target vehicles involved in the path following control design, as illustrated in Figure 2.3 of [Lapierre and Soetanto, 2003]. Obviously, only the along-path distance of the leader s_L is required to be sent to the follower, which presents a minimum load in the communication network and relieve the large amount information exchange under constrained underwater communication.

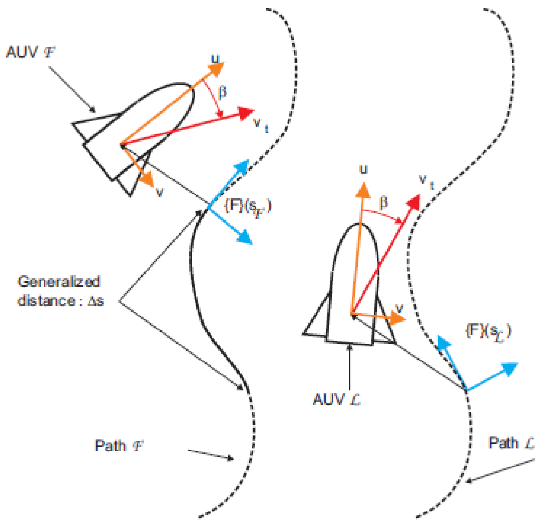

Figure 2.3 – Coordination of shifted paths following : leader-follower approach

However, two identical paths in three dimension space are assumed in [Lapierre and Soetanto, 2003], and the problem of coordinated path following with different path segments is receiving increased attentions from the practical field test view, such as desired paths including nested circumferences and parallel paths in the lawn-mowing maneuver for wide coverage of seabeds. This motivates the following question : How to choose of a good coordination variable for generalized CPF problem ? Actually, Axiom 1 in [Ren et al., 2005] shows that shared information is a necessary condition for group coordination. Underlying this axiom, there are two important questions :

- **Question 1 :** *What's kind of information should be shared ?*
- **Question 2 :** *Which one should information be shared with ?*

The first question indicates that the coordination variable is required for group coordination, and the second question indicates that communication topology between vehicles is required to define with whom does one share coordination variable in the group.

- Available solution for question 1 : choose a suitable coordination variable

For coordinated path following control, the coordination variable is instrumental in building the geometric formation. In the case of identical paths or straight line paths, the "along-path distance" is the suitable coordination variable to directly adjust the relative distance between vehicles and build the formation, as shown in Figure 2.3. However, in the case of nested or parallel paths, the along-path distance is not a good candidate of coordination variables anymore, how to choose a common variable for coordination or synchronization for parallel paths or general path is critical. Note that the coordination variable is also called synchronization variable where the term "synchronized path-following" is used instead of coordinated path-following in [Ihle, 2006, Ihle et al., 2007].

In [Ghabcheloo et al., 2007], the idea of re-parameterizing given paths via a new path variable with common property for coordination is proposed, to implement coordinated control of multiple wheeled vehicles following parallel straight lines and scaled circumferences paths. It means each given path $\Gamma_{di}(s_i)$ (i.e., parameterized by along-path distance s_i) is re-parameterized according to a conveniently defined variable ξ_i representing the "*normalized along-path distance*", such that the coordination is achieved along the paths if the agreement on the new path parameter $\xi_i = \xi_j, i \neq j$ is reached. The reparameterization of the path is denoted by $s_i = s_i(\xi)$ and define $R_i(\xi_i) = \partial s_i / \partial \xi_i$ in terms of the relative position of the i-th vehicle in the whole geometric formation. Henceforth, coordination error dynamics $\dot{\xi}_i$ can be built as $\dot{\xi}_i = \dot{s}_i / R_i(\xi_i)$ by using time-varying or constant scaling $R_i(\xi_i)$, and the coordinated control laws is derived based on it. Later, this idea is extended to coordinated control of multiple underwater vehicles in [Ghabcheloo et al., 2009], and achieve path following based cooperative control for multiple surface vessels in [Almeida et al., 2010].

However, applying path reparameterization to get normalized along-path distance, also leads to the extra coordination error dynamics. This solution makes an additional parameterization work and the resulted control design is not simple. In this thesis, there is another solution to this problem. By using the desired geometric relationship between virtual targets moving on different paths, the path is not required to be reparameterized and normalized along-path distance is represented in a simple way.

- Available solution for question 2 : build a communication topology

In practical application of coordinated multi-vehicle system, inter-vehicle communication network is a prerequisite to enable information sharing between vehicles and make the coordination be possible. Actually, the communication topology also indirectly defines the coordinated controller designed in a *centralized* or *decentralized* way. For example, leader-follower strategy gives a broadcasting-like communication topology so that centralized coordination strategy is the only choice.

Most of the early stage work seems to have been performed within a leader-follower framework and a centralized controller, e.g., in [Encarnacao and Pascoal, 2001, Lapierre and Soetanto, 2003], where an AUV tracks the planar projection of an ASC onto its nominal path, while the ASC follows its own path at sea ; In [Kyrkjebø et al., 2007] a leader-follower synchronization output feedback control scheme is presented for ship replenishment operation, in order to transfer fuel and supplies from one ship to the other while vessels are underway. In [Breivik et al., 2008], a so-called guided formation control scheme is developed for fully actuated ships within a leader-follower framework. However, in these early approaches to coordinated path-following, the communication constraints are not addressed explicitly and new techniques are required to make progress. The simple leader-follower strategy is effective for two vehicles, and in the multi-vehicle case (beyond three vehicles or much more of them), the inter-vehicle communication is a practical issue, which also enables the decentralized control laws to avoid the problem of single failure of the leader in the leader-follower approach. Algebraic graph theory[1] is an elegant methodology to represent the complex communication topology in a simple and formal mathematical way, where the concept of *graph Laplacian*, a matrix representation of the graph associated with a given communication topology, provides a classic method to rigorously analyze the formation stability of multi-vehicle system. In [Fax and Murray, 2002], it clearly shows how the graph Laplacian associated with a given inter-vehicle communication network plays a key role in assessing stability of the behavior of the vehicles in a formation. Later, there is an emerging trends to use graph theory for coordination and cooperation in literatures [Olfati-Saber and Murray, 2004, Lin et al., 2005, Moreau, 2005, Wei and Beard, 2005, Dimarogonas and Kyriakopoulos, 2006], to name but a few. In the case of coordinated path following control, graph theory is also widely used in the decentralized control design [Ghabcheloo et al., 2007, Ihle et al., 2007, Ghommam and Mnif, 2009].

- Cascade system theory and coordinated straight lines following

Most of the control design on coordinated path following, is based on Lyanpunov design and backstepping technique [Skjetne et al., 2002, Lapierre and Soetanto, 2003, Ghabcheloo et al., 2006a, Aguiar and Pascoal, 2007a, Do and Pan, 2007, Ghommam and Mnif, 2009]. However, there are a larger amount of attentions to deal with formation path following of straight lines, by means of building the interconnected structure of cross-track error dynamics and synchronization error dynamics, and using nonlinear cascaded systems theory to analyze the stability properties of the overall interconnected system [Børhaug et al., 2010].

[1]The preliminaries of algebraic graph theory and related Laplacian matrix will be introduced in section 6.1.3.1.

Actually, these research work on coordinated path following control, are inspired by the previous work of Pettersen where persistently excitation (PE) condition is required for trajectory tracking of nonholonomic and underactuated vehicles and straightline is excluded to be tracked [Pettersen and Nijmeijer, 2001]. In case of path following, the restrictive PE condition is relaxed under some mild assumptions and following straightline is possible. In [Pavlov et al., 2007], formation path following controller for 2D motion of 3DOF underactuated surface vessels is considered, consisting of a Line-of-Sight guidance law and a coordination control law, which makes each vessel asymptotically follow a given straight line path corresponding to a desired formation with a given forward speed profile. This work is extended to deal with constant ocean current in [Børhaug et al., 2008], where a modified Line-of-Sight guidance law with integral action and a pair of adaptive tracking controller is proposed to counteract environmental disturbances, and globally asymptotically achieve straight line formation path following. Furthermore, under the same control strategy, in order to deal with the presence of unknown ocean current, an adaptive yaw controller steers each vessel converging to its desired straight line path while rejecting ocean currents with unknown direction and magnitude, and a surge controller guarantees formation assembly with a desired forward speed [Burger et al., 2009]. The work [Pavlov et al., 2007] has also been extended to 3D motion of 5DOF underactuated underwater vehicles in [Børhaug et al., 2007], and the problem of straight line path following for formations of underactuated AUVs is solved under the topological constraints of the communication network. These research works are valid for a fleet of marine vehicles following straight-line paths and forming a desired formation. For ideas on how to extend the proposed control strategy to more general (curved) paths, there are some clues indicated in [BØrhaug, 2008].

2.3 Summary

In this thesis, the main concerns focus on two types of control design for nonholonomic autonomous vehicles, i.e., path following and path tracking control. Moreover, the derived controller steps from single vehicle system into multi-vehicle system under coordination, following a design principle from the simple case to complicated case. Note that the localization problem of vehicles is not considered herein when dealing with the motion control of single or multiple vehicles, by assuming that the positioning of the vehicles is perfect. The interested reader can refer to some established methods, for instance, Extended Kalman Filter localization [Jetto et al., 1999, Roumeliotis and Bekey, 2000], Monte Carlo localization [Fox et al., 1999, Thrun et al., 2001], and interval analysis based localization [Jaulin et al., 2000, Jaulin, 2009a].

After reviewing major important research work in the fields of motion control design, some classic and effective methods are adopted and combined with some new elements proposed in this thesis. In the case of single vehicle path following, the idea of introducing virtual target and the approaching angle guidance proposed in [Lapierre et al., 2003, Soetanto et al., 2003] is used to briefly introduce the path following control design for the unicycle-type vehicle, while the adapted LOS guidance design is used for marine vehicle and the computation of side-slip angle is analyzed in detail. Compared with MMTT, new strategy from path following to trajectory tracking is proposed to obtain path tracking control design.

Two solutions for coordinated formation control problems are introduced. One is based on coordinated path following control, and the other is based on coordinated path tracking control. Two strategies for each solution is proposed : the centralized strategy based on leader-follower and virtual structure respectively, and the decentralized control by using algebraic graph theory. Both of the individual and coordinated control are based on nonlinear Lyapunov's direct method design and backstepping technique.

CHAPTER 3

PROBLEM POSE

Due to the wide engineering applications in the last decades, there has been an increasing interest in the control of underactuated autonomous vehicles, which are most commonly subject to nonholonomic constraints [Oriolo and Nakamura, 1991]. These so-called nonholonomic constraints arise in mechanical systems where some constraints are imposed on the motion. This class of underactuated and nonholonomic systems are abundant in real life, which have been involved in all kinds of intelligent mechanical systems, including manipulators, mobile robots, surface vessels, underwater vehicles, helicopters, spacecrafts, etc. [Fantoni and Lozano, 2002].

This chapter sets the background for the main subject of the thesis : nonlinear motion control of nonholonomic and underactuated autonomous vehicles. Selected models of two types of autonomous vehicle systems are introduced, i.e., nonholonomic unicycle-type mobile vehicle and underactuated autonomous underwater vehicle, to illustrate the applications of motion control. The idea of control design extended from nonholonomic wheeled vehicle to underactuated underwater vehicles, is presented based on the similarity between these two vehicles in the kinematics stage, and the difference in the dynamics stage is shown as well. Basic notations for fundamental motion references are introduced. By choosing different reference frames, two types of error dynamics for motion control are derived, which are used for the motion control design in the following chapters.

3.1 Underactuated and nonholonomic autonomous vehicles

In this section, the definitions of underactuated system and nonholonomic constraints are firstly introduced, and the representative model of the underacutated underwater vehicles is recalled which suffers from the second-order nonholonomic constraints. Later, from the motion control point of view, the first-order nonholonomic autonomous vehicle, i.e., differential driven wheeled vehicle is presented. The similarity and difference between these two types of vehicles are described, which motivate the control design from simple underactuated wheeled mobile vehicle to complex underactuated underwater vehicles in the following chapters.

3.1.1 Definitions

This section introduces the definitions of underactuated systems and nonholonomic constraints, according to the formal mathematical representations.

3.1.1.1 Underactuated systems

Consider systems that can be written as

$$\ddot{q} = f(q, \dot{q}) + G(q)u$$

where q is the state vector of independent generalized coordinates, $f(.)$ is the vector field representing the dynamics of the systems, $\dot{q}$ is the generalized velocity vector, G is the input matrix, and u is a vector of generalized force inputs. The dimension of q is defined as the number of degrees of freedom. System is said to be underactuated if the external generalized forces are not able to command instanteneous accelerations in all directions in the configuration space (which is the space of possible positions that a physical system may attain), i.e. $rank(G) < dim(q)$ [Goldstein, 1980], rather that $dim(G(q)u) < dim(q)$.

The definition figures out that the *underactuated systems* are with fewer independent control actuators than degrees of freedom to be controlled. Whereas, a fully actuated system can independently control the motion of all its degrees of freedom simultaneously.

3.1.1.2 Nonholonomic constraints

Consider a system of generalized coordinates q, with the dynamics

$$\ddot{q} = f(q, \dot{q}, u)$$

where u is the vector of external generalized inputs, $f(\cdot)$ is the vector representing the dynamics. If the conditions of constraints limiting the motion of the system, can be expressed as the time-derivative of some functions of the generalized coordinates with the form

$$\Phi(q,t) = 0$$

then the constraints are said to be *holonomic* [Goldstein, 1980]. This type of constraint is so-called integrated, since the holonomic constraint can be solved by integration.

However, systems in classic mechanics with nonholonomic constraints, which are defined as linear constraints w.r.t. generalized coordinates q, having the form

$$\Phi(q,t)\dot{q}(t) = 0$$

That means the equations of motion constraints are irreducible, and can not be expressed as time derivative of some function of the state. Therefore, the constraints are non-integrable, which are called as *nonholonomic constraints* [Goldstein, 1980]. Within nonholonomic systems, the generalized coordinates are not independent of each other. The nonholonomic constraints can be classified into two principal categories, the first-order nonholonomic constraints and the second-order nonholonomic constraints.

The *first-order nonholonomic constraints* are defined as constraints on the generalized coordinates and velocities of the form $h(q,\dot{q}) = 0$ that are non-integrable, i.e. can not be written as $\Phi(q,t) = 0$. These constraints include nonholonomic constraints arising in classical mechanics and nonholonomic constraints arising from kinematics [Oriolo and Nakamura, 1991].

The *second-order nonholonomic constraints* are defined as constraints on the generalized coordinates, velocities and accelerations of the form $h(q,\dot{q},\ddot{q}) = 0$, which are non-integrable, i.e. can not be written as the time derivative of some function of the generalized coordinates and velocities, i.e. $\Phi(q,\dot{q}) = 0$. These nonholonomic constraints can not be solved by integration, as they are an essential part of the dynamics. The second-order nonholonomic constraints most commonly occurs in surface vessels, underwater vehicles, spacecraft and space robots.

- Example : holonomic system

Consider the following system given in [Lefeber, 2000]

$$\begin{cases} \dot{x} = uy \\ \dot{y} = -ux \end{cases} \tag{3.1}$$

where two state variables $(x,y)^T \in \Re^2$ denote absolute Cartesian position in the plane and u is the control input. This system contains a constraint on the velocities as follows

$$x\dot{x} + y\dot{y} = 0 \tag{3.2}$$

The equation (3.2) implies a holonomic constraint, since it can be integrated to yield

$$x^2 + y^2 = c \tag{3.3}$$

where c is a positive constant. It means the system (3.1) can be reduced to (3.3). Therefore, the system (3.1) is called a holonomic system, and the state trajectory is restricted by a circle. This example illustrates the concept of holonomic systems and integrable property. Examples of nonholonomic constraints and non-integrable properties will be given in (3.12) and (3.16) respectively.

3.1.2 Motivation for underactuated system applications

As underactuated mechanical systems are abundant in real life, the study of control methodologies are needed for underactuated systems that can be applied in practice. The motivation for underactuated system applications, includes the following advantages as follows :

- Wide engineering applications :
  There is a large number of underactuated marine vehicles operated in the open sea, and it is worth to attract much attention for control engineering practice.
- Cost-effectiveness considerations :
  Compared with fully-actuated vehicles, underactuated vehicles normally exhibit cost-effectiveness in the case of long range survey missions.
- Actuator efficiency :
  A fully actuated vehicle becomes underactuated while traveling at high speed, due to the dramatically decrease of the lateral thruster efficiency.
- Weight reduction :
  Heavy weight has a side effect for autonomous flight vehicles, and heavy weight also leads to extra efforts to balance the underwater vehicles to a neutral buoyant status in most of the cases.
- System reliability :
  Actuator failures render vehicles into underactuated configuration, whereas the underactuated control backup guarantees the safety as much as possible.

However, underactuated configuration brings more control challenges as having less control inputs than degree of freedom, and leads to increased control complexity.

Most underactuated systems can not be fully feedback linearized, and exhibit nonholonomic constraints. If classic motion control design for fully or over-actuated vehicle system, are directly applied to the underactuated ones, the resulting performance of the control system is poor or even the control objective cannot be achieved. This requires to study advanced control techniques for underactuated systems, in order to accommodate the reduced degrees of freedom available for controller and resulted nonholonomic constraints.

3.1.3 Model of underactuated underwater vehicle

Underactuated systems have a number of very important practical applications in the field of autonomous marine vehicles control. In this section, the mathematical models of underactuated autonomous marine vehicle are described, which will be used for the design of various control systems in the subsequent chapters .

Many marine vehicles, including ocean ships, autonomous underwater vehicles and surface crafts, are equipped with two actuators for surge and yaw motion controls only, but without any actuators for sway motion. In Figure 3.1(a), there is the underactuated AUV "Infante" propelled by two electric back thrusters, from Instituto Superior Técnico(IST), Portugal. The "Delfim" from IST is one of this kind of surface craft equipped with two propellers shown in Figure 3.1(b).

(a) Underactuated underwater vehicle : Infante in IST, Portugal

(b) Underactuated surface vehicle : Delfim in IST, Portugal

Figure 3.1 – Underactuated marine vehicles

SNAME Notation for marine vehicles :

Throughout this thesis, we use the standard notations in Table 3.1, which are defined by the Society of Naval Architects and Marine Engineers (SNAME) [SNAME and Engineers, 1950].

For a marine vehicle moving in six degree of freedom (DOF) defined as surge, sway, heave, roll, pitch and yaw, six independent coordinates are necessary to determine its position and orientation in two reference frames, the inertial coordinate frame $\{I\}$ and the body fixed coordinate frame $\{B\}$, as shown in Figure 3.2. Difference from aerial vehicles, the motion of the Earth rarely affects ocean vehicles, the earth-fixed frame can be considered to be inertial. The body-fixed frame $\{B\}$ is a moving coordinate which is fixed to the vehicle. In general, the body axe x_b is the longitudinal axis directed from aft to fore ; y_b is the transverse axis directed to starboard ; and z_b axe is the normal axis directed from top to bottom. Based on the definitions in Table 3.1, the following vectors can be used to describe the general motion of a marine vehicle :

$\eta_1 = [x, y, z]^T$: position of the origin of $\{B\}$ with respect to $\{I\}$, expressed in $\{I\}$.
$\eta_2 = [\phi, \theta, \psi]^T$: orientation of $\{B\}$ with respect to $\{I\}$, expressed in $\{I\}$.
$\nu_1 = [u, v, \omega]^T$: linear velocity of the origin of $\{B\}$ relative to $\{I\}$, expressed in $\{B\}$ (i.e., body-fixed linear velocity).
$\nu_2 = [p, q, r]^T$: angular velocity of $\{B\}$ relative to $\{I\}$, expressed in $\{B\}$ (i.e., body-fixed angular velocity).
$\tau_1 = [X, Y, Z]^T$: external force acting on the vehicle decomposed in $\{B\}$.
$\tau_2 = [K, M, N]^T$: external moment acting on the vehicle decomposed in $\{B\}$.

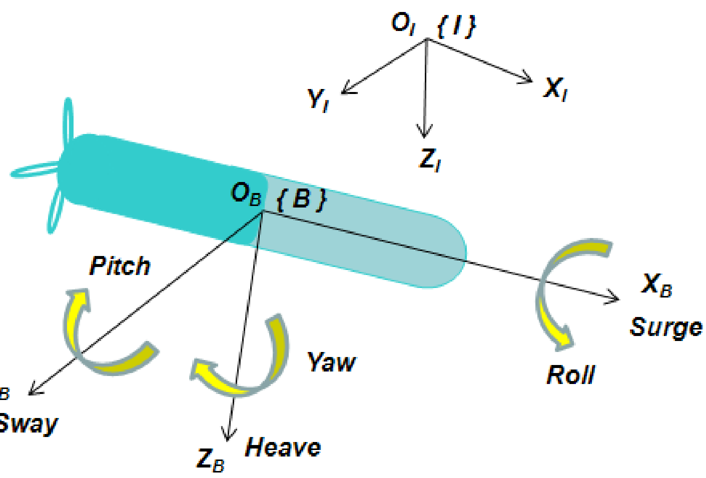

Figure 3.2 – Underwater vehicle in inertial frame

The standard 6-DOF kinematic and dynamics model of underwater vehicles is introduced in Appendix B. In the following section, the simplified horizontal motion model of underactuated AUVs is introduced, which will be used for the motion control design in this thesis.

3.1.3.1 Simplified underactuated horizontal motion model

The horizontal motion of an autonomous surface craft or an autonomous underwater vehicle moving in a horizontal plane is often described by the motion components in surge, sway, and yaw, while neglecting the motions in roll, pitch, heave, i.e., $(z, \phi, \theta)^T = 0_{3\times1}$. Hence, we choose motion variables vectors $\eta = (x, y, \psi)^T$ and $\nu = [u, v, r]^T$.

Table 3.1 – SNAME Notation for marine vehicles

Degree of freedom	Motion Components	Force and Moment	Linear and Angular Velocity	Position and Euler Angles
1^{st}	Surge	X	u	x
2^{nd}	Sway	Y	v	y
3^{rd}	Heave	Z	ω	z
4^{th}	Roll	K	p	ϕ
5^{th}	Pitch	M	q	θ
6^{th}	Yaw	N	r	ψ

Consider the planar motion of an autonomous underwater vehicle shown in Figure (3.3). The vehicle is equipped with two independent back thrusters, mounted symmetrically with respect to its longitudinal axis. Recruiting two different kinds of working mode of the thrusters, i.e. common and differential outputs, a force τ_u along the vehicle's longitudinal axis and a torque τ_r on its vertical axis are generated, respectively. As there is no lateral thruster and only two actuators for motion in three degrees of freedom, the vehicle is indeed underactuated. The two actuators are two propellers in this thesis. Practically, it can be a propeller and a rudder, or a jet propulsion system for underactuated ASVs that is either steerable or equipped with a rudder.

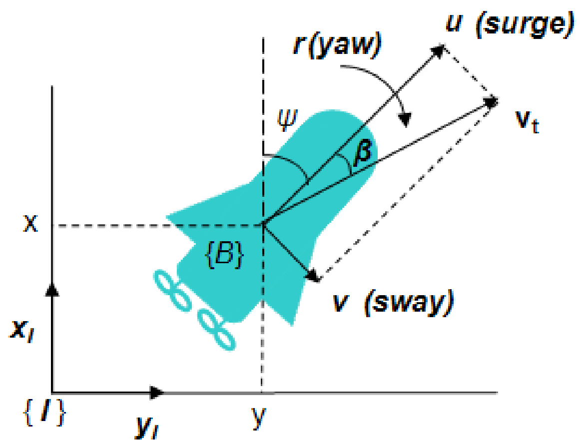

Figure 3.3 – 3-DOF underwater vehicle in horizontal plane

In the absence of ocean currents, the 3-DOF kinematic equations of the vehicle in the horizontal plane can be written as

$$\dot{\eta} = J(\eta)\nu \tag{3.4}$$

where the rotation matrix from the general 6-DOF expression (B.9) to one principal rotation about the z axis, i.e., $J(\eta) = R_{z,\psi}$.

For simplicity, it is assumed that the vehicle has homogeneous mass distribution and xz-plane symmetry, the vehicle is neutrally buoyant and the center of buoyancy (CB) coincides with the center of gravity (CG) located vertically on the z axis, such that $g(\eta) = 0_{3\times1}$. Neglecting the dynamics associated with the motion in heave, roll and pitch, i.e. $(\omega, p, q)^T = 0_{3\times1}$, and ignoring all elements of the nonlinear damping, the 3-DOF dynamic equations of the vehicle in the horizontal plane is simplified as

$$M\dot{\nu} = -C(\nu)\nu - D\nu + \tau \tag{3.5}$$

The matrices $J(\eta), M, C(\nu)$ and D are given by

$$J(\eta) = \begin{bmatrix} \cos\psi & -\sin\psi & 0 \\ \sin\psi & \cos\psi & 0 \\ 0 & 0 & 1 \end{bmatrix}, \qquad M = \begin{bmatrix} m_{11} & 0 & 0 \\ 0 & m_{22} & m_{23} \\ 0 & m_{23} & m_{33} \end{bmatrix},$$
$$D = \begin{bmatrix} d_{11} & 0 & 0 \\ 0 & d_{22} & d_{23} \\ 0 & d_{32} & d_{33} \end{bmatrix}, \qquad C(\nu) = \begin{bmatrix} 0 & 0 & -m_{22}v - m_{23}r \\ 0 & 0 & m_{11}u \\ m_{22}v + m_{23}r & -m_{11}u & 0 \end{bmatrix} \tag{3.6}$$

with

$$\begin{aligned} &m_{11} = m - X_{\dot{u}}, m_{22} = m - Y_{\dot{v}}, m_{23} = mx_g - Y_{\dot{r}}, m_{33} = I_z - N_{\dot{r}}, \\ &d_{11} = -X_u, d_{22} = -Y_v, d_{23} = -Y_r, d_{32} = -N_v, d_{33} = -N_r \end{aligned} \tag{3.7}$$

In (3.7), m is the mass of the vehicle, ; I_z is the vehicle's inertial about the z-axis of the body frame ; x_g is the along x-axis coordinate of the vehicle center of gravity ; $X(..), Y(..), N(..)$ express hydrodynamic derivatives of the system ; and other symbols denote the hydrodynamic derivatives [Fossen, 2002].

Since there is no independent actuator in the sway for the underactuated underwater vehicle under consideration, the propulsion force and moment vector can be expressed as $\tau = [\tau_u, 0, \tau_r]^T$.

3.1.3.2 Second-order nonholonomic constraints

Applying the following nonsingular kinematic transformations, there is

$$\begin{cases} v = J^{-1}(\eta)\dot{\eta} \\ \dot{v} = J^{-1}(\eta)(\ddot{\eta} - \dot{J}(\eta)J^{-1}(\eta)\dot{\eta}) \end{cases} \tag{3.8}$$

since $J(\eta)$ is a rotation matrix, it is invertible.

Now substituting (3.8) into the simplified 3-DOF dynamic equations in the horizontal plane (3.5), results in the mathematical dynamics model represented in the inertial frame :

$$M^{'}(\eta)\ddot{\eta} + C^{'}(v,\eta)\dot{\eta} + D^{'}(v,\eta)\dot{\eta} = \tau \tag{3.9}$$

where

$$\begin{cases} M^{'}(\eta) = MJ^{-1}(\eta),\ D(\eta) = D(v)J^{-1}(\eta),\ \eta = [x, y, \psi]^T \\ C^{'}(v,\eta) = [C(v) - MJ^{-1}(\eta)\dot{J}(\eta)]J^{-1}(\eta),\ \tau = [\tau_u, 0, \tau_r]^T \end{cases} \tag{3.10}$$

In this system, there are only two propellers to generate the force and the torque. Indeed, in the vector τ, there is only two physical terms on the first and third line, and one absent term on the third line. Therefore, this system is underactuated since it has three degree of freedom with only two control inputs ($dim(\tau) < dim(\eta)$).

From the second line of the dynamic equation in (3.9), we have

$$m_{22}(\ddot{x}\sin\psi - \ddot{y}\cos\psi) + (m_{22} - m_{11})\dot{\psi}(\dot{x}\cos\psi + \dot{y}\sin\psi) + d_{22}(\dot{x}\sin\psi - \dot{y}\cos\psi) - m_{23}\ddot{\psi} - d_{23}\dot{\psi} = 0 \tag{3.11}$$

or written in a compact form as

$$m_{22}\dot{v} + m_{23}\dot{r} + m_{11}ur + d_{22}v + d_{23}r = 0 \tag{3.12}$$

which is the nonholonomic second-order constraints, involving second-order time derivative of the configuration variables due to the underactuation in sway direction, that holds regardless of the control inputs τ_u and τ_r. In this sense, the second-order nonholonomic constraint is also named as acceleration constraints.

3.2 Motion control analysis of underactuated system

Underactuated system do arise in plenty of robotic vehicle control in both land and marine robotics when the number of actuators of an autonomous vehicle is less than its degree of freedom. For instance, a unicycle-type wheeled robot with two rear steering wheels, or an autonomous underwater vehicle without side thrusters. In this section, the problem of motion control of underactuated system is analyzed from the point of view of nonholonomic constraints. As a benchmark case, motion control of the first-order nonholonomic and underactuated unicycle-type wheeled robots is firstly discussed, and then the anlysis is extended to second-order nonholonomic underactuated AUVs, based on the similarity of control inputs and kinematics between them, as shown in Figure 3.5. The difference embedded in dynamics motivates the further treatment in the control design.

3.2.1 Benchmark case : nonholonomic unicycle-type mobile robot

In this section, the model of differential driven unicycle-type mobile robot is introduced, which is perhaps the most frequently investigated nonholonomic model in the literatures concerning motion control.

Consider a unicycle-type differential driven autonomous vehicle in Figure 3.4(a). There are following assumptions for this model as described in [Aguiar, 2001]. The vehicle has two identical parallel, non-deformable rear wheels and a passive steering front wheel. It is assumed that the plane of each wheel is perpendicular to the ground and the contact between the wheels and the ground is pure rolling and non-slipping, such that the velocity of the center of mass of the vehicle is orthogonal to the rear wheel axis. The masses and inertias of the wheels are negligible and the center of mass of the vehicle is located in the middle of the axis between the rear wheels .

Each real wheel is equipped one driver motor, such that it can turn independently forward or backward. Differential driven working mode enable different speeds at each rear wheel to cause the turn of the vehicle. A popular durable, differential-drive mobile robot platform for research named as Pioneeer P3-DX is shown is Figure 3.4(b).

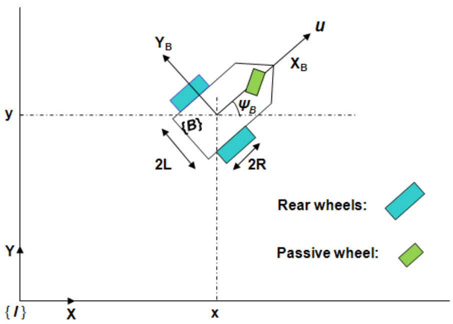

(a) Unicycle-type mobile robot

(b) Pioneer P3-Dx robot

Figure 3.4 – Differential driven unicycle-type mobile robot

3.2.1.1 Kinematics and dynamics model

Let $\{I\}$ be the (universal) inertial frame, and $\{B\}$ be the body frame with the origin coinciding with the center of the rear wheels axis. The robot is with coordinates $\mathbf{p} = (x, y, \psi_B)^T$ in $\{I\}$, and with velocity vector $\mathbf{q} = (u, r)^T$. Let $(x, y)^T$ express the position of the wheel axis center and ψ_B express the vehicle orientation with respect to the x-axis. Let u and r denote the linear (forward) and angular (rotational) velocity of the vehicle of $\{B\}$ with respect to $\{I\}$ respectively.

Kinematics model :

The kinematics of a unicycle-type autonomous vehicle is defined by the Jacobian matrix J

$$\dot{p} = \begin{pmatrix} \dot{x} \\ \dot{y} \\ \dot{\psi}_B \end{pmatrix} = Jq = \begin{pmatrix} \cos\psi_B & 0 \\ \sin\psi_B & 0 \\ 0 & 1 \end{pmatrix} \begin{pmatrix} u \\ r \end{pmatrix} \tag{3.13}$$

Furthermore, let ω_r and ω_l denote the angular velocity of the right-side and left side rear wheels generated by two independent motors respectively, and R denotes the radius of rear wheels, and L is the half length of the axis between them. Then the linear relationship between the control input (ω_r, ω_l) and (u, r) is

$$\begin{pmatrix} u \\ r \end{pmatrix} = \frac{R}{2} \begin{pmatrix} 1 & 1 \\ 1/L & -1/L \end{pmatrix} \begin{pmatrix} \omega_r \\ \omega_l \end{pmatrix} \tag{3.14}$$

Due to the differential driven property, it is easy to see that when $\omega_r = \omega_l > 0$, the vehicle moves straightly forward. Further, the vehicle rotates on the spot without any translation when the inputs with $\omega_r = -\omega_l \neq 0$ is applied.

Notice that the transformation between $(u, r)^T$ and $(\omega_r, \omega_l)^T$ is nonsingular, as the determinant of the transformation matrix is $-R/L \neq 0$. Consequently, the control transformations are globally well defined by substituting (3.14) to (3.13), the properties of controllability and stability of the system (3.13) hold for the physical model of a unicycle-type robot.

Dynamics model :

The wheels control provides the forward force F and angular torque N applied on the vehicle's center of mass. Let m and I denote the robot mass and the moment of inertia, respectively. Resorting to the Euler-Lagrangian equation of motion, the reduced-order dynamic model of the unicycle-type autonomous vehicle is obtained by augmenting (3.13) with the equations

$$\tau = \begin{pmatrix} F \\ N \end{pmatrix} = M\dot{q} = \begin{pmatrix} m & 0 \\ 0 & I \end{pmatrix} \begin{pmatrix} \dot{u} \\ \dot{r} \end{pmatrix} \tag{3.15}$$

3.2.1.2 First-order nonholonomic constraints

The differential driven unicycle mobile robot with kinematics model (3.13) is referred to as an *underactuated system*, since there are only two control inputs in the surge (moving forward) and yaw (rotating) directions, for three state variables and three motion degree of freedom as well. This representation of model (3.13) is also well known as Brockett's nonholonomic integrator and can be found quite frequently in the literature dealing with nonholonomic systems.

Actually, the nonholonomic constraints occurs on the velocity of the unicycle model, such that the linear velocity of the unicycle is always aligned with the longitudinal axis :

$$\dot{y}\cos\psi_B - \dot{x}\sin\psi_B = 0 \tag{3.16}$$

Contrary to the holonomic constraint (3.2), the constraint (3.16) can not be integrated which means this constraint can not be written as time derivative of some function of the generalized coordinates. Therefore, this non-integrable constraints on the generalized coordinates and velocities belong to the *first-order nonholonomic constraint*. It is also called the lateral zero-speed constraint in the case of unicycle-type differential driven autonomous vehicles, as the vehicle cannot directly move sideways perpendicularly to the direction of the rear wheels and should maneuver to approach position in the sway direction.

Control design analysis :

The laws of mechanics show that the trajectory of a moving vehicle is fully related to the amplitude and the orientation of its total speed. These variables must be driven to a desired value to control the trajectory. Due to the first-order nonholonomic constraints occurring on the speed, the total speed of a unicycle-type robot is permanently equal to its forward speed. In the case of path-following control problem, it can be solved for the unicycle-type robot by designing a kinematics controller that steers the vehicle onto the path and then guarantees that the orientation of the forward speed stays tangent to the path [Soetanto et al., 2003, Lapierre et al., 2003].

In the overall control loop, the kinematic controller actually acts as a reference, giving the desired signals for the control subsystem based on the dynamics level. Using backstepping techniques [M. Krstic and Kokotovic, 1995], the control law in kinematic level can be extended to deal with vehicle dynamics. Interestingly, the linear relationship between the actual control inputs (force and torque) in the dynamics stage and the virtual control inputs in the kinematics stage in (3.15), renders the implementation easier. Furthermore, the uncertainty of model parameters can also be addressed by Lyapunov based adaptive design as shown in [Lapierre et al., 2006].

3.2.2 Extended case : underactuated underwater vehicle

For the motion control of autonomous vehicles, the control strategy depends on the type of actuation. From the actuation point of view, there exists a visible similarity between the underactuated underwater vehicles and the classic unicycle-type wheeled robot, as the control inputs in the kinematics stage are the same : the forward and yaw speeds. This reveals the connection between unicycle-type vehicle and AUV control strategies [Lapierre and Jouvencel, 2008].

3.2.2.1 Similarity in the kinematic stage

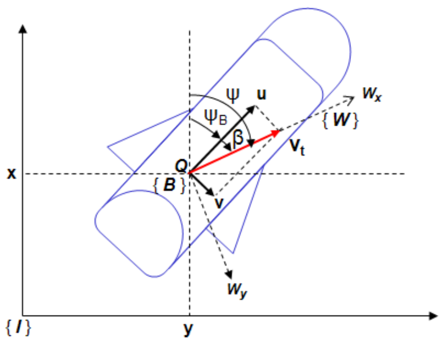

(a) autonomous underwater vehicle

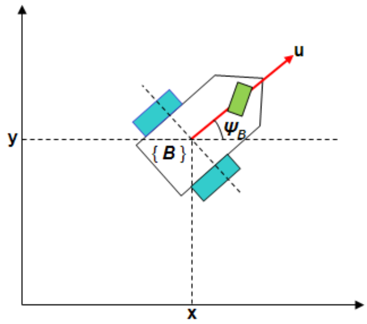

(b) unicycle-type mobile robot

Figure 3.5 – Similarity between underactuated AUV and unicycle-type mobile robot

In Figure 3.5, compared with a unicycle-type mobile robot, an autonomous underwater vehicle moving in horizontal plane is illustrated in Cartesian coordinates. In order to describe the motion of the AUV, three different reference frames are illustrated here.

1) Inertial frame $\{I\}$, which is also called as fixed reference frame or global coordinate frame in Cartesian space.

2) Body fixed frame $\{B\}$, with origin at the center mass of the vehicle and the x-axis in the surge direction.

3) Flow frame $\{W\}$, which is obtained from $\{B\}$ by rotating it around the Z_B axis through sideslip angle β in the positive direction.

The vehicle is with generalized coordinates $\mathbf{p} = (x, y, \psi)^T$ in inertial frame I. Let u and v are the longitudinal (surge) and transverse (sway) velocities, respectively. Let r is the angular speed (yaw rate). The kinematic equations of the AUV can be written as

$$\begin{cases} \dot{x} = ucos\psi_B - vsin\psi_B \\ \dot{y} = usin\psi_B + vcos\psi_B \\ \dot{\psi}_B = r \end{cases} \tag{3.17}$$

Assuming u is never equal to zero. Then, the sideslip angle β can be defined as $\arctan(v/u)$. Considering the flow frame $\{W\}$ which is obtained by rotating body frame $\{B\}$ around the z_B axis through the sideslip angle β, the kinematic equations can then be re-written to yield

$$\begin{cases} \dot{x} = v_t \cos\psi \\ \dot{y} = v_t \sin\psi \\ \dot{\psi} = r + \dot{\beta} \end{cases} \tag{3.18}$$

Where $\psi = \psi_B + \beta$ is the global heading of v_t with respect to $\{I\}$, and v_t is the total speed expressed in $\{W\}$. Clearly,

$$v_t = \sqrt{u^2 + v^2} \tag{3.19}$$

Notice that the control of an AUV system implies considering a ***permanent positive forward speed*** $u > 0$ ($v_t > 0$ as well), for an effective control action of the rudder/fin control surfaces.

The kinematics of underactuated vehicle is defined by a Jacobian matrix J

$$\begin{pmatrix} \dot{x} \\ \dot{y} \\ \dot{\psi} \end{pmatrix} = \dot{p} = Jq = \begin{pmatrix} \cos\psi & 0 \\ \sin\psi & 0 \\ 0 & 1 \end{pmatrix} q + \begin{pmatrix} 0 \\ 0 \\ \dot{\beta} \end{pmatrix} = \begin{pmatrix} v_t \cos\psi \\ v_t \sin\psi \\ r \end{pmatrix} + \begin{pmatrix} 0 \\ 0 \\ \dot{\beta} \end{pmatrix} \tag{3.20}$$

Thus, the vehicle can be taken as having velocity vector $\mathbf{q} = (v_t, r)^T$, and the yaw rate influenced by the side-slipping effect through the term $\dot{\beta}$.

- **Control similarities between unicycle-type robot and underactuated AUV :**

Note that the choice of a new frame in Figure 3.5, i.e., flow frame $\{W\}$, simplifies the first two kinematic equations of underwater vehicles in (3.20) and brings out their similarities with those of a wheeled robot in (3.13).

It indicates that in path following motion control, the unicycle case is solved by controlling the forward speed tangentially to the path, the underactuated case requires the control of the total speed defined in (3.19). The reason is that the total speed of a unicycle-type robot is permanently equal to its forward speed u due to the first-order nonholonomic constraints on speed (lateral zero-speed constraint and cannot directly move in the sway direction). This lateral speed constraints is relaxed in the underactuated AUVs suffering from the second-order nonholonomic constraints on acceleration but not directly on speed, such that the total speed of an underactuated vehicle results from both surge and sway components u and v in (3.19). There is no lateral speed constraints, so that the underwater vehicle can be side-slipping. Thus, designing a controller for a side-slipping underwater vehicle implies driving the amplitude and the orientation of the total speed to desired values, defined with respect to the motion objectives that the vehicle must reach and follow. However, due to the term $\dot{\beta}$ appears at the kinematics level in (3.20), the system dynamics must be carefully considered in the control design.

3.2.2.2 Difference in the dynamic stage

As discussed above, from the first-order nonholonomic underactuated unicycle type vehicle to the second-order nonholonomic underactuated underwater vehicle, the control design in the kinematics stage is similar.

However, the related variable $\beta = \arctan(v/u)$ exists in the case of underwater vehicles, such that control design based on kinematics is not enough and the controller design must resort to the vehicle dynamics. As v is not directly controllable, the dynamics of sway velocity v must be explicitly taken into account which depends on the equation ($m_v\dot{v} + m_u u_r r + d_v v_r = 0$ in (3.5)). This rules out any attempt to design the AUV controller only relying on its kinematic equations, which is a basic difference in control design between underactuated underwater vehicles and unicycle-type vehicles.

Essentially, the kinematic controller involves a computation of $\dot{\beta} = (u\dot{v} - v\dot{u})/v_t^2$, therefore a computation of $\dot{u}$ and $\dot{v}$, the longitudinal and transverse accelerations of the vehicle, depending on the dynamic model injects dynamic parameters at the kinematic level. Furthermore, the backstepping process, used to design the dynamic control from the kinematic solution, reveals the necessary computation of $\ddot{\beta}$, hence $\ddot{u}$ and $\ddot{v}$, the transverse and longitudinal system jerks. This is achieved by resorting to the dynamic model again, and it implies deriving longitudinal and transverse acceleration expressions from the dynamical model. Moreover, the nonlinearity in the AUV dynamics makes the control design more complex than the linear case in unicycle type vehicle. In the later section 5.1, one can see more details on the difference in control design of underactuated AUVs.

Summary :

Based on the explained connection between nonholonomic unicycle-type mobile robot and underactuated AUV, an important remark is that the research on underactuated AUV system is an extension of the research on the unicycle-type mobile robot systems. This is the theoretic root inspiring us to firstly address the problem of motion control of nonholonomic mobile robots, before going to underactuated underwater vehicles. At the same time, we can benefit from convenient experiments on nonholonomic mobile robots at the early stage, other than the high-cost and heavy experiments on underwater vehicles, especially when we deal with multiple vehicles.

In this thesis, we investigate the path following and path tracking control of underactuated unicycle-type vehicles in chapter 4, and then migrate the methodology and extend the control laws to underactuated AUVs in chapter 5. The coordinated motion control of both types of vehicles is given in chapter 6.

3.3 Basic notations and error dynamics for motion control

In this section, basic notations are given to describe three fundamental motion reference elements. Subsequently, mathematical methods to build error dynamics are introduced, as the motion control problem (i.e., path following and path tracking) can be converted into the stabilization problem of a tracking error vector between the vehicle and the moving target on a path or trajectory being stabilized to zero. [Walsh et al., 1994].

3.3.1 Basic notations

Before discussing different type of motion control problems, three main different references as desired targets for motion control, i.e., *posture*, *path* and *trajectory*, are describes and the definitions of these motion references will be given as well.

(1) **Posture**

Let $\Re^n$ be the configuration space. The term *posture* is corresponding to a specific target configuration, with definite position vector η_1 and orientation vector η_2 denoted in the n dimension configuration space. That is

$$\xi = [\eta_1 \ \eta_2]^T \in \Re^n \tag{3.21}$$

For instance, the posture of a 6-DOF AUV can be described as $\eta = [\eta_1 \ \eta_2]^T = [x, y, z, \phi, \theta, \psi]^T$.

(2) **Path**

A *path* $\Gamma(\tau)$ in the configuration space $\Re^n$, is a regular geometric curve parameterized by a continuous scalar τ in a closed subset $[0, \tau_f]$. A mathematic expression of path is

$$\Gamma(\tau) : \tau \longrightarrow \Re^n, \tau \in [0, \tau_f], \tau_f \in \Re^+ \tag{3.22}$$

where τ is called the path parameter.

In this framework, the path could be described as, there is a virtual target in the configuration space, freely moving forward in terms of time (i.e., the speed and acceleration along the path remains to be freely determined), and the trace of the moving target becomes a path.

(3) **Trajectory**

If the regular curve $\Gamma(t)$ in the configuration space $\Re^n$ described above, is parameterized by time t in a certain time interval $[0, t_f]$, it can be defined as a *trajectory*. A mathematic expression of trajectory is

$$\Gamma(t) : t \longrightarrow \Re^n, t \in [0, t_f], t_f \in \Re^+ \tag{3.23}$$

In this framework, the trajectory could be described as, there is a virtual target in the configuration space, moving forward with a defined function of time in order to arrive at the given position at the given time instant, and the temporally parameterized trace of the moving target becomes a trajectory.

These seemingly obvious concepts about posture, path and trajectory, are the fundmental pillars for the classification of motion control for autonomous vehicles. Roughly, the problem of motion control addressed can be classified into four categories in the contemporary literatures, i.e., posture stabilization, path following ,trajectory tracking and path tracking.

3.3.2 Error dynamics for motion control

In general, the motion control problem, can be rephrased as the stabilization to zero of a tracking error vector between the vehicle and the reference, using all the available control inputs. Hence, building a suitable error vector is the first step for motion control design. Depending on the different choices of reference frame in which the error vector is built, there are two main methods to build it, which is useful for motion control design. In this section, we build error model and corresponding error dynamics for unicycle type wheeled vehicle, and then extend it to underactuated underwater vehicles.

To the best knowledge of the author, the error dynamics usually is built in Cartesian coordinates, with respect to the body frame of the vehicle, or related to the reference target (moving target or virtual vehicle). The first one is widely used as reported in [Kanayama et al., 1990], [Jiang and Nijmeijer, 1997], [Fierro and Lewis, 1997], [Aguiar and Hespanha, 2007]. It is a natural way to map the error vector in the body frame of the vehicle itself.

In a converse way, the error vector is described in the frame of the reference target (virtual point-mass target or virtual vehicle) which is normally represented by the Frenet-Serret formulas. This special way is useful for path following control, as we can easily choose the velocity of the virtual target and let it collaborate with the movement of the real robot, and try to minimize the error space. This method is reported in [Diaz del Rio et al., 2001, Soetanto et al., 2003, Lapierre et al., 2003].

3.3.2.1 Error dynamics in body frame

Let the actual vehicle with generalized position vector be denoted by $p = (x, y, \psi)^T$ in the inertial frame $\{I\}$, where $(x, y)^T$ and ψ describe the position and orientation in $\{I\}$ respectively. Similarly, let $p_r = (x_r, y_r, \psi_r)^T$ denote the generalized position coordinate of the target reference in the inertial frame.

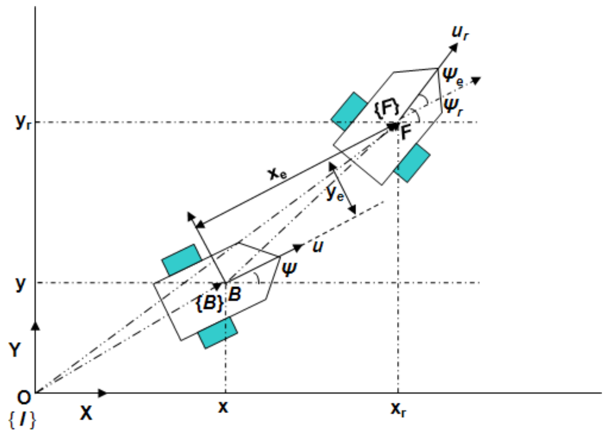

Figure 3.6 – Error vector in body frame

As depicted in Figure 3.6 , the error vector in the inertial frame can be formulated as

$$(\overrightarrow{BF})_I = (\overrightarrow{OF})_I - (\overrightarrow{OB})_I \tag{3.24}$$

Expressing the vector relationship in the vehicle's body frame $\{B\}$ yields

$$(\overrightarrow{BF})_B = R_I^B(\overrightarrow{BF})_I = R_I^B((\overrightarrow{OF})_I - (\overrightarrow{OB})_I) \tag{3.25}$$

where R_I^B is the rotation matrix from frame $\{I\}$ to frame $\{B\}$

$$R_I^B = \begin{bmatrix} \cos\theta & \sin\theta & 0 \\ -\sin\theta & \cos\theta & 0 \\ 0 & 0 & 1 \end{bmatrix}$$

Let $\mathbf{p}_{eB} = (x_e, y_e, \psi_e)^T$ be the error vector (or error space). We can simplify the error vector from (3.25), as

$$\mathbf{p}_{eB} = R_I^B(\theta)(\mathbf{p}_r - \mathbf{p}) \tag{3.26}$$

That is

$$\mathbf{p}_{eB} = \begin{bmatrix} x_e \\ y_e \\ \theta_e \end{bmatrix} = \begin{bmatrix} \cos\theta & \sin\theta & 0 \\ -\sin\theta & \cos\theta & 0 \\ 0 & 0 & 1 \end{bmatrix} \begin{bmatrix} x_r - x \\ y_r - y \\ \theta_r - \theta \end{bmatrix} \tag{3.27}$$

where $\mathrm{p}_{eB} = [x_e, y_e, \theta_e]^T$ consists of the *along-track error* x_e and the *cross-track error* y_e with respect to the vehicle body frame $\{B\}$, and the *heading error* θ_e with respect to the inertial frame $\{I\}$. The along-track error represents the distance from p_r to p along the x-axis of the body frame, the cross-track error represents the distance along the y-axis of the body frame, while the heading error represents the heading difference between the target and the vehicle along the x-axis of the inertial frame.

Assume the vehicle moves with velocities $q = (u, \omega)^T$, where u denotes the linear velocity and ω denotes angular velocity. The reference robot moves with velocities $q_r = (u_r, \omega_r)^T$. Differentiating the error coordinates, yields error dynamics

$$\begin{bmatrix} \dot{x}_e \\ \dot{y}_e \\ \dot{\theta}_e \end{bmatrix} = \begin{bmatrix} \omega y_e - u + u_r \cos\theta_e \\ -\omega x_e + u_r \sin\theta_e \\ \omega_r - \omega \end{bmatrix} \tag{3.28}$$

In [Kanayama et al., 1990], direct computation is used to get the error dynamics, but it results in heavy computation burden. The first-order non-holonomic constraint $\dot{x}\sin\theta - \dot{y}\cos\theta = 0$ imposed on the unicycle-type robot, is the important additional condition to get (3.28). However, in the case of other non-holonomic vehicles, such as under-actuated marine vehicle, $\dot{x}\sin\theta - \dot{y}\cos\theta = 0$ is not true due to the presence of side-slip velocity imposed by second-order non-holonomic constraints. The derivation of error dynamics in under-actuated vehicle is more complex than the case of unicycle-type vehicle. One way to simplify the derivation of error dynamics is to adopt the flow-frame by rotating body frame $\{B\}$ around the z_B axis through the sideslip angle β.

Another way to simplify the derivation of error-dynamics, is using the specific orthogonal characteristics of rotation matrix, to deduce the equations of error dynamics. In this sense, this method is universal to all kinds of vehicles. As the rotation matrix R_I^B has the following property

$$\dot{R}_I^B(\theta) = R_I^B(\theta)'\dot{\theta} = R_I^B(\theta)S(\theta)\dot{\theta} \tag{3.29}$$

where $S(\theta)$ is skew-symmetrical with elements $0, -1, 1$, i.e.,

$$S(\theta) = \begin{bmatrix} 0 & 1 & 0 \\ -1 & 0 & 0 \\ 0 & 0 & 0 \end{bmatrix} \tag{3.30}$$

There is, $S(\theta) = -S(\theta)^T$ and $X^T S X = 0, X \in \Re^3$.

Rewriting (3.27) as

$$\begin{bmatrix} x_e \\ y_e \\ \theta_e \end{bmatrix} = R_I^B \begin{bmatrix} x_r - x \\ y_r - y \\ \theta_r - \theta \end{bmatrix} \tag{3.31}$$

Differentiating above equation, results in

$$\begin{bmatrix} \dot{x}_e \\ \dot{y}_e \\ \dot{\theta}_e \end{bmatrix} = \dot{R}_I^B \begin{bmatrix} x_r - x \\ y_r - y \\ \theta_r - \theta \end{bmatrix} + R_I^B \begin{bmatrix} \dot{x}_r - \dot{x} \\ \dot{y}_r - \dot{y} \\ \dot{\theta}_r - \dot{\theta} \end{bmatrix} = \dot{\theta} S(\theta) R_I^B(\theta) \begin{bmatrix} x_r - x \\ y_r - y \\ \theta_r - \theta \end{bmatrix} + R_I^B \begin{bmatrix} \dot{x}_r - \dot{x} \\ \dot{y}_r - \dot{y} \\ \dot{\theta}_r - \dot{\theta} \end{bmatrix}$$

$$= \begin{bmatrix} 0 & \omega & 0 \\ -\omega & 0 & 0 \\ 0 & 0 & 0 \end{bmatrix} R_I^B \begin{bmatrix} x_r - x \\ y_r - y \\ \theta_r - \theta \end{bmatrix} + R_I^B \begin{bmatrix} u_r \cos\theta_r - u\cos\theta \\ u_r \sin\theta_r - u \sin\theta \\ \dot{\theta}_r - \dot{\theta} \end{bmatrix}$$

$$= \begin{bmatrix} 0 & \omega & 0 \\ -\omega & 0 & 0 \\ 0 & 0 & 0 \end{bmatrix} \begin{bmatrix} x_e \\ y_e \\ \theta_e \end{bmatrix} + \begin{bmatrix} u_r \cos(\theta_r - \theta) - u \\ u_r \sin(\theta_r - \theta) \\ \omega - \omega_r \end{bmatrix}$$

Or, rather that the same error dynamics as that in (3.28).

3.3.2.2 Error dynamics in target frame

In Figure 3.7, the target reference based frame $\{F\}$ is selected, to build the error vector $\mathbf{p}_{eF} = (x_e, y_e, \psi_e)^T$. Be aware the geometric relationship is different in Figure 3.7 and Figure 3.6, although the error vector has same elements $(x_e, y_e, \psi_e)^T$ as that in vehicle's body based frame.

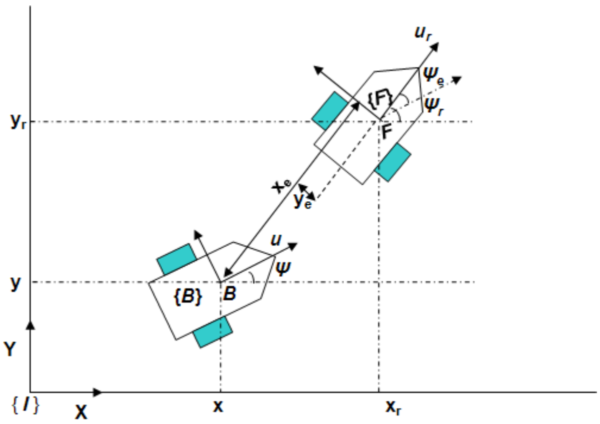

Figure 3.7 – Error vector in target frame

Similarly, expressing the error vector $(\overrightarrow{FB})_I = (\overrightarrow{OB})_I - (\overrightarrow{OF})_I$ in the inertial frame $\{I\}$, yields

$$(\overrightarrow{FB})_F = R_I^F((\overrightarrow{OB})_I - (\overrightarrow{OF})_I) \tag{3.32}$$

where R_I^F is the rotation matrix from frame I to frame F

$$R_I^F = \begin{bmatrix} \cos\psi_r & \sin\psi_r & 0 \\ -\sin\psi_r & \cos\psi_r & 0 \\ 0 & 0 & 1 \end{bmatrix}$$

and ψ_r is the orientation of the virtual vehicle.

By introducing the error vector $\mathbf{p}_{eF} = (x_e, y_e, \psi_e)^T$, (3.32) can be rewritten as $\mathbf{p}_{eF} = R_I^F(\psi_r)(\mathbf{p} - \mathbf{p}_r)$, that is

$$\begin{bmatrix} x_e \\ y_e \\ \psi_e \end{bmatrix} = \begin{bmatrix} \cos\psi_r & \sin\psi_r & 0 \\ -\sin\psi_r & \cos\psi_r & 0 \\ 0 & 0 & 1 \end{bmatrix} \begin{bmatrix} x - x_r \\ y - y_r \\ \psi - \psi_r \end{bmatrix} \tag{3.33}$$

where $p_{eF} = [x_e, y_e, \psi_e]^T$ consists of the *along-track error* x_e, the *cross-track error* y_e and the *heading error* θ_e with respect to the target reference frame $\{F\}$, and the *heading error* θ_e between the virtual and actual vehicle. The along-track error represents the distance from p to p_r along the x-axis of the target reference frame, the cross-track error represents the distance along the y-axis of the target reference frame, while the heading error represents the heading difference between the actual vehicle and the virtual target.

Assume the velocity vector of the vehicle is $(u, \omega)^T$, and the velocity vector of the reference target is $(u_r, \omega_r)^T$. By using the property of the rotation matrix R_I^F in (3.29), we can get the error dynamics in reference frame

$$\begin{bmatrix} \dot{x}_e \\ \dot{y}_e \\ \dot{\psi}_e \end{bmatrix} = \dot{R}_I^F \begin{bmatrix} x - x_r \\ y - y_r \\ \psi - \psi_r \end{bmatrix} + R_I^F \begin{bmatrix} \dot{x} - \dot{x}_r \\ \dot{y} - \dot{y}_r \\ \dot{\psi} - \dot{\psi}_r \end{bmatrix} = \begin{bmatrix} \omega_r y_e - u_r + u\cos\psi_e \\ -\omega_r x_e + u\sin\psi_e \\ \omega - \omega_r \end{bmatrix} \tag{3.34}$$

In another way to get the error dynamics, one can also propagate the vehicle linear velocities from the vehicle's body frame to the target reference frame by using the classic law of Mechanics [Craig, 1986], rendering the error dynamics as reported in [Micaelli and Samson, 1993], [Encarnacao and Pascoal, 2000], and [Lapierre et al., 2006].

Furthermore, the error dynamics (3.34) in target frame, can be rewritten as

$$\begin{bmatrix} \dot{x}_e \\ \dot{y}_e \\ \dot{\psi}_e \end{bmatrix} = \begin{bmatrix} -u_r \\ 0 \\ -\omega_r \end{bmatrix} + \begin{bmatrix} 0 & \omega_r & 0 \\ -\omega_r & 0 & 0 \\ 0 & 0 & 0 \end{bmatrix} \begin{bmatrix} x_e \\ y_e \\ \psi_e \end{bmatrix} + \begin{bmatrix} \cos\psi_e & 0 \\ \sin\psi_e & 0 \\ 0 & 1 \end{bmatrix} \begin{bmatrix} u \\ \omega \end{bmatrix} \tag{3.35}$$

It decouples the derivative of error variables into the form related to the actual states (u, ω), tracking errors (x_e, y_e, ψ_e) and desired states (u_r, ω_r) of the vehicle.

3.3.2.3 Error dynamics extended to AUV

In this part, by using the same strategy for unicycle-type mobile robot, the error model and corresponding error dynamics are built for autonomous underwater vehicles, based on the motion model of AUV.

Error dynamics in body frame :

Let the actual AUV with generalized position vector (position and orientation) denoted by $p = (x, y, \psi)^T$ in the inertial frame $\{I\}$ as illustrated in Figure 3.8(a), where $\psi = \psi_B + \beta$ is the course angle, and let $p_r = (x_r, y_r, \psi_r)^T$ denote the generalized position coordinate of the target reference in the inertial frame.

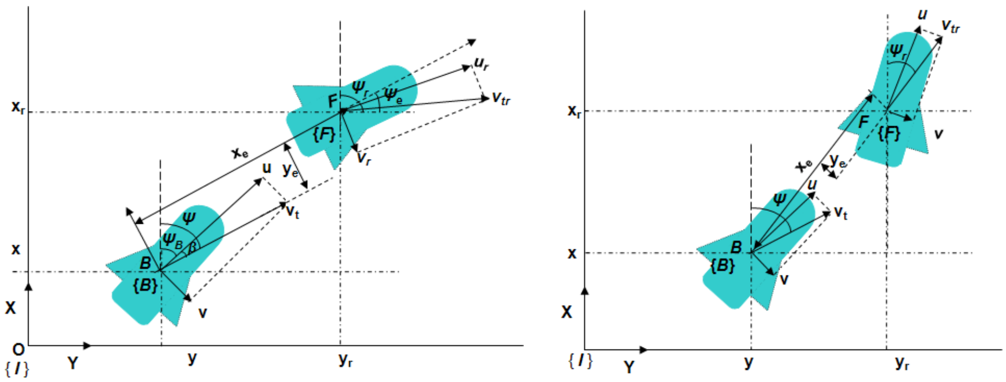

(a) AUV error vector in body frame (b) AUV error vector in target frame

Figure 3.8 – AUV error vectors in different reference frame

Similarly with that of in unicycle-type vehicle, the error vector for autonomous underwater vehicle built in body frame $\{B\}$, is described as

$$\mathbf{p}_{eB} = R_I^B(\psi)(\mathbf{p}_r - \mathbf{p}) \tag{3.36}$$

Assume the vehicle moves with velocities $q = (v_t, \omega)^T$, where v_t denotes the total linear velocity and r denotes angular velocity in (3.18). The reference vehicle moves with velocities $q_r = (v_{tr}, \omega_r)^T$. Differentiating the error coordinates (3.36), yields error dynamics

$$\begin{aligned}
\begin{bmatrix} \dot{x}_e \\ \dot{y}_e \\ \dot{\psi}_e \end{bmatrix} =& \dot{R}_I^B(\psi) \begin{bmatrix} x_r - x \\ y_r - y \\ \psi_r - \psi \end{bmatrix} + R_I^B(\psi) \begin{bmatrix} \dot{x}_r - \dot{x} \\ \dot{y}_r - \dot{y} \\ \dot{\psi}_r - \dot{\psi} \end{bmatrix} \\
=& \dot{\psi} S(\psi) R_I^B(\psi) \begin{bmatrix} x_r - x \\ y_r - y \\ \omega_r - \omega \end{bmatrix} + R_I^B(\psi) \begin{bmatrix} \dot{x}_r - \dot{x} \\ \dot{y}_r - \dot{y} \\ \dot{\psi}_r - \dot{\psi} \end{bmatrix} \\
=& \begin{bmatrix} 0 & r & 0 \\ -\omega & 0 & 0 \\ 0 & 0 & 0 \end{bmatrix} \begin{bmatrix} x_e \\ y_e \\ \psi_e \end{bmatrix} + \begin{bmatrix} v_{tr}\cos(\psi_r - \psi) - v_t \\ v_{tr}\sin(\psi_r - \psi) \\ \omega - \omega_r \end{bmatrix}
\end{aligned}$$

where $\dot{\psi} = \omega + \dot{\beta}$ is used.

Consequently, there is

$$\begin{bmatrix} \dot{x}_e \\ \dot{y}_e \\ \dot{\psi}_e \end{bmatrix} = \begin{bmatrix} \omega y_e - v_t + v_{tr}\cos\psi_e \\ -\omega x_e + v_{tr}\sin\psi_e \\ \omega_r - \omega - \dot{\beta} \end{bmatrix} \tag{3.37}$$

Error dynamics in target frame :

Again, similarly with that of in unicycle-type vehicle, the error vector for autonomous underwater vehicle built in target frame $\{F\}$ as illustrated in Figure 3.8(b), is described as

$$\mathbf{p}_{eF} = R_I^F(\psi)(\mathbf{p} - \mathbf{p}_r) \tag{3.38}$$

Suppose the vehicle moves with velocities $q = (v_t, \omega)^T$, where v_t denotes the total linear velocity and r denotes angular velocity. The target moves with velocities $q_r = (v_{tr}, \omega_r)^T$. Let the total velocity of the vehicle be aligned with the tangent vector of the path, that means the flow frame coincides with the target frame.

Differentiating the error coordinates (3.38), yields error dynamics

$$\begin{bmatrix} \dot{x}_e \\ \dot{y}_e \\ \dot{\psi}_e \end{bmatrix} = \begin{bmatrix} \omega_r y_e - v_{tr} + v_t\cos\psi_e \\ -\omega_r x_e + v_t\sin\psi_e \\ \omega + \dot{\beta} - \omega_r \end{bmatrix} \tag{3.39}$$

3.4 Summary

In this chapter, the definitions of underactuated system and nonholonomic constraints are introduced. The first-order and seconder-order nonholonomic constraints imposed on unicycle-type wheeled robots and underactuated AUVs are presented respectively. According to this fact, the similarity and difference for control design between them are indicated, which enables the strategies of motion control for nonholonomic mobile robots to be extended for underactuated underwater vehicles in this thesis. Finally, basic notations for motion control is described, and error dynamics is introduced which is useful for control design in the following chapters.

CHAPTER 4

MOTION CONTROL OF SINGLE NONHOLONOMIC UNICYCLE VEHICLE

In this chapter, the motion control problems of three main motion types : trajectory tracking, path following and path tracking for nonholonomic unicycle-type wheeled vehicles, are formulated and the control design for each motion type is proposed in detail, by using Lyapunov-based state-feedback control laws and backstepping technique. Whereas, the control problem of point stabilization is not our interest in this thesis, one can refer to the solutions reviewed in section 2.1.1. Simulation results illustrate the performance of the control laws derived and describes the difference of three motion controllers. Finally, concluding remarks are given to show the exclusive characteristics of these three main motion behaviors.

4.1 Trajectory tracking control of nonholonomic unicycle vehicle

Although trajectory tracking is not a new issue to be solved, we propose the dedicated controller with the error dynamics built in reference target frame but not in vehicle body frame, by choosing the control input to avoid the potential singularity. Moreover, we introduce the control design procedure in this part, as a preparation and comparison for path following and path tracking according to the control objective.

4.1.1 Problem formulation

In the problem of path following, the desired linear velocity of the vehicle is predefined. The vehicle is required to adapt its orientation to approach the path, and the speed of the virtual target moving along the path complies with that of the vehicle, in order to achieve the control objective.

However, in trajectory tracking, the desired linear velocity of the vehicle cannot be chosen freely, and it absolutely complies with the reference trajectory parameterized through time t. In other words, there is one virtual reference vehicle moving with pre-defined velocity $[u_r(t), \omega_r(t)]^T$ at time instant t, generating the trajectory to be tracked by the actual vehicle as shown in Figure. (4.1). Therefore, the trajectory tracking problem requires the vehicle to track the specific position defined by the virtual vehicle at each given time instant, through adapting its linear and angular velocities.

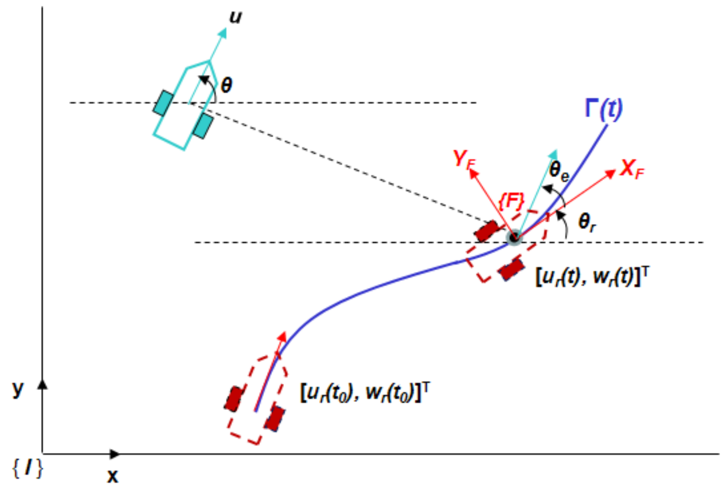

Figure 4.1 – Trajectory tracking of nonholonomic autonomous vehicle

Generally, trajectory tracking controller is designed in the vehicle body frame $\{B\}$, see [Kanayama et al., 1990], [Fierro and Lewis, 1997], [Aguiar and Hespanha, 2007] among many others. Herein, we propose the controller derived from the error dynamics which is built in reference based frame $\{F\}$, and choose the control inputs to avoid the singularity in the control design.

Let the tracking error state vector $\mathbf{p}_{eF} = [x_e, y_e, \theta_e]$ be built in the target frame $\{F\}$, where the target is the virtual vehicle, generating the desired trajectory. As described in section 3.3.2.2, we can define the error vector as

$$\mathbf{p}_{eF} = \begin{bmatrix} x_e \\ y_e \\ \theta_e \end{bmatrix} = \begin{bmatrix} \cos\theta_r & \sin\theta_r & 0 \\ -\sin\theta_r & \cos\theta_r & 0 \\ 0 & 0 & 1 \end{bmatrix} \begin{bmatrix} x - x_r \\ y - y_r \\ \theta - \theta_r \end{bmatrix} \tag{4.1}$$

where $[x, y, \theta]^T$ is the vehicle state vector and $[x_r, y_r, \theta_r]^T$ is the reference state vector in the inertial frame $\{I\}$.

The corresponding error state dynamics can be derived as follows :

$$\begin{bmatrix} \dot{x}_e \\ \dot{y}_e \\ \dot{\theta}_e \end{bmatrix} = \begin{bmatrix} \omega_r y_e - u_r + u\cos\theta_e \\ -\omega_r x_e + u\sin\theta_e \\ \omega - \omega_r \end{bmatrix} \tag{4.2}$$

where $[u, \omega]^T$ is the vehicle state vector and $[u_r, \omega_r]^T$ is the reference velocity vector.

With respect to the error model (4.1) and (4.2), the control objective of trajectory tracking in kinematics stage, is to choose suitable vehicle inputs u and ω, such that the tracking error asymptotically converges to zero, i.e.,

$$\lim_{t\to\infty} \|\mathbf{p}_{eF}\| = 0 \tag{4.3}$$

4.1.2 Controller design

In the reference target frame $\{F\}$, the candidate Lyapunov function is selected in a positive definite quadratic form.

$$V = \frac{1}{2}(x_e^2 + y_e^2 + \theta_e^2)$$

Clearly, V is positive definite, only equal to zero with $\mathbf{p}_{eF} = 0^3$.

We propose the trajectory tracking control laws as follows :

$$q = \begin{bmatrix} u \\ \omega \end{bmatrix} = \begin{bmatrix} u_r\cos\theta_e - k_1 x_e\cos\theta_e - k_1 y_e\sin\theta_e \\ \omega_r + u_r(x_e\frac{\sin\theta_e}{\theta_e}\sin\theta_e - y_e\frac{\sin\theta_e}{\theta_e}\cos\theta_e) - k_2\theta_e \end{bmatrix} \tag{4.4}$$

where k_1, k_2 are positive scalar.

Then, the derivative of V is

$$\begin{aligned}
\dot{V} =& \dot{x}_e x_e + \dot{y}_e y_e + \theta_e\dot{\theta}_e \\
=& x_e(\omega_r y_e - u_r + u\cos\theta_e) + y_e(u\sin\theta_e - \omega_r x_e) + (\dot{\theta} - \dot{\theta}_r)\theta_e \\
=& -u_r x_e + u x_e\cos\theta_e + u y_e\sin\theta_e + (\omega - \omega_r)\theta_e \\
=& -u_r x_e + (u_r\cos\theta_e - k_1 x_e\cos\theta_e - k_1 y_e\sin\theta_e)(x_e\cos\theta_e + y_e\sin\theta_e) \\
& + \theta_e(u_r(x_e\frac{\sin\theta_e}{\theta_e}\sin\theta_e - y_e\frac{\sin\theta_e}{\theta_e}\cos\theta_e) - k_2\theta_e) \\
=& -u_r x_e + u_r x_e\cos^2\theta_e + u_r y_e sin\theta_e\cos\theta_e - k_1 x_e^2\cos^2\theta_e - k_1 x_e y_e\cos\theta_e\sin\theta_e \\
& - k_1 x_e y_e\sin\theta_e\cos\theta_e - k_1 y_e^2\sin^2\theta_e + u_r x_e\sin^2\theta_e - u_r y_e\sin\theta_e\cos\theta_e - k_2\theta_e^2 \\
=& -k_1(x_e\cos\theta_e + y_e\sin\theta_e)^2 - k_2\theta_e^2 \\
\leq& 0
\end{aligned}$$

Proposition 4.1.1 (Trajectory tracking :unicycle type vehicle)

Assume that one virtual vehicle moves with bounded velocity $u_r(t)$ and $\omega_r(t)$ on $t \in [0, \infty)$, generating the trajectory continuously. Given the kinematic control inputs u and ω for the tracking vehicle in (4.4), the control objective (4.3) of trajectory tracking is achieved and the equilibrium point $(x_e, y_e, \theta_e)^T = (0, 0, 0)^T$ is globally asymptotically stable.

Proof As V is positive definite and $\dot{V}$ is negative semi-definite, V is nonincreasing and converges to some limit : $V \to V_{lim} \geq 0$. It is assumed u_r, ω_r are bounded, such that $\ddot{V}$ is bounded. By Barbalat's lemma, $\dot{V} \to 0$, there are $x_e \to 0$, $\dot{x}_e \to 0$, and the same for θ_e and $\dot{\theta}_e$. By checking the first terms in (4.2), $\lim_{t\to\infty} \dot{x}_e \to \omega_r y_e$ as $\lim_{t\to\infty} u \cos\theta_e = \lim_{t\to\infty} u_r$ by recalling the control input u in (4.4). In order to prove the convergence of $y_e \to 0$, we are proving by contradiction. Suppose $\lim_{t\to\infty} y_e \neq 0$, there is $y_e \to y_{e,lim}$ due to the boundedness of V. Thus, for any $\omega_r \neq 0$, it gives the convergence solution :

$$\lim_{t\to\infty} \dot{x}_e \to \omega_r y_{e,lim}$$

which is paradoxical with $\dot{x}_e \to 0$ no matter the state of ω_r. Hence, $\lim_{t\to\infty} y_e = 0$. Now, we can conclude that $\lim_{t\to\infty} \|p_{eF}\| = 0$. ∎

Notice that the term $\frac{\sin\theta_e}{\theta_e}$ in control laws (4.4) is well defined and continuous at zero. Using L'Hopital's rule, it is easy to see that $\frac{\sin\theta_e}{\theta_e} = 1$ when $\theta_e = 0$. Therefore, the trajectory tracking controller is continuous and nonsingular in the whole time horizon.

4.2 Path following control of nonholonomic unicycle vehicle

In this section, the Frenet-Serret formulas is reviewed firstly, and path following problem is formulated based on the moving Frenet-Serret reference frame attached to the virtual target on the path. Kinematic controller is derived by elaborating heading guidance design to shape the transient maneuvers as proposed in [Micaelli and Samson, 1993], and LaSalle's invariance principle is involved to simplify the nonlinear path following control law firstly presented in [Soetanto et al., 2003]. Finally, backstepping technique is used to deal with vehicle dynamics.

4.2.1 Problem formulation

Given a path S, let a moving point P along S be the desired reference point of the following vehicle. In trajectory tracking, P is time-parameterized. However, in path following, P is parameterized by the path variable s, which is the along path distance.

Frenet-Serret frame :

In order to properly build the reference target frame attached to the moving point P on the path, we introduce the *Frenet-Serret frame*, which is the main tool in the differential geometry to represent curves as it is far easier and more natural to describe local properties (e.g. curvature, torsion) in terms of a local reference system than using a global one, i.e., the cartesian coordinate.

In Figure. 4.2, a Frenet-Serret frame $\{F\}$ in $\Re^3$ is a moving frame of three orthonormal vectors, that provides a coordinate system at each point of the curve. Let $s(t)$ represent the signed curvilinear abscissa along the curve C. It means the curve is parameterized by its arc length, also called along-path distance, and the Frenet-Serret frame is defined as follows :

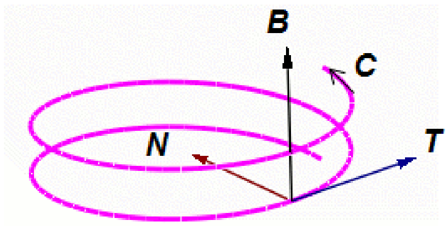

Figure 4.2 – Frenet-Serret frame in $\Re^3$

- T is the unit vector tangent to the curve, pointing in the direction of motion.
- N is the derivative of T with respect to the arclength parameter of the curve, divided by its length.
- B is the cross product of T and N, i.e., $B = T \times N$.

The *curvature* $c_c(t)$ at point P, measures the deviation of N from being a straight line relative to the osculating plane T. The reciprocal of the curvature $1/c_c(t)$ is called the radius of curvature. For instance, the curvature of a straight line is 0, and the curvature of a circle with radius r is $1/r$.

Path following formulation :

Assume that the desired path is parameterized by a virtual target P moving forward in Figure. 4.3, with along path length denoted by s. Q is the center of mass of an autonomous vehicle moving with predefined speed. Attached to $\{P\}$, the Frenet-Serret frame $\{F\}$ is built by choosing the tangent vector along the path as the x-direction of $\{F\}$, the principal normal vector as the y-direction of $\{F\}$. Let the rotations from $\{I\}$ to $\{F\}$ and $\{I\}$ to $\{B\}$ be denoted by the yaw angles ψ_F and ψ_B respectively. Let (x_e, y_e) denote the coordinates of Q in $\{F\}$. Furthermore, let $\psi = \psi_B - \psi_F$, $c_c(s)$ and $g_c(s)$ denote the path curvature and its derivative respectively, and then $\dot{\psi}_F = c_c(s)\dot{s}$, $g_c(s) = \frac{\partial c(s)}{\partial s}$.

Let the path following error state vector $\mathbf{p}_{eF} = [x_e, y_e, \psi_e]$ be built in the Frenet-Serret

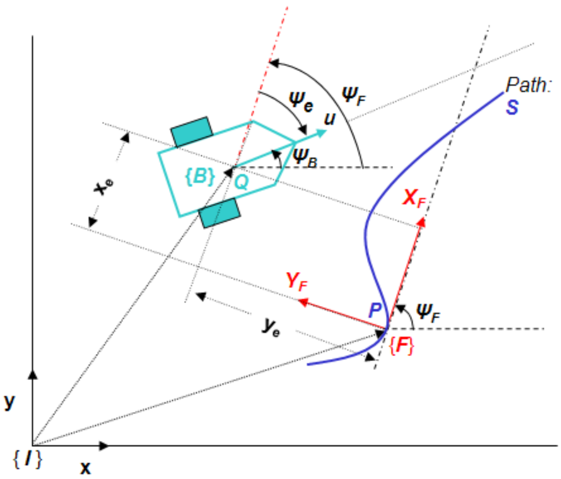

Figure 4.3 – Path following of nonholonomic autonomous vehicle

frame $\{F\}$. As described in section 3.3.2.2, we can define the error vector as described in (3.33), that is

$$\begin{bmatrix} x_e \\ y_e \\ \psi_e \end{bmatrix} = \begin{bmatrix} \cos\psi_F & \sin\psi_F & 0 \\ -\sin\psi_F & \cos\psi_F & 0 \\ 0 & 0 & 1 \end{bmatrix} \begin{bmatrix} x - x_r \\ y - y_r \\ \psi_B - \psi_F \end{bmatrix} \tag{4.5}$$

where $[x, y, \psi_B]^T$ is the vehicle state vector and $[x_F, y_F, \psi_F]^T$ is the reference state vector in the inertial frame $\{I\}$. According to the definition of Frenet-Serret frame, there is $u_r(s) = \dot{s}$ and $\omega_r(s) = c_c(s)\dot{s}$. Hence, the corresponding error state dynamics in Frenet-Serret based target frame $\{F\}$ described in (3.28), can be rewritten as follows :

$$\begin{bmatrix} \dot{x}_e \\ \dot{y}_e \\ \dot{\psi}_e \end{bmatrix} = \begin{bmatrix} c_c(s)\dot{s}y_e - \dot{s} + u\cos\psi_e \\ -c_c(s)\dot{s}x_e + u\sin\psi_e \\ \omega - c_c(s)\dot{s} \end{bmatrix} \tag{4.6}$$

where $[u, \omega]^T$ is the vehicle velocity vector.

The control objective of path following is to design a controller and achieve the following tasks :

$$\begin{aligned} \lim_{t\to\infty} \|P_{eF}\| &= 0 \\ \lim_{t\to\infty} |u(t) - u_d(t)| &= 0 \end{aligned} \tag{4.7}$$

where $P_{eF} = (x_e, y_e, \psi_e)^T$ is the path following error vector built in Frenet-Serret frame $\{F\}$, and $u_d(t)$ is the predefined speed for the vehicle moving along the path.

4.2.2 Kinematics controller design

An intuitive solution to this problem was first proposed at a kinematic level in [Micaelli and Samson, 1993], from which the objective of path following controller should look at

- the distance from the vehicle to the path,
- the angle between the vehicle's velocity vector and the tangent to the path,

and reduce both to zero. Therefore, the controller design can be structured into two steps :

(1) design a heading guidance to steer the vehicle towards the path ;

(2) design control inputs to force the vehicle move onto the path.

Step 1. Heading guidance design :

In [Micaelli and Samson, 1993] and [Lapierre et al., 2003], a heading guidance δ performs as an "approaching angle", which is instrumental in shaping the transient maneuvers during the path approaching phase, chosen as

$$\delta(y_e, u) = -sign(u)\theta_a \tanh(k_\delta y_e) \tag{4.8}$$

where the shaping coefficient $k_\delta > 0$, $0 < \theta_a < \pi/2$, and $sign(\cdot)$ is the sign function.

In the ideal situation, ψ_e should be equal to the desired heading δ. Hence, consider the Lyapunov function $V_1 = (\psi_e - \delta)^2/2$. It is straightforward to show that the choice of the yaw rate control $\dot{\psi}_e = \dot{\delta} - k_\theta(\psi_e - \delta)$ yields $\dot{V}_1 = -k_\theta(\psi_e - \delta)^2 \leq 0$. That means $(\theta - \delta)$ is bounded, such that $\ddot{V} = 2k_\theta(\psi_e - \delta)^2$, which is bounded. By using Barbalat's Lemma, we can conclude that $\psi_e = \delta$ as $t \to \infty$. It means the ψ_e will globally asymptotically approach to the guidance angle. Hence, the trajectories of the system will asymptotically reach the invariant set Ω_{guid} defined as $\{\Omega_{guid} | (x, y) \in \Re^2, \psi_e = \delta\}$.

Furthermore, the desired yaw rate of the autonomous vehicle is

$$r = \dot{\psi}_F + \dot{\psi}_e = \dot{\psi}_F + \dot{\delta} - k_\theta(\psi_e - \delta) = c_c \dot{s} + \dot{\delta} - k_\theta(\psi_e - \delta) \tag{4.9}$$

Step 2. control inputs design :

The second step for path following control mentioned above, can be represented as minimizing the distance error between the vehicle and virtual target such that $(x_e, y_e)^T = 0$. In this step, the motion control of a virtual target moving along the path is designed, in order to "help" the actual vehicle converge to the path.

Consider a positive definite quadratic Control Lyapunov function $V_2 = \frac{1}{2} P_e^T P_e$ where $P_e = (x_e, y_e)^T$. Recalling (4.5), the derivative $\dot{V}_2 = u x_e \cos(\psi_e) + u y_e \sin(\psi_e) - \dot{s} x_e$. Let choose the auxiliary input $\dot{s}$ as :

$$\dot{s} = u \cos \psi_e + k_x x_e \tag{4.10}$$

Actually, the auxiliary input $\dot{s}$ is the kinematics control of the virtual target moving along the path. By defining $\dot{s}$ in (4.10), the motion behavior of the virtual target is compliant with the actual vehicle. With the heading guidance δ defined in (4.8), the system trajectories reach the invariant set $\{\Omega_{guid}|(x,y) \in \Re^2, \psi_e = \delta\}$, rendering that $\dot{V}_2 = uy_e \sin\delta - k_x x_e^2 = -k_0\theta_a|u|y_e \tanh(k_\delta y_e) - k_x x_e^2 \leq 0$.

Since $\dot{V}_2$ is negative definite, V_2 is bounded as well as all of the variables included in V_2. Thus, it is straightforward to show that $\ddot{V}_2$ is bounded. Now, we can conclude that $\lim_{t\to\infty} x \to 0$ and $\lim_{t\to\infty} y \to 0$ (as $\lim_{t\to\infty} u \neq 0$ assumed) by using Brablat's Lemma. Hence, the system trajectories will asymptotically reach the invariant set Ω_{pos} defined as $\{\Omega_{pos}|(x,y) \in \Re^2, (x_e, y_e) = 0^2$ and $\psi_e = \delta\}$.

During the kinematic stage, perfect velocity tracking is normally assumed [Kanayama et al., 1990]. Consequently, the kinematics control law $u = \alpha_u$ and $r = \alpha_r$ can be given as

$$\begin{bmatrix} \alpha_u \\ \alpha_r \\ \dot{s} \end{bmatrix} = \begin{bmatrix} u_d \\ c_c\dot{s} + \dot{\delta} - k_\theta(\psi_e - \delta) \\ u_d \cos\psi_e + k_x x_e \end{bmatrix} \tag{4.11}$$

where u_d is the desired speed assignment for the actual vehicle, the second term is the yaw rate control, and the last term is a virtual control input which introducing an additional degree of freedom for control design.

Proposition 4.2.1 (Path following 1 : unicycle type vehicle)

Given a spatial path $\Gamma(s)$ to be followed by a unicycle type vehicle with desired speed profile $u_d(t)$ and $\lim_{t\to\infty} u_d \neq 0$. Given the kinematic control inputs u and ω , and the virtual control input $\dot{s}$ for path parameter given in (4.11) . The control objective (4.7) of path following is achieved and the equilibrium point $(x_e, y_e, \psi_e)^T = (0,0,0)^T$ is globally asymptotically stable.

Proof Assume the desired speed u_d is constant and the system can be taken as autonomous. It allows the application of LaSalle's invariance principle to concatenate the two previous convergence properties.

In the first design step, for any initial state $(x,y)^T$ starting in $\Omega = \Re^2$, the heading design drive the system trajectories into the invariant set $\{\Omega_{guid}|(x,y) \in \Re^2, \psi_e = \delta\}$.

In the second step, it show that the largest invariant set of Ω_{guid} is $\{\Omega_{pos}|(x,y) \in \Re^2, (x_e, y_e)^T = 0^2$ and $\psi_e = \delta\}$. Furthermore, $\delta(y_e, u) = -sgn(u)\theta_a \tanh(k_\delta y_e)$, $\lim_{t\to\infty} \delta \to 0$ can be deduced from $\lim_{t\to\infty} y_e \to 0$. It eventually renders $\lim_{t\to\infty} \psi_e \to 0$ due to $\psi_e = \delta$ in set Ω_{pos}.

Therefore, every bounded solution starting in $\Re^2$ asymptotically converges to invariant manifold M which indeed is $\{M|(x_e, y_e, \psi_e)^T = (0,0,0)^T\}$, as t tends to ∞. ∎

- **Remark :**

In [Micaelli and Samson, 1993] and [Encarnacao and Pascoal, 2001], the moving point P is chosen to be the closest point by the orthogonal projection of Q on the path, i.e., $x_e \equiv 0$, such that $\dot{s} = \frac{u cos\psi_e}{1-y_e c_c(s)}$ by solving the first equation in (4.6) with $\dot{x}_e = 0$. Although the convergence of x_e is directly achieved, the singularity at $y_e = 1/c_c(s)$ arises. For any point on the path, there exists an associated tangent circle with radius $r(s) = 1/c_c(s)$. This circle is known as the osculating circle [Skjetne and Fossen, 2001]. The physical interpretation of the singularity is that, once the vehicle is located at the origin of the osculating circle, the projected point on the path will move infinitely fast, resulting in the instantaneously explosion of the control system.

Samson avoids this problem by restricting the initial position of vehicle to a tube around the path, the radius of which must be less than $1/\max(c_c(s))$ in the whole path [Micaelli and Samson, 1993]. Only local convergence to the path is guaranteed, and the restriction is very conservative since a large $\max(c_c(s))$ might appear in a small part of the path and impose a strict constraint even if the vehicle starts far away from the "problematic" section. By endowing the virtual target with free mobility on the path and introducing an additional degree of freedom to the virtual control input $\dot{s}$ in (4.11), the singularity problem is relieved by specifying how fast the virtual target moves, and global asymptotical convergence is achieved [Lapierre et al., 2003].

4.2.3 Backstepping Dynamics

In the previous step of control design, the kinematics control (4.11) has been derived, to address the path following problem by assuming "perfect velocities tracking" ($u = \alpha_u, r = \alpha_r$, where α_u, α_r are desired velocities), which may not hold in most practical case.

Actually, in the overall control loop, the kinematic controller acts as a reference subsystem, giving the desired signals for the control subsystem based on the dynamics level. A better alternative to the unrealistic assumption is using the backstepping techniques [M. Krstic and Kokotovic, 1995] to deal with vehicle dynamics. Hence, the control law in kinematic level can be extended to deal with vehicle dynamics.

Let u and r be virtual control inputs, α_u and α_r in (4.11) be the corresponding virtual control laws. Introduce the velocity error variables

$$z = \begin{pmatrix} z_u \\ z_r \end{pmatrix} = \begin{pmatrix} u - \alpha_u \\ r - \alpha_r \end{pmatrix}$$

Consider the Lyapunov function $V_{kin} = V_1 + V_2$, augmented with the quadratic terms of z_u and z_r, that is

$$V_{dyn} = V_{kin} + \frac{1}{2} z^T M z \tag{4.12}$$

where the positive definite matrix $M = \begin{pmatrix} m & 0 \\ 0 & I \end{pmatrix}$ is defined in (3.15).

The time derivative of V_{dyn} can be written as

$$\begin{aligned}
\dot{V}_{dyn} &= (\psi_e - \delta)(\dot{\psi} - \dot{\psi}_F - \dot{\delta}) + uy_e \sin\delta - k_x x_e^2 + m z_u \dot{z}_u + I z_r \dot{z}_r \\
&= (\psi_e - \delta)(z_r + \alpha_r - \dot{\psi}_F - \dot{\delta}) + uy_e \sin\delta - k_x x_e^2 + z_u(m\dot{u} - m\dot{\alpha}_u) + I z_r \dot{z}_r \\
&= (\psi_e - \delta)(z_r - k_1(\psi_e - \delta)) + uy_e \sin\delta - k_x x_e^2 + z_u(m\dot{u} - m\dot{\alpha}_u) + I z_r \dot{z}_r \\
&= -k_\theta(\psi_e - \delta)^2 + z_r(I\dot{z}_r + (\psi_e - \delta)) + z_u(m\dot{u} - m\dot{\alpha}_u) + uy_e \sin\delta - k_x x_e^2
\end{aligned}$$

Let the control laws for F and N be chosen as

$$\begin{cases} F = m\dot{u} = m\dot{\alpha}_u - k_3 z_u = m\dot{u}_d - k_3(u - u_d) \\ N = I\dot{r} = I\dot{\alpha}_r - (\psi_e - \delta) - k_4 z_r \end{cases} \tag{4.13}$$

where k_3 and k_4 are positive constants. Then

$$\dot{V}_{dyn} = -k_0|u|\theta_a y_e \tanh(k_\delta y_e) - k_\theta(\psi_e - \delta)^2 - k_x x_e^2 - k_3 z_u^2 - k_4 z_r^2 \leq 0$$

That means, $\dot{V}_{dyn}$ is negative definite anywhere except the equilibrium, and all the states $(x_e, y_e, \psi_e, z_u, z_r)$ globally asymptotically converge to its equilibrium. Moreover, it can be concluded that the equilibrium is $(x_e, y_e, \psi_e, z_u, z_r) = 0^5$ from the Barbalat's lemma as we have done for the kinematic control laws. Moreover, as $\lim_{t\to\infty} u \neq 0$ is required, $\lim_{t\to\infty} z_u = \lim_{t\to\infty}(u - u_d) \neq 0$ means $\lim_{t\to\infty} u_d \neq 0$ is the equivalent statement. Therefore, we can propose the following proposition for dynamic path following control.

Proposition 4.2.2 (Path following 2 : unicycle type vehicle)

Given a spatial path $\Gamma(s)$ to be followed by a unicycle type vehicle with desired speed profile $u_d(t)$ and $\lim_{t\to\infty} u_d \neq 0$. Given the dynamics control inputs F and N in (4.13), and the virtual control input $\dot{s}$ in (4.11). The control objective (4.7) of path following is achieved and the equilibrium point $(x_e, y_e, \psi_e, (u-u_d))^T = (0, 0, 0, 0)^T$ is globally asymptotically stable.

4.3 Path tracking control of nonholonomic unicycle vehicle

In this section, path parameterized with time evolution is introduced to formulate the path tracking problem. The extra control degree of freedom on the virtual target related to path parameter $\tau(t)$, results in singularity free control law for any regular path. It is also used for tracking error feedback, which enable the system robustness, and keep the benefits from both trajectory tracking and path following behaviors. Moreover, the path variable $\tau(t)$ is generalized to any meaningful parameter and is not limited to arc-length anymore as proposed in the standard path following control design [Soetanto et al., 2003].

Under this framework, formation control of multiple vehicles will be easily achieved by the coordinated paths tracking, which is shown in later chapter 6.2.

4.3.1 Problem formulation

Given a geometric reference path $\Gamma_r(\tau_d) = [x_r(\tau_d), y_r(\tau_d), \theta_r(\tau_d)]^T$ with τ_d being the path parameter, where $x_r(\tau_d), y_r(\tau_d)$ are arbitrary $\mathcal{C}^1$ functions of path parameter τ_d constructing the reference paths. This reference path can be taken as a primary trajectory tracking target (**TT target**) moving along the predefined reference path with speed $\dot{\tau}_d(t)$. On the other hand, we consider that there is a secondary path tracking target (**PT target**) moving along the predefined reference path, according to the time evolution $\dot{\tau}(t)$, and generates the virtual reference path $\Gamma_r(\tau(t))$ online. That is :

$$\begin{bmatrix} \dot{x}_r(\tau) \\ \dot{y}_r(\tau) \\ \theta_r(\tau) \end{bmatrix} = \begin{bmatrix} x_r^\tau(\tau)\dot{\tau} \\ y_r^\tau(\tau)\dot{\tau} \\ \text{atan2}(y_r^\tau(\tau)/x_r^\tau(\tau)) \end{bmatrix} \tag{4.14}$$

where

$$x_r^\tau(\tau) := \frac{\partial x_r(\tau)}{\partial \tau},\ y_r^\tau(\tau) := \frac{\partial y_r(\tau)}{\partial \tau}$$

denotes the partial derivative of $x_r(\tau)$, $y_r(\tau)$ with respect to path parameter τ, and atan2$(\cdot)$ function is used in computer simulation for implementation of $\arctan(\cdot)$ to obtain correct quadrant mapping.

Notice that the virtual reference path $\Gamma_r(\tau(t))$ is the same with the desired reference path $\Gamma_r(\tau_d(t))$ until certain time instant t_f, if there is $\tau(t_f) = \tau_d(t_f)$ which means the PT target coincides with the TT target on the desired path at time instant t_f. However, the virtual parameter τ has an extra degree of freedom in the following control design, in order to achieve path tracking performance, that is, smooth spatial convergence and time convergence as well.

Let the path tracking error state vector $\mathbf{p}_{eB} = [x_e, y_e, \theta_e]^T$ be built in the vehicle body frame $\{B\}$. As described in section 3.3.2.1, we can define the tracking error vector as

$$\mathbf{p}_{eB} = \begin{bmatrix} x_e \\ y_e \\ \theta_e \end{bmatrix} = \begin{bmatrix} \cos\theta & \sin\theta & 0 \\ -\sin\theta & \cos\theta & 0 \\ 0 & 0 & 1 \end{bmatrix} \begin{bmatrix} x_r - x \\ y_r - y \\ \theta_r - \theta \end{bmatrix} \tag{4.15}$$

where $[x, y, \theta]^T$is the vehicle state vector and $[x_r, y_r, \theta_r]^T$ is the reference state vector in the inertial frame $\{I\}$.

According to the strategy of path tracking, the vehicle is forced to follow the secondary PT target, and the PT target with extra degree of freedom is forced to track the main TT target. Whereas, similarly to the path following control, we have to properly describe the reference (PT target) velocity which is parameterized by path parameter τ, such that the velocity of the PT target can be related to the velocity of the path parameter. Consequently, we have the desired linear and angular velocity of the PT target on the path

$$\begin{bmatrix} u_r(\tau) \\ \omega_r(\tau) \end{bmatrix} = \begin{bmatrix} \bar{u}_r(\tau)\dot{\tau} \\ \bar{w}_r(\tau)\dot{\tau} \end{bmatrix} \tag{4.16}$$

where

$$\begin{cases} \bar{u}_r(\tau) = \sqrt{x_r^\tau(\tau)^2 + y_r^\tau(\tau)^2} \\ \bar{w}_r(\tau) = \frac{x_r^\tau(\tau){y_r^\tau}^2(\tau) - {x_r^\tau}^2(\tau)y_r^\tau(\tau)}{x_r^\tau(\tau)^2 + y_r^\tau(\tau)^2} \end{cases} \tag{4.17}$$

Resorting to the velocity vector $(u_r, \omega_r)^T$ expressed by path parameter in (4.16), the corresponding error state dynamics (3.28) expressed in vehicle body frame $\{B\}$, can be rewritten as follows :

$$\begin{bmatrix} \dot{x}_e \\ \dot{y}_e \\ \dot{\theta}_e \end{bmatrix} = \begin{bmatrix} \omega y_e - u + \bar{u}_r\dot{\tau}\cos\theta_e \\ -\omega x_e + \bar{u}_r\dot{\tau}\sin\theta_e \\ \bar{\omega}_r\dot{\tau} - \omega \end{bmatrix} \tag{4.18}$$

where $[u, \omega]^T$ is the vehicle state vector and $[u_r, \omega_r]^T$ is the reference velocity vector of the PT target.

The expressions in (4.16) and (4.17) also stand for the reference velocity vector of the TT target on the path :

$$\begin{cases} u_r(\tau_d) = \sqrt{x_r^{\tau_d}(\tau_d)^2 + y_r^{\tau_d}(\tau_d)^2}\dot{\tau}_d := \bar{u}_r(\tau_d)\dot{\tau}_d \\ \omega_r(\tau_d) = \dot{\theta}_r(\tau_d) = \theta_r^{\tau_d}(\tau_d)\dot{\tau}_d = \frac{x_r^{\tau_d}(\tau_d){y_r^{\tau_d}}^2(\tau_d) - {x_r^{\tau_d}}^2(\tau_d)y_r^{\tau_d}(\tau_d)}{x_r^{\tau_d}(\tau_d)^2 + y_r^{\tau_d}(\tau_d)^2}\dot{\tau}_d := \bar{w}_r(\tau_d)\dot{\tau}_d \end{cases} \tag{4.19}$$

Before going on with the controller design, we first give the following assumptions for the desired geometric path.

Assumption 4.3.1 *The following assumptions are hold throughout for path tracking.*

- *Uniqueness*

  For each value of path parameter τ, there exists a unique value of $x_r(\tau)$ and $y_r(\tau)$. It means the unique solvability of one path from its parameter.

- *Regularity*

$$0 < \sqrt{x_r^\tau(\tau)^2 + y_r^\tau(\tau)^2} < k$$

It means that the desired path is regularly parameterized. For any non-regular path, it can be split into piecewise regular paths. This is also the case of point-to-point navigation, where regular curve segments connect desired points in sequence.

- *Persistent excitation.*

$$\lim_{t\to\infty} \dot{\tau}(t) \neq 0$$

The path parameter is persistently excited, which means the TT target on the path always moves. Therefore, the path tracking problem will not degenerate into point stabilization problem.

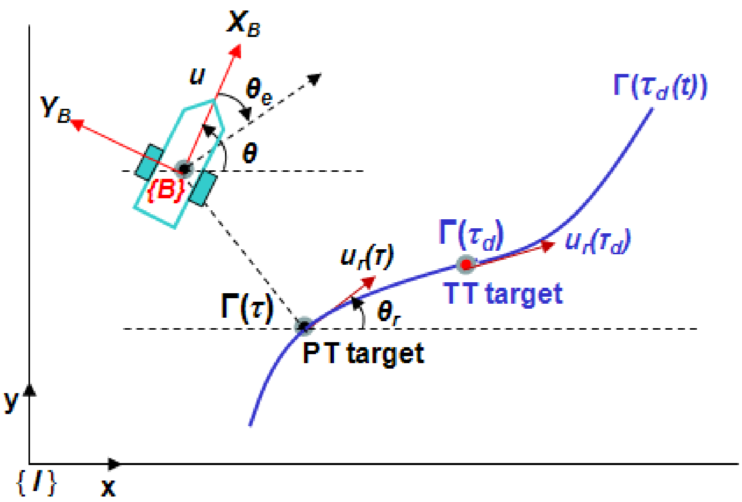

Figure 4.4 – Path tracking of nonholonomic autonomous vehicle

For the problem of path tracking shown in Figure. 4.4, there are two assignments assembled in the sense that :

(1) Geometric assignment :
requests that the position and orientation of the vehicle coincides with those of the PT target moving on the path $\Gamma(\tau)$, such that the vehicle tracks the PT target and its linear velocity is tangential to the path ;

(2) Dynamic assignment :
demands the speed of the PT target $\dot{\tau}(t)$ to respect the given speed assignment imposed on the TT target as $\dot{\tau}_d(t)$, and demands the PT target to catch up with the TT target.

Notice that the speed assignment is assigned to the path parameter $\tau_d(t)$ in path tracking, whereas the speed assignment $u_d(t)$ is assigned to the vehicle in path following. In Figure. 4.4, τ, τ_d is the virtual and desired path parameter respectively, where τ has a beneficial property to introduce the tracking error feedback for path tracking to wait (by slowing down) or catch (by speeding up) the vehicle.

Therefore, the control objective of path tracking is to design a controller and achieve the following tasks :

$$\begin{aligned} &\lim_{t\to\infty} \|\mathbf{p}_{eB}\| = 0 \\ &\lim_{t\to\infty} |\tau(t) - \tau_d(t)| = 0,\ \lim_{t\to\infty} |\dot{\tau}(t) - \dot{\tau}_d(t)| = 0 \end{aligned} \tag{4.20}$$

where $P_{eB} = (x_e, y_e, \theta_e)^T$ is the tracking error vector built in vehicle body frame $\{B\}$, and $\dot{\tau}_d(t)$ is the desired speed assignment for the actual target moving along the path. Apparently, the first term in (4.20) declares the geometric assignment of path tracking, and the second term declares the dynamic assignment.

4.3.2 Controller design

Similarly to the path following control design, we introduce the approaching angle $\delta(y_e, \dot{\tau}_d)$ to shape the desired orientation during transient path tracking behavior, such that

$$\begin{cases} \delta(0, \dot{\tau}_d) = 0 \\ -y_e \dot{\tau}_d \sin\delta \geq 0 \end{cases} \tag{4.21}$$

Thus, the function $\delta(y_e, \dot{\tau}_d)$ can be chosen as a sigmoid function

$$\delta(y_e, \dot{\tau}_d) = -sign(\dot{\tau}_d)\theta_a \tanh(k_\delta y_e) \tag{4.22}$$

where the shaping coefficient $k_\delta > 0$, $0 < \theta_a < \pi/2$, and $sign(\cdot)$ is the sign function.

The Control Lyapunov function is selected as new one in a positive definite quadratic form

$$V = \frac{1}{2}[x_e^2 + y_e^2 + \frac{1}{\gamma}(\theta_e - \delta)^2 + k_\tau(\tau - \tau_d)^2] \tag{4.23}$$

where τ, τ_d is the actual and desired path parameter respectively, and $\lim_{t\to\infty} \dot{\tau}_d \neq 0$.

The time derivative of (4.23) along the solution of (4.19) is

$$\begin{aligned} \dot{V} =& x_e(y_e\omega - u + u_r\cos\theta_e) + y_e(-x_e\omega + u_r\sin\theta_e) + \frac{1}{\gamma}(\theta_e - \delta)(\dot{\theta}_e - \dot{\delta}) + k_\tau(\tau - \tau_d)(\dot{\tau} - \dot{\tau}_d) \\ =& -x_e u + u_r x_e\cos\theta_e + u_r y_e\sin\theta_e + \frac{1}{\gamma}(\theta_e - \delta)(\dot{\theta}_e - \dot{\delta}) + k_\tau(\tau - \tau_d)(\dot{\tau} - \dot{\tau}_d) \end{aligned}$$

Adding $u_r y_e \sin\delta - u_r y_e \sin\delta$ to above equation, there is

$$\dot{V} = -x_e u + u_r x_e\cos\theta_e + u_r y_e\sin\delta + \frac{1}{\gamma}(\theta_e - \delta)(\dot{\theta}_e - \dot{\delta} + \gamma u_r y_e\frac{\sin\theta_e - \sin\delta}{\theta_e - \delta}) + k_\tau(\tau - \tau_d)(\dot{\tau} - \dot{\tau}_d)$$

In order to introduce the tracking error feedback, define the auxiliary variable $\tilde{\tau}$, such that :

$$\dot{\tilde{\tau}} = \dot{\tau} - v_\tau(t, x_e, y_e, \theta_e) \tag{4.24}$$

where $\dot{\tilde{\tau}}$ can be considered as speed disagreement variable of path tracking.

Substituting (4.16), (4.17) and (4.24) into the derivative of Lyapunov control function, yields

$$\begin{aligned}\dot{V} =& x_e(\bar{u}_r\dot{\tau}\cos\theta_e - u) + y_e\bar{u}_r\dot{\tau}\sin\delta + \frac{1}{\gamma}(\theta_e - \delta)(\dot{\theta}_e - \dot{\delta} + \gamma\bar{u}_r\dot{\tau}y_e\frac{\sin\theta_e - \sin\delta}{\theta_e - \delta})\\
&+k_\tau(\tau - \tau_d)(\dot{\tilde{\tau}} + v_\tau - \dot{\tau}_d)\\
=& x_e(\bar{u}_r v_\tau\cos\theta - u) + y_e\bar{u}_r v_\tau\sin\delta + \dot{\tilde{\tau}}[x_e\bar{u}_r\cos\theta_e + y_e\bar{u}_r\sin\theta_e + \frac{1}{\gamma}(\theta - \delta)\bar{\omega}_r]\\
&+\frac{1}{\gamma}(\theta_e - \delta)(\bar{\omega}_r v_\tau - \omega - \dot{\delta} + \gamma y_e\bar{u}_r v_\tau\frac{\sin\theta_e - \sin\delta}{\theta_e - \delta}) + k_\tau(\tau - \tau_d)(\dot{\tilde{\tau}} + v_\tau - \dot{\tau}_d)\end{aligned}$$

Proposing the control input as

$$\begin{bmatrix} u \\ \omega \end{bmatrix} = \begin{bmatrix} k_x x_e + \bar{u}_r v_\tau\cos\theta_e \\ \bar{\omega}_r v_\tau - \dot{\delta} + \gamma y_e\bar{u}_r v_\tau\frac{\sin\theta_e - \sin\delta}{\theta_e - \delta} + k_\theta(\theta_e - \delta) \end{bmatrix} \tag{4.25}$$

and choosing

$$\begin{bmatrix} v_\tau \\ \dot{\tilde{\tau}} \end{bmatrix} = \begin{bmatrix} \dot{\tau}_d \\ -k_v\tanh[x_e\bar{u}_r\cos\theta_e + y_e\bar{u}_r\sin\theta_e + \frac{1}{\gamma}(\theta_e - \delta)\bar{\omega}_r + k_\tau(\tau - \tau_d)] \end{bmatrix} \tag{4.26}$$

and utilizing the first element in (4.16), yields

$$\dot{V} = -k_x x_e^2 - k_v\Phi_e\tanh(\Phi_e) + y_e\bar{u}_r\dot{\tau}_d\sin\delta - \frac{k_\theta}{\gamma}(\theta_e - \delta)^2 \tag{4.27}$$

where $\Phi_e := x_e\bar{u}_r\cos\theta_e + y_e\bar{u}_r\sin\theta_e + \frac{1}{\gamma}(\theta_e - \delta)\bar{\omega}_r + k_\tau(\tau - \tau_d)$ for simplified notation.

Replacing (4.24) into the combination of (4.25) and (4.26), yields the control laws for path tracking

$$\begin{bmatrix} u \\ \omega \\ \dot{\tau} \end{bmatrix} = \begin{bmatrix} k_x x_e + \bar{u}_r\dot{\tau}_d\cos\theta_e \\ \bar{\omega}_r\dot{\tau}_d - \dot{\delta} + \gamma y_e\bar{u}_r\dot{\tau}_d\frac{\sin\theta_e - \sin\delta}{\theta_e - \delta} + k_\theta(\theta_e - \delta) \\ \dot{\tau}_d - k_v\tanh(\Phi_e) \end{bmatrix} \tag{4.28}$$

The first two elements in (4.28) are the kinematic control inputs of the vehicle, and the third element is the additional control input for the speed updating law of path parameter τ , which is related to the speed of the virtual target moving on the path defined in (4.16).

Moreover, $\dot{\tau}$ is critical for path tracking, as it has the freedom to speed up or slow down according to the tracking error feedback $k_v\tanh(\Phi_e)$.

Proposition 4.3.2 (Path tracking 1 : unicycle type vehicle)

Under assumption 4.3.1 for a predefined $\mathcal{C}^1$ path given in (4.14) with desired speed $\dot{\tau}_d(t)$ for the time derivative of path parameter $\tau_d(t)$, the kinematic control inputs u and ω, and the virtual control input $\dot{\tau}$ expressing time evolution law for path parameter given in (4.28). The control objective (4.20) of path tracking is achieved and the equilibrium point $[x_e, y_e, \theta_e, (\tau - \tau_d)]^T = 0^4$ is globally asymptotically stable.

Proof The control Lyapunov function V is positive definite and radially unbounded from(4.23). Notice $y_e\bar{u}_r\dot{\tau}_d \sin\delta \leq 0$ in (4.27) as δ is chosen as a sigmoid function in (4.22). The path is regular such that $0 < \bar{u}_r(\tau) < k$ as $\bar{u}_r = \sqrt{x_d^\tau(\tau)^2 + y_d^\tau(\tau)^2}$. Therefore, $\dot{V} \leq 0$ is semi-negative definite. We have

$$0 \leq V(t) \leq V(t_0), t \geq t_0$$

such that all the signals $x_e(t), y_e(t), \theta_e(t) - \delta(t), \tau(t) - \tau_d(t)$ constituting $V(t)$ are bounded. $\delta(t)$ is sigmoid function such that $\theta_e(t)$ is bounded. In addition, $\dot{\tau}_d(t)$ is assumed bounded, yielding that $\dot{\tau}(t)$ is bounded by directly checking the third element in (4.28). Due to the boundedness of these signals and that of vehicle velocity, revisiting (4.18) , $\dot{x}_e, \dot{y}_e, \dot{\theta}_e$ are also bounded. Furthermore, noticing the boundedness of δ and Φ_e, directly computing the derivative of (4.27), we can conclude the second derivative $\ddot{V}(t)$ exists and is bounded. Resorting to the Barbalat's Lemma, it follows

$$\lim_{t\to\infty} \dot{V}(t) = 0$$

Therefore, $x_e, \Phi_e, y_e\bar{u}_r\dot{\tau}_d \sin\delta, (\theta_e - \delta)$ vanish as $t \to \infty$.

As δ is given as a sigmoid function in (4.22), $\lim_{t\to\infty} y_e\bar{u}_r\dot{\tau}_d \sin\delta \to 0$ means that $\lim_{t\to\infty} \bar{u}_r|\dot{\tau}_d|y_e^2 \to 0$. The path is persistent exciting such that $\lim_{t\to\infty} \dot{\tau}_d \neq 0$, and $0 < \bar{u}_r < k$. Hence, $\lim_{t\to\infty} y_e \to 0$. It follows $\lim_{t\to\infty} \delta \to 0$, such that $\lim_{t\to\infty} \theta_e \to 0$ as $\lim_{t\to\infty}(\theta_e - \delta) \to 0$. We can conclude that

$$\lim_{t\to\infty} \|P_{eB}\| = \lim_{t\to\infty} \sqrt{x_e^2 + y_e^2 + \theta_e^2} \to 0$$

which fulfils the first control objective in (4.20).

On the other hand, due to $\lim_{t\to\infty} \|P_{eB}\| \to 0$, and $\lim_{t\to\infty} \Phi_e \to 0$ where $\Phi_e = x_e\bar{u}_r \cos\theta_e + y_e\bar{u}_r \sin\theta_e + \frac{1}{\gamma}(\theta_e - \delta)\bar{\omega}_r + k_\tau(\tau - \tau_d)$, it follows that

$$\lim_{t\to\infty} |\tau(t) - \tau_d(t)| \to 0$$

Moreover, as $\lim_{t\to\infty} \Phi_e \to 0$, $\dot{\bar{\tau}} = -k_v \tanh(\Phi_e)$ and $\dot{\tau} = \dot{\bar{\tau}} + v_\tau$, there is

$$\lim_{t\to\infty} |\dot{\tau}(t) - \dot{\tau}_d(t)| \to 0 \tag{4.29}$$

It means the autonomous vehicle eventually moves along the path according to the desired speed assignment $\dot{\tau}_d(t)$. Consequently, it meets the second control objective in (4.20). $\blacksquare$

Path tracking features :

- Blending path following into trajectory tracking

  By choosing proper positive gain k_v in the speed control of virtual target, we can designate its moving behavior by

$$\dot{\tau} = \dot{\tau}_d - k_v \tanh(\Phi_e) \tag{4.30}$$

  If the total tracking error Φ_e is positive, the evolution speed of the PT target $\dot{\tau}$ will slow down (less than the evolution speed of the TT target), such that the PT target will "wait" for the vehicle although the TT target will move at its own will ; otherwise, the PT target will speed up in order to catch up the vehicle. It means the path tracking has similar property with the path following in this aspect.

  Interestingly, path tracking behaviors like trajectory tracking, when the tracking error Φ_e tends to zero such that $\dot{\tau} = \dot{\tau}_d - k_v \tanh \Phi_e = \dot{\tau}_d$, i.e., the vehicle moves at the same speed of the predefined one of the virtual target. It means the initial path following-like behavior will evolve into the trajectory tracking-like behavior eventually. Therefore, path tracking strategy tries to keep the trajectory tracking performance with respect to time as possible as it can be achieved, while possible unreachable tracking state due to speed saturation can be rejected and smoother convergence is achieved owing to the benefit of path following control.

  This feature indicates that path tracking can be considered as a behavior evolving from path following to trajectory tracking. It is different from the work of Hindman [Hindman and Hauser, 1996] and Encarnacao [Encarnacao and Pascoal, 2001], where maneuvering modified trajectory tracking (MMTT) is considered as a behavior evolving from trajectory tracking to path following. The interesting point is that the path tracking algorithm is more easier to be implemented, compared with the algorithm from trajectory tracking to path following.

- Dealing with speed saturation

  In (4.28), the tracking speed of the vehicle is given as

$$u = k_x x_e + \bar{u}_r \dot{\tau}_d \cos \theta_e \tag{4.31}$$

  Actually, the vehicle speed u is upper bounded due to the physical limitation of actuators. In order to avoid an infeasible speed given to u when the initial along-track error x_e is very large, we can use the saturation function to bound the tracking error x_e, for instance, let

$$u = k_x \tanh(x_e) + \bar{u}_r \dot{\tau}_d \cos\theta_e \tag{4.32}$$

we still have $\dot{V} = -k_x x_e tanh(x_e) - k_v \Phi_e \tanh \Phi_e + y_e \bar{u}_r \dot{\tau}_d \sin\delta - \frac{k_\theta}{\lambda}(\theta_e - \delta)^2 \leq 0$ to guarantee the convergence of the system state trajectories.
Now the first element of the tracking speed $k_1 \tanh(x_e)$ is bounded. In order to bound $\bar{u}_r \dot{\tau}_d$, we can fix $\bar{u}_r \dot{\tau}_d = u_d$ ($u_d < u_{max}$) and leave the desired speed $\dot{\tau}_d$ be time-varying for the virtual target, as done in [Skjetne et al., 2005].
Note that, $u_d < u_{max}$ ***means the speed of the target is less than the maximum speed of the vehicle, such that the vehicle is able to catch up with the TT target.***
Furthermore, if we choose $0 < k_1 < u_d, u_{min} < u_d + k_1 < u_{max}$ where u_{min}, u_{max} is the minimum and the maximum speed of the vehicle respectively. Then, the actual tracking speed $|u| < u_{max}$ is bounded under the physical limitation of the vehicle.

- Filtered path parameter updating
Actually, the updating law of path parameter in path tracking controller (4.30) can be described as

$$\begin{cases} \dot{\tau} = \dot{\tau}_d + \omega_\tau \\ \omega_\tau = -k_\tau \tanh(\Phi_e) \end{cases} \tag{4.33}$$

Obviously, this updating law for path parameter $\omega_\tau(t)$ during path tracking is a static updating function.
However, there is an alternative dynamic method to the static design for updating the path parameter. As pointed out in [Skjetne et al., 2002], practical experience shows that the dynamic filtered updating law brings an improved numerical response for static updating of $\dot{\tau}(t)$ in the presence of measurement noise. We can instead apply a filtered design inspired by the work of [Skjetne et al., 2002, Skjetne et al., 2004, Skjetne et al., 2005], to dynamically update the path parameter $\tau(t)$.
The path tracking control Lyapunov function V is augmented to construct a 1^{st} order $\dot{\omega}_s$ update law as follows

$$V_F = V + \frac{1}{2\lambda\mu}\omega_\tau^2, \ \lambda > 0, \mu > 0 \tag{4.34}$$

Recalling (4.27), its time-derivative along the solution (4.15) is

$$\begin{aligned}\dot{V}_F =&\dot{V} + \frac{1}{\lambda\mu}\omega_\tau\dot{\omega}_\tau \\ =&-k_x x_e^2 + y_e u_r \sin\delta - \frac{k_\theta}{\gamma}(\theta_e-\delta)^2 + \Phi_e\omega_\tau + \frac{1}{\lambda\mu}\omega_\tau\dot{\omega}_\tau \\ =&-k_x x_e^2 + y_e u_r \sin\delta - \frac{k_\theta}{\gamma}(\theta_e-\delta)^2 + \omega_\tau(\Phi_e + \frac{1}{\lambda\mu}\dot{\omega}_\tau)\end{aligned} \tag{4.35}$$

The last term becomes negative by setting

$$\dot{\omega}_\tau = -\lambda(\omega_\tau + \mu\Phi_e) \tag{4.36}$$

resulting in

$$\dot{V}_F = -k_x x_e^2 + y_e u_r \sin\delta - \frac{k_\theta}{\gamma}(\theta_e-\delta)^2 - \frac{1}{\mu}\omega_\tau^2 \tag{4.37}$$

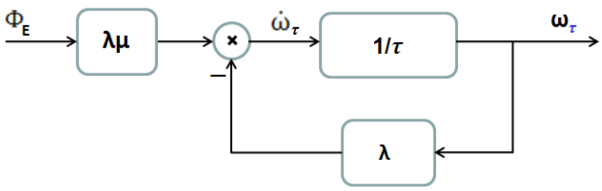

Figure 4.5 – Second order filtered updating law for path parameter

The dynamic version of a 2nd order path updating law now is constructed as

$$\begin{cases}\dot{\tau} = \dot{\tau}_d + \omega_\tau \\ \dot{\omega}_\tau = -\lambda\omega_\tau - \lambda\mu\Phi_e\end{cases} \tag{4.38}$$

The new updating law (4.38), is called a filtered updating law, because the path update term is filtered in the Laplace domain by $\omega_\tau(\tau) = -H(\tau)\tau(\tau)$, where $H(\tau) = \mu\frac{\lambda}{\tau+\lambda}$ is a stable single-input single-output(SISO) transfer function, shown in Figure. 4.5. The cut-off frequency λ of this filter is used to mitigate state measurement noise versus bandwidth.
For the differential equation,

$$\dot{\omega}_\tau = -\lambda\omega_\tau - \lambda\mu\Phi_e$$

the solution is

$$\omega_\tau(t) = [\omega_\tau(0) + \mu\Phi_e]e^{-\lambda t} - \mu\Phi_e$$

Consequently, if there is no state measurement noise, one can increase λ, and the solution $\omega_\tau = -\mu\Phi_e$ as $\lambda \to \infty$. In this case, dynamic path parameter updating law

(4.38) degenerated into the static version as $\dot{\tau} = \dot{\tau}_d - \mu\Phi_e$. However, it is different from the bounded static version without filter as $\dot{\tau} = \dot{\tau}_d - k_\tau \tanh(\Phi_e)$, where the virtual target can always moving forward by using the saturation function and chosing $0 < k_\tau < \max(\dot{\tau}_d)$. Clearly, $\dot{\tau} = \dot{\tau}_d - \mu\Phi_e < 0$ is possible if $\mu\Phi_e$ is large enough. It means the virtual target will move backward to comply with the actual vehicle's motion because of large tracking error.
Hence, the dynamic updating law (4.38) can be considered as a more relaxed version compared with the bounded static path parameter updating law (4.33), where the virtual target always moving forward can slow down its speed to wait for the vehicle, is more tightly approaching the trajectory tracking-like behavior in the sense of fulfilling time constraints and keeping time performance in the control loop. The caveat of filtered path parameter updating, is higher order resulted in the path tracking controller than that in static updating law [Skjetne et al., 2002].

4.3.3 Backstepping Dynamics

Let u and ω be virtual control inputs, α_u and α_ω in (4.28) be the corresponding virtual control laws. Introduce the velocity error variables

$$z = \begin{pmatrix} z_u \\ z_\omega \end{pmatrix} = \begin{pmatrix} u - \alpha_u \\ \omega - \alpha_\omega \end{pmatrix}$$

Consider the Lyapunov function V in (4.23), augmented with the quadratic terms of z_u and z_r, that is

$$V_{dyn} = V + \frac{1}{2} z^T M z \tag{4.39}$$

The time derivative of V_{dyn} can be written as

$$\begin{aligned}
\dot{V}_{dyn} &= x_e(\bar{u}_r v_\tau \cos\theta_e - u) + y_e \bar{u}_r v_\tau \sin\delta + \dot{\tilde{\tau}}[x_e \bar{u}_r \cos\theta_e + y_e \bar{u}_r \sin\theta_e + \frac{1}{\gamma}(\theta_e - \delta)\bar{\omega}_r + k_\tau(\tau - \tau_d)] \\
&\quad + \frac{1}{\gamma}(\theta_e - \delta)(\bar{\omega}_r v_\tau - \omega - \dot{\delta} + \gamma y_e \bar{u}_r v_\tau \frac{\sin\theta_e - \sin\delta}{\theta_e - \delta}) + k_\tau(\tau - \tau_d)(v_\tau - \dot{\tau}_d) + m z_u \dot{z}_u + I z_\omega \dot{z}_\omega \\
&= x_e(\bar{u}_r v_\tau \cos\theta_e - z_u - \alpha_u) + y_e \bar{u}_r v_\tau \sin\delta + \dot{\tilde{\tau}}[x_e \bar{u}_r \cos\theta_e + y_e \bar{u}_r \sin\theta_e + \frac{1}{\gamma}(\theta_e - \delta)\bar{\omega}_r + k_\tau(\tau - \tau_d)] \\
&\quad + \frac{1}{\gamma}(\theta_e - \delta)(\bar{\omega}_r v_\tau - z_\omega - \alpha_\omega - \dot{\delta} + \gamma y_e \bar{u}_r v_\tau \frac{\sin\theta_e - \sin\delta}{\theta_e - \delta}) + k_\tau(\tau - \tau_d)(v_\tau - \dot{\tau}_d) + m z_u \dot{z}_u + I z_\omega \dot{z}_\omega
\end{aligned}$$

$$\begin{aligned}
\dot{V}_{dyn} &= x_e(\bar{u}_r v_\tau \cos\theta_e - \alpha_u) + y_e \bar{u}_r v_\tau \sin\delta + \dot{\tilde{\tau}}[x_e \bar{u}_r \cos\theta_e + y_e \bar{u}_r \sin\theta_e + \frac{1}{\gamma}(\theta_e - \delta)\bar{\omega}_r + k_\tau(\tau - \tau_d)] \\
&\quad + \frac{1}{\gamma}(\theta_e - \delta)(\bar{\omega}_r v_\tau - \alpha_\omega - \dot{\delta} + \gamma y_e \bar{u}_r v_\tau \frac{\sin\theta_e - \sin\delta}{\theta_e - \delta}) + k_\tau(\tau - \tau_d)(v_\tau - \dot{\tau}_d) + z_u(m\dot{z}_u - x_e) \\
&\quad + z_\omega[I\dot{z}_\omega - \frac{1}{\gamma}(\theta_e - \delta)]
\end{aligned}$$

Let the control laws for F and N be chosen as

$$\begin{cases} F = m\dot{u} = m\dot{\alpha}_u + x_e - k_3 z_u \\ N = I\dot{\omega} = I\dot{\alpha}_\omega + \frac{1}{\gamma}(\theta_e - \delta) - k_4 z_\omega \end{cases} \tag{4.40}$$

where $k_3,\ k_4$ are positive constants, and α_u, α_ω are given according to (4.28) as follows :

$$\begin{bmatrix} \alpha_u \\ \alpha_\omega \end{bmatrix} = \begin{bmatrix} k_x x_e + \bar{u}_r \dot{\tau}_d \cos\theta_e \\ \bar{\omega}_r \dot{\tau}_d - \dot{\delta} + \gamma y_e \bar{u}_r \dot{\tau}_d \frac{\sin\theta_e - \sin\delta}{\theta_e - \delta} + k_\theta(\theta_e - \delta) \end{bmatrix}$$

There is

$$\dot{V}_{dyn} = -k_x x_e^2 - k_s \Phi_e \tanh(\Phi_e) + y_e \bar{u}_r \dot{\tau}_d \sin\delta - \tfrac{k_\theta}{\gamma}(\theta_e - \delta)^2 - k_3 z_u^2 - k_4 z_\omega^2$$

That means, $\dot{V}_{dyn}$ is negative definite and all the states $(x_e, y_e, \theta_e, \Phi_e, z_u, z_\omega)$ globally asymptotically converge to its equilibrium. Moreover, it can be concluded that the equilibrium is $(x_e, y_e, \theta_e, (\tau - \tau_d), z_u, z_\omega) = 0^6$ from the Barbalat's lemma. Therefore, we can propose the following proposition for dynamic path tracking control. Note that $\lim_{t\to\infty} |\dot{\tau}(t) - \dot{\tau}_d(t)| \to 0$ is achieved as the same state in (4.29).

Proposition 4.3.3 (Path tracking 2 : unicycle type vehicle)

Under assumption 4.3.1 for a predefined C^1 path given in (4.14) with desired speed $\dot{\tau}_d(t)$ for the time derivative of the virtual path parameter $\tau(t)$, given the dynamics control inputs F and N in (4.40), and the virtual control input $\dot{\tau}$ in (4.28). The control objective (4.20) of path tracking is achieved and the equilibrium point $[x_e, y_e, \theta_e, (\tau - \tau_d)]^T = 0^4$ is globally asymptotically stable.

4.3.4 Transition between path tracking and trajectory tracking

This section illustrate how a control transition between path tracking and trajectory tracking is realized.

Checking the derivative of the Lyapunov candidate function in (4.27), there is

$$\dot{V} = -k_x x_e^2 - k_v \Phi_e \tanh(\Phi_e) + y_e \bar{u}_r \dot{\tau}_d \sin\delta - \frac{k_\theta}{\gamma}(\theta_e - \delta)^2 \tag{4.41}$$

Directly setting $k_v = 0$, is also one choice to make the close-loop system asymptotically stable by rendering $\dot{V} \leq 0$, as $\dot{V}$ in (4.27) can be simply rewritten as

$$\dot{V} = -k_x x_e^2 + y_e \bar{u}_r \dot{\tau}_d \sin\delta - \frac{k_\theta}{\gamma}(\theta_e - \delta)^2 \tag{4.42}$$

where $k_v = 0$ drives

$$\dot{\tilde{\tau}} = \dot{\tau} - \dot{\tau}_d = (\dot{\tau}_d - k_\tau \tanh\Phi_e) - \dot{\tau}_d = 0 \tag{4.43}$$

according to the third item in the control law (4.28).

Actually, $\dot{\tilde{\tau}} = 0$ means $\dot{\tau}(t) = \dot{\tau}_d(t)$ at any time instant t, so that the extra degree of $\dot{\tau}(t)$ in path tracking strategy is completely deprived. Consequently, path tracking reduces to trajectory tracking as the dynamic task is equivalent to a trajectory tracking design in the case of $\dot{\tau}(t) \equiv \dot{\tau}_d(t)$, and the control laws (4.28) become

$$\begin{bmatrix} u \\ \omega \end{bmatrix} = \begin{bmatrix} k_x x_e + u_r \cos\theta_e \\ \omega_r - \dot{\delta} + \gamma y_e u_r \frac{\sin\theta_e - \sin\delta}{\theta_e - \delta} + k_\theta(\theta - \delta) \end{bmatrix} \tag{4.44}$$

where $u_r = \bar{u}_r \dot{\tau}_d, \omega_r = \bar{\omega}_r \dot{\tau}_d$ as $\dot{\tau} = \dot{\tau}_d$.

Note that the trajectory tracking controller (4.44) is derived by building the tracking error dynamics in body frame $\{B\}$, which is different with the proposed one in (4.4) by building the error dynamics in target reference frame $\{F\}$ in section 4.1.

Hence, by directly setting $k_v = 0$ or $k_v \neq 0$, we can get the smooth transition of control laws for trajectory tracking or path tracking depending on the requirements of various tasks, where k_v determines whether the extra degree of freedom for $\tau(t)$ exists or not.

On the other hand, as we discussed in section 4.3.2, in the case of $k_v \neq 0$, when the tracking error Φ_e converges to zero such that $\dot{\tau} = \dot{\tau}_d$, i.e., the vehicle moves at the same speed of the predefined one for the TT target. It means path tracking evolves from path following-like behavior to trajectory tracking-like behavior. Therefore, path tracking controller tries to keep the trajectory tracking performance with respect to time as possible as it can achieve, and smoother convergence is achieved as the benefit of path following control.

4.4 Motion control examples

Simulations results are included to illustrate the dynamic behavior of the nonholonomic underactuated unicycle vehicle system and the proposed control laws for trajectory tracking, path following and path tracking described in this chapter.

Case 1 : Reference path : straight line

In this simulation, motion controllers of trajectory tracking, path following and path tracking in kinematics stage, are used for the comparison of three different types motion control. The reference path is a straight line, set as $x(\gamma) = \gamma, y(\gamma) = 0$ with $\dot{\gamma}(t) = 0.8m/s$.

All the initial conditions are the same for the trajectory tracking, path following and path tracking, there are :

the initial vehicle surge and angular speeds are $u(0) = 1.0ms^{-1}, r(0) = 0rads^{-1}$, and the initial posture is set as $x(0) = 20m, y(0) = -3m, \psi(0) = \pi/2$.

Moreover, the speed limitation $0 < u(t) < 1.2m/s$ and $-1.5\pi rad/s < r(t) < 1.5\pi rad/s$ are assumed in the simulation.

In the case of trajectory tracking, the controller (4.4) has been used for the trajectory tracking versus path following in Figure 1.12. Herein, the trajectory tracking controller (4.44) transited from path tracking controller (4.28) is used. The kinematics controller set up is shown in Table 4.4. Note that the trajectory tracking control parameters are the same as those in path tracking except $k_v = 0$, which reveals the smooth transition between path tracking and trajectory tracking.

In the first column of Figure 4.6, the spatial convergence of the path is compared through three sub-figures, where the trajectory tracking renders an aggressive convergence, the path following renders a smooth convergence, and path tracking has a compromise on spatial convergence as shown in the upper part of Figure 4.6(a), 4.6(c) and 4.6(e) respectively. In the lower part of these figures, all position errors relative to the virtual target in x, y-directions and yaw errors tend to zero asymptotically.

In the second column of Figure 4.6, the temporal performance is shown by comparing the relative posture between the vehicle and the actual target on the reference path, where both the trajectory tracking and path following achieve the temporal convergence, as all position errors relative to the actual target in x, y-directions and yaw errors at the same time instants tending to zero asymptotically in Figure 4.6(b) and 4.6(f). While path following do not need to respect the time specification, as there is only spatial assignment is required in path following control. Although the tracking error in y-direction and yaw error converge to zero due to the reference path is straight line, the tracking error in x-direction clearly holds as shown in Figure 4.6(d).

Case 2 : Reference path : sinusoid path

In this part, motion control of path tracking in dynamics stage is simulated, compared with the simulation results of trajectory tracking and path following illustrated in Figure 1.12. Hence, the same sinusoid path and initial conditions are used to show the path tracking control in dynamics stage.

The reference path : $x(\gamma) = 0, y(\gamma) = -6 + 6cos(0.04\pi\gamma)$ with $\dot{\gamma}(t) = 1.0m/s$.

Initial conditions : $u(0) = 1.0ms^{-1}, r(0) = 0rads^{-1}$, $x(0) = 10m, y(0) = -15m, \psi(0) = \pi/2$.

The speed limitation $0 < u(t) < 1.2m/s$ and $-1.5\pi rad/s < r(t) < 1.5\pi rad/s$ are assumed in the simulation. The physical parameters of the unicycle-type vehicle are assumed as :

$$\begin{bmatrix} m \\ I \end{bmatrix} = \begin{bmatrix} 1.0kg \\ 1.0kg\ m^2 \end{bmatrix}$$

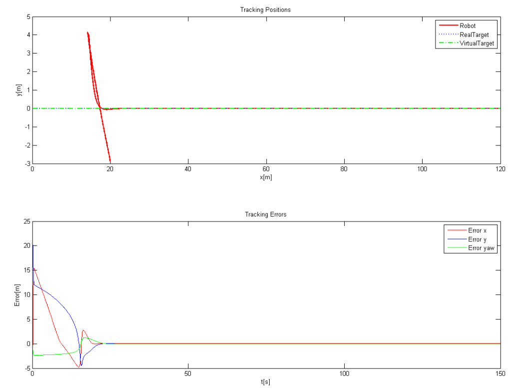

(a) Spatial convergence of trajectory tracking

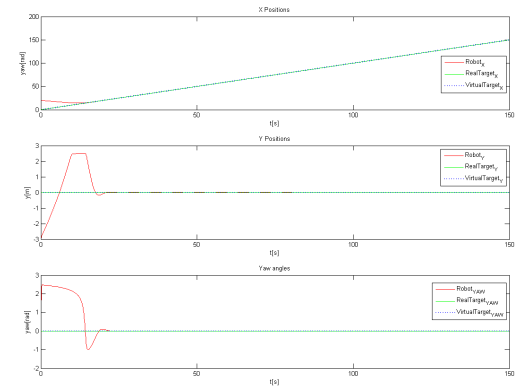

(b) Temporal convergence of trajectory tracking

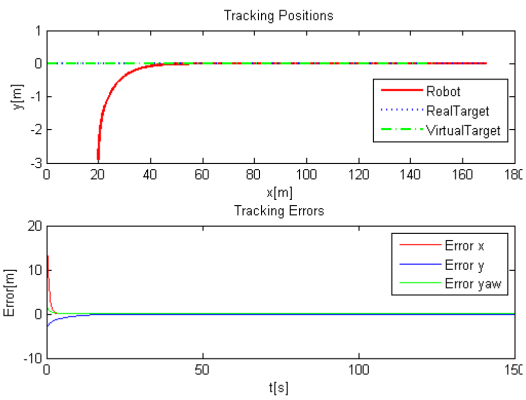

(c) Spatial convergence of path following

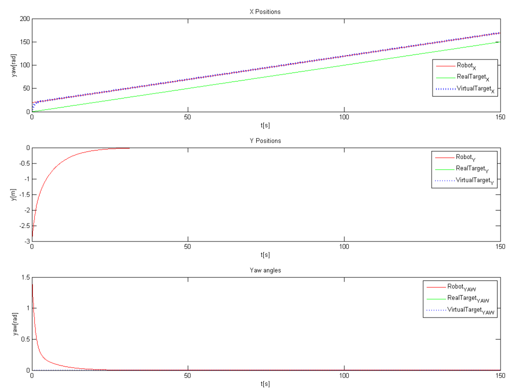

(d) Temporal convergence of path following

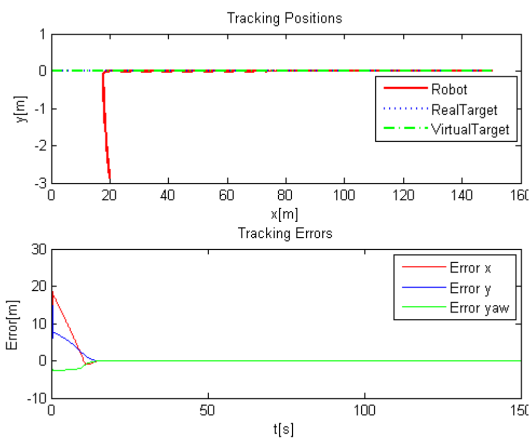

(e) Spatial convergence of path tracking

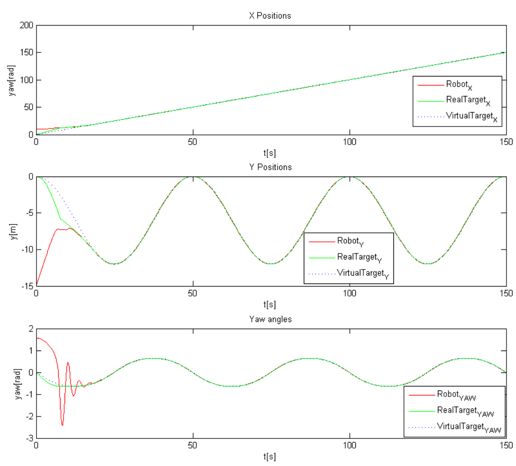

(f) Temporal convergence of path tracking

Figure 4.6 – Comparison of TT, PF & PT control : spatial and temporal convergence

Table 4.1 – Control parameters of three motion controllers

	Trajectory Tracking	Path Following	Path Tracking
Controller	(4.44) [a]	(4.11)	(4.28)
Control parameters			
k_x	1.5	1.5	1.5
k_θ	1.0	1.0	1.0
γ	1.0	–	1.0
k_τ	0.5	–	0.5
k_v	0 [b]	–	0.6
Heading parameters			
θ_a	$\pi/2$	$\pi/2$	$\pi/2$
k_δ	0.1	0.1	0.1

[a] Trajectory tracking controller (4.44) is smoothly transited from path tracking controller (4.28).
[b] By setting $k_v = 0$, path tracking controller (4.28) is degenerated into trajectory tracking controller.

The control design parameters are displayed in Table 4.2.

Table 4.2 – Control parameters of sinusoid path tracking

$k_x = 1.5$	$k_\theta = 1.0$	$\gamma = 1.0$	$k_\tau = 0.5$	
$k_v = 0.6$	$k_3 = 1.0$	$k_4 = 1.0$	$\theta_a = \pi/2$	$k_\delta = 0.1$

In the upper part of Figure 4.7, the smooth spatial convergence is achieved by recalling Figure 1.12, and the tracking errors converge to zero asymptotically shown in the lower part. In Figure 4.8, the vehicle velocity profiles (forward and yaw speeds) converge to those of the TT target, and notice how the PT target change its speed to bridge the gap between the vehicle and the TT target. It clearly shows that the virtual target increase its forward speed when the vehicle is in advance of the actual target at the initial stage, and then slow down and lead the vehicle to move together with the actual target. In Figure 4.9, the temporal convergence is achieved as the vehicle coincides with the actual target after certain time instants. The control inputs, force and torque, are shown in Figure 4.10 by applying the dynamics control law in (4.40).

4.5 Summary

In this chapter, the nonlinear motion control design based on Lyapunov theory and backstepping technique are proposed. Namely, trajectory tracking, path following and

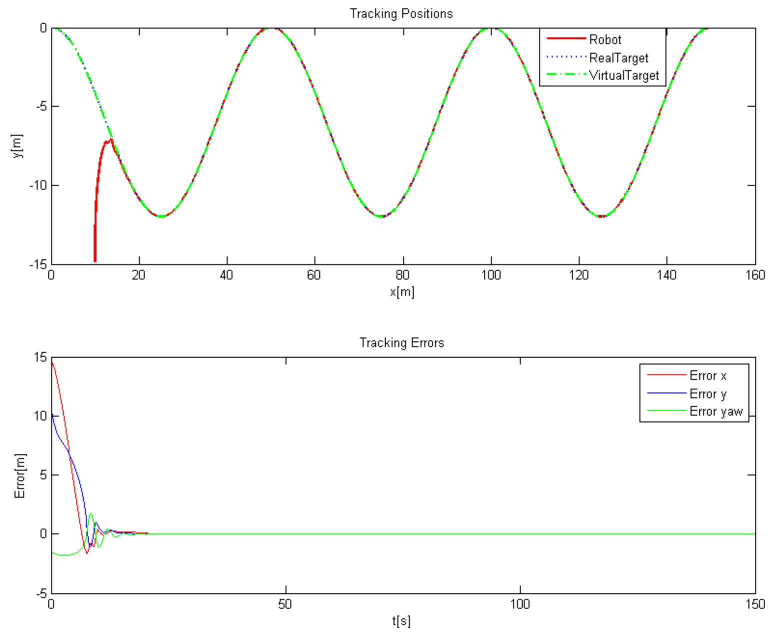

Figure 4.7 – Spatial convergence of path tracking

path tracking control problems are addressed for nonholonomic underactuated autonomous mobile vehicles. From the control objectives and corresponding control design procedure, we can conclude the exclusive characteristics of these three main kinds motion behaviors :

- Trajectory tracking :
  The trajectory is parameterized by time, which can be considered as generated by a virtual vehicle moving at certain velocity $[u(t), \omega(t)]^T$ of which is strictly constrained by time. The actual vehicle is passively tracks the virtual vehicle with stringent time constraints. Hence, trajectory tracking solves the geometric assignment (spatial convergence) and dynamic assignment (temporal limitation) together in a single task.
- Path following :
  The path is predefined and parameterized by along-path distance s, and an autonomous vehicle is requested to follow the path with predefined speed. A virtual target is introduced to collaboratively move along the path according to the vehicle's speed, to help the vehicle converging to the path. It means that the vehicle is active to do path following with predefined speed, while the virtual target moves on the path complying with the vehicle's speed to slow down and speed up. Hence, path following solves the geometric assignment (spatial convergence) primarily,

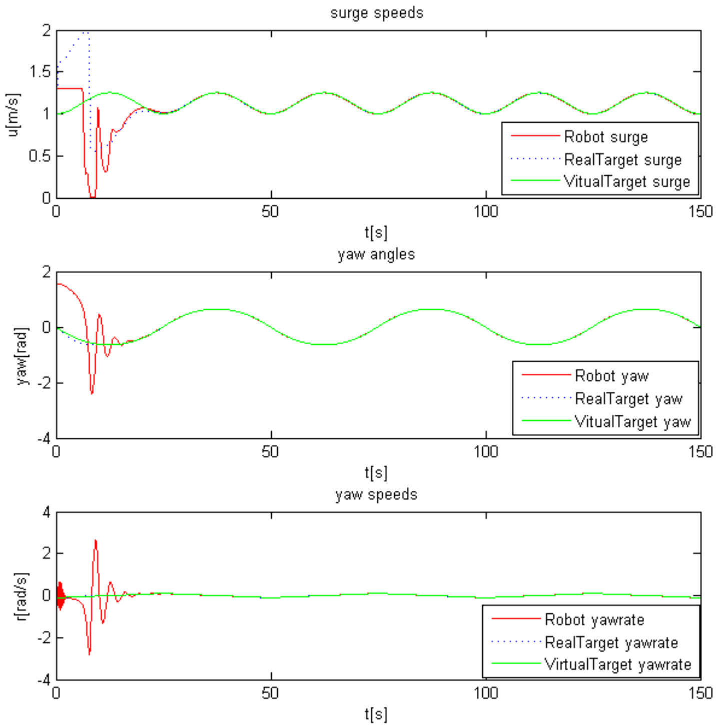

Figure 4.8 – Speed profile of path tracking

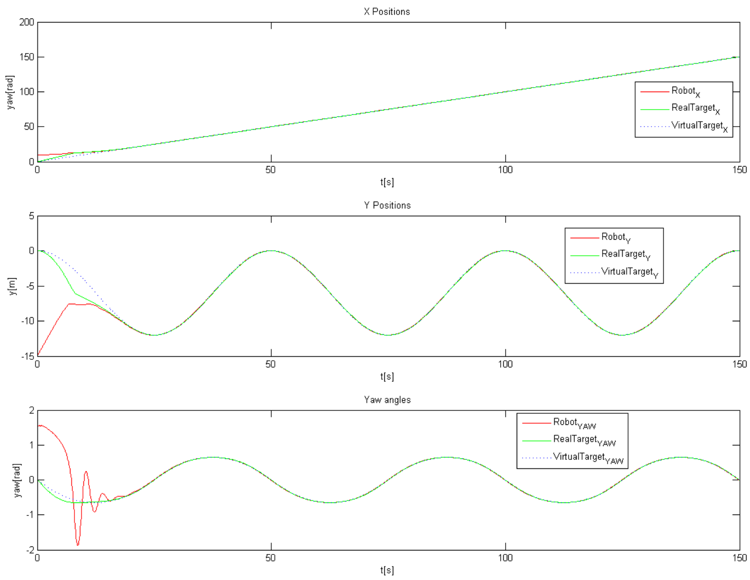

Figure 4.9 – Temporal convergence of path tracking

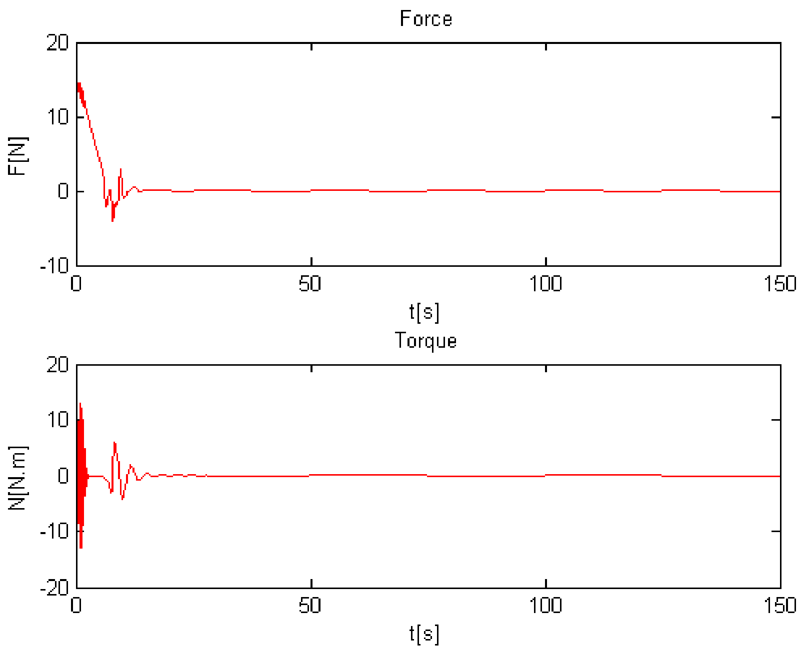

Figure 4.10 – Control efforts of path tracking

and the dynamic assignment (temporal limitation) is the secondary interest partially achieved by designating the desired speed of the vehicle.

- Path tracking :

  The path is parameterized by actual path parameter τ_d, pursuing the desired speed profile predefined by $\dot{\tau}_d(t)$ which is constrained by time instant. However, a virtual path parameter τ is introduced, and the evolution speed of the virtual path parameter $\dot{\tau}(t)$ has an extra degree of freedom, in order to comply with the status of the tracking vehicle. The actual and virtual path can be considered as one trajectory tracking target (TT target) and another path tracking target (PT target) moving along respectively. When the tracking error is large, the PT target will slow down or speed up to collaborate with the vehicle's movement, and path tracking is prone to path following-like behavior ; otherwise, under certain small tracking error, PT target will catch up with the TT target, and path tracking acts as trajectory tracking-like behavior to keep the temporal performance as possible as it can achieve. Therefore, the smoother spatial convergence is achieved and the temporal performance is guaranteed in the end.

Finally, the simulation results illustrate the efficiency of the proposed control laws, and the different characteristics among three motion control categories can be perceived therein.

Chapter 5

Motion control of single underactuated AUVs

In the previous chapter, the motion control problem is addressed for nonholonomic unicycle-type mobile vehicles. In this chapter, the solution is extended to motion control of path following and path tracking for underactuated AUVs in horizontal plane, based on the motion modeling and error dynamics of underactuated underwater vehicles described in section 3.1.3 and 3.3.2.3. Furthermore, smooth transitions from underactuated to fully actuated AUVs are proposed for both path following and path tracking control.

The main differences between the control design for nonholonomic unicycle vehicles and underactated AUVs, are listed as follows :

1. The side-slip angle β existing in underactuated AUV, results in that not only the total speed is required to align with the tangential direction of the path, but also leading to the difficulty in computation of acceleration of β, where the stern-dominancy property of underactuated vehicles is highlighted for well-posed control computation.
2. In the path following control design, the adapted Line-of-Sight (LOS) heading guidance with embedded helmsman behavior built in Frenet-Serret frame, is used for underwater vehicles instead of approaching angle guidance used for unicycle-type vehicle.
3. In the path tracking control design, the weighting factor is introduced in path tracking of AUVs, and the new control design with implicit heading guidance (neither explicit approaching angle or LOS) is adopted to simplify the derived controller.

5.1 Path following control of underactuated AUV

As it is shown in the comparison results of three motion control modes for nonholonomic unicycle-type mobile vehicles in section 4.4, trajectory tracking has a performance limitation due to the occurrence of aggressive maneuvers. Hence, for underactuated AUVs, only path following and path tracking control are studied, and trajectory tracking control is not addressed in this chapter.

5.1.1 Problem formulation

As depicted in Figure 5.1, an underactuated AUV follows a predefined spatial path S, P is an arbitrary point on the path to be followed, and Q is the center of mass of the moving vehicle. Associated with P, consider the corresponding Frenet-Serret frame $\{F\}$. The path S is parameterized by the moving target P on the path, with curvilinear abscissa (along path length) denoted by s. Let (x_e, y_e) denote the coordinates of Q in $\{F\}$, where the along-track error x_e represents the distance from vehicle to the desired position along the x-axis of the Frenet-Serret frame, and the cross-track error y_e represents the distance along the y-axis of the Frenet-Serret frame. Let the rotations from $\{I\}$ to $\{F\}$ and $\{I\}$ to $\{B\}$ be denoted by the yaw angles ψ_F and ψ_B, respectively. Furthermore, let $c_c(s)$ and $g_c(s)$ denote the path curvature and its spatial derivative respectively, and then $\dot{\psi}_F = c_c(s)\dot{s}, g_c(s) = \frac{\partial c_c(s)}{\partial s}$.

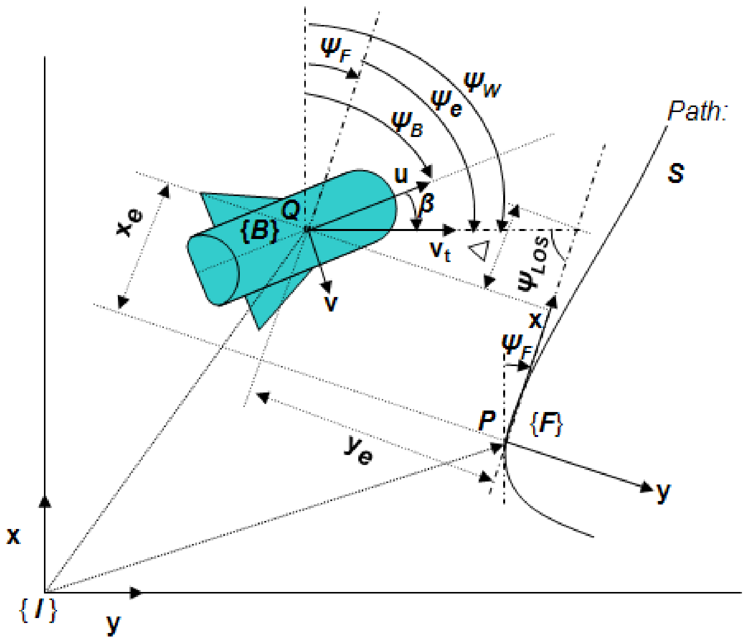

Figure 5.1 – Frame definitions of path following : underactuated AUV

Now, the problem of path-following control for underactuated AUV can be briefly stated as follows :

Given a spatial path S, develop feedback control laws for the surge forces and yaw torque acting on the underactuated underwater vehicle, such that its center of mass asymptotically converges to the path, while its total speed tracks a desired profile and aligns with the tangent vector of the path.

The solution to this problem is similar to that given in section 4.2 for nonholonomic unicycle-type vehicle, with some extra concerns for underactuated AUVs due to non-zero side-slip angle, and dedicated effort on the computation of its acceleration.

5.1.2 Controller design

Notice how the choice of a new frame simplifies the first two kinematic equations in (3.18) and brought out their similarities with those (3.13) of an underactuated unicycle vehicle. If the constraints are different between underactuated unicycle and AUV systems, the control inputs are the same : the forward and yaw speeds in kinematics stage and forward force and yaw torque in dynamics stage. This explains the connection between unicyle-type vehicle and AUV path following control design. The only difference is that the absence of a side thruster due to the underactuated design in the AUV system, making the total speed v_t resulted from both surge and sway components u, v. While the first-order nonholonomic constraint imposing on unicycle-type vehicle, make the total speed is permanently equal to its forward speed u.

Furthermore, as the desired path is parameterized by a virtual target P moving along path length denoted by s, the Frenet-Serret frame $\{F\}$ attached to $\{P\}$ can be chosen as the target frame. According to (3.36), the path following error vector $\mathbf{p}_{eF}$ built in the Frenet-Serret frame $\{F\}$ can be written as

$$\mathbf{p}_{eF} = \begin{bmatrix} x_e \\ y_e \\ \psi_e \end{bmatrix} = \begin{bmatrix} \cos\psi_F & \sin\psi_F & 0 \\ -\sin\psi_F & \cos\psi_F & 0 \\ 0 & 0 & 1 \end{bmatrix} \begin{bmatrix} x - x_F \\ y - y_F \\ \psi_W - \psi_F \end{bmatrix} \tag{5.1}$$

where $\psi_W = \psi_B + \beta$ and $r = \dot{\psi}_B$.

Replacing $\dot{\psi}_F = c_c(s)\dot{s}$ in (3.39), the error dynamics built in the target frame $\{F\}$, can be expressed as

$$\begin{bmatrix} \dot{x}_e \\ \dot{y}_e \\ \dot{\psi}_e \end{bmatrix} = \begin{bmatrix} -\dot{s}(1 - c_c y_e) + v_t cos\psi_e \\ -c_c\dot{s}x_e + v_t sin\psi_e \\ r + \dot{\beta} - c_c\dot{s} \end{bmatrix} \tag{5.2}$$

5.1.2.1 LOS heading guidance

Line-of-Sight (LOS) is a popular guidance method applied in marine surface vehicle system. Traditional LOS is built in the inertial frame and can be used for path following of straight-line constructed by way points [Fossen, 2002]. Herein, the LOS heading guidance is proposed for path following of underwater vehicles, in stead of approaching angle proposed for that of unicycle-type vehicle. However, the traditional LOS built in the inertial frame [Pettersen and Lefeber, 2001] [Fossen et al., 2003], is adapted and built in a moving Frenet-Serret frame, for underwater vehicles following both straight-line and curved path in this chapter.

In order to follow the desired path, the most important thing is to steer the vehicle with the right heading, and desired surge speed is arbitrary. However, the convergence performance towards the path could be quite different, depending on the situation whether a reasonable heading is chosen and a wise computerized 'helmsman' is onboard [Pettersen and Lefeber, 2001]. Classic LOS law for heading guidance is popularly applied to marine surface vehicles and ships for tracking straight-line path generated by given way-points during navigation [Fossen, 2002] [Fossen et al., 2003], and this method drives us on designing the heading guidance for underwater vehicle to track curved path here.

As depicted in Figure 5.2(a), the coordinate origin of the AUV is (x, y), and the LOS point on the straightline path is (x_{los}, y_{los}). Thus, the desired yaw angle under LOS guidance is

$$\psi_{los} = \arctan(\frac{y_{los} - y}{\Delta})$$

Originally, the control parameter $\Delta(> 0)$ is interpreted as the distance ahead of the ship along the x-axis, i.e. the straight-line path, which the ship should reach [Pettersen and Lefeber, 2001]. This important parameter, look ahead distance Δ (or so-called 'visibility distance' in the LOS strategy), is constant in LOS design, used to shape the vessel moving towards the straight-line path. Note that the straight-line path is perpendicular to y-axis in Figure 5.2(a), but it can be generalized to straight-line path with an arbitrary slope, and the generalized LOS angle is $\psi_{los} = \arctan(\frac{y_{los}-y}{x_{los}-x})$ as illustrated in [Fossen, 2002].

Unlike the traditional LOS built in the inertial frame for following straight-line in Figure 5.2(a), the LOS law is built in a moving Frenet-Serret frame and chosen as a heading guidance herein. When the AUV tracks arbitrary regular path (straight line or curved path), the parameter Δ is extended to look at the distance along the tangential path in Frenet-Serret frame as illustrated in Figure 5.2(b).

Elaborating more efforts on the heading design, Helmsman-like behavior is in-

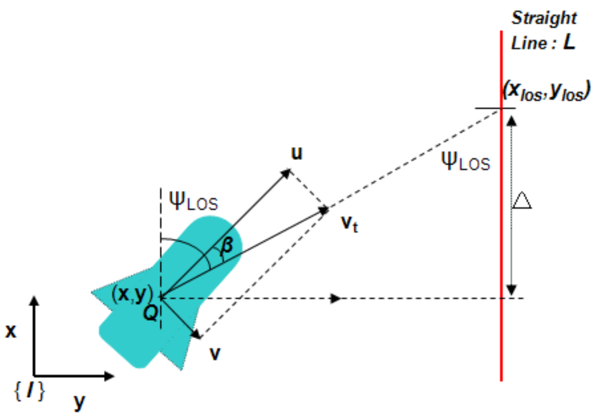

(a) Traditional LOS for straight line represented in Inertial frame {I}

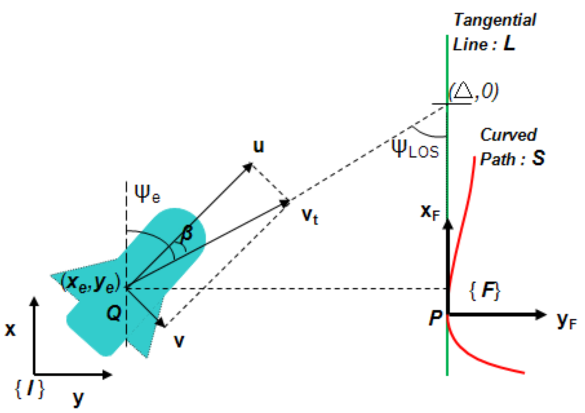

(b) Modified LOS for curved path represented in Frenet-Serret frame {F}

Figure 5.2 – Illustration for the LOS guidance in different frames

troduced. In order to steer a ship towards the straight line, a good helmsman will choose the magnitude of heading in function of the distance from the straight line [Fossen et al., 2003]. In order to follow an arbitrary curvilinear path, a wise helmsman on board is important. When the path has a small radius of the tangent osculating circle (i.e. large curvature in Frenet-Serret frame) at one point, a good helmsman will catch this information, and increase the heading to adhere to the sharp turning path at that moment. On the contrary, the heading guidance is decreased when the path is smooth. In this point of view, the LOS angle is adjusted by the helmsman when the path is not straight, so that Δ is a variable ($\Delta > 0$ and upper bounded). One solution is that, Δ can be a function of curvature $c_c(s)$.

Revisiting Figure 5.1, in the perfect case of ψ_e equal to the desired heading ψ_{los}, we can see that $\psi_e = \psi_W - \psi_F$ in the Frenet-Serret frame, is the corresponding LOS angle

ψ_{los} described in Figure 5.2(b). That means the guidance yaw angle can be defined as

$$\psi_{los} = \arctan(\frac{-y_e}{\Delta}) \tag{5.3}$$

or rather that

$$\psi_{los} = -\arcsin(\frac{y_e}{\sqrt{y_e^2 + \Delta^2}}) \tag{5.4}$$

and Δ can be given by

$$\Delta = 2L - L\text{sat}(k_0|c_c(s)|) \tag{5.5}$$

where $0 < k_0 < k_{0max}$, L is the longitudinal length of the vehicle, and sat$(\cdot)$ is the saturation function in $(-1, 1)$, such as $\tanh(\cdot)$, atan$(\cdot)$, etc. In the case of straight-line path where $c_c(s) = 0$, Δ is equal to two vehicle's length, which is corresponding to a standard choice in LOS algorithms .

As depicted in Figure 5.2(a), the LOS angle enables the vehicle to turn right ($y_{los} - y > 0$ such that $\psi_{los} > 0$) to follow the straight-line path, when it is on the left side of path, and turn left in the reversal situation. In the situation of arbitrary curved path in Figure 5.2(b), a wise helmsman will steer the vehicle onto the tangential path, and command a large Δ giving a mild approach to the smooth curve, while a small Δ brings more aggressive approach to the sharp curve. Explicitly, it is convenient for controller in the Frenet-Serret frame to provide the information of curvature, which means the helmsman behavior can be embedded in the path following design proposed in this chapter.

In a word, the heading reference under LOS guidance law with helmsman-like behavior illustrated in (5.3) is physically meaningful, driving the vehicle to turn sharper in advance where the path curvature will be larger. Moreover, as we can see later, the adapted LOS guidance is also instrumental in path following controller design to sharpen the convergence with ULES or UGES performance.

5.1.2.2 Kinematic controller

As the main objective of the path following control is to drive x_e, y_e an ψ_e to zero, the following Lyapunov function candidate can be considered

$$V_1 = \frac{1}{2}[x_e^2 + y_e^2 + (\psi_e - \psi_{los})^2] \tag{5.6}$$

Resorting to the error dynamics model (5.2), the derivative of V_1 is

$$\dot{V}_1 = -x_e\dot{s} + v_t s_1 cos\psi_e + v_t y_e sin\psi + (\psi_e - \psi_{los})(\dot{\psi}_e - \dot{\psi}_{los})$$

It is straightforward to show that the choice

$$\begin{cases} \dot{s} = k_1 x_e + v_t cos\psi_e \\ \dot{\psi}_e = \dot{\psi}_{los} - y_e v_t \frac{\sin\psi_e - \sin\psi_{los}}{\psi_e - \psi_{los}} - k_2(\psi_e - \psi_{los}) \end{cases} \tag{5.7}$$

where k_1 and k_2 are positive gains, lead to

$$\dot{V}_1 = -k_1 {x_e}^2 + y_e v_t \sin\psi_{los} - k_2(\psi_e - \psi_{los})^2$$

With the heading reference designed in (5.4), there is

$$\dot{V}_1 = -k_1 {x_e}^2 - \frac{v_t {y_e}^2}{\sqrt{{y_e}^2 + \Delta^2}} - k_2(\psi_e - \psi_{los})^2 \tag{5.8}$$

That means $\dot{V}_1 < 0$ anywhere except the origin.

On the other hand, as the error between the actual orientation and guidance LOS angle is $\dot{\psi}_e = r + \dot{\beta} - c_c\dot{s}$, the yaw rate in kinematics stage can be represented as :

$$r = \dot{\psi}_{los} - y_e v_t \frac{\sin\psi_e - \sin\psi_{los}}{\psi_e - \psi_{los}} - k_2(\psi_e - \psi_{los}) - \dot{\beta} + c_c\dot{s} \tag{5.9}$$

5.1.2.3 Dynamics controller

In the overall control loop, the kinematics controller acts as a reference subsystem, giving the desired signal to the control subsystem based on the dynamics level. Using backstepping techniques, the control law in kinematic level can be extended to deal with vehicle dynamics.

The underactuated AUV model adopted in this thesis, is based on the model and parameters of the SIRENE AUV, and more details about this AUV can be found in [Aguiar, 2001]. According to the standard motion model in (3.5), neglecting the motions in heave, roll and pitch, the simplified motion equations of SIRENE AUV in surge, sway and heading directions yield [Aguiar, 2001]

$$\begin{cases} \tau_u = m_u\dot{u} - m_v vr + d_u u \\ 0 = m_v\dot{v} + m_u ur + d_v v \\ \tau_r = m_r\dot{r} - m_{uv} uv + d_r r \end{cases} \tag{5.10}$$

where

$$\begin{aligned} m_u &= m - X_{\dot{u}} & d_u &= -X_u - X_{|u|u}|u| \\ m_v &= m - Y_{\dot{v}} & d_v &= -Y_v - Y_{|v|v}|v| \\ m_r &= I_z - N_{\dot{r}} & d_r &= -N_r - N_{|r|r}|r| \\ m_{uv} &= m_u - m_v \end{aligned}$$

I_z is the moment of inertia w.r.t. the z-axis. $m_{\{.\}}$ captures the effect of mass and hydrodynamic added mass terms, and $d_{\{.\}}$ captures the hydrodynamic damping effects [Aguiar, 2001]. τ_u and τ_r define the external force input in surge direction and torque input about the z axis of the AUV respectively, generated by the back thrusters. In these equations, and for clarity of presentation, it was assumed that the AUV is neutrally buoyant and that the center of buoyancy coincides with the center of mass. We can clearly see that there is no control input in the second equation in (5.10) due to the absence of thruster on sway direction, usually in an underactuated AUV system.

Assuming the desired forward speed of the AUV is known as u_d, it is easily to get the derivative of the actual forward speed $\dot{u}$ by

$$\dot{u} = \dot{u}_d - k_4(u - u_d) \tag{5.11}$$

where k_4 is an arbitrary positive gain.

Let r_d (desired yaw rate) be the reference signal of r (actual yaw rate), which derived from kinematic model. That means the desired yaw rate as a reference for dynamics controller can be written as :

$$r_d = \dot{\psi}_{los} - y_e v_t \frac{\sin\psi_e - \sin\psi_{los}}{\psi_e - \psi_{los}} - k_2(\psi_e - \psi_{los}) - \dot{\beta} + c_c\dot{s} \tag{5.12}$$

Then, applying backstepping technique, the difference between the actual yaw rate and the desired yaw rate, must be reduced to zero. This inspires us to design the Lyapunov candidate function :

$$V_2 = \frac{1}{2}[x_e^2 + y_e^2 + (\psi_e - \psi_{los})^2 + (r - r_d)^2] \tag{5.13}$$

With $\dot{x}_e$, $\dot{y}_e$ and $\dot{\psi}_e$ in error dynamics (5.2) and $\dot{s} = k_1 x_e + v_t cos(\psi_e)$ is given in kinematics formulation (5.7), the derivative of V_2 is

$$\dot{V}_2 = -k_1 x_e^2 + y_e v_t sin\psi_{los} + (\psi_e - \psi_{los})(\dot{\psi}_e - \dot{\psi}_{los}) + (r - r_d)(\dot{r} - \dot{r}_d)$$

Choose

$$\dot{r} = \dot{r}_d - k_3(r - r_d) - (\psi_e - \psi_{los}) \tag{5.14}$$

then

$$\dot{V}_2 = -k_1 x_e^2 + y_e v_t sin\psi_e + (\psi_e - \psi_{los})[(\dot{\psi}_e - \dot{\psi}_{los}) - (r - r_d)] - k_3(r - r_d)^2$$

As desired yaw rate is a reference signal from kinematic controller given in (5.12). After tedious calculation, we can get

$$\begin{aligned} \dot{V}_2 &= -k_1 x_e^2 - k_2(\psi_e - \psi_{los})^2 + y_e v_t sin\psi_{los} - k_3(r - r_d)^2 \\ &= -k_1 x_e^2 - k_2(\psi_e - \psi_{los})^2 - y_e^2 \frac{v_t}{\sqrt{y_e^2 + \Delta^2}} - k_3(r - r_d)^2 \end{aligned} \tag{5.15}$$

That means $\dot{V}_2 < 0$ anywhere except the origin.

Consequently, by using (5.7), (5.11) and (5.14), the control laws of virtual input $\dot{s}$ and input force and toque τ_u, τ_r are :

$$\begin{cases} \dot{s} = k_1 x_e + v_t cos\psi_e \\ \tau_u = m_u \dot{u} - m_v vr + d_u u = m_u(\dot{u}_d - k_4(u - u_d)) - m_v vr + d_u u \\ \tau_r = m_r \dot{r} - m_{uv} uv + d_r r = m_r(\dot{r}_d - k_3(r - r_d) - (\psi_e - \psi_{los})) - m_{uv} uv + d_r r \end{cases} \tag{5.16}$$

where $\tau_v = 0$ due to the underactuation in sway direction.

Proposition 5.1.1 (Path following : underactuated underwater vehicle)

Consider an underactuated underwater vehicle with the dynamics equations in (3.17) and (5.10). Assume $v_t \geq v_{tmin} > 0$ and the LOS heading guidance is given by (5.3). Let control laws be given by (5.16) for some $k_i > 0(i = 1, 2, 3, 4)$, the equilibrium point $(x_e, y_e, \psi_e) = 0^3$ is uniformly globally asymptotically and locally exponentially stable (UGAS&ULES).

Proof The Lyapunov function V_2 given by (5.13) is positive definite and radially unbounded. The derivative of Lyapunov function $\dot{V}_2$ given by (5.15) is negative definite as $v_t \geq v_{tmin} > 0$. Hence, by standard Lyapunov arguments, x_e, y_e, $(r - r_d)$, and $(\psi_e - \psi_{los})$ uniformly global asymptotically converge to 0. Recalling (5.3), ψ_{los} converges to y_e, and y_e converges to 0, such that ψ_e has the same characteristics with y_e, and also uniformly global asymptotically converges to 0 in the end.

For $|y_e| \leq \bar{y}_e$, there is $\frac{v_t}{\sqrt{{y_e}^2+\Delta^2}} \geq \frac{v_{tmin}}{\sqrt{\bar{y}_e^2+\Delta^2}} > 0$. By choosing $\min\{k_1, k_2, k_3, \frac{v_{tmin}}{\sqrt{\bar{y}_e^2+\Delta^2}}\} = k_{min}$, the derivative of Lyapunov function (5.15) becomes

$$\dot{V}_2 \leq -k_{min}[x_e^2 + y_e^2 + (\psi_e - \psi_{los})^2 + (r - r_d)^2] \leq -2k_{min} V_2$$

It means the derivative of the Lyapunov candidate function is quadratically negative definite. Hence, the equilibrium point $(x_e, y_e, \psi_e) = 0^3$, is uniformly locally exponentially stable (ULES), with convergent rate of $2k_{min}$, and the region of ULES depends on Δ. ∎

- **Remarks :**

1. Actually, this is a sharp solution to the traditional path following control, both on physic level (performance of helmsman like LOS heading guidance) and mathematic level (performance of convergence). In [Lapierre et al., 2003], only global asymptotically stability is guaranteed. With LOS guidance and helmsman like behavior embedded in the controller design, the performance of globally asymptotically and locally exponentially stable (ULES) achieved herein is indeed stronger.

2. The convergence performance of uniformly global asymptotically stable (UGES) is attainable, if the speed of the vehicle is chosen as

$$v_t = k_v \sqrt{{y_e}^2 + \Delta^2} \tag{5.17}$$

where $k_v > 0$. Then, the derivative of Lyapunov candidate is

$$\dot{V}_2 = -k_1 x_e^2 - k_2(\psi_e - \psi_{los})^2 - k_v y_e^2 - k_3(r - r_d)^2 \leq 2\text{min}\{k_1, k_2, k_3, k_v\}V_2$$

which results in UGES of the system. This is indeed a strong convergence performance, but it is constrained by the maximum available speed of the physical vehicle system, i.e., $\max(k_v\sqrt{{y_e}^2 + \Delta^2}) \leq v_{tmax}$ is required. Even in the case that this requirement is not fulfilled, ULES convergence still holds for the whole system.

5.1.3 Computation of side-slip angle

Clearly, $\ddot{\beta}$ is requested for control computation of torque input τ_r in (5.16) as $\dot{r}_d = f(\ddot{\beta})$ shown in (5.12), but the second derivative of side slip angle $\ddot{\beta}$ can not be directly measured in practice. Moreover, β is not directly controllable for underactuated AUV and can not converge to a desired side slip angle rigorously, as there is no lateral thruster contributing force to steer sway speed v in an underactuated AUV. It is different from the case of fully actuated AUV where β is controllable by the surge and sway forces and converges to a desired sideslip angle β_d. Therefore, one must resort to the original dynamic model of the AUV for the computation of $\beta, \dot{\beta}, \ddot{\beta}$. Furthermore, ***stern-dominant*** property of AUV is required during the computation of $\ddot{\beta}$.

As $v_t = \sqrt{u^2 + v^2}$, there is

$$\dot{v}_t = (u\dot{u} + v\dot{v})/\sqrt{u^2 + v^2} = (u\dot{u} + v\dot{v})/v_t$$

The side-slip angle $\beta = \arctan(v/u)$, such that

$$\dot{\beta} = (u\dot{v} - v\dot{u})/(u^2 + v^2) = (u\dot{v} - v\dot{u})/v_t^2 \tag{5.18}$$

Hence, the acceleration of side-slip angle is

$$\begin{aligned}\ddot{\beta} &= \frac{(\dot{u}v + u\ddot{v} - \dot{v}\dot{u} - v\ddot{u})v_t^2 - 2(u\dot{v} - v\dot{u})v_t\dot{v}_t}{v_t^4} \\ &= \frac{u\ddot{v} - v\ddot{u}}{v_t^2} - 2\frac{u\dot{v} - v\dot{u}}{v_t^3}\dot{v}_t\end{aligned}$$

Replacing (5.18) to above equation, there is

$$\ddot{\beta} = \frac{u\ddot{v} - v\ddot{u}}{v_t^2} - 2\frac{\dot{v}_t}{v_t}\dot{\beta} \tag{5.19}$$

Hence, in order to get $\ddot{\beta}$, the jerks $\ddot{u}$ and $\ddot{v}$ have to be prior-known. Actually, the jerks can not be directly measured. One possible way to solve this problem, is to compute $\ddot{u}$ through the desired forward speed information, while $\ddot{v}$ is computed by resorting to the AUV dynamics model.

Computation of jerk $\ddot{u}$

As the forward speed control is given by

$$\dot{u} = \dot{u}_d - k_4(u - u_d)$$

Thus, the jerk $\ddot{u}$ can be computed by the following equation :

$$\ddot{u} = \ddot{u}_d + k_4^2(u - u_d)$$

If the system is traveling with a constant forward speed, there is $\dot{u}_d = 0$ and $\ddot{u}_d = 0$. Hence, it makes above expression simpler since the desired acceleration term disappears.

Computation of jerk $\ddot{v}$

By using the dynamics model (5.10), there is

$$\ddot{v} = -(m_u \dot{u} r + m_u u \dot{r} + \dot{d}_v v + d_v \dot{v})/m_v \tag{5.20}$$

Thus, computing $\ddot{\beta}$ in (5.19) is converted into getting the knowledge of acceleration $\dot{r}$. We can simplify the computation procedure by revisiting the dynamic model,.

Actually, we can simplify the yaw rate control of AUV in (5.12), as we have done for unicycle-type vehicle by using LaSalle's invariance principle to concatenate three-step control design in section 4.2.2, i.e., firstly stabilize $(\psi_e - \psi_{los}) = 0$ by $V_1 = \frac{1}{2}(\psi_e - \psi_{los})^2$, then stabilize $(x_e, y_e)^2 = 0^2$ by $V_2 = \frac{1}{2}(x_e^2 + y_e^2)$, and finally choose $V = V_1 + V_2 + \frac{1}{2}[(u - \alpha_u)^2 + (r - \alpha_r)^2]$ to stabilize all the error state to zero within the system dynamics, where α_u, α_r represent the virtual control laws u_d, r_d respectively. Thus, we can have the virtual control inputs as

$$\alpha_r = \dot{\psi}_{los} - \dot{\beta} + c_c(s)\dot{s} - k_2(\psi_e - \psi_{los}) \tag{5.21}$$

where α_r in (5.21) is simplified by canceling the term $y_e v_t \frac{\sin\psi_e - \sin\psi_{los}}{\psi_e - \psi_{los}}$, compared with that in (5.12).

Using the equivalent symbol α_r to replace r_d in (5.14), there is

$$\dot{r} = \dot{\alpha}_r - (\psi_e - \psi_{los}) - k_3(r - \alpha_r)$$

Furthermore, $\dot{r}$ can be simplified by $\dot{\alpha}_r$ in (5.21) as follows :

$$\dot{r} = \ddot{\psi}_{los} - \ddot{\beta} + c_c\ddot{s} + g_c\dot{s}^2 - k_2(\dot{\psi}_e - \dot{\psi}_{los}) - (\psi_e - \psi_{los}) - k_3(r - \alpha_r)$$

Let the intermediate variable B be

$$B = \ddot{\psi}_{los} + c_c\ddot{s} + g_c\dot{s}^2 - k_2(\dot{\psi}_e - \dot{\psi}_{los}) - (\psi_e - \psi_{los}) - k_3(r - \alpha_r) \tag{5.22}$$

such that $\dot{r} = B - \ddot{\beta}$.

From the second term in the dynamics model (5.10), there is $\dot{v} = \frac{-m_u ur - d_v v}{m_v}$, and $u = v_t \cos\beta$, then $\dot{\beta}$ in (5.18) can be rewritten as

$$\dot{\beta} = \frac{u\dot{v} - v\dot{u}}{v_t^2} = \frac{1}{v_t^2}[u\frac{-m_u u\alpha_r - d_v v}{m_v} - v\dot{u}] = -\frac{m_u}{m_v}\cos^2\beta\alpha_r - \frac{uvd_v}{m_v v_t^2} - \frac{v\dot{u}}{v_t^2} \tag{5.23}$$

Let the intermediate variable A be

$$A = \dot{\psi}_{los} + c_c\dot{s} - k_2(\psi_e - \psi_{los}) \tag{5.24}$$

Replacing (5.23) into (5.21), there is

$$\alpha_r = [A + \frac{1}{v_t^2}(v\dot{u} + \frac{uvd_v}{m_v})]/(1 - \frac{m_u}{m_v}\cos^2\beta)$$

As $\ddot{\beta}$ given in (5.19) and $\ddot{v}$ given in (5.20), using the intermediate variable B in (5.22), there is

$$\begin{aligned}
\dot{r} =& B + \frac{\ddot{u}v}{v_t^2} + 2\frac{\dot{v}_t}{v_t}\dot{\beta} - \frac{u}{v_t^2}[\frac{-(m_u\dot{u}r + m_u u\dot{r} + \dot{d}_v v + d_v\dot{v})}{m_v}] \\
=& B + \frac{\ddot{u}v}{v_t^2} + 2\frac{\dot{v}_t}{v_t}\dot{\beta} + \frac{u}{v_t^2}(\frac{m_u\dot{u}r + m_u u\dot{r} + \dot{d}_v v}{m_v}) + \frac{u}{v_t^2}\frac{m_u}{m_v}u\dot{r} \\
=& C + \frac{u^2}{v^2}\frac{m_u}{m_v}\dot{r} = C + \frac{m_u}{m_v}\cos^2\beta\dot{r}
\end{aligned}$$

Hence, we get

$$\dot{r} = C/(1 - \frac{m_u}{m_v}\cos^2\beta) \tag{5.25}$$

where the intermediate variable C is :

$$\begin{aligned}
C =& B + \frac{\ddot{u}v}{v_t^2} + 2\frac{\dot{v}_t}{v_t}\dot{\beta} + \frac{u}{v_t^2}(\frac{m_u\dot{u}r + m_u u\dot{r} + \dot{d}_v v}{m_v}) \\
=& \ddot{\psi}_{los} + c_c\ddot{s} + g_c\dot{s}^2 - k_1(\dot{\psi}_e - \dot{\psi}_{los}) - (\psi_e - \psi_{los}) - k_3(r - \alpha_r) \\
&+ \frac{\ddot{u}v}{v_t^2} + 2\frac{\dot{v}_t}{v_t}\dot{\beta} + \frac{u}{v_t^2}(\frac{m_u\dot{u}r + \dot{d}_v v + d_v\dot{v}}{m_v})
\end{aligned} \tag{5.26}$$

Now, we can have a summary about the algebraic computation for the acceleration of side-slip angle, and the computation process is shown in Figure 5.3.

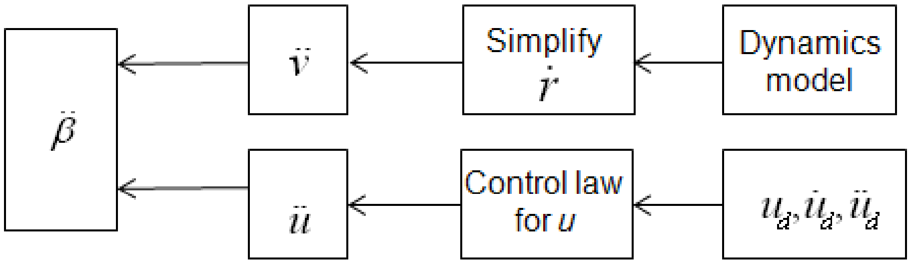

Figure 5.3 – Diagram of computation for acceleration of side-slip angle

1. Computation on side-slip angle

$$\begin{cases} \beta = \arctan v/u \\ \dot{\beta} = \frac{1}{v_t^2}(u\dot{v} - v\dot{u}) \\ \ddot{\beta} = \frac{1}{v_t^2}(u\ddot{v} - v\ddot{u}) - 2\frac{v_t^2}{v_t}\dot{\beta} \end{cases}$$

2. Computation on acceleration of speed by resorting to dynamic model

$$\begin{cases} \ddot{u} = \ddot{u}_d + k_4^2(u - u_d) \\ \ddot{v} = -(m_u\dot{u}r + m_u u\dot{r} + \dot{d}_v v + d_v\dot{v})/m_v \end{cases}$$

3. Computation on angular speed and its acceleration

$$\begin{cases} \alpha_r = [A + \frac{1}{v_t^2}(u\dot{v} + \frac{uvd_v}{m_v})]/(1 - \frac{m_u}{m_v}\cos^2\beta) \\ \dot{r} = C/(1 - \frac{m_u}{m_v}\cos^2\beta) \end{cases} \tag{5.27}$$

where the intermediate variables A, C are stated in (5.24) and (5.26).

Condition of stern-dominant vehicle :

With similar analysis in [Lapierre and Jouvencel, 2008], it is noted that $\dot{r}$ is causal and well defined in (5.27) if

$$\frac{m_u}{m_v} = \frac{m - X_{\dot{u}}}{m - Y_{\dot{v}}} < 1$$

Note that added mass terms $X_{\dot{u}}$ and $Y_{\dot{v}}$ are standard notations of SNAME [SNAME and Engineers, 1950]. For instance, the hydrodynamic added mass force Y along the y-axis due to an acceleration $\dot{v}$ in the y-direction, is written as :

$$Y = -Y_{\dot{v}}\dot{v}$$

where the hydrodynamic derivatives $Y_{\dot{v}} := \frac{\partial Y}{\partial \dot{v}}$, can be considered as the added mass resulted by Newton's second laws of motion.

Checking the signs of the hydrodynamic parameters of an AUV reveals following properties :

1. The added mass $X_{\dot{u}}$ and $Y_{\dot{v}}$ are negative in a real fluid ([Fossen, 2002], pages :$66-67$) .
2. If the vehicle is **stern dominant**, $-Y_{\dot{v}} > -X_{\dot{u}} > 0$ as the added mass act on the vehicle have more influence in the sway direction than that in the surge direction.
3. If the vehicle is **bow dominant**, $-X_{\dot{u}} > -Y_{\dot{v}} > 0$ as the added mass act on the vehicle have more influence on the surge direction than that in the sway direction.

Hence, in the case of a stern-dominant vehicle such as one considered in this thesis, the control computation is well posed. For a definition of bow and stern dominant vehicles, see (Lewis [Lewis, 1989], Chapter 9, Section 4.2).

As a conclusion, the underactuated property of AUVs leads the side-slip angle to be not directly controllable, and it brings difficulty in computation of the acceleration of side-slip angle, which is usually ignored by neglecting it in many other literatures. However, the simulation result in section (5.3) will exposes that $\ddot{\beta}$ can not be simply set as zero if high precision performance of path following is expected. In this part, the computation problem is solved by resorting the dynamics model and stern-dominant structure of AUVs is required to get the well-posed computation.

5.1.4 Smooth Transition from underactuated to fully-actuated AUV

Underactuated vehicle systems exhibit so-called second order nonholonomic constraints, i.e. non-integrable conditions imposed on the acceleration, such that the vehicle lacks capability to command instantaneous accelerations in one or more DOFs. However, fully-actuated vehicle systems have the same dimension of the control input space as that of the configuration space. This gives full actuation for applications like low-speed maneuvering in harbours and confined waters, and eases docking. But since such lateral thrusters loose their efficiency at higher speeds, mainly because of the relative perpendicular water flow, adding them doesn't solve the situation for high-speed applications. At such instances, these vehicles just behave like underactuated as the rest.

On the other hand, fully actuated vehicles can be exposed to actuator failure rendering them into underactuated case. This can be partially solved by introducing redundancy in the actuator configuration, but only at increased costs. Even so, the control system of these vehicles should be equipped with algorithms allowing the vehicles to be controlled using only the remaining actuator capability. In practice, this represents a software solution to handling faults in the event of a failure, that is having both software and hardware redundancy.

For marine vehicles, it is desirable to automatically control the vehicles through all the feasible stages from low speed positioning [Riedel and Healey, 1998] to high-speed maneuvering [Do et al., 2004b]. Traditionally, the vehicle is fully actuated for low-speed application, while under-actuated vehicle is assumed for high-speed maneuvering. It results in the development of structurally different controllers, and an intelligent supervisor is required to perform a heuristics and hybrid switch between two controllers. For example, a hybrid switching design involving a low-speed dynamic positioning controller and a high-speed track-keeping controller is proposed in [Bertin and Branca, 2000] for marine surface vehicles, and a unified design throughout the whole non-zero speed envelope is proposed in [Breivik and Fossen, 2006] for autonomous underwater vehicles. However, we propose a control law for fully-actuated vehicle, which is adapted from the control laws for underactuated vehicles in (5.16). Thus, both underactuated and fully actuated AUVs under the same control framework, except that the control computation for $\ddot{\beta}$ is different due to the different controllability of β in these two cases.

Motion control design for fully actuated AUV :

Consider the simplified dynamics of a fully actuated underwater vehicle in body fixed frame [Ghabcheloo et al., 2006a], written as :

$$\begin{cases} \tau_u = m_u\dot{u} - m_v vr + d_u u \\ \tau_v = m_v\dot{v} + m_u ur + d_v v \\ \tau_r = m_r\dot{r} - m_{uv} uv + d_r r \end{cases} \tag{5.28}$$

It degenerates into the underactuated AUV dynamics in (5.10) when $\tau_v = 0$.

Notice that the side-slip angle β exists in both the fully actuated vehicle and underactuated vehicle, and the difference is that β is directly controllable in fully actuated case, but not directly controllable in underactuated case. However, the kinematic equations in (3.20) are with the same form for both the fully-actuated vehicle and under-actuated vehicle.

Using the fact that

$$\begin{cases} \beta = \arctan(v/u) \\ v_t = \sqrt{u^2 + v^2} \\ u = v_t \cos\beta \\ v = v_t \sin\beta \end{cases}$$

Replacing above equations into (5.28), the dynamics of fully actuated AUV can be re-written in terms of (v_t, β, r) as

$$\begin{cases} \dot{v}_t = f_{vt}(v_t, \beta, r) + \tau_{vt}(\tau_u, \tau_v, v_t, \beta) \\ \dot{\beta} = f_{\beta}(v_t, \beta, r) + \tau_{\beta}(\tau_u, \tau_v, v_t, \beta) \\ \dot{r} = f_r(v_t, \beta, r) + \tau_r/m_r \end{cases} \tag{5.29}$$

where

$$\begin{cases} f_{vt} = (\frac{m_v}{m_u} - \frac{m_u}{m_v})v_t r \sin\beta\cos\beta - (\frac{d_u}{m_u}\cos^2\beta + \frac{d_v}{m_v}\sin^2\beta)v_t \\ f_\beta = -(\frac{m_v}{m_u} r \sin^2\beta + \frac{m_u}{m_v} r\cos^2\beta) + (\frac{d_u}{m_u} - \frac{d_v}{m_v})\sin\beta\cos\beta \\ f_r = -\frac{d_r}{m_r} + \frac{m_{ur}}{m_r} v_t^2 \sin\beta\cos\beta \end{cases} \tag{5.30}$$

and

$$\begin{cases} \tau_{vt} = \frac{\cos\beta}{m_u}\tau_u + \frac{\sin\beta}{m_v}\tau_v \\ \tau_\beta = -\frac{\sin\beta}{v_t m_u}\tau_u + \frac{\cos\beta}{v_t m_v}\tau_v \end{cases} \tag{5.31}$$

The transformation between (τ_{vt}, τ_β) and (τ_u, τ_v) is nonsingular due to the determinate of the transformation $m_u m_v v_t \neq 0$, which can also be written as follows

$$\begin{cases} \tau_u = (m_u \cos\beta)\tau_{vt} - (m_u v_t \sin\beta)\tau_\beta \\ \tau_v = (m_v \sin\beta)\tau_{v_t} + (m_v v_t \cos\beta)\tau_\beta \end{cases} \tag{5.32}$$

where τ_u, τ_v, τ_r denote the surge force, sway force and torque applied to the fully-actuated vehicle respectively, and m's and d's are vehicle parameters.

As the side-slip angle β is directly controllable by the control input τ_v, we can guarantee the desired side-slip angle. This is the main difference from under-actuated vehicle. Hence, the desired side-slip angle can be predefined as β_d, and choose the Lyapunov function $V_\beta = \frac{1}{2}(\beta - \beta_d)^2$, it renders

$$\dot\beta = \dot\beta_d - k_5(\beta - \beta_d) \tag{5.33}$$

where the gain $k_5 > 0$.

Therefore, the control input of τ_β in (5.29) is

$$\tau_\beta = -f_\beta + \dot\beta_d - k_5(\beta - \beta_d) \tag{5.34}$$

drives β asymptotically converges to β_d.

The only different between fully and underactuated vehicle, exists if the side-slip angle β is directly controllable or not. The common point is that control inputs for τ_u and τ_r are the same for both of the cases. Directly using the same surge and yaw control inputs as proposed in (5.16), and replacing (5.34) into (5.32) to get the sway control input τ_v, there is

$$\begin{cases} \tau_u = m_u(\dot u_d - k_4(u - u_d)) - m_v v r + d_u u \\ \tau_r = m_r(\dot r_d - k_3(r - r_d) - (\psi_e - \psi_{los})) - m_{uv} uv + d_r r \\ \tau_v = \frac{m_v u}{\cos^2\beta}[\frac{\sin^2\beta}{m_u v}\tau_u - f_\beta + \dot\beta_d - k_5(\beta - \beta_d)] \end{cases} \tag{5.35}$$

Note that the control law for τ_v is singular when $\beta = \frac{\pi}{2} + 2k\pi, k \in \Re^+$. However, $\beta = \frac{\pi}{2} + 2k\pi$ means that the surge velocity $u = 0$ and only sway velocity v exists. Actually, the desired surge velocity u_d is not zero in path following problem , so that $u \neq 0$ which rules out this singularity problem.

Proposition 5.1.2 (Path following : fully actuated underwater vehicle)

Consider a fully actuated underwater vehicle with the dynamics equations in (3.17) and (5.28). Given the desired surge speed $u_d > 0$ and the LOS heading guidance in (5.3). Let control laws be given by (5.35) for some $k_i > 0 (i = 1, 2, 3)$, the equilibrium point $(x_e, y_e, \psi_e) = 0^3$ is uniformly globally asymptotically and locally exponentially stable (UGAS&ULES).

Proof The proof follows the same steps adopted in the proof of Proposition 5.1.1. ∎

Furthermore, the acceleration of side-slip angle $\ddot{\beta}$ is still required to compute control input τ_r, as $\ddot{\beta}$ is implicitly included in $\dot{r}_d$ which appears in τ_r. Fortunately, it is far more easier to get it compared with that in the underactuated model. As the β is directly controllable in (5.33), there is

$$\ddot{\beta} = \ddot{\beta}_d - k_5(\dot{\beta} - \dot{\beta}_d) = \ddot{\beta}_d + k_5^2(\beta - \beta_d) \tag{5.36}$$

We can conclude that the difference between two path following controllers for underactuated and fully actuated AUV is that, the side-slip angle is directly controllable in fully actuated vehicle due to the available control input τ_v, so we can use (5.36) to replace (5.19) in underactuated AUV controller. The control inputs for τ_u and τ_r are the same for both of the cases.

From this point of view, we can keep the control framework consistent for both underactuated and fully actuated AUVs, as we just need to switch the control computation for $\ddot{\beta}$ from (5.19) to (5.36). However, the smooth control transition is preferred to the hard switch in practical case.

Control design of smooth transition between fully and under-actuated AUV :

The smooth transition design is proposed as follows :

Define the total speed of the vehicle as

$$0 < v_{tmin} \leq v_{t1} < v_{t2} \leq v_{tmax} \tag{5.37}$$

where v_{tmin} is the minimum value of v_t when the vehicle is still fully actuated, and v_{tmax} is the maximum value of v_t when the vehicle becomes underactuated.

In order to achieve a smooth transition between a fully actuated and an underactuated vehicle, a natural choice is constructing the transition factor $f(v_t)$ as a function of the instantaneous vehicle total speed v_t :

$$f(v_t) = \frac{\frac{\pi}{2} + \arcsin[k_{vt}(v_t - \frac{v_{t1}+v_{t2}}{2})/(\frac{v_{t2}-v_{t1}}{2})]}{\pi} \tag{5.38}$$

where $k_{vt} > 0$ is a slack variable and $0 \leq f(v_t) \leq 1$. Note some sigmoid functions, for instance, $\tanh(\cdot)$, atan$(\cdot)$, are excluded as only $0 < f(v_t) < 1$ is guaranteed.

Revisiting (5.35) in fully actuated control laws and using the fact of null sway force in underactuated case, the control input in sway direction can be written as

$$\tau_v = \begin{cases} \tau_{v1} = 0, & \text{underactuated case : high speed} \\ \tau_{v2} = \frac{m_v u}{\cos^2\beta}[\frac{\sin^2\beta}{m_u v}\tau_u - f_\beta + \dot{\beta}_d - k_5(\beta - \beta_d)], & \text{fully-actuated case : low speed} \end{cases} \tag{5.39}$$

The smooth transition of control force in sway direction, from low speed to high speed maneuvering, can be proposed as

$$\tau_v = f(v_t)\tau_{v1} + (1 - f(v_t))\tau_{v2} \tag{5.40}$$

where $f(v_t)$ is given in (5.38) and τ_{v1}, τ_{v2} are given in (5.39). When the vehicle maneuvers in high speed approaching to v_{t2}, it tends to $\tau_v = \tau_{v1}$. It tends to $\tau_v = \tau_{v2}$ vice versa.

Hence, we can get the proposition for path following control of autonomous underwater vehicles maneuvering in the whole speed profile (from low speed to high speed) as follows :

Proposition 5.1.3 (Path following : smooth transition between fully and underactuated AUVs)

Consider an underwater vehicle with the kinematics equations in (3.17), and dynamics equations (5.28) and (5.10) in fully and under-actuated case respectively. Given the desired surge speed $u_d > 0$ and the LOS heading guidance in (5.3). The control input of τ_u, τ_r are given in (5.35). Let control law for control force in sway direction be given by (5.40), the smooth transition between low-speed and high speed maneuvering of AUVs can be achieved.

Remark :

Actually, there is another control representation for path following control of fully-actuated AUVs. As the side-slip angle is directly controllable for the fully actuated AUVs, the desired total speed v_{td} ($v_{td} \geq v_{tdmin} > 0$) can be directly given other than setting the desired surge speed u_d in the Proposition 5.1.2.

Then the control laws can be chosen as

$$\begin{cases} \tau_{vt} = -f_{vt} + \dot{v}_{td} - k_6(v_t - v_{td}) \\ \tau_\beta = -f_\beta + \dot{\beta}_d - k_5(\beta - \beta_d) \\ \tau_r = m_r(\dot{r}_d - k_3(r - r_d) - (\psi_e - \psi_{los})) - m_{uv}uv + d_r r \end{cases} \tag{5.41}$$

where f_{vt}, f_β are given in (5.30).

Note the composite control input τ_{vt} is simply derived by choosing the Lyapunov function $V_{vt} = \frac{1}{2}(v_t - v_{td})^2$, while τ_β, τ_r are derived in the same way as shown in (5.35).

Subsequently, the control inputs τ_u and τ_v can be derived by using the mapping between τ_u, τ_v and τ_β, τ_{vt} in (5.32).

5.2 Path tracking control of underactuated AUV

In this section, the problem of path tracking for underactuated AUVs in horizontal plane is addressed, based on the solution for nonholonomic unicycle-type mobile vehicle in previous chapter. The difference is that the total speed of the underactuated vehicle is required to track a desired speed profile.

5.2.1 Problem formulation

As depicted in Figure 5.4, an underactuated AUV is required to track a reference path $\Gamma(\tau_d(t))$ parameterized by path parameter $\tau_d(t)$. The reference path can be considered as a trajectory tracking target (TT target) moving along the path with desired speed profile $\dot{\tau}_d(t)$, and a path tracking target (PT target) moving on the path is introduced to generate the virtual reference path $\Gamma(\tau(t))$ online. Apparently, the path of TT target coincides with the path of PT target if the time-related path parameters are the same, i.e., $\tau(t_f) = \tau_d(t_f)$ at certain time instant t_f. However, the virtual path parameter $\tau(t)$ has an extra degree of freedom in order to bridge the behaviors of the tracking vehicle and the TT target on the path, such that both smooth spatial convergence and time convergence can be achieved, which are the characteristics of path tracking control, with the performance to combine both the path following and trajectory tracking control behaviors.

As the reference path $\Gamma(\tau(t))$ is parameterized by $\tau(t)$, there is :

$$\begin{bmatrix} \dot{x}(\tau) \\ \dot{y}(\tau) \\ \psi_r(\tau) \end{bmatrix} = \begin{bmatrix} x^\tau(\tau)\dot{\tau} \\ y^\tau(\tau)\dot{\tau} \\ \text{atan2}(y^\tau(\tau)/x^\tau(\tau)) \end{bmatrix} \tag{5.42}$$

where $x^\tau(\tau) = \frac{\partial x(\tau)}{\partial \tau}$ and $y^\tau(\tau) = \frac{\partial y(\tau)}{\partial \tau}$.

Compared with the path tracking of nonholonomic unicycle-type vehicle, the total speed of the underactuated AUV v_t is required to align with the tangent speed of the path v_{tr}. Let the path tracking error state vector $\mathbf{p}_{eB} = [x_e, y_e, \psi_e]^T$ be built in the vehicle

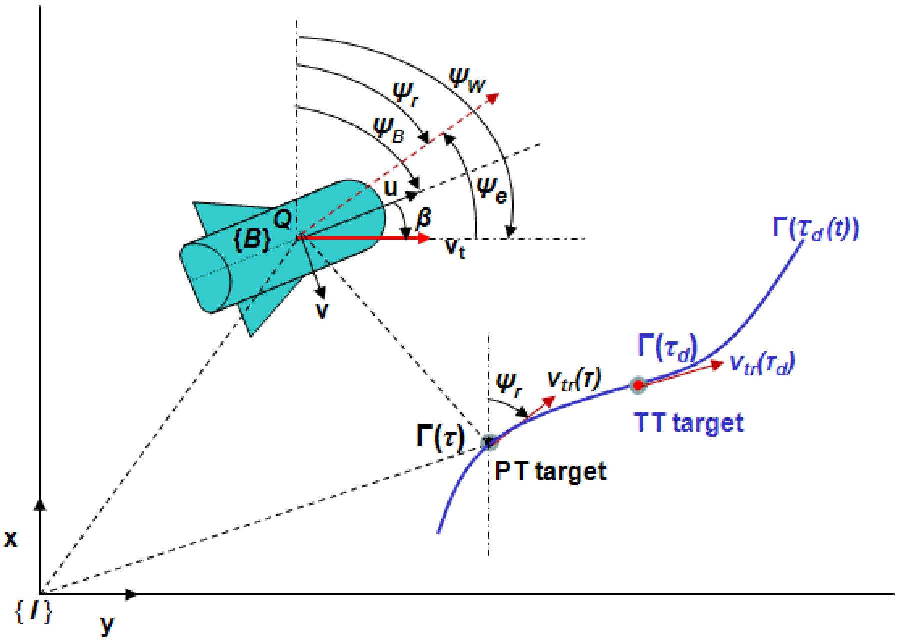

Figure 5.4 – Path tracking of underactuated AUV

body frame $\{B\}$, there is

$$\mathbf{p}_{eB} = \begin{bmatrix} x_e \\ y_e \\ \psi_e \end{bmatrix} = \begin{bmatrix} \cos\psi_W & \sin\psi_W & 0 \\ -\sin\psi_W & \cos\psi_W & 0 \\ 0 & 0 & 1 \end{bmatrix} \begin{bmatrix} x_r - x \\ y_r - y \\ \psi_r - \psi_W \end{bmatrix} \tag{5.43}$$

where $[x, y, \psi_W]^T$is the AUV state vector with the course angle $\psi_W = \psi_B + \beta$, and $[x_r, y_r, \psi_r]^T$ is the reference state vector in the inertial frame $\{I\}$.

Similarly with (4.16), the velocity vector of the PT target on the path $(v_{tr}, \omega_r)^T$ can be expressed by path parameter τ as

$$\begin{bmatrix} v_{tr}(\tau) \\ \omega_r(\tau) \end{bmatrix} = \begin{bmatrix} \bar{v}_{tr}(\tau)\dot{\tau} \\ \bar{w}_r(\tau)\dot{\tau} \end{bmatrix} \tag{5.44}$$

where

$$\begin{cases} \bar{v}_{tr}(\tau) = \sqrt{x_r^\tau(\tau)^2 + y_r^\tau(\tau)^2} \\ \bar{w}_r(\tau) = \frac{x_r^\tau(\tau) y_r^{\tau^2}(\tau) - x_r^{\tau^2}(\tau) y_r^\tau(\tau)}{x_r^\tau(\tau)^2 + y_r^\tau(\tau)^2} \end{cases} \tag{5.45}$$

Hence, the corresponding error state dynamics (3.39) expressed in AUV body frame $\{B\}$, can be rewritten as follows :

$$\begin{bmatrix} \dot{x}_e \\ \dot{y}_e \\ \dot{\psi}_e \end{bmatrix} = \begin{bmatrix} \omega y_e - v_t + \bar{v}_{tr}\dot{\tau}\cos\psi_e \\ -\omega x_e + \bar{v}_{tr}\dot{\tau}\sin\psi_e \\ \bar{\omega}_r\dot{\tau} - \omega - \dot{\beta} \end{bmatrix} \tag{5.46}$$

where $[v_t, \omega_W]^T$ is the vehicle state vector with $\omega_W = \dot{\psi}_B + \dot{\beta} = \omega + \dot{\beta}$,and $[v_{tr}, \omega_r]^T$ is the reference velocity vector of the PT target.

Note that three properties of the path, uniqueness, regularity and persisting excitation, are still assumed for path tracking as expressed in Assumption 4.3.1.

Therefore, the control objective of path tracking of underactuated AUV is to design a controller and achieve the following tasks :

$$\begin{aligned} &\lim_{t\to\infty} \|\mathbf{p}_{eB}\| = 0 \\ &\lim_{t\to\infty} |\tau(t) - \tau_d(t)| = 0,\ \lim_{t\to\infty} |\dot{\tau}(t) - \dot{\tau}_d(t)| = 0 \end{aligned} \tag{5.47}$$

where the first term declares the spatial assignment of path tracking, requiring the position and total velocity of the vehicle coincide with those of the PT target on the path ; the second term declares the dynamic assignment, requiring the speed of the PT target $\dot{\tau}(t)$ respect that of the TT target $\dot{\tau}_d(t)$ and force the PT target to asymptotically catch up with the TT target.

5.2.2 Controller design

In this part, the control law for underactuated AUV path tracking is derived based on Lyapunov stability theorem and backstepping technique. However, a new control Lyapunov function is chosen in a concise pattern, where neither the approaching angle nor the LOS guidance is used. Moreover, a weighting factor λ is introduced to flexibly tune the weighting of the path following and trajectory tracking behaviors, which are blended in the path tracking control design.

5.2.2.1 Kinematics controller

In the kinematics stage, the control Lyapunov function is selected as

$$V = (1-\lambda)\frac{(x_e^2 + y_e^2 + \frac{1}{\gamma}\psi_e^2)}{2} + \lambda\frac{k_\tau(\tau-\tau_d)^2}{2} \tag{5.48}$$

where γ, k_τ are scale factors to guarantee dimensional homogeneity of position x_e, y_e, angle ψ_e and time τ. Meanwhile τ, τ_d is the virtual and desired path parameter respectively with $\lim_{t\to\infty} \dot{\tau}_d \neq 0$.

The first part $\frac{(x_e^2+y_e^2+\frac{1}{\gamma}\psi_e^2)}{2}$ in (5.48) concerns the spatial tracking property, while the second part $(\tau-\tau_d)^2$ is the addition of a time dependent penalty.

The parameter $\lambda \in (0, 1)$ is the weighting factor. Obviously, large λ let the time specification $(\tau - \tau_d)$ plays more important roles in the path tracking design, which represents the characteristics of trajectory tracking. While small λ let the spatial specification x_e, y_e, ψ_e plays more important roles, which represents the characteristics of path following.

The time derivative of (5.48) along the solution of (5.46) is

$$\dot{V} = (1-\lambda)[-x_e v_t + v_{tr} x_e \cos\psi_e + v_{tr} y_e \sin\psi_e + \frac{1}{\gamma}\psi_e(\omega_r - \omega - \dot{\beta})] + \lambda k_\tau(\tau - \tau_d)(\dot{\tau} - \dot{\tau}_d)$$

In order to introduce the extra degree of freedom to the virtual path parameter τ, define an auxiliary variable $\tilde{\tau}$ and let its time derivative as

$$\dot{\tilde{\tau}} = \dot{\tau} - v_\tau(t, x_e, y_e, \psi_e) \tag{5.49}$$

Substituting (5.44), (5.44) and (5.49) into above equation, yields

$$\begin{aligned}
\dot{V} =&(1-\lambda)\{-x_e v_t + \bar{v}_{tr}(\dot{\tilde{\tau}} + v_\tau) x_e \cos\psi_e + \bar{v}_{tr}(\dot{\tilde{\tau}} + v_\tau) y_e \sin\psi_e + \frac{1}{\gamma}\psi_e[\bar{\omega}_r(\dot{\tilde{\tau}} + v_\tau) - \omega - \dot{\beta}]\} \\
&+ \lambda k_\tau(\tau - \tau_d)(\dot{\tilde{\tau}} + v_\tau - \dot{\tau}_d) \\
=&(1-\lambda)[(\bar{v}_{tr} v_\tau \cos\psi_e - v_t) x_e + \bar{v}_{tr} v_\tau y_e \sin\psi_e + \frac{1}{\gamma}\psi_e(\bar{\omega}_r v_\tau - \omega - \dot{\beta})] + \lambda k_\tau(\tau - \tau_d)(v_\tau - \dot{\tau}_d) \\
&+ \dot{\tilde{\tau}}[(1-\lambda)(\bar{v}_{tr} x_e \cos\psi_e + \bar{v}_{tr} y_e \sin\psi_e + \frac{1}{\gamma}\psi_e \bar{\omega}_r) + \lambda k_\tau(\tau - \tau_d)]
\end{aligned}$$

Let

$$\Phi_e = (1-\lambda)(\bar{v}_{tr} x_e \cos\psi_e + \bar{v}_{tr} y_e \sin\psi_e + \frac{1}{\gamma}\psi_e \bar{\omega}_r) + \lambda k_\tau(\tau - \tau_d) \tag{5.50}$$

Proposing the control input as

$$\begin{bmatrix} v_t \\ \omega \end{bmatrix} = \begin{bmatrix} k_x x_e + \bar{v}_{tr} v_\tau \cos\psi_e \\ \bar{\omega}_r v_\tau - \dot{\beta} + \gamma y_e \bar{v}_{tr} v_\tau \frac{\sin\psi_e}{\psi_e} + k_\psi \psi_e \end{bmatrix} \tag{5.51}$$

and choosing

$$\begin{bmatrix} v_\tau \\ \dot{\tilde{\tau}} \end{bmatrix} = \begin{bmatrix} \dot{\tau}_d \\ -k_v \tanh\Phi_e \end{bmatrix} \tag{5.52}$$

yields

$$\dot{V} = -(1-\lambda)(k_x x_e^2 + \frac{k_\psi}{\gamma}\psi_e^2) - k_v \Phi_e \tanh\Phi_e \tag{5.53}$$

Replacing (5.49) into the combination of (5.51) and (5.52), yields the control laws for path tracking

$$\begin{bmatrix} v_t \\ \omega \\ \dot{\tau} \end{bmatrix} = \begin{bmatrix} k_x x_e + \bar{v}_{tr} \dot{\tau}_d \cos\psi_e \\ \bar{\omega}_r \dot{\tau}_d - \dot{\beta} + \gamma y_e \bar{v}_{tr} \dot{\tau}_d \frac{\sin\psi_e}{\psi_e} + k_\psi \psi_e \\ \dot{\tau}_d - k_v \tanh\Phi_e \end{bmatrix} \tag{5.54}$$

The above path tracking controller is nonsingular, as the term $\frac{\sin\psi_e}{\psi_e}$ is well defined and continuous at zero.

Remark :

Note that neither explicit approaching angle δ nor LOS angle ψ_{LOS} is used as a heading guidance in control design, by building the Lyapunov candidate function (5.48). However, the implicit heading guidance is embedded as the the x_e, y_e, ψ_e tending to zero will be still achieved in the subsequent proof of Proposition 5.2.1. And this implicit heading guidance simplifies the derived control input of yaw rate in (5.54) compared with that in (4.28).

Proposition 5.2.1 (Path tracking 1 : underactuated AUV)

Under assumption 4.3.1 for a predefined $\mathcal{C}^1$ path given in (5.42) with desired speed $\dot{\tau}_d(t)$ for the time derivative of path parameter $\tau(t)$, the kinematic control inputs v_t and ω, and the virtual control input $\dot{\tau}$ rendering time evolving law for path parameter given in (5.54). The control objective of path tracking is achieved and the equilibrium point $[x_e, y_e, \psi_e, (\tau - \tau_d)]^T = 0^4$ is globally asymptotically stable.

Proof The control Lyapunov function V in (5.48) is positive definite, and its time derivative $\dot{V}$ in (5.53) is semi-negative definite. We have

$$0 \leq V(t) \leq V(t_0), t \geq t_0$$

such that all the signals $x_e(t), y_e(t), \psi_e(t), \tau(t) - \tau_d(t)$ constituting $V(t)$ are bounded.

As the path is $\mathcal{C}^1$, there is $\bar{v}_{tr}, \bar{\omega}_r$ are bounded. $\dot{\tau}_d$ is assumed to be bounded. The boundedness of $\bar{v}_{tr}, \bar{\omega}_r, \dot{\tau}_d$ renders that v_t is bounded from the first term in (5.54). Furthermore, the boundedness of v_t renders the same for u, v and $\dot{u}, \dot{v}$, such that $\dot{\beta} = (\cos\psi_e \dot{v} - \sin\psi_e \dot{u})/v_t$ is bounded. Moreover, $|\sin\psi_e/\psi_e| \leq 1$. Consequently, ω is bounded by checking the second term in (5.54). Now, $\dot{x}_e, \dot{y}_e, \dot{\psi}_e$ can be claimed as bounded by checking (5.46). In addition, the functions $\tanh(\cdot), \mathrm{sech}(\cdot)$ are bounded. Therefore, the double derivative of Lyapunov function

$$\ddot{V} = -2(1-\lambda)(k_x x_e \dot{x}_e - k_\psi \psi_e \dot{\psi}_e) - k_v \dot{\Phi}_e(\tanh\Phi_e - \Phi_e \mathrm{sech}^2 \Phi_e)$$

is also bounded. By resorting to Barbalat's lemma, there is

$$\lim_{t\to\infty} \dot{V}(t) = 0$$

Therefore, x_e, ψ_e, Φ_e vanish as $t \to \infty$, which renders

$$\lim_{t\to\infty} (\tau - \tau_d) = 0$$

by checking the the expression of Φ_e in (5.50). Moreover, as $\dot{\tau} = \dot{\tau}_d - k_v \tanh \Phi_e$ in (5.54), $\lim_{t\to\infty} \Phi_e = 0$ renders

$$\lim_{t\to\infty} |\dot{\tau} - \dot{\tau}_d| = 0$$

It means the second control objective in (5.47) is fulfilled.

From (5.46), we have $\lim_{t\to\infty} \dot{x}_e = \lim_{t\to\infty}(\omega y_e - v_t + \bar{v}_{tr}\dot{\tau}\cos\psi_e) = 0$. Since $v_t \to \bar{v}_{tr}\dot{\tau}_d$ from the control law and $\dot{\tau} \to \dot{\tau}_d$ as $t \to \infty$, there is $v_t \to \bar{v}_{tr}\dot{\tau}$. It yields $\lim_{t\to\infty} \omega y_e = 0$. By checking the control law for ω and $\lim_{t\to\infty} \dot{\psi}_e = 0$ in (5.46), there is $\omega \to \omega_r - \dot{\beta}$ as $t \to \infty$. By resorting the dynamics model in (5.10), there is $\lim_{t\to\infty} \dot{\beta} = -m_u\omega/m_v$. Therefore, $\omega \to \omega_r/(1-m_u/m_v)$. Thus, for any $\omega_r \neq 0$, there is $\omega \neq 0$. Suppose $\lim_{t\to\infty} y_e \neq 0$, there is $y_e \to y_{e,lim}$ due to the boundedness of y_e. It gives the convergence solution :

$$\lim_{t\to\infty} \dot{x}_e \to \omega y_{e,lim}$$

which is paradoxical with $\dot{x}_e \to 0$ no matter the state of ω_r. Hence, $\lim_{t\to\infty} y_e = 0$. Now, we can conclude that the first control objective in (5.47) is also fulfilled. ∎

5.2.2.2 Backstepping Dynamics

Let v_t and ω be virtual control inputs, α_{v_t} and α_ω in (5.54) be the corresponding virtual control laws. Introduce the velocity error variables

$$z = \begin{pmatrix} z_{v_t} \\ z_\omega \end{pmatrix} = \begin{pmatrix} v_t - \alpha_{v_t} \\ \omega - \alpha_\omega \end{pmatrix}$$

Augmenting the Lyapunov function V in (5.48) with the quadratic terms of z_u and z_r, there is

$$V_{dyn} = V + \frac{1}{2} z^T M z \tag{5.55}$$

Denote the positive definite matrix $M = \begin{pmatrix} m_u & 0 \\ 0 & m_r \end{pmatrix}$, where m_u, m_r are defined in (5.10).

The time derivative of V_{dyn} can be written as

$$\begin{aligned}\dot{V}_{dyn} &= (1-\lambda)[(\bar{v}_{tr}v_\tau\cos\psi_e - v_t)x_e + \bar{v}_{tr}v_\tau y_e\sin\psi_e + \frac{1}{\gamma}\psi_e(\bar{\omega}_r v_\tau - \omega - \dot{\beta})] + \lambda k_\tau(\tau-\tau_d)(v_\tau - \dot{\tau}_d)\\
&\quad + \dot{\tilde{\tau}}[(1-\lambda)(\bar{v}_{tr}x_e\cos\psi_e + \bar{v}_{tr}y_e\sin\psi_e + \frac{1}{\gamma}\psi_e\bar{\omega}_r) + \lambda k_\tau(\tau-\tau_d)] + +m_u z_{v_t}\dot{z}_{v_t} + m_r z_\omega\dot{z}_\omega\\
&= (1-\lambda)[(\bar{v}_{tr}v_\tau\cos\psi_e - z_{v_t} - \alpha_{v_t})x_e + \bar{v}_{tr}v_\tau y_e\sin\psi_e + \frac{1}{\gamma}\psi_e(\bar{\omega}_r v_\tau - z_\omega - \alpha_\omega - \dot{\beta})] + m_u z_{v_t}\dot{z}_{v_t}\\
&\quad + \lambda k_\tau(\tau-\tau_d)(v_\tau - \dot{\tau}_d) + \dot{\tilde{\tau}}[(1-\lambda)(\bar{v}_{tr}x_e\cos\psi_e + \bar{v}_{tr}y_e\sin\psi_e + \frac{1}{\gamma}\psi_e\bar{\omega}_r) + \lambda k_\tau(\tau-\tau_d)] + m_r z_\omega\dot{z}_\omega\\
&= (1-\lambda)[(\bar{v}_{tr}v_\tau\cos\psi_e - \alpha_{v_t})x_e + \bar{v}_{tr}v_\tau y_e\sin\psi_e + \frac{1}{\gamma}\psi_e(\bar{\omega}_r v_\tau - \alpha_\omega - \dot{\beta})] + z_{v_t}(m_u\dot{z}_{v_t} - (1-\lambda)x_e)\\
&\quad + \lambda k_\tau(\tau-\tau_d)(v_\tau - \dot{\tau}_d) + \dot{\tilde{\tau}}\Phi_e + z_\omega(m_r\dot{z}_\omega - \frac{1}{\gamma}\psi_e)\end{aligned}$$

Let the control laws for v_t and ω be chosen as

$$\begin{cases}\dot{v}_t = \dot{\alpha}_{v_t} + ((1-\lambda)x_e - k_{v_t}z_{v_t})/m_u\\ \dot{\omega} = \dot{\alpha}_\omega + (\frac{1}{\gamma}\psi_e - k_\omega z_\omega)/m_r\end{cases} \tag{5.56}$$

where k_{v_t}, k_ω are positive constants, and $\alpha_{v_t}, \alpha_\omega$, and the updating law for the virtual parameter $\tau(t)$ are given according to (5.54) as follows :

$$\begin{bmatrix}\alpha_{v_t}\\ \alpha_\omega\\ \dot{\tau}\end{bmatrix} = \begin{bmatrix}k_x x_e + \bar{v}_{tr}\dot{\tau}_d\cos\psi_e\\ \bar{\omega}_r\dot{\tau}_d - \dot{\beta} + \gamma y_e\bar{v}_{tr}\dot{\tau}_d\frac{\sin\psi_e}{\psi_e} + k_\psi\psi_e\\ \dot{\tau}_d - k_v\tanh\Phi_e\end{bmatrix} \tag{5.57}$$

Recalling the transformation between (τ_{vt}, τ_β) and (τ_u, τ_v) for fully-actuated AUV in (5.29),(5.30) and (5.31). By setting $\tau_v = 0$ in those equations, the corresponding transformation for underactuated AUV can be written as

$$\begin{cases}\tau_u = m_u\tau_{vt}/\cos\beta\\ \tau_\beta = -\tau_{vt}\tan\beta/v_t\end{cases} \tag{5.58}$$

Note that $\beta = \frac{\pi}{2}$ is impossible, as the surge velocity $u > 0$ is assumed for underwater vehicles.

In (5.58), there is

$$\begin{cases}\dot{v}_t = f_{vt}(v_t,\beta,r) + \tau_{vt}(\tau_u,\tau_v,v_t,\beta)\\ \dot{\beta} = f_\beta(v_t,\beta,r) + \tau_\beta(\tau_u,\tau_v,v_t,\beta)\\ \dot{r} = f_r(v_t,\beta,r) + \tau_r/m_r\end{cases} \tag{5.59}$$

and

$$\begin{cases}f_{vt} = (\frac{m_v}{m_u} - \frac{m_u}{m_v})v_t r\sin\beta\cos\beta - (\frac{d_u}{m_u}\cos^2\beta + \frac{d_v}{m_v}\sin^2\beta)v_t\\ f_\beta = -(\frac{m_v}{m_u}r\sin^2\beta + \frac{m_u}{m_v}r\cos^2\beta) + (\frac{d_u}{m_u} - \frac{d_v}{m_v})\sin\beta\cos\beta\\ f_r = -\frac{d_r}{m_r} + \frac{m_{ur}}{m_r}v_t^2\sin\beta\cos\beta\end{cases} \tag{5.60}$$

Hence, the control inputs in dynamics stage can be written as

$$\begin{cases} \tau_u = m_u(\dot{v}_t - f_{vt})/\cos\beta = [m_u\dot{\alpha}_{v_t} + ((1-\lambda)x_e - k_{v_t}z_{v_t}) - m_u f_{vt}]/\cos\beta \\ \tau_r = m_r\dot{r} - m_{uv}uv + d_r r = m_r\dot{\alpha}_\omega + (\frac{1}{\gamma}\psi_e - k_\omega z_\omega) - m_{uv}uv + d_r r \end{cases} \tag{5.61}$$

Replacing (5.56) and (5.57) into the derivative of V_{dyn}, there is

$$\dot{V}_{dyn} = -(1-\lambda)(k_x x_e^2 + \frac{k_\psi}{\gamma}\psi_e^2) - k_v \Phi_e \tanh\Phi_e - k_{v_t} z_{v_t}^2 - k_\omega z_\omega^2$$

That means, $\dot{V}_{dyn}$ is semi-negative definite and all the states $(x_e, \psi_e, (\tau - \tau_d), z_{v_t}, z_\omega)$ globally asymptotically converge to their equilibrium. Similarly with the kinematics controller design, it can be concluded that the equilibrium is $(x_e, y_e, \psi_e, (\tau - \tau_d), z_{v_t}, z_\omega) = 0^6$ by using Barbalat's lemma. Therefore, we can state the following proposition for dynamic path tracking control of underactuated AUV.

Proposition 5.2.2 (Path tracking 2 : underactuated AUV)

Under assumption 4.3.1 for a predefined $\mathcal{C}^1$ path given in (4.14) with desired speed $\dot{\tau}_d(t)$ for the time derivative of the path parameter $\tau_d(t)$, given the dynamics control inputs in (5.61), and the virtual control laws in (5.57). The control objective (5.47) of path tracking is achieved and the equilibrium point $[x_e, y_e, \psi_e, (\tau - \tau_d)]^T = 0^4$ is globally asymptotically stable.

- **Remarks :**

1. **Computation of side-slip angle**

   As the computation of side-slip angle is required in path following control in section 5.1.3, the same problem arises for path tracking control, due to $\ddot{\beta}$ appearing in the control computation of torque input τ_r in (5.61) as $\dot{\alpha}_\omega = f(\ddot{\beta})$ shown in (5.57). The same strategy is used to solve this problem, by resorting to the original dynamic model of the underactuated AUV.

   Firstly, recalling $\dot{\omega}$ in (5.56) and differentiating α_ω in (5.57), we can redefine $\dot{\omega}$ as

$$\dot{\omega} = B_1 - \ddot{\beta}$$

   where the intermediate variable

$$B_1 = \gamma(\dot{\bar{u}}_r y_e \dot{\tau}_d \frac{\sin\psi_e}{\psi_e} + \bar{u}_r \dot{y}_e \dot{\tau}_d \frac{\sin\psi_e}{\psi_e} + \bar{u}_r y_e \ddot{\tau}_d \frac{\sin\psi_e}{\psi_e} + \bar{u}_r y_e \dot{\tau}_d \frac{\cos\psi_e \psi_e \dot{\psi}_e - \sin\psi_e \dot{\psi}_e}{\psi_e^2})$$
$$+ \dot{\bar{\omega}}_r \dot{\tau}_d + \bar{\omega}_r \ddot{\tau}_d + k_\psi \dot{\psi}_e + (\frac{1}{\gamma}\psi_e - k_\omega z_\omega)/m_r$$

Secondly, define the intermediate variable A_1 as

$$A_1 = \bar{\omega}_r \dot{\tau}_d + \gamma y_e \bar{v}_{tr} \dot{\tau}_d \frac{\sin \psi_e}{\psi_e} + k_\psi \psi_e$$

Using the same expression (5.23) to represent β, such that α_ω in (5.57) can be rewritten as

$$\alpha_\omega = [A_1 + \frac{1}{v_t^2}(v\dot{u} + \frac{uvd_v}{m_v})]/(1 - \frac{m_u}{m_v}\cos^2\beta)$$

Finally, as $\ddot{\beta}$ given in (5.19), there is

$$\dot{\omega} = C_1/(1 - \frac{m_u}{m_v}\cos^2\beta)$$

where

$$C_1 = B_1 + \frac{\ddot{u}v}{v_t^2} + 2\frac{\dot{v}_t}{v_t}\dot{\beta} + \frac{u}{v_t^2}(\frac{m_u \dot{u} r + m_u u \dot{r} + \dot{d}_v v}{m_v})$$

Hence, the acceleration of side-slip angle $\ddot{\beta}$ can be computed through these intermediate variables.

Note that the term $(1 - \frac{m_u}{m_v}\cos^2\beta)$ appears in the denominator, the stern-dominant property of the underactuated AUV is still required, in order to let the computation of $\ddot{\beta}$ be well posed.

2. **Smooth transition from underactuated to fully actuated AUV**

The methodology to design the control law of path tracking for fully actuated AUV, is the same as that adopted for fully actuated AUV path following in section 5.1.4. The essential idea is that the side-slip angle is directly controllable in the case of fully actuated vehicle, such that the tedious algebraic computation of $\ddot{\beta}$ can be avoided. Similarly with (5.41), the control laws of path tracking for fully actuated AUV can be derived, by modifying the control laws for underactuated AUV in (5.61)

$$\begin{cases} \tau_{vt} = -f_{vt} + \dot{\alpha}_{v_t} + ((1-\lambda)x_e - k_{v_t} z_{v_t})/m_u \\ \tau_\beta = -f_\beta + \dot{\beta}_d - k_5(\beta - \beta_d) \\ \tau_r = m_r \dot{r} - m_{uv} uv + d_r r = m_r \dot{\alpha}_\omega + (\frac{1}{\gamma}\psi_e - k_\omega z_\omega) - m_{uv} uv + d_r r \end{cases} \tag{5.62}$$

where f_{vt}, f_β are given in (5.30).

Notice that $\dot{v}_t, \dot{\omega}$ in (5.56) are used to get above control laws for τ_{vt}, τ_r, while τ_β is directly derived from the Lyapunov function $V_\beta = \frac{1}{2}(\beta - \beta_d)^2$ due to the direct controllability of β in fully-actuated vehicles.

Then, the control inputs τ_u and τ_v can be derived by using the mapping between τ_u, τ_v and τ_β, τ_{vt} in (5.32).

Table 5.1 – SIRENE AUV : parameters of simplified model

$m = 4000$ Kg	$I_z = 2600$ Kg m^2	
$X_u = -360$ kg/s	$Y_v = -420$ kg/s	$N_r = -110$ Kg m/s
$X_{\dot{u}} = -290$ Kg	$Y_{\dot{v}} = -310$ Kg	$N_{\dot{r}} = -95$ Kg m^2
$X_{u\|u\|} = -805$ kg/m	$Y_{v\|v\|} = -1930$ kg/m	$N_{r\|r\|} = -555$ Kg m

Finally, after getting the control laws τ_u, τ_v, τ_r, similarly with the smooth path following transition from underactuated vehicle to fully-actuated vehicle in section 5.1.4, we can get the smooth path tracking transition, by means of bridging the control force in fully and under-actuated case with transition faction $f'(v_t)$:

$$f'(v_t) = \frac{\frac{\pi}{2} + \arcsin[k'_{vt}(v_t - \frac{v_{t1}+v_{t2}}{2})/(\frac{v_{t2}-v_{t1}}{2})]}{\pi} \tag{5.63}$$

where $k'_{vt} > 0$ is a slack variable and v_{t1}, v_{t2} are defined in (5.37), so that $0 \leq f'(v_t) \leq 1$.

Then, the smooth transition of path tracking control from underactuated vehicle to fully actuated vehicle can be chosen as :

$$\tau_v = f'(v_t)\tau_{v1} + (1 - f('v_t))\tau_{v2} \tag{5.64}$$

where $\tau_{v1} = 0$ is the control force in underactuated operating mode, and τ_{v2} is derived by the mapping from τ_β, τ_{vt} in (5.62) to τ_u, τ_v in (5.32).

5.3 Motion control examples

This section includes the simulation results, in order to illustrate the performance of the proposed path following and path tracking control laws for underactuated autonomous underwater vehicles.

Case 1 : path following of underactuated AUV

In this simulation, the simplified model of underactuated SIRENE AUV [Aguiar, 2001], is used and parameters are shown in Table 5.1.

The AUV is required to follow a 'S'-shape path given in Cartesian coordinates, which is parameterized as

$$x_s(\eta) = \sum_{i=1}^{5} a_i \eta^{i-1}, y_s(\eta) = \sum_{i=1}^{5} b_i \eta^{i-1} \tag{5.65}$$

where the path coefficients are given in Table.5.2.

Actually, the path in the path following problem is parameterized by along path distance s. The evolution of s is constrained by the virtual control law of $\dot{s}$ in (5.16),

Table 5.2 – The path parameters of AUV path following

coefficients/index	1	2	3	4	5
a_i	0	0.87	-0.02	-10^{-6}	1.5×10^{-6}
b_i	0	0.5	-10^{-3}	-10^{-5}	10^{-7}

Table 5.3 – Control parameters of AUV path following

$k_0 = 0.1$	$k_1 = 0.5$	$k_2 = 0.1$	$k_3 = 0.1$	$k_4 = 0.1$

such that $s(t)$ can be computed. Hence, s is known in the simulation while a precise estimation of the function $\eta(s)$ is unknown. However, it can be achieved by integration of

$$\frac{d\eta}{ds} = \frac{1}{\sqrt{x_s^\eta(\eta)^2 + y_s^\eta(\eta)^2}}$$

where $x_s^\eta(\eta) = \frac{\partial x_s(\eta)}{\partial\eta}$ and $y_s^\eta(\eta) = \frac{\partial y_s(\eta)}{\partial\eta}$.

The heading of the virtual target in inertial frame is $\psi_F(s) = \arctan\frac{y_s^\eta(\eta)}{x_s^\eta(\eta)}$, and the path curvature at the target position is $c_c(s) = \frac{\partial\psi_F(s)}{\partial\eta}\frac{d\eta}{ds}$.

The objective is to regulate the distance to the path and the heading of the total speed of the underactuated AUV to zero relative to the given path. Initial conditions of the AUV are as follows :

$u(0) = 0.1ms^{-1}, v(0) = 0ms^{-1}, r(0) = 0rads^{-1}$, $x(0) = 60m, y(0) = -20m, \psi(0) = \pi/2rad/s$. The desired surge speed is $u_d = 1.5m/s$ and $\dot{u}_d = 0, \ddot{u}_d = 0$. The initial value of along path distance is $s(0) = 0m$.

As SIRENE vehicle is $4.0m$ long, the parameter L in the LOS looking ahead distance (5.5) is chosen as $4.0m$. The control parameters are given in Table 5.3.

The actual and reference paths are shown in Figure 5.5, and the path following errors of AUV, x_e, y_e, ψ_e, are asymptotically converging to zero in Figure 5.6. The velocity profiles of AUV are illustrated in Figure 5.7, and the underactuated control efforts are shown in Figure 5.8.

Notice in Figure 5.9 how the virtual target moving along the path collaboratively adjust its speed (slow down-wait-speed up) to help the AUV to follow the path, and keep the same speed with the AUV at the desired value $u_d = 1.5m/s$ in the end.

In Figure 5.10, it clearly shows that the side-slip angle can not be ignored as its maximum value is around $0.5rad$, and its acceleration also varies during the path following stage. It proves the computation effort on the side-slip angle is valuable.

Case 2 : path tracking of underactuated AUV

In this simulation, the underactuated SIRENE AUV is required to track a reference

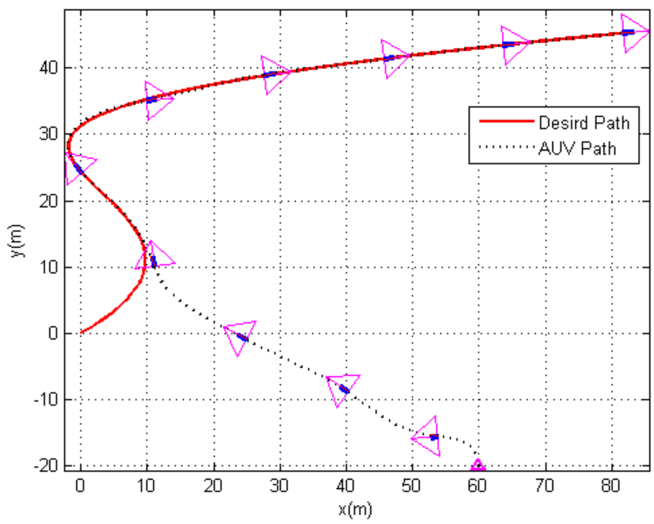

Figure 5.5 – Spatial convergence of AUV path following

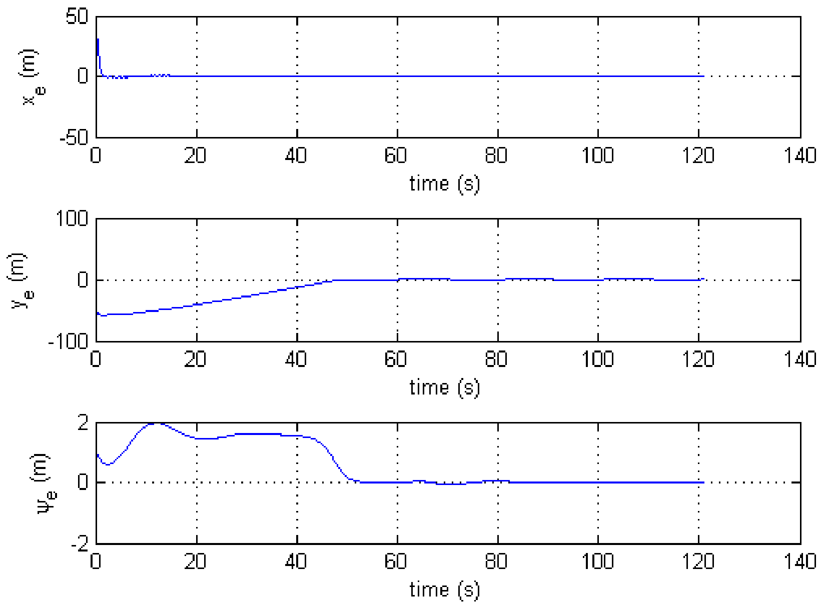

Figure 5.6 – Relative posture errors between AUV and target

sinusoid path, given by :

$x(\gamma) = 0, y(\gamma) = -6 + 6cos(0.04\pi\gamma), \dot{\gamma}(t) = 1.0m/s$

The objective is to regulate the distance to the path and the heading of the total speed of the vehicle to zero relative to the given path, while keeping the time convergence.

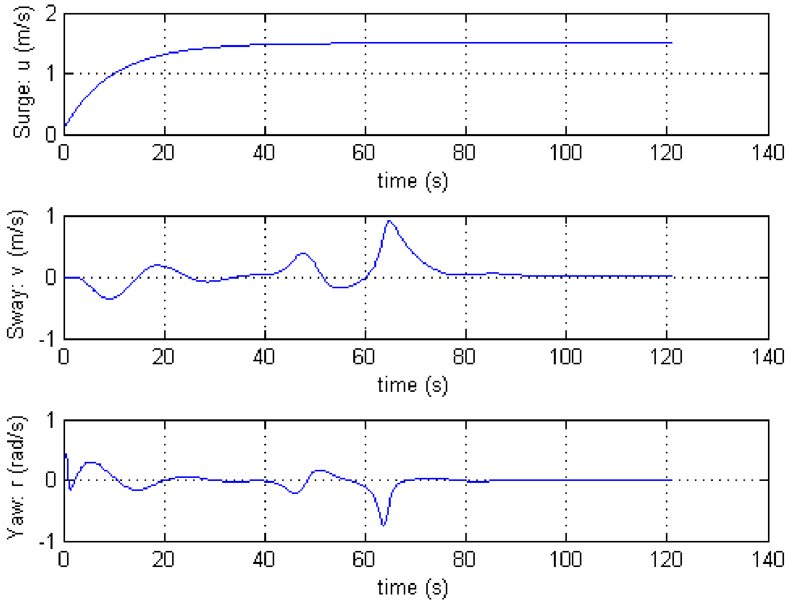

Figure 5.7 – Velocities profiles of AUV

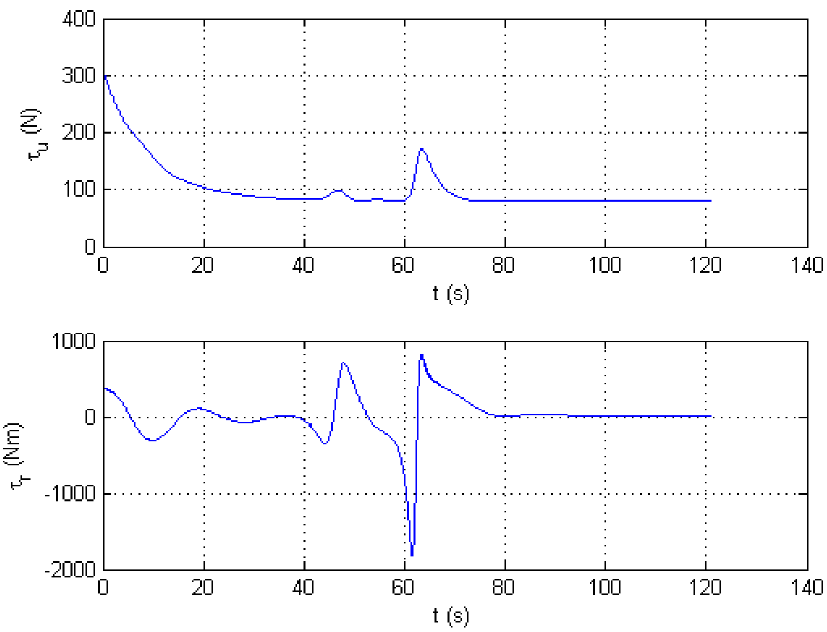

Figure 5.8 – Control inputs of AUV

Path tracking control law with weighting factor is adopted, while different weighting factors are chosen to compare the different path tracking behaviors. For each weighting factor, all initial conditions of the AUV are the same as follows :

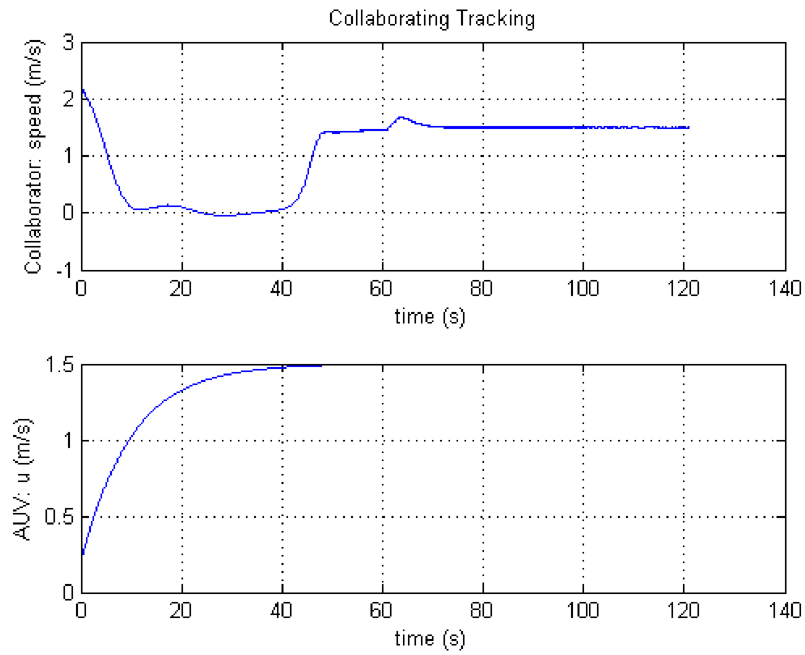

Figure 5.9 – Velocities of virtual target and AUV

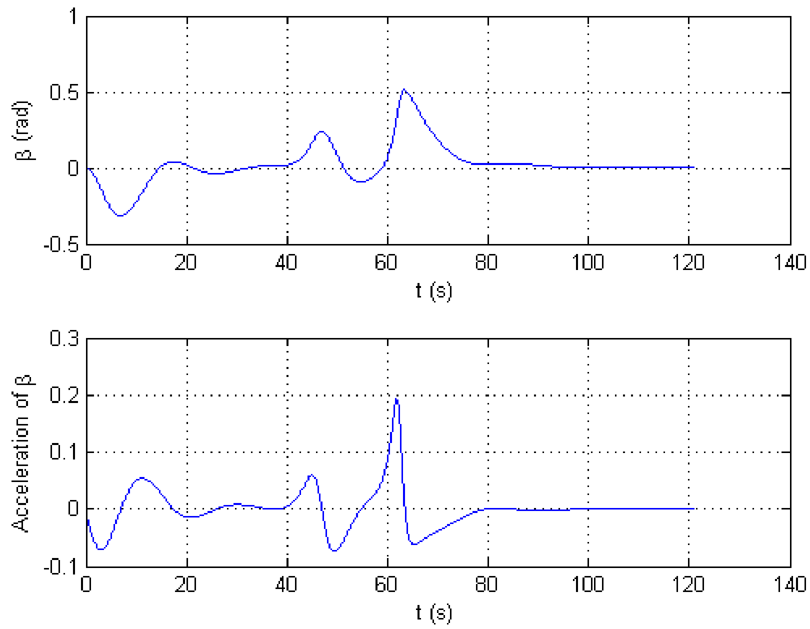

Figure 5.10 – Computation of underactuated AUV side-slip angle

$u(0) = 1.0ms^{-1}, v(0) = 0ms^{-1}, r(0) = 0rads^{-1}$, $x(0) = -10m, y(0) = 10m, \psi(0) = \pi/2$

For each weighting factor λ, control parameters are chosen as the same, as displayed

Table 5.4 – Control parameters of AUV path tracking

$k_x = 1.0$	$k_\psi = 1.0$	$\gamma = 1.0$	$k_\tau = 0.5$	$k_v = 0.3$

in Table 5.4.

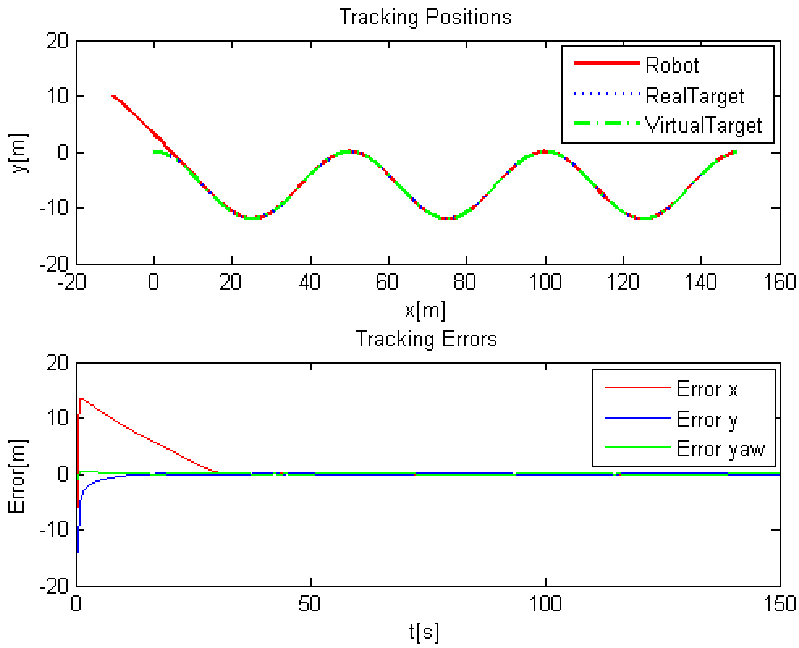

Figure 5.11 – Spatial convergence of PT : $\lambda = 0.1$

As path tracking merges the path following and trajectory tracking behaviors, λ is the key parameter to determine how much weights of the path following and trajectory tracking play in the whole path tracking design respectively. From the Lyapunov control function (5.48), it clearly shows that large λ means more trajectory tracking weighting added in the path tracking control.

In the Figures 5.11, 5.12 and 5.13, the spatial tracking performance is shown by comparing the spatial convergence and tracking errors between the vehicle and the path. From Figure 5.11 to 5.13, show that the performance of spatial convergence is decreased, and the speed of tracking error tending to zero slows down. This happens because increasing λ means decreasing the weighting of path following behavior, such that the spatial tracking convergence performance is degenerated.

In the Figures 5.14, 5.15 and 5.16, the temporal performance is shown by comparing the relative posture between the AUV and the TT target on the path. From Figure 5.14 to 5.16, the speed of temporal convergence is increased. This happens because increasing λ means increasing the weighting of trajectory tracking behavior, which has the advantage

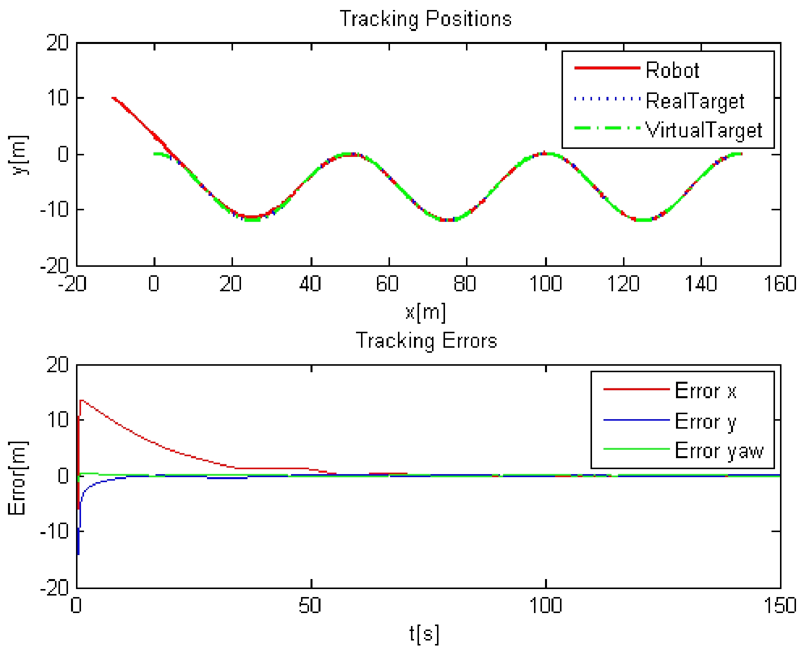

Figure 5.12 – Spatial convergence of PT : $\lambda = 0.5$

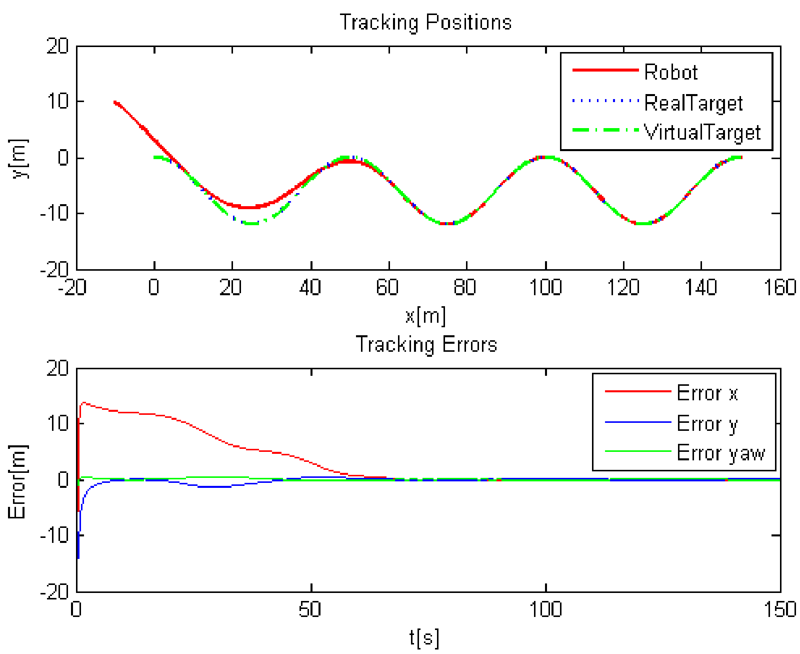

Figure 5.13 – Spatial convergence of PT : $\lambda = 0.99$

of keeping the temporal performance in motion control.

Hence, through this simulation, the path tracking behavior is well understood as a motion control strategy which blends the path following and trajectory tracking together

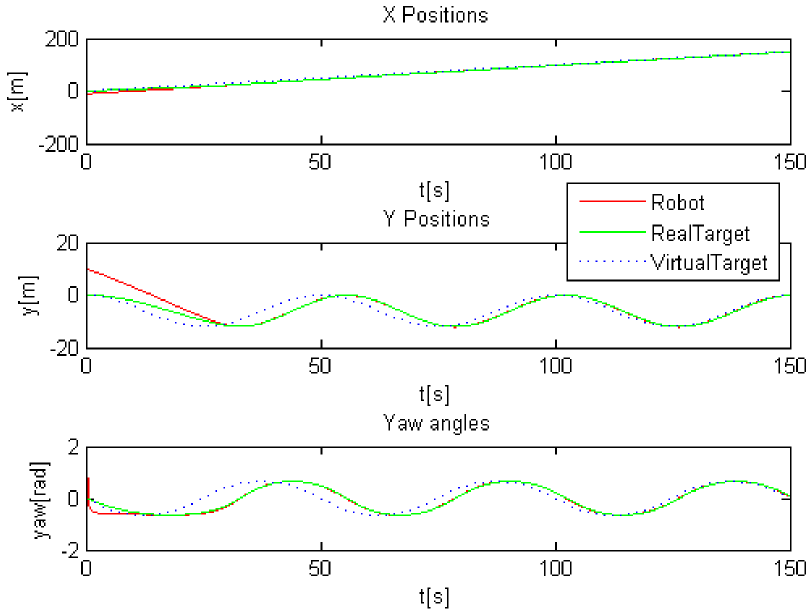

Figure 5.14 – Temporal convergence of PT : $\lambda = 0.1$

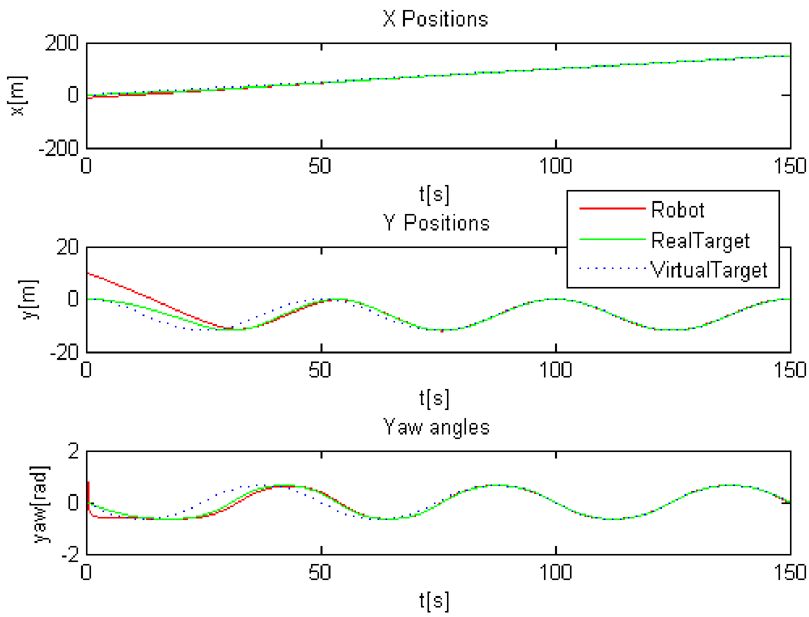

Figure 5.15 – Temporal convergence of PT : $\lambda = 0.5$

through the tunable weighting factor λ.

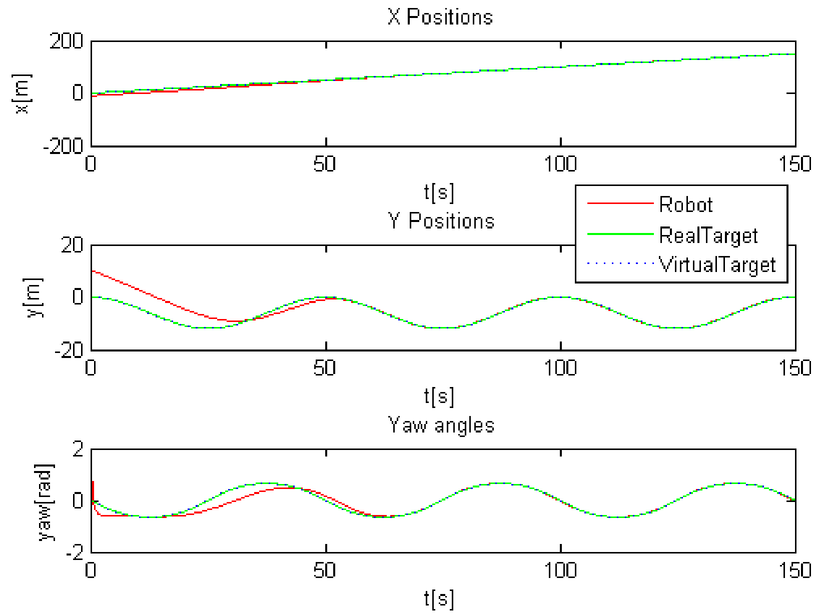

Figure 5.16 – Temporal convergence of PT : $\lambda = 0.99$

5.4 Summary

In this chapter, the problems of nonlinear motion control of path following and path tracking in case of underactuated AUVs, are addressed based on Lyapunov theory and backstepping technique.

- Traditional LOS guidance for following straight line is adapted for following curved path in the path following design, by building LOS in Frenet-Serret frame with helmsman-like behavior embedded.
- New control design without approaching angle or LOS guidance is proposed for path tracking design, and tunable weighting factor is introduced to blend the trajectory tracking and path following behaviors in path tracking strategy.
- The solution to computation of the acceleration of side-slip angle is given for both path following and trajectory tracking control where stern-dominant AUV is required for well-posed computation. Moreover, smooth control transitions from underactuated to fully actuated AUVs are also proposed for both control cases.

Finally, the simulation results illustrate the performance of the derived controllers.

CHAPTER 6

COORDINATED MOTION CONTROL OF MULTIPLE AUTONOMOUS VEHICLES

In this chapter, coordinated motion control design is proposed to address the problem of steering a group of autonomous underactuated and nonholonomic vehicles along given paths, while building and then keeping a desired inter-vehicle formation pattern. Two main coordinated control strategies are proposed, i.e., coordinated paths following and coordinated paths tracking, where the control of virtual targets moving along the paths is the fundmental issue. Moreover, each type of coordinated motion control is firstly solved under centralized framework based on leader-follower and virtual structure approaches respectively, and then solved under decentralized framework by using algebraic graph theory.

6.1 Coordinated paths following of multiple autonomous vehicles

In this section, centralized coordination based on leader-follower approach is firstly addressed for multiple vehicles following predefined paths, and then this idea is extended by considering each vehicle as a leader of other neighboring vehicles, or leaderless in the team, to build the decentralized coordination.

6.1.1 Problem formulation

In this section, the classification of multiple paths for coordinated path following control is firstly introduced. Then the mathematical formulation is build for parallel paths.

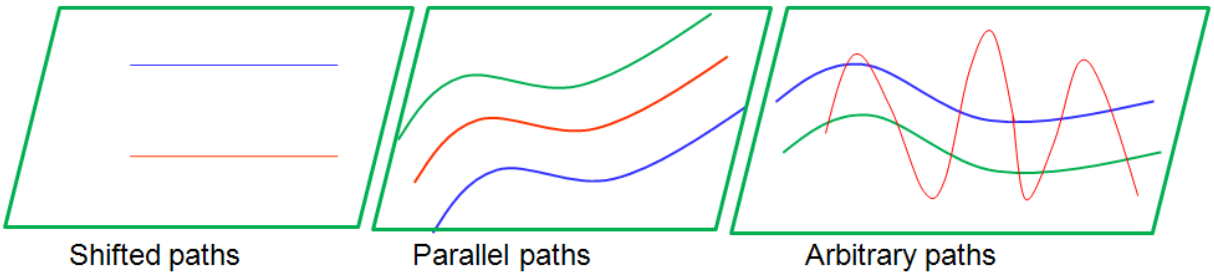

Figure 6.1 – Multiple paths for coordinated control illustrated in horizontal plane

6.1.1.1 Multiple paths classification

Generally, the definitions of three types of multiple paths, i.e., shifted paths, parallel paths and arbitrary paths in Figure 6.1, can be given as follows :

- **Shifted paths**
  Shifted paths means some identical paths, others being spatially shifted versions of one baseline path [Lapierre et al., 2003]. In an envisioned coordinated manner, shifted paths are requested in such a typical scenario : one autonomous surface craft (ASC) is required to follow a desired path, and an AUV operating at a fixed depth is required to follow a vertically shifted version of the same path while tracking the ASC motion along the path, in order to achieve fast underwater communication channel between them, exploiting the fact that high rate communication is achieved when the emitter and the receiver are aligned along the same vertical line.
- **Parallel paths**
  Parallel paths means some similar paths with the same shape, i.e., the same curvatures at the corresponding points on the paths. Normally, parallel paths are defined in the same horizontal plane. In an envisioned coordinated manner, parallel paths are planned for multiple vehicles in a formation, while vehicles follow them in order to get fast acoustic coverage without missing blocks, which is achieved by overlapping the acoustic coverage along parallel paths in a defined sea area.
- **Arbitrary paths**
  Arbitrary paths, mean no shifted or parallel relationships between planned paths. These kinds of paths can be predefined for irregular tasks. For instance, several AUVs act as mobile sensor suites to acquire scientific data, while one autonomous surface vehicle plays the role of a fast communication relay to collect all data from AUVs in a coordinated team. Hence, the path of the surface vehicle has to cross

the paths of AUVs in order to get a vertical communication channel. Obviously, paths of ASC and AUVs are not in a shifted or parallel pattern in this case.

The problem of coordinated control based on shifted paths has been solved in [Lapierre et al., 2003]. Hence, the coordinated paths following control based on parallel paths is of the main interest in this thesis, while the strategy to solve the coordinated problem of arbitrary paths will be described in the coordinated path tracking part.

6.1.1.2 Parallel paths formulation

Predefined parallel paths are in general not straight lines, but feasible curves. A in-line formation with n vehicles is created by a set of shifted vectors d_{yi}, relative to the baseline path of the virtual leader, as depicted in Figure 6.2. The individual path for vehicle i is

$$s_i(\mu) = s(\mu) + R_B^I d_{yi} \tag{6.1}$$

where μ is the path parameters, and R_B^I is the rotation matrix from a moving body frame B to the inertial frame I.

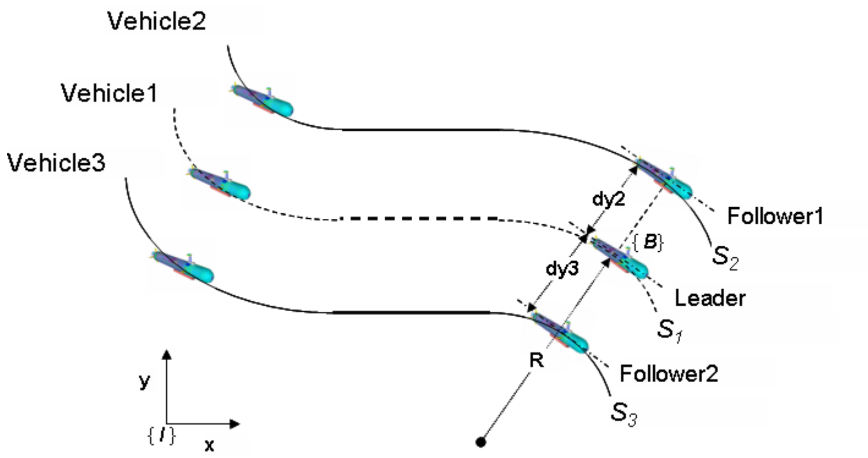

Figure 6.2 – Illustration of parallel paths setup

For underwater vehicle moving on the 2D plane, the desired path which a virtual leader is following, is then given by $s(\mu) = [x(\mu), y(\mu), \theta(\mu)]^T$. The tangent vector along the path in the (x, y) directions is chosen as the x axis of the moving body frame B. The angle of the tangent vector in the inertial frame I gives the heading $\theta(\mu) = arctan(\frac{y(\mu)'}{x(\mu)'})$. Therefore, the rotation matrix for the parallel paths is given by

$$R_B^I = \begin{pmatrix} cos\theta(\mu) & -sin\theta(\mu) & 0 \\ sin\theta(\mu) & cos\theta(\mu) & 0 \\ 0 & 0 & 1 \end{pmatrix}$$

Note that the paths generated by the baseline should be feasible, which can be guaranteed by the path planning stage.

6.1.2 Centralized control of coordinated paths following

In order to get centralized controller, the classic leader-follower strategy is adopted. That means one vehicle in the multi-vehicle team is chosen as the leader, to coordinate other follower vehicles achieving the desired geometric formation pattern.

6.1.2.1 Strategy of coordinated parallel paths following

In order to simplify the control design, one vehicle is elected as a leader, with the formation shifted vector $d_1 = [0, 0, 0]^T$. This means that the virtual leader coincides with the vehicle 1 in Figure 6.2, and the other vehicles i will be followers with shifted vector $d_i = [0, d_{yi}, 0]^T, i = 2, 3, ..., n$.

In the case of in-line formation for parallel paths as depicted in Figure 6.2, there is always a relationship between the along-path position of the virtual target of the leader vehicle s_1, and the desired along-path position of the virtual target of the follower s_2^d. That is

$$\dot{s}_2^d(\mu) = \frac{c_{c1}}{c_{c2}}\dot{s}_1(\mu) \tag{6.2}$$

Since $c_{ci} \in \Re$ and $c_{ci} = 1/R_i$, where R_i is the radii of the tangent circle (i.e. the circle of curvature which is tangent to the curve) at one point of the path. According to the path formulation, there is $R_2 = R_1 + d_{y2}$, such that

$$\frac{c_{c1}}{c_{c2}} = \frac{R_2}{R_1} = 1 + d_{y2}c_{c1}(\mu) \tag{6.3}$$

Substituting (6.3) into (6.2), there is

$$\dot{s}_2^d(\mu) = (1 + d_{y2}c_{c1}(\mu))\dot{s}_1(\mu)$$

Hence,

$$s_2^d(t) = s_1(t) + d_{y2}\int_0^t c_{c1}(t,\mu)\dot{s}_1(t,\mu)dt \tag{6.4}$$

6.1.2.2 Leader-follower Control

The design of control input τ_u in dynamics level for AUVs, is repeated here. Consider Lyapunov function candidate, $V_u = \frac{1}{2}(u - u_d)^2$. It is trivial to choose the control law $\dot{u} = \dot{u}_d - k_4(u - u_d)$ where $k_4 > 0$.

Consequently, the control force is

$$\tau_u = m_u\dot{u} - m_v vr + d_u u = m_u(\dot{u}_d - k_4(u - u_d)) - m_v vr + d_u u \tag{6.5}$$

By means of (6.5), surge force only drives the vehicle speed u converge to desired speed u_d (assuming $u_d(t) \geq u_{min} > 0$), with performance of globally uniformly exponentially stable.

It indicates that controlling u is totally decoupled with other control behaviors, i.e., steering the vehicle onto the path with x_e, y_e, ψ_e equal to zero through the yaw torque, is decoupled from driving u_t to u_{td}. This important theoretic root endows the path following controller with another dedicated ability of speed adaptation among vehicles, without degrading the steering performance of vehicle's convergence to the path.

Therefore, considering n vehicles tracking n paths, the feasible strategy for coordinated paths following based on centralized strategy is to perform two tasks, as :

(1) Geometric task : each vehicle (either the leader or the follower) recruit its own path following control law to track the dedicated path,

(2) Coordination task : adjusting the desired speed $u_{Fi}^d(i = 1, 2, \cdots, n)$ of the follower vehicles according to the speed of the leader u_L^d, make the coordinated parameter, i.e., the desired curvilinear abscissa (along path distance) $s_i^d(i = 1, 2, \cdots, n)$, to converge to some desired values.

Note that the total speed v_t is required to be aligned with the tangent direction of the path in the path following control. Hence, in the case of homogenous AUVs, driving u_i to u_{di} for each vehicle is enough to enable the AUVs to follow the n paths in a coordinated pattern, as the u_{di} leads to the appropriate v_{tdi}. While, in the case of heterogenous AUV, the total speed v_{ti} is required to approach to v_{tdi}, as the same u_{di} does not bring the same v_{tdi} due to the different dynamics of heterogenous AUVs [Lapierre and Soetanto, 2003]. Therefore, a specific transformation from u_i to v_{ti} is necessary in that case.

- **Leader Control**

In the case of the leader, a path following controller is easily obtained by directly recruiting control laws of individual AUV proposed in (5.7). That is,

$$\begin{cases} \dot{s}_L = k_1 x_{eL} + v_{tL} cos\psi_{eL} \\ \dot{\psi}_{eL} = \dot{\delta}_1 - y_{eL} v_t \frac{\sin\psi_{eL} - \sin\delta_L}{\psi_{eL} - \delta_L} - k_2(\psi_{eL} - \delta_L) \\ \dot{u}_L = \dot{u}_L^d - k_4(u_L - u_L^d) \end{cases} \tag{6.6}$$

where $(\cdot)_L$ represents the states of the leader, u_L^d is the desired speed profile of the leader, and $\dot{u}_L^d$ is the desired acceleration of the leader.

The first two equations in (6.6) contribute to minimize the along-tracking and cross-track errors, and the third one contributes to speed control.

- **Followers Control**

The follower recruits similar path following control laws to those recruited by the leader.

$$\begin{cases} \dot{s}_{F1} = k_1 x_{eF1} + v_{tF1} cos\psi_{eF1} \\ \dot{\psi}_{eF1} = \dot{\delta}_{eF1} - y_{eF1} v_{tF1} \frac{\sin\psi_{eF1} - \sin\delta_{eF1}}{\psi_{eF1} - \delta_{eF1}} - k_2(\psi_{eF1} - \delta_{eF1}) \\ \dot{u}_{F1} = \dot{u}^d_{F1} - k_4(u_{F1} - u^d_{F1}) \end{cases} \tag{6.7}$$

where $(\cdot)_{F1}$ represent the states of the first follower (AUV2) in Figure 6.2.

The only difference between the control of the leader and that of the follower is that, the follower's forward speed u_{F1} must be adapted to reduce the generalized along-path distance between the two vehicles to zero.

A solution proposed to speed adaption is

$$u^d_{F1} = u^d_L + \frac{2}{\pi} k_u \arctan(\Delta s_{LF1}) \tag{6.8}$$

where $\Delta s_{LF1} = s^d_{F1}(t) - s_{F1}(t) = [s_L(t) + d_{y2} \int_0^t c_{cL}(t,\mu))\dot{s}_L(t,\mu)dt] - s_{F1}(t)$ is the generalized along-path distance between the two vehicles, derived from (6.4).

Straightforward computations show that the derivative of the follower's speed is

$$\dot{u}^d_{F1} = \dot{u}^d_L + \frac{2}{\pi} k_u \frac{((1 + d_{y2} c_{cL}) u_L - \dot{s}_{F1})}{1 + (\Delta s_{LF1})^2} \tag{6.9}$$

where c_{cL} is the path curvature, and $k_u > 0$ is a slack variable to impose restrictions on how much the follower's speed is allowed to catch up with the leader.

There is one thing highlighted in the controller design, that only the generalized along-path length of the leader $s^d_i (= [s_L(t) + d_{yi} \int_0^t c_{cL}(t,\mu))\dot{s}_L(t,\mu)dt])$ is required for the follower, as c_{cL} can be estimated by means of the value of s_L and predefined path information. With the error of along-path distance (Δs_{LF1}) between the leader and the follower, the follower is able to reduce the relative distance, and then keep the relative position according to the leader. Neither speed nor Cartesian position of the leader is needed, such that the amount of information exchanged between two vehicles are minimal.

In the case of the second follower (AUV3) in Figure 6.2, the follower recruits similar path following and speed adaptation controls with those recruited by the first follower (AUV2). The only difference between the controllers of the follower AUV2 and AUV3, is that the error of along path distance Δs_{13} between the leader (AUV1) and the follower (AUV3) is different with Δs_{12} in mathematical formulation. As the follower AUV3 has the desired path on the left side of the leader's path, the error of along path distance is as follows

$$\begin{cases} u_{F2}^{d} = u_{L}^{d} + \frac{2}{\pi} k_{u} \arctan(\Delta s_{LF2}) \\ \dot{u}_{F2}^{d} = \dot{u}_{L}^{d} + \frac{2}{\pi} k_{v} \frac{((1-d_{y2}c_{cL})u_{L} - \dot{s}_{F2})}{1+(\Delta s_{LF2})^{2}} \\ \Delta s_{LF2} = [s_{L}(t) + d_{y3} \int_{0}^{t} c_{cL}(t,\mu)) \dot{s}_{L}(t,\mu) dt] - s_{F2}(t) \end{cases} \tag{6.10}$$

With control laws proposed here, both the leader and the follower asymptotically converge to the paths, and their relative along-path distance is guaranteed in terms of geometric constraints of the formation.

Proposition 6.1.1 (Centralized control of coordinated paths following : underactuated underwater vehicles)

Consider n underactuated AUVs with the dynamics equations in (3.17) and (5.10). Let n parallel paths be generated through (6.1). Assume $u_{L}^{d} \geq u_{Lmin}^{d} > 0$ is the desired speed for the leader vehicle. The feedback control laws in (6.6) for the leader, (6.7) and (6.10) for the followers, drive all vehicles converging to the predefined paths, and the error of generalized along-path distance $\Delta s_{LFi}, i = 1, 2., ..., n$ defined in the geometric formation, asymptotically converge to zero.

Proof The nonlinear coordinated controller design for path following in an in-line formation, is derived in four steps.

i) Adopting the first two equations of individual path following control laws in (6.6) for the leader and (6.7) for followers, the multi-AUV system will uniformally globally exponentially reach the largest invariant set $\{\Omega_{Path} | (x_{e,i}, y_{e,i}) = 0^{2}, \psi_{e,i} = 0, i = L, F_{1}, F_{2}, \cdots, F_{n}\}$.

ii) Adopting the last equation in (6.6) and (6.7), the multi-AUV system will uniformly globally exponentially reach the largest invariant set $\{\Omega_{v} | (x_{e,i}, y_{e,i}) \in \Re^{2}, \psi_{e,i} \in \Re, u_{ti} = u_{ti}^{d}, i = L, F_{1}, F_{2}, \cdots, F_{n}\}$.

iii) Under these two invariant sets, $\Omega_{path} \cap \Omega_{v}$ let's select the Lyapunov candidate function $V_{s} = \frac{1}{2} \Delta S_{LFi}^{2}$, and then we can get the derivative of Lyapunov function with the speed adaptation law in (6.8), such that

$$\dot{V}_{s} = \Delta S_{LFi}(u_{L}^{d} - u_{Fi}^{d}) = -\frac{1}{2} k_{v} \Delta S_{LFi} \arctan \Delta S_{1i}$$

That means, $\dot{\Delta} S_{LFi} < 0$ except the origin $\Delta S_{LFi} = 0$. Then, V_{s} is positive definite and radially unbounded. Therefore, we can conclude by standard Lyapunov arguments, the equilibrium point ($\Delta S_{LFi} = 0$) is global uniform asymptotic stable. For other followers, there are similar Lyapunov candidate functions to prove the along path distance of each follower approaching to that of the leader. Such that the state of the system converges to the largest invariant subset $\Omega_S = (\Delta S_{LF1}, \Delta S_{LF2}, \cdots, \Delta S_{LFn}) \in \Re^n | \Delta S_{LF1} = \Delta S_{LF2} = \cdots = \Delta S_{LFn} = 0\}$.

iv) we use LaSalle's invariance principle to concatenate the two previous convergence properties. The first and second step of the proof showed that every solution starting in $\{\Omega | (x_i, y_i) \in \Re^2\}$ where (x_i, y_i) is the initial position of vehicle, asymptotically converges to the invariant $\Omega_{path} \bigcap \Omega_v$. The third step showed that the largest invariant set of $\Omega_{path} \bigcap \Omega_v$, is the invariant manifold Ω_S. Therefore, every bounded solution starting in $\Re^2$ converges to invariant manifold Ω_S which indeed is $\Delta S_{LF1} = \Delta S_{LF2} = \cdots = \Delta S_{LFn} = 0$. Hence, all AUVs will be coordinated to follow the assigned paths in an in-line formation. ∎

Remark :

In the case of other formation patterns other than in-line formation, such as building a triangle formation, geometric specification has to be taken into account. Assuming vehicle1 is the leader, there is $\Delta_{1i} = [s_{1i} \pm d_{yi} \int_0^t c_{c1}(t, \mu)) \dot{s}_1(t, \mu) dt] - s_{1i} - l_i, i = 2, \cdots, n$, where l_i is the desired along track offset of the triangle formation.

6.1.3 Decentralized control of coordinated paths following

In the case of decentralized coordination, it means there is no leader in the multi-vehicle team and each vehicle plays an equal roles in the team, or rather than each vehicle is the "leader" of its neighboring vehicles inside communication range [Xiang et al., 2009b]. Therefore, considering n vehicles tracking n paths, the feasible strategy for coordinated paths following based on decentralized strategy is that

(1) Geometric task :

each vehicle recruits its own path following control law to track the path, such that $(x_{ei}, y_{ei}, \psi_{ei})^T = (0, 0, 0)^T$.

(2) Coordination task :

adjusting the desired speed $u_i^d, (i = 1, 2, \cdots, n)$ of each vehicle depending on the status of neighboring vehicles, make the coordination parameters, i.e., the desired curvilinear abscissa (along path distance) $s_i^d (i = 1, 2, \cdots, n)$, to converge to some desired values, such that $s_i^d = s_j^d, i \neq j, i, j \in \{1, 2, ..., N\}$.

With the above notation, the problem of coordinated path following for multiple underactuated vehicles can be formulated as below :

Coordinated path following of multiple Underactuated AUVs.

Consider n homogenous underactuated AUVs with kinematic and dynamic models given by (3.17) and (5.10) respectively. Given n spatial parallel paths to be followed by AUVs, *and a desired profile u_d for the final speed along the paths, derive feedback control laws, so that x_{ei}, y_{ei}, ψ_{ei}, $u_i - u_i^d$, and $s_i^d - s_j^d$ tend to zero asymptotically.*

Furthermore, information flow among vehicles in the communication network must be carefully treated, which plays a key role in decentralized control of multiple vehicles. In [Fax and Murray, 2004], [Olfati-Saber and Murray, 2004], algebraic graph theory is introduced to represent communication network, where each vehicle is one node and each communication link is one edge in the graph. Subsequently, algebraic graph theory supports a rigorous methodology to explicitly interpret the relationship between information flow and stability of the coordinated behavior of multiple vehicles. Hopefully, the elegant technique sheds some light on the problem of coordinated control for multi-vehicle system.

6.1.3.1 Algebraic graph theory

In this section, we will review the basic concept of graph and matrices associated with graph, which are the preliminaries of algebraic graph theory and Laplacian matrix. See for example [Godsil and Royle, 2001] and the references therein.

A communication topology is defined by a ***graph*** $G(V, E)$ with N vertices in a set of vertices V, and a set of edges E with edges $e_{ij} = (v_i, v_j) \in E$ and $v_i, v_j \in V$. We say that vertex v_i and v_j are connected if $(v_i, v_j) \in E$, and two vertices on the same edge or two edges with a common vertex are adjacent. If two edges have a common vertex, then they are incident with this vertex. The adjacent matrix A of graph G, is a positive square matrix of size $|V|$, whose ijth element $a_{ij} = 1$ if $(v_i, v_j) \in E$, and is zero otherwise. The degree matrix $D = D(A)$ of an undirected graph G, is the diagonal matrix with the number of its neighbors of each vertex along the diagonal denoted by $deg(v_i) = \sum_{j=1}^{n} a_{ij}$, where the set of neighbors of node i is denoted by $N_i = \{j : (v_i, v_j) \in E\}$.

The scalar *graph Laplacian matrix* $L = [l_{ij}]$ of an undirected graph is an $n \times n$ matrix associated with graph G, defined as

$$L = D(A) - A \tag{6.11}$$

Laplacian matrix L always has a right eigenvector of $\vec{1}_n = (1, \ldots, 1)^T$ associated with eigenvalue $\lambda_1 = 0$.

A *path* in the graph is a sequence of edges from v_i to v_j, such that two consecutive vertices are adjacent. A graph is said ***connected*** if there is a *path* between any distinct pair of vertices.

***Lemma* 1** *From [Godsil and Royle, 2001], the laplacian potential L of a (connected) undirected graph is positive semi-define and satisfies the following sum-of-squares (SOS) identity,*

$$S^T LS = \sum_{i,j \in E} (s_i - s_j)^2 \geq 0 \tag{6.12}$$

where $S = [s_1, s_2, ..., s_n]^T$ is the state vector of vertices, and s_i can be position, velocity, acceleration, etc.

***Lemma* 2** *From [Godsil and Royle, 2001], the Laplacian matrix of a connected graph, only has one single zero eigenvalue and the corresponding eigenvector is the vector of ones, $\vec{1}$.*

The following lemma summarizes the basic properties of graph Laplacians :

***Lemma* 3** *Let $G(V, E)$ be an undirected graph of order n with a non-negative adjacency matrix $A = A^T$.*

i) The graph G has $m \leq 1$ connected components iff rank$(L) = n - m$. Particularly, G is connected iff rank$(L) = n - 1$;

ii) Let G be a connected graph, then $\lambda_2(L) = \underline{min}_{z \perp \vec{1}_n} \frac{z^T Lz}{\|z\|^2} > 0$.

Proof : All three results are well-known in the field of algebraic graph theory and their proofs can be found in Godsil and Royle [Godsil and Royle, 2001].

Note that the quantity $\lambda_2(L)$ is known as *algebraic connectivity* of a graph. In [Olfati-Saber, 2006], it was shown that the speed of convergence of a linear consensus protocol is equal to $\lambda_2(L) > 0$.

All of above statements are very important characteristic of Laplacian matrix, and they are instrumental in designing decentralized controller for coordination of multiple autonomous vehicles. As a defined communication topology in a multi-vehicle system can be consider as a graph, and each vehicle is a vertex and each bi-directional communication channel is an edge in the corresponding graph. In Figure 6.3(a), the communication topology of a multi-vehicle system constructed by four underwater vehicles, is represented by a graph, and the corresponding Laplacian matrix is shown in Figure 6.3(b), according to the definition of the Laplacian matrix.

In this thesis, the communication topology of a multiple vehicles system is assumed that :

(1) the communication link between any pair of vehicle is reciprocal (i.e. bidirectional link) such that L is symmetric.

(2) the communication graph is connected, i.e., there is no vehicle is isolated from other vehicles in the team.

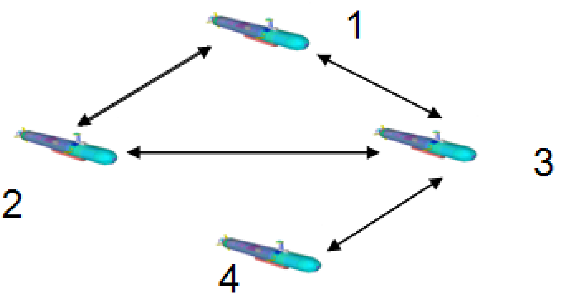

(a) Graph of a multi-vehicle communication topology

$$L = D - A = \begin{array}{cc} \begin{matrix} 1 & \;\;2 & \;\;3 & \;\;4 \end{matrix} & \\ \begin{pmatrix} 2 & -1 & -1 & 0 \\ -1 & 2 & -1 & 0 \\ -1 & -1 & 3 & -1 \\ 0 & 0 & -1 & 1 \end{pmatrix} & \begin{matrix} 1 \\ 2 \\ 3 \\ 4 \end{matrix} \end{array}$$

(b) Laplacian matrix of the corresponding graph

Figure 6.3 – Graph representation of a multiple underwater vehicle systems

6.1.3.2 Controller design

The coordinated controller design for synchronized path following of homogenous underactuated AUVs, is derived in three steps as following.

Step1 : Given individual path following control law (5.16) for each vehicle, the multi-vehicle system uniformly globally exponentially reach the largest invariant set $\{\Omega_{Path}|(x_{ei}, y_{ei})^T = 0^2, \psi_{ei} = 0, i = 1, 2, \cdots, n\}$

Step2 : Given individual path following control law (6.5) for each vehicle, the multi-vehicle system uniformly globally exponentially reach the largest invariant set $\{\Omega_u|(x_{ei}, y_{ei})^T \in \Re^2, \psi_{ei} \in \Re, u_i = u_{d_i}, i = 1, \cdots, n\}$

Step3 : Let's study the trajectories of the vehicles onto the largest invariant set Ω_{Path} and Ω_u. Under these two invariant sets, that is $\{\Omega_{Path} \cap \Omega_u\}$, all vehicles are on their own paths and will move along these paths with desired speeds. That means, each vehicle coincides with the corresponding virtual target moving on the individual path. So, we can claim that $\dot{S} = U_d$ as long as the control laws exist, where the desired speed profile is $U_d = [u_{d1}, u_{d2}, \ldots, u_{dn}]^T$, and $S = [s_1, s_2, \ldots, s_n]^T$.

Let consider Lyapunov candidate function

$$V_S = \frac{1}{2} S^T L S \tag{6.13}$$

As illustrated in Lemma 1, V_S has a quadric form such that $V_S \geq 0$. With the condition that, there are reciprocal communication links among each pair of nodes, which contributes to symmetric Laplacian matrix $L = L^T$. The time-derivative of V_S is

$$\mathbf{\dot{V}_S} = \frac{1}{2}\dot{S}^T L S + \frac{1}{2} S^T L \dot{S} = S^T L \dot{S}$$

Let the desired speed profile be

$$\mathbf{U_d} = \frac{u_{max} + u_{min}}{2}\vec{1} - (\frac{u_{max} - u_{min}}{2\pi}) \cdot arctan(LS)$$

Where : $u_{min} = [u_{1min}, u_{2min}, \ldots, u_{nmin}]^T$, and $u_{max} = [u_{1max}, u_{2max}, \ldots, u_{nmax}]^T$. u_{imin} and u_{imax} are the minimum and maxim speed of vehicle i ($i = 1, 2, \ldots, n$), respectively.

In order to simplify the matrix manipulation, special notations are made as following :

(1)$arctan(LS) = [arctan(L_1S), \ldots, arctan(L_nS)]^T$, and L_iS represents the ith row of Laplacian matrix L.

(2) $(\frac{u_{max}-u_{min}}{2\pi}) \cdot arctan(LS)$, represents *Hadamard product* of matrix $(\frac{u_{max}-u_{min}}{2\pi})$ and matrix $arctan(LS)$. For two matrices with the same dimensions, Hadamard product, is also known as the entrywise product and the Schur product, with the definition of $(A \cdot B)_{i,j} = A_{i,j} \cdot B_{i,j}$.

For homogenous AUVs, assuming that

$$(u_{imax} + u_{imin})/2 = (u_{jmax} + u_{jmin})/2 = u_{d0} \tag{6.14}$$

where $i \neq j, i, j \in \{1, 2, \cdots, n\}$, there is

$$\mathbf{U_d} = u_{d0}\vec{1} - (\frac{u_{max} - u_{min}}{2\pi}) \cdot arctan(LS) \tag{6.15}$$

Proposition 6.1.2 (Decentralized path following) *Consider the communication topology of multi-vehicle system represented by a connected graph with reciprocal links, let individual path following controller be given by (5.16) and (6.5). Let decentralized speed adaptation be given by (6.15) under the condition of (6.14). Then the homogenous underactuated multi-vehicle system globally asymptotically spatially synchronized to an invariant manifold $\{\Omega_S | LS = 0\}$, that is $s_1 = s_2 = \ldots = s_n$. Meanwhile, the speeds of all vehicles globally asymptotically convergence to a constant value $(u_{imax} + u_{imin})/2$.*

Proof As the trajectories of the system onto the invariant set Ω_{Path} and Ω_v, $\dot{S}$ equals to U_d, then there is

$$\begin{aligned}\dot{\mathbf{V}}_\mathbf{S} =& U_d S^T L\vec{1} - (LS)^T((\frac{u_{max} - u_{min}}{2\pi}) \cdot arctan(LS)) \\ =& -(LS)^T((\frac{u_{max} - u_{min}}{2\pi}) \cdot arctan(LS))\end{aligned}$$

There are three steps to simplify the derivative of Lyapunov function :

(1) Due to the fact that the sum of row vector of L equals to zero, $L\vec{1} = 0$, such that $U_d S^T L\vec{1} = 0$.

(2) $(LS)^T((\frac{u_{max}-u_{min}}{2\pi}) \cdot arctan(LS)) = \frac{1}{2\pi}\sum_{i=1}^{n}(u_{imax} - u_{imin})(L_iS)arctan(L_iS)$. As the function $f(x) = (x)arctan(x) \geq 0$, $(L_iS)arctan(L_iS) \geq 0$. In addition, $(u_{imax} - u_{imin}) > 0$, such that $(u_{imax} - u_{imin})(L_iS)arctan(L_iS) \geq 0$.

(3) As there is $U_d S^T L\vec{1} = 0$ in above step (1), and $(u_{imax} - u_{imin})(L_iS)arctan(L_iS) \geq 0$ in

step (2), $\dot{V}_S \leq 0$. That is, V_S is a nonnegative and monotonically non-increasing function up to a well-defined limit $lim_{t\rightarrow\infty} V_S = l_1$, which means $V_S = S^T LS$ is bounded.

Moreover, it is straightforward to show that $\ddot{V}_S$ is bounded so that $\dot{V}_S$ is uniformly continuous. Then, using Barbalat's lemma, $\dot{V}_S$ tends to 0 as t tends to ∞. That is $\dot{V}_S = \frac{1}{2\pi}\sum_{i=1}^{n}(u_{imax} - u_{imin})(L_i S)arctan(L_i S)$ tends to 0, which means $(L_i S)arctan(L_i S) = 0$, and $L_i S = 0$ at last.

Now, we can conclude that the state of the system converges to the largest invariant subset, i.e. invariant manifold $M = \{S \in \Re^n | LS = 0\}$, with decentralized control law (6.15) under speed condition in (6.14).

Interestingly, the invariant manifold M implies that, S are eigenvectors of L corresponding to the zero eigenvalue. In another word, S belong to span $\{\vec{1}\}$ when the corresponding graph is connected. That is, $M = \{S \in \Re^n | s_1 = s_2 = \ldots = s_n\}$.

Finally, we use LaSalle's invariance principle to concatenate the two previous convergence properties. Let $\Omega = \Re^2$. The first and second step of the proof showed that every solution starting in Ω asymptotically converges to the invariant $\{\Omega_{path} \cap \Omega_u\}$. The third step showed that the largest invariant set of $\{\Omega_{path} \cap \Omega_u\}$, is the invariant manifold M. Therefore, every bounded solution starting in Ω converges to invariant manifold M which indeed is $s_1 = s_2 = \ldots = s_n$, as t tends to ∞.

Consequently, $u_d = U_{d0}\vec{1} - (\frac{u_{max}-u_{min}}{2\pi}) \cdot arctan(LS) = U_{d0}\vec{1} = (u_{imax} + u_{imin})/2$, which means each vehicle will always have the same velocity, to keep the same state value of s_i upon synchronizing the state S, so the vehicles will be synchronized to follow the predefined paths. ∎

Remark :

Note that the application of LaSalle's invariance principle is restricted to autonomous system. Although the speeds of the vehicles in the team are varying due to the speed adaptation according to the neighbors' speeds and the paths information, the varying speeds depend on the system internal states, as $u_i = f_i(u_i, u_j, s_i, s_j, c_{ci})$ and u_d is constant. Hence, it still can be considered as an autonomous system and LaSalle's invariance stands in this case. If u_d is arbitrary time-varying, the whole system is nonautonomous. We need to resort to Barbalat's Lemma, which is used to address the time-varying formation problem in the following case of coordinated paths tracking.

6.2 Coordinated paths tracking of multiple autonomous vehicles

In this section, individual path tracking control is extended to coordinated path tracking of multiple vehicles. Both the centralized and decentralized control strategy are adopted. In case of centralized control, the formation reference point(FRP) with formation feedback constructing the virtual formation structure, is proposed to coordinate the multi-vehicle team while achieving robustness of single vehicle perturbation. In case of decentralized control, shared information from neighboring vehicles is used to design the decentralized controller of coordinated paths tracking based on the algebraic graph theory and virtual structure framework. For sake of simplicity, nonholonomic unicycle-type vehicles are considered for coordinated paths tracking, however the same control problem for underactuated AUVs can be casted into the same strategy.

6.2.1 Problem formulation

In [Ren et al., 2004], the virtual structure method is used to design coordinated formation control and applied to spacecrafts. The coordination vector $\xi = [r_F, v_F, q_F, \omega_F, \lambda_F, \dot{\lambda}_F]$ representing the desired states of the virtual structure including six elements, is the necessary amount of information broadcasted by each spacecraft to coordinate its motion with the group. However, this approach leads to a heavy communication load for underwater vehicles if one uses this strategy for multi-AUV system. It is worthy to pursue other possible strategies with a single exchanging variable for coordinated control. Indeed, in our approach to coordinated paths tracking, the path parameter τ in the paths tracking setup is one suitable candidate to achieve this performance.

For a general setup of coordinated formation control of nonholonomic unicycle-type vehicles under a virtual structure framework, one is given a team of $n \geq 2$ vehicles, and each vehicle is required to track a set of individual reference paths $\Gamma_i(\tau_i), i \in \{1, \ldots, n\}$, which are continuously parameterized by scalar variable $\tau_i \in \Re$ and related to the center of the virtual structure. Furthermore, vehicles are required to move along the paths to maintain a desired formation pattern with specific geometric constraints, such as "in-line", "triangle" or "polygonal" formation pattern, etc.

For the coordinated formation problem, the i-th path $\Gamma_i(\tau_i) = [x_{ri}(\tau_i), y_{ri}(\tau_i), \psi_{ri}(\tau_i)]^T$ can be designated as a general offset (not limited by parallel translation) of a "baseline" path $\Gamma_i(\tau_0) = [x_{r0}(\tau_0), y_{r0}(\tau_0), \psi_{r0}(\tau_0)]^T$ in horizontal plane, illustrated in Figure 6.4. When the virtual target moves along the baseline $\Gamma_i(\tau_0)$ with time evolving law $\dot{\tau}_0(t)$,

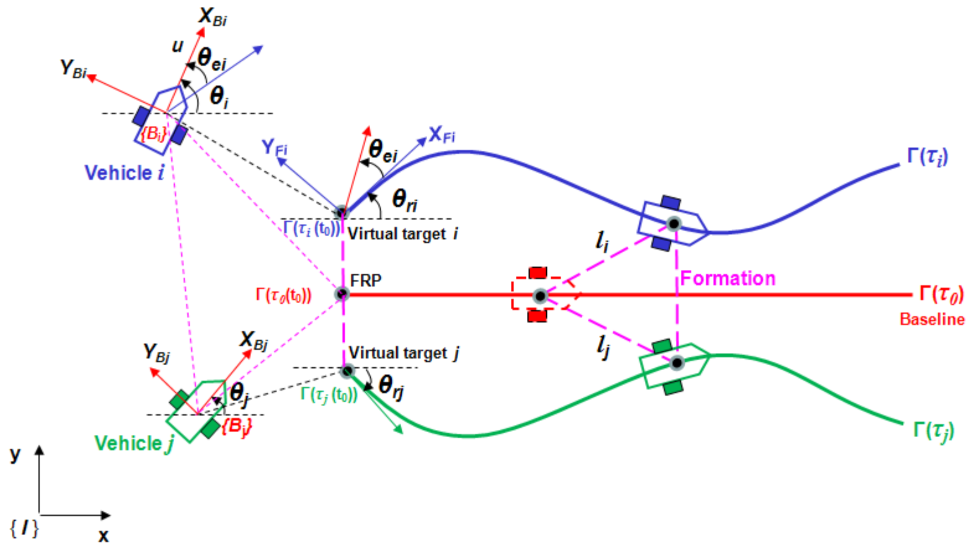

Figure 6.4 – Paths setup for coordinated formation tracking

there is a corresponding virtual target moving along the designated path $\Gamma_i(\tau_i)$ with timing law $\dot{\tau}_i(t)$. Obviously, if the path parameters $\tau_i(t)$ are synchronized, the vehicle member i will be in the desired in-line formation. In other words, the virtual target in the baseline acts as the center of the virtual structure, or rather than a **formation reference point** (***FRP***) [Skjetne et al., 2002]. As long as the FRP moves along the baseline, the i-th vehicle will then follow the individual desired path generated by the arbitrary translation operation as follows :

$$\Gamma_i(\tau_i) = \Gamma_{r0}(\tau_i) + R(\psi_{r0}(\tau_i))l_i(x_{r0}(\tau_i), y_{r0}(\tau_i)) \tag{6.16}$$

The rotation matrix $R(\psi_{r0}(\tau_i))$ from a frame $\{F\}$ associates the virtual target on the baseline to the inertial frame $\{I\}$, which is given by :

$$R(\psi_{r0}(\tau_i)) = \begin{bmatrix} \cos(\psi_{r0}(\tau_i)) & -\sin(\psi_{r0}(\tau_i)) & 0 \\ \sin(\psi_{r0}(\tau_i)) & \cos(\psi_{r0}(\tau_i)) & 0 \\ 0 & 0 & 1 \end{bmatrix}$$

where

$$\begin{cases} \psi_{r0}(\tau_i) = \text{atan2}(y_{r0}^{\tau_i}(\tau_i)/x_{r0}^{\tau_i}(\tau_i)) \\ x_{r0}^{\tau_i}(\tau_i) = \frac{\partial x_{r0}(\tau_i)}{\partial \tau_i} \\ y_{r0}^{\tau_i}(\tau_i) = \frac{\partial y_{r0}(\tau_i)}{\partial \tau_i} \end{cases}$$

The offset vector l_i is constructed as

$$l_i(x_{ri}(\tau_i), y_{ri}(\tau_i)) = \begin{bmatrix} f_{xi}(x_{ri}(\tau_i), y_{ri}(\tau_i)) \\ f_{yi}(x_{ri}(\tau_i), y_{ri}(\tau_i)) \\ 0 \end{bmatrix}$$

where $f(\cdot)$ is the offset function related to the different geometric formation constraints, and $f(\cdot)$ is possible varying to allow for varied formation patterns.

Similarly with (4.16) and (4.17), the desired linear and angular velocity of the virtual target i on the path $\Gamma_i(\tau_i)$, are

$$\begin{bmatrix} u_{ri}(\tau_i) \\ \omega_{ri}(\tau_i) \end{bmatrix} = \begin{bmatrix} \bar{u}_{ri}(\tau_i)\dot{\tau}_i \\ \bar{w}_{ri}(\tau_i)\dot{\tau}_i \end{bmatrix} \tag{6.17}$$

with

$$\begin{cases} \bar{u}_{ri}(\tau_i) = \sqrt{x_{ri}^{\tau_i}(\tau_i)^2 + y_{ri}^{\tau_i}(\tau_i)^2} \\ \bar{w}_{ri}(\tau_i) = \frac{x_{ri}^{\tau_i}(\tau_i) y_{ri}^{\tau_i^2}(\tau_i) - x_{ri}^{\tau_i^2}(\tau_i) y_{ri}^{\tau_i}(\tau_i)}{x_{ri}^{\tau_i}(\tau_i)^2 + y_{ri}^{\tau_i}(\tau_i)^2} \end{cases} \tag{6.18}$$

where $x_{ri}^{\tau_i^2}(\tau_i) = \partial^2(x_{ri}(\tau_i))/\partial\tau_i^2$ and $y_{ri}^{\tau_i^2}(\tau_i) = \partial^2(y_{ri}(\tau_i))/\partial\tau_i^2$.

Notice that in the traditional virtual structure approach, the distance from each virtual target to the structure center is constant such that the shape of the structure is rigid and cannot be changed [Lewis and Tan, 1997] . However, the flexible virtual structure proposed here can build varied formation shapes, by easily changing the offset vector in real time depending on the situations, for instance, changing a column formation to a row formation in order to enable a team of vehicles pass a narrow scope.

After the formulation of each reference path for each vehicle, the next step is to design a controller such that each vehicle tracks its own desired path, and all the path parameters of the reference paths are coordinated (that is, synchronizes the motions of the virtual targets along the paths in temporal specification) in order to build the formation shape.

Let the individual path tracking error state vector $\mathbf{p}_{eiB} = [x_{ei}, y_{ei}, \theta_{ei}]^T = 0^3$ be built in the i-th vehicle body frame $\{B_i\}$. As described in section 3.3.2.1, we can define the tracking error vector as

$$\mathbf{p}_{eiB} = \begin{bmatrix} x_{ei} \\ y_{ei} \\ \theta_{ei} \end{bmatrix} = \begin{bmatrix} \cos\theta_i & \sin\theta_i & 0 \\ -\sin\theta_i & \cos\theta_i & 0 \\ 0 & 0 & 1 \end{bmatrix} \begin{bmatrix} x_{ri} - x_i \\ y_{ri} - y_i \\ \theta_{ri} - \theta_i \end{bmatrix} \tag{6.19}$$

where $P_{iI} = [x_i, y_i, \theta_i]^T$ is the i-th vehicle state vector and $\Gamma_{iI} = [x_{ri}, y_{ri}, \theta_{ri}]^T$ is the corresponding reference state vector attached to the i-th reference path in the inertial frame $\{I\}$.

Resorting to the velocity vector $(u_{ri}, \omega_{ri})^T$ of the i-th vehicle expressed by path parameter in (6.17), the corresponding error state dynamics in the i-th vehicle body frame $\{B_i\}$ can be rewritten as follows :

$$\begin{bmatrix} \dot{x}_{ei} \\ \dot{y}_{ei} \\ \dot{\theta}_{ei} \end{bmatrix} = \begin{bmatrix} \omega y_{ei} - u_i + \bar{u}_{ri}\dot{\tau}_i \cos\theta_{ei} \\ -\omega x_{ei} + \bar{u}_{ri}\dot{\tau}_i \sin\theta_{ei} \\ \bar{\omega}_{ri}\dot{\tau}_i - \omega_i \end{bmatrix} \tag{6.20}$$

where $[u_i, \omega_i]^T$ is the i-th vehicle state vector and $[u_{ri}, \omega_{ri}]^T$ is the i-th reference velocity vector.

- **Remark** :

The proposed virtual-structure concept can be extended to the dynamic virtual structure with rotation and scaling. In this case, the paths can be defined as follows :

$$\Gamma_i(\tau_i) = \Gamma_{r0}(\tau_i) + R(\theta)SR(\psi_{r0}(\tau_i))l_i(x_{r0}(\tau_i), y_{r0}(\tau_i)) \tag{6.21}$$

The rotation matrix $R(\theta)$ is

$$R(\theta) = \begin{bmatrix} \cos\theta(t) & \sin\theta(t) \\ -\sin\theta(t) & \cos\theta(t) \end{bmatrix} \tag{6.22}$$

where $\theta(t)$ is the rotation angle.

The scaling matrix S is

$$S = \begin{bmatrix} s_1(t) & 0 \\ 0 & s_2(t) \end{bmatrix} \tag{6.23}$$

where $s_1(t)$ and $s_2(t)$ are scaling factors. It means that the desired virtual structure expands as long as the scaling factor decreases, shrinks vice versa.

Assumption 6.2.1 ***paths for multiple vehicles***

For each desired geometric reference path, assumption 1 in section 4.3.1 holds. That means each path has the characteristics of :

- *Uniqueness : Each τ_i maps into a unique value of $(x_{ri}(\tau_i), y_{ri}(\tau_i))$*
- *Regularity :* $0 < \sqrt{x_{ri}^{\tau_i}(\tau_i)^2 + y_{ri}^{\tau_i}(\tau_i)^2} < k$
- *Persistent excitation :* $\lim_{t\to\infty} \dot{\tau}_i(t) \neq 0$

Assumption 6.2.2 ***global information feedback for multiple vehicles***

The following assumption is hold throughout for ***centralized coordination with formation feedback****.*

- *Global information share*

  Each vehicle in the coordination team broadcasts its error state $P_{eiB} = (x_{ei}, y_{ei}, \psi_{ei})^T$ to the rest of the vehicles. And, it can receive error states from other vehicles in the team, in order to build global formation feedback.

These information exchanges guarantee the implementation of formation information feedback, such that the motion behavior of each vehicle will take into account motion states of other vehicles, and the formation can be still achievable even in the case of speed saturations or disturbances on some vehicles [Egerstedt et al., 1998, Beard et al., 2001b, Ogren et al., 2002, Do, 2008]. The trade-off is that the additional information about other team members are required, while each vehicle requires only the path parameter and measurement of its own state for centralized coordination without formation feedback, which is prone to collapse due to saturation and disturbance.

For the problem of path tracking shown in Figure. 6.4, there are two assignments assembled in the sense that :

(1) Geometric assignment :
ensures each individual vehicle converges to the virtual target and moves along the path with its linear velocity tangential to the path ;

(2) Dynamic assignment :
guarantees synchronization of all the path parameters such that vehicles in the team keep the desired relative distance to the formation reference point in the formation.

The coordinated path tracking control methodology also belongs to "Divide to Conquer" strategy, original proposed for coordinated paths following control in [Almeida et al., 2010]. Using this framework, path convergence (in space) and inter-vehicle coordination (in time) can be essentially decoupled. Path convergence for each vehicle aims at minimizing tracking error vector to zero. Inter-vehicle coordination is achieved by adjusting the "speed" of each virtual target along its path according to information on the positions of a set of neighboring virtual targets. Complicated kinematic or dynamic information is not required to be exchanged among the vehicles.

Therefore, the control objective of coordinated path tracking is to design a controller and achieve the following tasks :

$$\begin{aligned} &\lim_{t\to\infty} \|P_{eiB}\| = 0 \\ &\lim_{t\to\infty} |\tau_i(t) - \tau_0(t)| = 0 \end{aligned} \tag{6.24}$$

where τ_i is the path parameter of reference path Γ_i, and τ_0 determining the "pace" of the formation team, is the path parameter of the baseline Γ_0. $P_{eiB} = (x_{ei}, y_{ei}, \theta_{ei})^T$ is the tracking error vector of the i-th vehicle with respect to the virtual target evolving with timing law $\dot{\tau}_i(t)$, built in the i-th vehicle body frame $\{B_i\}$, and $\dot{\tau}_0(t)$ is the desired speed assignment for the FRP moving along the baseline path.

6.2.2 Centralized coordination of paths tracking

When addressing the centralized coordination problem, the formation reference point (FRP) receives formation feedback information, which is used to design the controller. Later, the controller is extended to the case where the individual physical vehicle in the team get formation feedback, to achieve robustness to vehicle failure or actuator saturation.

6.2.2.1 FRP with global formation feedback

Similarly to the individual path tracking control design, we introduce the approaching angle $\delta_i(y_{ei}, \dot{\tau}_i)$ for each vehicle to shape the desired orientation during transient path tracking behavior, such that

$$\begin{cases} \delta_i(0, \dot{\tau}_i) = 0 \\ -y_{ei}\dot{\tau}_i \sin\delta_i \geq 0 \end{cases} \tag{6.25}$$

Thus, the function $\delta_i(y_{ei}, \dot{\tau}_i)$ can be chosen as a sigmoid function

$$\delta_i(y_{ei}, \dot{\tau}_i) = -sign(\dot{\tau}_i)\theta_a \tanh(k_\delta y_{ei}) \tag{6.26}$$

where the shaping coefficient $k_\delta > 0$, $0 < \theta_a < \pi/2$, and $sign(\cdot)$ is the sign function.

In order to introduce the tracking error feedback, define the variable $\tilde{\tau}$, such that its derivative is :

$$\dot{\tilde{\tau}}_i = \dot{\tau}_i - v_{\tau i}(t, x_{ei}, y_{ei}, \theta_{ei}) \tag{6.27}$$

where $\dot{\tilde{\tau}} = [\dot{\tilde{\tau}}_i]_{n\times 1}$ can be considered as speed disagreement error vector of formation tracking.

The Control Lyapunov function is selected as new one in a positive definite quadratic form

$$V = \frac{1}{2}\sum_{i=1}^{n}[x_{ei}^2 + y_{ei}^2 + \frac{1}{\gamma}(\theta_{ei} - \delta_i)^2] + \frac{1}{2}\sum_{i=1}^{n} k_\tau(\tau_i - \tau_0)^2 \tag{6.28}$$

where τ_i is the actual path parameter of i-th vehicle, and τ_0 is the desired path parameter for the whole formation team where $\lim_{t\to\infty} \dot{\tau}_0 \neq 0$.

The time derivative of (6.28) along the solution of (6.20) is

$$\begin{aligned}\dot{V} &= \sum_{i=1}^{n}[x_{ei}(y_{ei}\omega_i - u_i + u_{ri}\cos\theta_{ei}) + y_{ei}(-x_{ei}\omega_i + u_{ri}\sin\theta_{ei}) + \frac{1}{\gamma}(\theta_{ei} - \delta_i)(\dot{\theta}_{ei} - \dot{\delta}_i) \\ &+ k_\tau(\tau_i - \tau_0)(\dot{\tau}_i - \dot{\tau}_0)] \\ &= \sum_{i=1}^{n}[-x_{ei}u_i + u_{ri}x_{ei}\cos\theta_{ei} + u_{ri}y_{ei}\sin\theta_{ei} + \frac{1}{\gamma}(\theta_{ei} - \delta_i)(\dot{\theta}_{ei} - \dot{\delta}_i) + k_\tau(\tau_i - \tau_0)(\dot{\tau}_i - \dot{\tau}_0)]\end{aligned}$$

Adding $u_{ri}y_{ei}\sin\delta_i - u_{ri}y_{ei}\sin\delta_i$ to above equation, there is

$$\begin{aligned}\dot{V} &= \sum_{i=1}^{n}[-x_{ei}u_i + u_{ri}x_{ei}\cos\theta_{ei} + u_{ri}y_{ei}\sin\delta_i + \frac{1}{\gamma}(\theta_{ei} - \delta_i)(\dot{\theta}_{ei} - \dot{\delta}_i + \gamma u_{ri}y_{ei}\frac{\sin\theta_{ei} - \sin\delta_i}{\theta_{ei} - \delta_i}) \\ &+ k_\tau(\tau_i - \tau_0)(\dot{\tau}_i - \dot{\tau}_0)]\end{aligned}$$

Substituting (6.17), (6.18) and (6.27) into the derivative of Lyapunov control function, yields

$$\begin{aligned}
\dot{V} &= \sum_{i=1}^{n}[x_{ei}(\bar{u}_{ri}\dot{\tau}_i\cos\theta_{ei} - u_i) + y_{ei}\bar{u}_{ri}\dot{\tau}_i\sin\delta_i + \frac{1}{\gamma}(\theta_{ei}-\delta_i)(\dot{\theta}_{ei} - \dot{\delta}_i + \gamma\bar{u}_{ri}\dot{\tau}y_{ei}\frac{\sin\theta_{ei}-\sin\delta_i}{\theta_{ei}-\delta_i}) \\
&+k_\tau(\tau_i-\tau_0)(\dot{\tilde{\tau}}_i + v_{\tau i} - \dot{\tau}_0)] \\
&= \sum_{i=1}^{n}\{x_{ei}(\bar{u}_{ri}v_{\tau i}\cos\theta_{ei} - u_i) + y_{ei}\bar{u}_{ri}v_{\tau i}\sin\delta_i + \dot{\tilde{\tau}}_i[x_{ei}\bar{u}_{ri}\cos\theta_{ei} + y_{ei}\bar{u}_{ri}\sin\delta_i + \frac{1}{\gamma}(\theta_{ei}-\delta_i)\bar{\omega}_{ri}] \\
&+\frac{1}{\gamma}(\theta_{ei}-\delta_i)(\bar{\omega}_{ri}v_{\tau i} - \omega_i - \dot{\delta}_i + \gamma y_{ei}\bar{u}_{ri}v_{\tau i}\frac{\sin\theta_{ei}-\sin\delta_i}{\theta_{ei}-\delta_i}) + k_\tau(\tau_i-\tau_0)(\dot{\tilde{\tau}}_i + v_{\tau i} - \dot{\tau}_0)\}
\end{aligned} \tag{6.29}$$

Proposing the control inputs as

$$\begin{bmatrix} u_i \\ \omega_i \end{bmatrix} = \begin{bmatrix} k_1 x_{ei} + \bar{u}_{ri}v_{\tau i}\cos\theta_{ei} \\ \bar{\omega}_{ri}v_{\tau i} - \dot{\delta}_i + \gamma y_{ei}\bar{u}_{ri}v_{\tau i}\frac{\sin\theta_{ei}-\sin\delta_i}{\theta_{ei}-\delta_i} + k_\theta(\theta_{ei}-\delta_i) \end{bmatrix} \tag{6.30}$$

and choosing

$$\begin{bmatrix} v_{\tau i} \\ \dot{\tilde{\tau}}_i \end{bmatrix} = \begin{bmatrix} \dot{\tau}_0 \\ -k_v\tanh[x_{ei}\bar{u}_{ri}\cos\theta_{ei} + y_e\bar{u}_{ri}\sin\delta_i + \frac{1}{\gamma}(\theta_{ei}-\delta_i)\bar{\omega}_{ri} + k_\tau(\tau_i-\tau_0)] \end{bmatrix} \tag{6.31}$$

utilizing the first element in (6.17) again, yields

$$\dot{V} = \sum_{i=1}^{n}[-k_e x_{ei}^2 - k_v\Phi_{Ei}\tanh(\Phi_{Ei}) + y_{ei}\bar{u}_{ri}\dot{\tau}_0\sin\delta_i - \frac{k_\theta}{\gamma}(\theta_{ei}-\delta_i)^2] \tag{6.32}$$

where $\Phi_{Ei} := x_{ei}\bar{u}_{ri}\cos\theta_{ei} + y_{ei}\bar{u}_{ri}\sin\delta_i + \frac{1}{\gamma}(\theta_{ei}-\delta_i)\bar{\omega}_{ri} + k_\tau(\tau_i-\tau_0)$ for simplified notation.

By enforcing tracking error feedback on virtual target which partially considers the motion behavior of the vehicle [Ogren et al., 2002, Do, 2008], $\dot{\tau}_0$ can be chosen as the function of the tracking error P_{eB} :

$$\dot{\tau}_0 = \omega_0(t)(1 - k_f\tanh(\sum_{i=1}^{n} P_{eiB}^T W P_{eiB})) \tag{6.33}$$

where k_f is strictly positive feedback gain, W is a positive definite weighting matrix determining how much the tracking errors are taken into account in the tracking error feedback, and $\omega_0(t)$ is a bounded positive function denoting the desired speed of the virtual target generating the path as $u_{ri} = \sqrt{x_{ri}^{\tau_{ri}}(\tau_{ri})^2 + y_{ri}^{\tau_{ri}}(\tau_{ri})^2}\dot{\tau}_{ri}$.

Replacing (6.27) into the combination of (6.30) and (6.31), we get the control laws for path tracking

$$\begin{bmatrix} u_i \\ \omega_i \\ \dot{\tau}_i \end{bmatrix} = \begin{bmatrix} k_1 x_{ei} + \bar{u}_{ri}\dot{\tau}_0\cos\theta_{ei} \\ \bar{\omega}_{ri}\dot{\tau}_0 - \dot{\delta}_i + \gamma y_{ei}\bar{u}_{ri}\dot{\tau}_0\frac{\sin\theta_{ei}-\sin\delta_i}{\theta_{ei}-\delta_i} + k_\theta(\theta_{ei}-\delta_i) \\ \dot{\tau}_0 - k_v\tanh(\Phi_{Ei}) \end{bmatrix} \tag{6.34}$$

where $\dot{\tau}_0$ given in (6.33), is a function of tracking error and critical for path tracking.

The first two elements in (6.34) are the kinematic control inputs of the vehicle, and the third element is the additional control input for the speed updating law of path parameter τ_i , which is related to the speed of the virtual target moving on the path by (6.17).

Proposition 6.2.3 (Coordinated path tracking 1 : multiple unicycle type vehicles)

Under assumption 6.2.1 and 6.2.2, the kinematic control inputs u_i and ω_i, and the virtual control input $\dot{\tau}_i$ expressing time evolution law for path parameter given in (6.34). The control objective (6.24) of coordinated path tracking is achieved and the equilibrium point $[x_{ei}, y_{ei}, \theta_{ei}, (\tau_i - \tau_0)]^T = 0^4$ is globally asymptotically stable.

Proof Since the control Lyapunov function V is positive definite and radially unbounded from(6.28). Notice $y_{ei}\bar{u}_{ri}\dot{\tau}_0 \sin\delta_i \leq 0$ in (6.32) as δ_i is chosen as a sigmoid function in (6.26). The path is regular such that $0 < \bar{u}_{ri}(\tau) < k$ as $\bar{u}_{ri} = \sqrt{x_{ri}^{\tau_i}(\tau_i)^2 + y_{ri}^{\tau_i}(\tau_i)^2}$. Therefore, $\dot{V} \leq 0$ is semi-negative definite. We have

$$0 \leq V(t) \leq V(t_0), t \geq t_0$$

such that all the signals $x_{ei}(t), y_{ei}(t), \theta_{ei}(t) - \delta_i(t), \tau_i(t) - \tau_0(t)$ constituting $V(t)$ is bounded. $\delta_i(t)$ is sigmoid function such that $\theta_{ei}(t)$ is bounded. In addition, $\omega_0(t)$ is a bounded function such that the same for $\dot{\tau}_0(t)$, yielding that $\dot{\tau}_i(t)$ is bounded by directly checking the third element in (6.34). Due to the boundedness of these signals and that of vehicle velocity, revisiting (6.20) , $\dot{x}_{ei}, \dot{y}_{ei}, \dot{\theta}_{ei}$ are also bounded. Furthermore, noticing the boundedness of δ_i and Φ_{Ei}, directly computing the derivative of (6.32), we can conclude the second derivative $\ddot{V}(t)$ exists and is bounded. Resorting to the Barbalat's Lemma, it follows

$$\lim_{t\to\infty} \dot{V}(t) = 0$$

Therefore, $x_{ei}, \Phi_{Ei}, y_{ei}\bar{u}_{ri}\dot{\tau}_0 \sin\delta_i, (\theta_{ei} - \delta_i)$ vanish as $t \to \infty$.

As δ_i is given as a sigmoid function in (6.26), $\lim_{t\to\infty} y_{ei}\bar{u}_{ri}\dot{\tau}_0 \sin\delta_i \to 0$ means that $\lim_{t\to\infty} \bar{u}_{ri}|\dot{\tau}_0|y_{ei}^2 \to 0$. The path is persistent exciting such that $\lim_{t\to\infty} \dot{\tau}_0 \neq 0$, and $0 < \bar{u}_{ri} < k$. Hence, $\lim_{t\to\infty} y_{ei} \to 0$. It follows $\lim_{t\to\infty} \delta_i \to 0$, such that $\lim_{t\to\infty} \theta_{ei} \to 0$ as $\lim_{t\to\infty}(\theta_{ei} - \delta_i) \to 0$. We can conclude that

$$\lim_{t\to\infty} \|P_{eiB}\| = \lim_{t\to\infty} \sqrt{x_{ei}^2 + y_{ei}^2 + \theta_{ei}^2} \to 0$$

which fulfils the first control objective in (6.24).

On the other hand, due to $\lim_{t\to\infty} \|P_{eiB}\| \to 0$, and $\lim_{t\to\infty} \Phi_{Ei} \to 0$ where $\Phi_{Ei} = x_{ei}\bar{u}_{ri}\cos\theta_{ei} + y_{ei}\bar{u}_{ri}\sin\theta_{ei} + \frac{1}{\gamma}(\theta_{ei} - \delta_i)\bar{\omega}_r + k_\tau(\tau - \tau_0)$, it follows that

$$\lim_{t\to\infty} |\tau_i(t) - \tau_0(t)| \to 0$$

Moreover, as $\lim_{t\to\infty}\Phi_{Ei} \to 0$, $\dot{\tilde{\tau}}_i = -k_\tau \tanh(\Phi_{Ei})$ and $\dot{\tau}_i = \dot{\tilde{\tau}}_i + v_{\tau i}$, there is

$$\lim_{t\to\infty} |\dot{\tau}_i(t) - \dot{\tau}_0(t)| \to 0$$

Substituting $\dot{\tau}_0 = \omega_0(t)(1 - k_f \tanh(\Sigma_{i=1}^n P_{eiB}^T W P_{eiB}))$, we have

$$\lim_{t\to\infty} \dot{\tau}_i(t) \to \omega_0(t)$$

It means the autonomous vehicle eventually moves along the path according to the desired speed assignment $\omega_0(t)$. Consequently, it meets the second control objective in (6.24). ∎

Formation tracking features :

- By choosing proper gains in the speed control of virtual target in (6.34), we can designate its moving behavior, defined by

  $$\dot{\tau}_i = \dot{\tau}_0 - k_v \tanh(\Phi_{Ei}) = \omega_0(t)(1 - k_f \tanh(\Sigma_{i=1}^n P_{eiB}^T W P_{eiB})) - k_v \tanh(\Phi_{Ei})$$

  Apparently, the gain for enforced tracking error feedback can be chosen as $0 < k_f < 1$. If one choose the gain $k_v < \omega_0(t)(1 - k_f)$, there is

  $$\dot{\tau}_i = \omega_0(t)(1 - k_f \tanh(\Sigma_{i=1}^n P_{eiB}^T W P_{eiB})) - k_v \tanh(\Phi_{Ei}) > \omega_0(t)(1 - k_f) - k_v > 0$$

  It means the virtual target will always move forward, and how fast the virtual target should move depending on how much the predefined speed assignment of FRP is affected by the tracking error feedback. This feature is suitable in practice as it avoids using a high gain control for large tracking error $\|P_{eiB}\|$.

- Actually, FRP gets the global formation tracking feedback by $\dot{\tau}_0 = \omega_0(t)(1 - k_f \tanh(\Sigma_{i=1}^n P_{eiB}^T W P_{eiB}))$. If some vehicles get saturated or disturbed, formation can still be achieved due to the global formation feedback imposed on the FRP traveling speed, such that $\dot{\tau}_0(t)$ decreases and the speed of FRP tolerates the problematic vehicle. Without this feature, formation cannot be achieved under these situations, although the individual vehicle can still track the path well. The formation is robust to the actuation saturation or partial actuation failure of vehicles, therefore this dedicated control demonstrates increased safety.

- As individual path tracking, smooth transitions between paths tracking and trajectories tracking stands for formation tracking, by setting $k_v = 0$ or $k_v \neq 0$, we can get the smooth transitions of control laws for formation paths tracking and trajectories tracking depending on the various tasks, where k_v determines if the degree of freedom for $\tau_0(t)$ exists or not.

Dynamics backstepping :

Let u_i and ω_i be virtual control inputs, α_{ui} and $\alpha_{\omega i}$ in (6.34) be the corresponding virtual control laws. Introduce the velocity error variables

$$z_i = \begin{pmatrix} z_{ui} \\ z_{\omega i} \end{pmatrix} = \begin{pmatrix} u_i - \alpha_{ui} \\ \omega_i - \alpha_{\omega i} \end{pmatrix}$$

Consider the Lyapunov function V in (6.28), augmented with the quadratic terms of z_{ui} and z_{ri}, that is

$$V_{dyn} = V + \frac{1}{2}\sum_{i=1}^{n} z^T M z \tag{6.35}$$

where $M = \begin{pmatrix} m_i & 0 \\ 0 & I_i \end{pmatrix}$, and m_i, I_i denotes the mass and moment of inertia of the i-th vehicle.

The time derivative of V_{dyn} can be written as

$$\begin{aligned}
\dot{V}_{dyn} = & \sum_{i=1}^{n}\{x_{ei}(\bar{u}_{ri}v_{\tau i}\cos\theta - u_i) + y_{ei}\bar{u}_{ri}v_{\tau i}\sin\delta_i + k_\tau(\tau_i - \tau_0)(v_{\tau i} - \dot{\tau}_0) \\
& + \dot{\tilde{\tau}}_i[x_{ei}\bar{u}_{ri}\cos\theta_{ei} + y_{ei}\bar{u}_{ri}\sin\theta_{ei} + \frac{1}{\gamma}(\theta_{ei} - \delta_i)\bar{\omega}_{ri} + k_\tau(\tau_i - \tau_0)] \\
& + \frac{1}{\gamma}(\theta_{ei} - \delta_i)(\bar{\omega}_{ri}v_{\tau i} - \omega_i - \dot{\delta}_i + \gamma y_{ei}\bar{u}_{ri}v_{\tau i}\frac{\sin\theta_{ei} - \sin\delta_i}{\theta_{ei} - \delta_i}) + m_i z_{ui}\dot{z}_{ui} + I_i z_{\omega i}\dot{z}_{\omega i}\} \\
= & \sum_{i=1}^{n}\{x_{ei}(\bar{u}_{ri}v_{\tau i}\cos\theta_{ei} - z_{ui} - \alpha_{ui}) + y_{ei}\bar{u}_{ri}v_{\tau i}\sin\delta_i \\
& + \dot{\tilde{\tau}}_i[x_{ei}\bar{u}_{ri}\cos\theta_{ei} + y_{ei}\bar{u}_{ri}\sin\delta_i + \frac{1}{\gamma}(\theta_{ei} - \delta_i)\bar{\omega}_{ri} + k_\tau(\tau_i - \tau_0)] + k_\tau(\tau_i - \tau_0)(v_{\tau i} - \dot{\tau}_0) \\
& + \frac{1}{\gamma}(\theta_{ei} - \delta_i)(\bar{\omega}_{ri}v_{\tau i} - z_{\omega i} - \alpha_{\omega i} - \dot{\delta}_i + \gamma y_{ei}\bar{u}_{ri}v_{\tau i}\frac{\sin\theta_{ei} - \sin\delta_i}{\theta_{ei} - \delta_i}) + m_i z_{ui}\dot{z}_{ui} + I_i z_{\omega i}\dot{z}_{\omega i}\} \\
= & \sum_{i=1}^{n}\{x_{ei}(\bar{u}_{ri}v_{\tau i}\cos\theta_{ei} - \alpha_{ui}) + y_{ei}\bar{u}_{ri}v_{\tau i}\sin\delta_i + k_\tau(\tau_i - \tau_0)(v_{\tau i} - \dot{\tau}_0) \\
& + \dot{\tilde{\tau}}_i[x_{ei}\bar{u}_{ri}\cos\theta_{ei} + y_{ei}\bar{u}_{ri}\delta_i + \frac{1}{\gamma}(\theta_{ei} - \delta_i)\bar{\omega}_{ri} + k_\tau(\tau_i - \tau_0)] \\
& + \frac{1}{\gamma}(\theta_{ei} - \delta_i)(\bar{\omega}_{ri}v_{\tau i} - \alpha_{\omega i} - \dot{\delta}_i + \gamma y_{ei}\bar{u}_{ri}v_{\tau i}\frac{\sin\theta_{ei} - \sin\delta_i}{\theta_{ei} - \delta_i}) + z_{ui}(m_i\dot{z}_{ui} - x_{ei}) \\
& + z_{\omega i}[I_i\dot{z}_{\omega i} - \frac{1}{\gamma}(\theta_{ei} - \delta_i)]\}
\end{aligned}$$

Let the control laws for $\dot{\tau}_i$, F_i and N_i be chosen as

$$\begin{cases} F_i = m_i\dot{u}_i = m_i\dot{\alpha}_{ui} + x_{ei} - k_3 z_{ui} \\ N_i = I_i\dot{\omega}_i = I_i\dot{\alpha}_{\omega i} + \frac{1}{\gamma}(\theta_{ei} - \delta_i) - k_4 z_{\omega i} \\ \dot{\tau}_i = \dot{\tau}_0 - k_v\tanh(\Phi_{Ei}) \end{cases} \tag{6.36}$$

where $k_3,\ k_4$ are positive constants, $\dot{\tau}_0$ is given in (6.33), and $\alpha_{ui}, \alpha_{\omega i}$ are given according to (6.34) as follows :

$$\begin{bmatrix} \alpha_{ui} \\ \alpha_{\omega i} \end{bmatrix} = \begin{bmatrix} k_1 x_{ei} + \bar{u}_{ri}\dot{\tau}_0 \cos\theta_{ei} \\ \bar{\omega}_{ri}\dot{\tau}_0 - \dot{\delta}_i + \gamma y_{ei}\bar{u}_{ri}\dot{\tau}_0 \frac{\sin\theta_{ei} - \sin\delta_i}{\theta_{ei} - \delta_i} + k_\theta(\theta_{ei} - \delta_i) \end{bmatrix}$$

There is

$$\dot{V}_{dyn} = \sum_{i=1}^n [-k_e x_{ei}^2 - k_s \Phi_{Ei}\tanh(\Phi_{Ei}) + y_{ei}\bar{u}_{ri}\dot{\tau}_0 \sin\delta_i - \tfrac{k_\theta}{\gamma}(\theta_{ei} - \delta_i)^2 - k_3 z_{ui}^2 - k_4 z_{\omega i}^2]$$

That means, $\dot{V}_{dyn}$ is negative semi-definite and all the states $(x_{ei}, y_{ei}, \theta_{ei}, z_{ui}, z_{\omega i})$ globally converge to its equilibrium. Moreover, it can be concluded that the equilibrium is $(x_{ei}, y_{ei}, \theta_{ei}, z_{ui}, z_{\omega i}) = 0^5$ from the Barbalat's lemma. Therefore, we can propose the following proposition for dynamic path tracking control.

Proposition 6.2.4 (Coordinated Path tracking 2 : multiple unicycle type vehicles)
Under assumption 6.2.1 and 6.2.2, the dynamics control inputs F_i and N_i, and the virtual control input $\dot{\tau}_i$ expressing time evolution law for path parameter given in (6.36). The control objective (6.24) of coordinated path tracking is achieved and the equilibrium point $[x_{ei}, y_{ei}, \theta_{ei}, (\tau_i - \tau_0)]^T = 0^4$ is globally asymptotically stable.

6.2.2.2 Individual vehicle with global formation feedback

Formation feedback is realized by enforcing the tracking error to the desired speed of FRP $\dot{\tau}_d$ in previous section.

Here, the formation feedback is realized by directly embedded in the actual speed of virtual target $\dot{\tau}_i$ in each path, not depending on the FRP speed $\dot{\tau}_0$ any more. This can be achieved by choosing

$$\begin{bmatrix} v_{\tau i} \\ \dot{\tilde{\tau}}_i \end{bmatrix} = \begin{bmatrix} \dot{\tau}_0 \\ -k_v \sum_{i=1}^n \Phi_{Ei} \end{bmatrix} \tag{6.37}$$

Obviously, $\dot{\tilde{\tau}}_i = \dot{\tilde{\tau}}_j$ due to the summation of the feedback from the states of all vehicles. However, in the third term of (6.34), $\dot{\tilde{\tau}}_i \neq \dot{\tilde{\tau}}_j$ as each one only get the feedback from its own states. This is the basic difference between the FRP formation feedback and individual vehicle formation feedback methods.

By replacing (6.37) into (6.29), the derivative of Lyapunov function is

$$\dot{V} = \sum_{i=1}^n [-k_e x_{ei}^2 + y_{ei}\bar{u}_{ri}\dot{\tau}_0 \sin\delta_i - \frac{k_\theta}{\gamma}(\theta_{ei} - \delta_i)^2] - k_v(\sum_{i=1}^n \Phi_{Ei})^2 \tag{6.38}$$

Now, the updating law for path parameter is

$$\dot{\tau}_i(t) = \dot{\tau}_0 - k_v \sum_{i=1}^n \Phi_{Ei} \tag{6.39}$$

Note that the difference between Lyapunov candidate functions (6.38) and (6.32), such that the ***global formation feedback*** acting on ***each individual vehicle*** in (6.39), but only on the ***formation reference point (FRP)*** from the third equation in (6.34).

By carefully checking the derivative of Lyapunov candidate funtion (6.29), we can declare

$$\Phi_{Ei} = -\frac{\partial V}{\partial \tau_i}(x_{ei}, y_{ei}, \theta_{ei}, u_i, \omega_i, \tau_i)$$

Hence, the updating law is actually a gradient descent algorithm, see the similar statement in [Skjetne et al., 2002] and [Ihle et al., 2004].

By using the global formation information feedback for individual vehicle in (6.39), the formation is robust to the actuation saturation or actuation failure of one vehicle, therefore this dedicated control demonstrates increased safety. As the time evolution of $\dot{\tau}(t)$ along the path is equally influenced by the states of all vehicles through the updating law (6.39), it means if one vehicle experiences a actuation problem, all the vehicles will act upon it.

However, in the traditional leader-follower control framework, only if the leader experiences a problem will the formation as a whole act robustly on it. A failure in one of the other following vehicles will not call for attention for other vehicles and can easily lead to an accident, due to the absence of formation feedback to the leader.

6.2.3 Decentralized control of coordinated paths tracking

Decentralized coordinated control is more suitable when a large number of vehicles are involved in the team, where inter-vehicle communication constraints are exerted [Ren et al., 2004]. Algebraic graph theory introduced in section 6.1.3.1, is the instrumental tool to illustrate the communication topology of multi-vehicle system and provide a theoretical way to rigorously prove the dedicated coordination laws.

The Control Lyapunov function candidate is selected as new one in a positive definite quadratic form

$$V = \frac{1}{2}\sum_{i=1}^{n}[x_{ei}^2 + y_{ei}^2 + \frac{1}{\gamma}(\theta_{ei} - \delta_i)^2] \tag{6.40}$$

Define the following variable :

$$\dot{\tau}_i = \dot{\tilde{\tau}}_i + v_{\tau i} \tag{6.41}$$

And choose the approaching angle δ_i as the same sign function in (6.26).

The time derivative of (6.40) along the solution of (6.20) is

$$\begin{aligned}\dot{V} &= \sum_{i=1}^{n}[x_{ei}(y_{ei}\omega_i - u_i + u_{ri}\cos\theta_{ei}) + y_{ei}(-x_{ei}\omega_i + u_{ri}\sin\theta_{ei}) + \frac{1}{\gamma}(\theta_{ei}-\delta_i)(\dot{\theta}_{ei}-\dot{\delta}_i)\\ &= \sum_{i=1}^{n}[-x_{ei}u_i + u_{ri}x_{ei}\cos\theta_{ei} + u_{ri}y_{ei}\sin\delta_i + \frac{1}{\gamma}(\theta_{ei}-\delta_i)(\dot{\theta}_{ei}-\dot{\delta}_i + u_{ri}y_{ei}\frac{\sin\theta_{ei}-\sin\delta_i}{\theta_{ei}-\delta_i})\end{aligned}$$

Substituting (6.17), (6.18) and (6.27) into the derivative of Lyapunov control function, yields

$$\begin{aligned}\dot{V} &= \sum_{i=1}^{n}[x_{ei}(\bar{u}_{ri}\dot{\tau}_i\cos\theta_{ei} - u_i) + y_{ei}\bar{u}_{ri}\dot{\tau}_i\sin\delta_i + \frac{1}{\gamma}(\theta_{ei}-\delta_i)(\dot{\theta}_{ei}-\dot{\delta}_i + \bar{u}_{ri}\dot{\tau}y_{ei}\frac{\sin\theta_{ei}-\sin\delta_i}{\theta_{ei}-\delta_i})]\\ &= \sum_{i=1}^{n}[x_{ei}(\bar{u}_{ri}v_{\tau i}\cos\theta_i - u_i) + y_{ei}\bar{u}_{ri}v_{\tau i}\sin\delta_i + \dot{\tilde{\tau}}_i[x_{ei}\bar{u}_{ri}\cos\theta_{ei} + y_{ei}\bar{u}_{ri}\sin\delta_i + \frac{1}{\gamma}(\theta_i-\delta_i)\bar{\omega}_{ri}]\\ &+\frac{1}{\gamma}(\theta_{ei}-\delta_i)(\bar{\omega}_{ri}v_{\tau i} - \omega_i - \dot{\delta}_i + \gamma y_{ei}\bar{u}_{ri}v_{\tau i}\frac{\sin\theta_{ei}-\sin\delta_i}{\theta_{ei}-\delta_i})]\end{aligned}$$

Proposing the control input as

$$\begin{bmatrix} u_i \\ \omega_i \end{bmatrix} = \begin{bmatrix} k_1 x_{ei} + \bar{u}_{ri}v_{\tau i}\cos\theta_{ei} \\ \bar{\omega}_{ri}v_{\tau i} - \dot{\delta}_i + \gamma y_{ei}\bar{u}_{ri}v_{\tau i}\frac{\sin\theta_{ei}-\sin\delta_i}{\theta_{ei}-\delta_i} + k_\theta(\theta_{ei}-\delta_i) \end{bmatrix} \tag{6.42}$$

and utilizing the first element in (6.17) again, yields

$$\dot{V} = -\sum_{i=1}^{n}[\phi_i\dot{\tilde{\tau}}_i + k_e x_{ei}^2 + y_{ei}\bar{u}_{ri}\dot{\tau}_0\sin\delta_i + \frac{k_\theta}{\gamma}(\theta_{ei}-\delta_i)^2] \tag{6.43}$$

where $\phi_i := x_{ei}\bar{u}_{ri}\cos\theta_{ei} + y_{ei}\bar{u}_{ri}\sin\delta_i + \frac{1}{\gamma}(\theta_{ei}-\delta_i)\bar{\omega}_{ri}$ for simplified notation.

To make the presentation clear, we use the vector notion $\Omega_\tau = [\dot{\tilde{\tau}}_1, \ldots, \dot{\tilde{\tau}}_n]^T$, $\mathcal{T} = [\tau_1, \ldots, \tau_n]^T$, and $v_\tau = [v_{\tau 1}, \ldots, v_{\tau n}]^T$. Thus, (6.41) can be rewritten as

$$\dot{\mathcal{T}} = \Omega_\tau + v_\tau \tag{6.44}$$

Augmenting the Lyapunov function (6.40) as

$$V_{aug} = V + \frac{1}{2}\Omega_\tau^T K_1^{-1}K_2^{-1}\Omega_\tau + \frac{1}{2}\mathcal{T}^T L\mathcal{T} \tag{6.45}$$

where L is the Laplacian matrix of the connected graph $\mathcal{G}$, which describes the inter-vehicle communication topology, K_1, K_2 are diagonal positive-definite matrices.

Supposing the communication graph $\mathcal{G}$ is bi-directional and connected, we can declare L is a symmetric positive semi-definite matrix by using Lemma 1, such that $L^T = L$. There is

$$\frac{d}{dt}(\mathcal{T}^T L\mathcal{T}/2) = (\dot{\mathcal{T}}^T L\mathcal{T} + \mathcal{T}^T L\dot{\mathcal{T}})/2 = ((L\dot{\mathcal{T}})^T\mathcal{T} + \mathcal{T}^T(L\dot{\mathcal{T}}))/2 = \mathcal{T}^T L\dot{\mathcal{T}}$$

Hence, the time derivative of (6.45) along the solutions of (6.19) gives :

$$\dot{V}_{aug} = \Phi^T \Omega_\tau - \sum_{i=1}^{n} [k_e x_{ei}^2 + y_{ei} \bar{u}_{ri} \dot{\tau}_0 \sin \delta_i + \frac{k_\theta}{\gamma} (\theta_{ei} - \delta_i)^2] + \dot{\Omega}_\tau^T K_1^{-1} K_2^{-1} \Omega_\tau + \mathcal{T}^T L \dot{\mathcal{T}} \tag{6.46}$$

where $\Phi = [\phi_1, \ldots, \phi_n]^T$.

Proposing the updating law for path parameters

$$\begin{bmatrix} \dot{\mathcal{T}} \\ \dot{\Omega}_\tau \end{bmatrix} = \begin{bmatrix} \Omega_\tau + v_\tau \\ -K_1 K_2 (L\mathcal{T} + \Phi) - K_1 \Omega_\tau \end{bmatrix} \tag{6.47}$$

where $v_\tau = [v_{\tau i}]_{n \times 1} = v_{\tau 0} \vec{1}$ with $\vec{1} = [1]_{n \times 1}$, and $\lim_{t \to \infty} v_{\tau 0} \neq 0$.

It means the desired time evolving speed $v_{\tau i}$ is common for each vehicle and equal to $v_{\tau 0}$, but $v_{\tau 0}$ needs not be constant and it could be time-varying.

Now, we can propose the solution to the coordinated paths tracking problem, with decentralized feedback updating law for $\mathcal{T}$ as a function of the information received from the neighboring vehicles.

Proposition 6.2.5 (Decentralized coordination of paths tracking)

Under assumption 1 and 2, the kinematic control inputs u_i and ω_i, and the virtual control input $\dot{\tau}_i$ expressing time evolution law for path parameter given in (6.34). The control objective (6.24) of coordinated path tracking is achieved and the equilibrium point $[x_{ei}, y_{ei}, \theta_{ei}, (\tau_i - \tau_j)]^T = 0^4$ is globally asymptotically stable.

Proof Given the solution (6.47), the derivative of Lyapunov candidate function in (6.46), can be further written as

$$\begin{aligned}
\dot{V}_{aug} =& \Phi^T \Omega_\tau + \dot{\Omega}_\tau^T K_1^{-1} K_2^{-1} \Omega_\tau + \mathcal{T}^T L (\Omega_\tau + v_\tau) - \sum_{i=1}^{n} [k_e x_{ei}^2 + y_{ei} \bar{u}_{ri} \dot{\tau}_0 \sin \delta_i + \frac{k_\theta}{\gamma} (\theta_{ei} - \delta_i)^2] \\
=& (\Phi^T + \dot{\Omega}_\tau^T K_1^{-1} K_2^{-1} + \mathcal{T}^T L) \Omega_\tau + v_{\tau 0} \mathcal{T}^T L \vec{1} - \sum_{i=1}^{n} [k_e x_{ei}^2 + y_{ei} \bar{u}_{ri} \dot{\tau}_0 \sin \delta_i + \frac{k_\theta}{\gamma} (\theta_{ei} - \delta_i)^2] \\
=& - \Omega_\tau^T K_2^{-1} \Omega_\tau - \sum_{i=1}^{n} [k_e x_{ei}^2 + y_{ei} \bar{u}_{ri} \dot{\tau}_0 \sin \delta_i + \frac{k_\theta}{\gamma} (\theta_{ei} - \delta_i)^2] \leq 0
\end{aligned}$$

where $v_{\tau 0} \mathcal{T}^T L \vec{1} = 0$ is applied due to the property of Laplacian matrix L of the connected undirected graph, according to Lemma 2.

Since the control Lyapunov function V_{aug} is positive definite and radially unbounded from(6.45), and $\dot{V}_{aug} \leq 0$, for any initial condition of the state $X = (x_{ei}, y_{ei}, \theta_{ei}, \delta_i, \Omega_\tau^T)^T$, there exists a constant ϵ such that $\|X(t)\| \leq \epsilon$ fora all $t \geq t_0$. Therefore, $\|X(t)\|$ is uniformly continuous in t on $[0, \infty)$, and $\dot{X}(t)$ exist and is bounded therein. It follows that

$\dot{V}_{aug}(t, X_1(t))$ is also uniformly continuous. Using the Barbalat Lemma, we can conclude that

$$\lim_{t\to\infty} \dot{V}_{aug}(t, X_1(t)) = 0$$

Therefore, $x_{ei}, y_{ei}, \theta_{ei}, \delta_i, \Omega_\tau$ vanishes as $t \to \infty$. $\lim_{t\to\infty} \Omega_\tau = 0$ implies that $\lim_{t\to\infty} \dot{\Omega}_\tau = 0$. $\lim_{t\to\infty}(x_{ei}, y_{ei}, \theta_{ei}, \delta_i) = 0^4$ such that $\lim_{t\to\infty} \Phi = 0$. By using the fact that $\dot{\Omega}_\tau = L\mathcal{T} - \Phi - K\Omega_\tau$ in (6.47), we have $\lim_{t\to\infty} L\mathcal{T} = 0$. It means

$$\lim_{t\to\infty} (\tau_i - \tau_j) = 0$$

Hence, the proof is completed. ∎

Remarks :

(1) Actually, (6.47) is a 2^{nd} filter updating law of path parameter. One can refer to the section 4.3.2 in Chapter 4 to know the details about filtered path parameter updating.

(2) We know examine the compact form of the updating law proposed in (6.47), which can be written in a decentralized form as

$$\begin{cases} \dot{\tau}_i = \dot{\tilde{\tau}}_i + v_{\tau_i} \\ \ddot{\tilde{\tau}}_i = -k_{1i}[\dot{\tilde{\tau}}_i + k_{2i}(\sum_{j\in J_i}(\tau_i - \tau_j) + \phi_i)] \end{cases} \tag{6.48}$$

Recall that J_i denotes the set of neighboring vehicles (vertices in the communication graph) that communicate with vehicle i. Notice how the updating law of path parameter $\dot{\tau}_i$ for vehicle i is a function of its own path parameter errors with respect to path parameters of other vehicles included in the communication set J_i. Clearly, the updating law is decentralized, which meets the constraints imposed by the communication network.

(3) The dynamics version of decentralized coordinated path tracking, can be derived by adopting backstepping technique as we have done for single nonholonomic vehicle. Let u_i, ω_i be virtual control inputs, and $\alpha_{ui}, \alpha_{\omega i}$ be the corresponding virtual control laws in (6.47). The control law for F_i and N_i be chosen as

$$\begin{bmatrix} F_i \\ N_i \end{bmatrix} = \begin{bmatrix} m_i\dot{\alpha}_{ui} + x_{ei} - k_{3i}z_{ui} \\ I_i\dot{\alpha}_{\omega i} + \frac{1}{\gamma}(\theta_{ei} - \delta_i) - k_{4i}z_{\omega i} \end{bmatrix} \tag{6.49}$$

where m_i, I_i denotes the mass and moment of inertia of the i-th vehicle.

The decentralized updating law keeps the same as one in (6.47), when extending vehicle kinematics to dynamics.

Table 6.1 – INFANTE AUV : simplified model parameters

$m = 2234.5kg$	$I_z = 2000Nm^2$	
$X_{uu} = -35.4kgm^{-2}$	$X_{vv} = -128.4kgm^{-1}$	
$X_{\dot{u}} = -142kg$	$Y_{\dot{v}} = -1715kg$	$N_{\dot{r}} = -1350Nm^2$
$Y_r = 435kg$	$Y_v = -346kgm^{-1}$	$Y_{v\|v\|} = -667kgm^{-1}$
$N_v = -686kg$	$N_{v\|v\|} = 443kg$	$N_r = -1427kgm$

6.3 Examples of coordinated motion control

This section contains the results of simulation, illustrating the performance obtained by the control laws developed.

6.3.1 Examples of coordinated paths following

With the proposed coordinated paths following algorithms, two cases of simulations are illustrated.

6.3.1.1 Example 1 : in-line circle paths

Four homogenous underactuated AUVs with dynamics model of the INFANTE AUV in Table 6.1 [Silvestre, 2000], are required to follow 4 circumferences, which are with the same center but different radii R_i ($i = 1, 2, 3, 4$) respectively, while keeping synchronization with in-line formation.

The normalization of the along paths lengths for each underactuated AUVs is $\hat{s}_i = s_i/R_i$ and normalized speed is $\hat{u}_i = u_i/R_i$, will be the same in the case of circumferences. Actually, these normalized parameters make the truth, that the rotating speeds of virtual vehicles with respect to the same center of circles (i.e., angular frequencies), as well as normalized lengths along paths, are synchronized. Therefore, the in-line formation of multi-vehicle system is built.

The radius of the circumferences are $R = [5, 10, 15, 20]^T m$. Four vehicles (scaled model) are with initial velocities of $u_0 = [2, 2, 2, 2]^T m/s, v_0 = [0, 0, 0, 0]^T m/s, r_0 = [0, 0, 0, 0]^T rad/s$. The maximum and minimum speed of the vehicles are, $u^d_{max} = 5.0m/s$ and $u^d_{min} = 0.1m/s$. The initial positions are $x = [0, 0, 0, 0]^T m$ and $y = [0, -5, -10, -15]^T m$. The initial tracing error vectors are $x_{e0} = [5, 5, 5, 5]^T m$ and $y_{e0} = [5, 5, 5, 5]^T m$. The initial error angles are $\psi_0 = [\pi/2, \pi/2, \pi/2, \pi/2]^T$.

The Laplacian matrix, corresponding to the communication topology of the multi-vehicle system, is

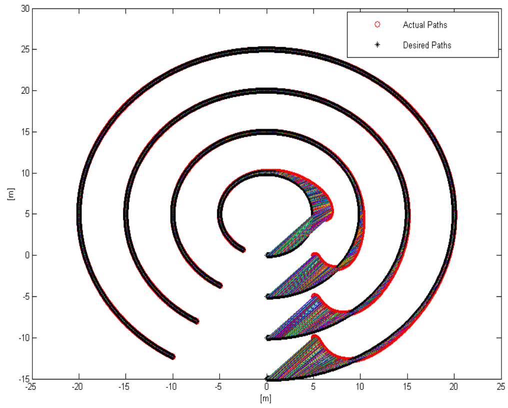

(a) Coordinated in-line path following

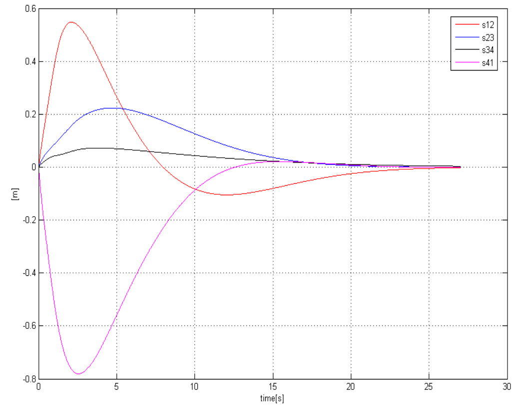

(b) Normalized along path errors in path following

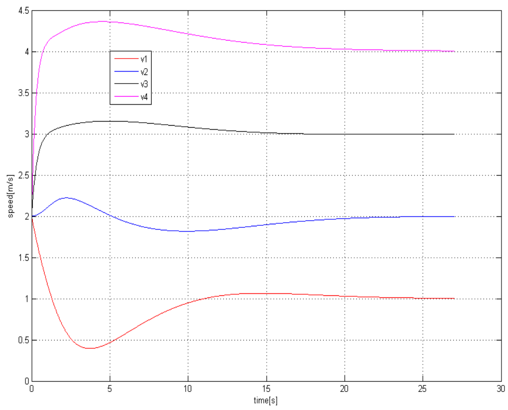

(c) Coordinated speed in in-line path following

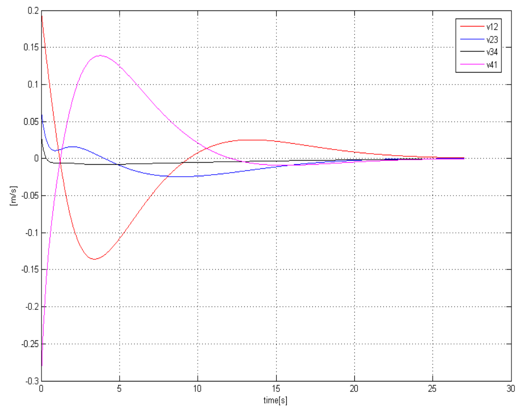

(d) Normalized speed errors in path following

Figure 6.5 – Coordinated in-line circle paths following of underactuated AUVs

$$L = D - A = \begin{pmatrix} 1 & -1 & 0 & 0 \\ -1 & 3 & -1 & -1 \\ 0 & -1 & 2 & -1 \\ 0 & -1 & -1 & 2 \end{pmatrix}$$

As illustrated in Figure 6.5(a), the along path lengths of different vehicles converge to the same normalized value. The speed converge to the desired speed profile $U_d = [1, 2, 3, 4]^T m/s$, as illustrated in Figure 6.5(b). The normalized synchronized errors s_{ij} $(= \hat{s}_i - \hat{s}_j)$ and u_{ij} $(= \hat{u}_i - \hat{u}_j)$ are illustrated in Figure 6.5(c) and 6.5(d), decaying to 0 respectively.

6.3.1.2 Example 2 : parallel paths

This section illustrates the performance of coordinated paths following control based on leader-follower strategy and decentralized strategy respectively, where three homogenous underactuated AUVs with dynamics model of the INFANTE AUV, are required to inspect underwater pipeline illustrated in Figure 6.6.

In the scenario of underwater pipeline inspection, there are three parallel paths followed by three AUVs in 3D space, which are elevated from the seabed and offset from the underwater pipeline, and the speeds of vehicles along the pipeline should be the same as that determined by the end-user. Therefore, in the point of view of control design, the challenging of underwater pipeline inspection falls into the category of path following control. Most importantly, the vehicles are requested to keep synchronously moving along the paths to stay in a formation, to cooperatively acquire complete 3D images of the pipeline. Therefore, proper coordinated control strategy has to be adopted to accomplish the mission of pipeline inspection [Xiang et al., 2010a].

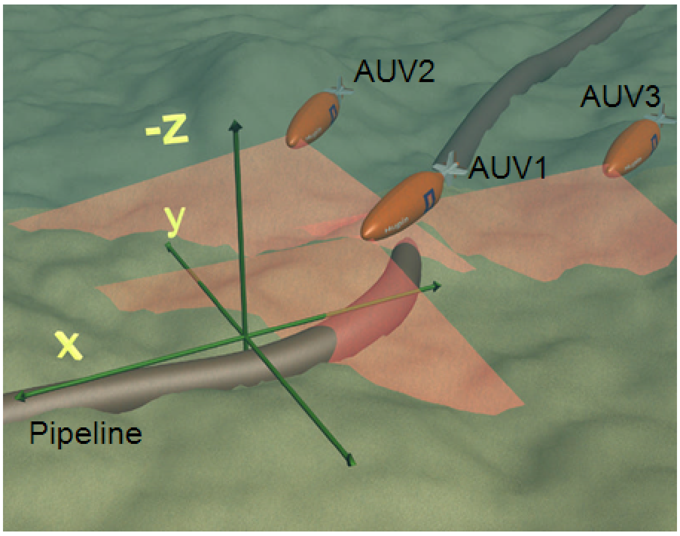

Figure 6.6 – Three AUVs swimming in formation along a pipeline. The coordinate axes indicates the formation reference frame with origin in the FRP. Courtesy : Anders S. Wroldsen

Assuming that the pipeline information is prior-known, the pipeline can be taken as a parameterized path. For instance, it is given by

$$x(\lambda) = \sum_{i=1}^{5} a_i \lambda^{i-1}, y(\lambda) = \sum_{i=1}^{5} b_i \lambda^{i-1}$$

where the path coefficients are given in Table. 6.2.

Table 6.2 – The path parameters for coordinated path following control

coefficients/index	1	2	3	4	5
a_i	0	0.87	-0.02	10^{-5}	1.5×10^{-6}
b_i	0	0.5	-5×10^{-4}	10^{-5}	10^{-7}

The initial position of the three AUVs are $x = [30, 20, 40]^T m$ and $y = [-30, -30, -30]^T m$. The initial velocities of $u_0 = [0.1, 0.1, 0.1]^T m/s, v_0 = [0, 0, 0]^T m/s, r_0 = [0, 0, 0]^T rad/s$, and the initial orientation are $\psi_0 = [\pi/2, \pi/2, \pi/2]^T$.

- **Leader-follower based centralized paths following control**

The leader and the followers are required to keep a triangle formation with $l_0 =$ 5m, and the leader flies above the pipeline with 5m depth. The leader coincided with the AUV1 in Figure 6.2, such that the shifted vector of corresponding pipeline path is $d_{y1} = [0m, 0m, 0m]^T$. Both AUV2 and AUV3 are followers, whose parallel paths are with shifted vector $d_{y2} = [0m, 7m, 0m]^T$ and $d_{y3} = [0m, -7m, 0m]^T$ according to the 2D projection of the leader's path (the actual track of pipeline) respectively.

For the "triangle formation", the along-path space between the "front" AUV and its two "wingman" AUVs is $5m$. This along-path space inside "triangle"-shape can be introduced as an offset of the along-path distance s_i, such that the same synchronized path following control laws can be used.

As depicted in Figure 6.7, the underwater pipeline and AUVs paths are illustrated in 3D. The projected 2D graph is showed in Figure 6.8, both the leader, left/right followers converge to the assigned paths, and keep the triangle formation. In Figure 6.9(a), the error spaces of three vehicles with respect to the paths are driven to zero. The forward speed adaptations of the followers are illustrated in the top subplot of Figure 6.9(b), while the forward speeds asymptotically converge to $u_d = 1m/s$. The orientations the followers are the same as that of the leader in the bottom subplot of Figure 6.9(b) when the desired triangle formation is built. In Figure 6.10, the errors of generalized along-path distance $\Delta S_i, (i = LF1, LF2, F12)$ between the leader and followers are asymptotically decaying to 0, where the geometric constraints of l_0 is already incorporated.

- **Decentralized paths following control**

In this simulation, three AUVs follow three parallel curved paths based on the actual track of pipeline by using decentralized control strategy, while building varied geometric formation from "triangle" to "in-line" pattern, and then back to "triangle" formation pattern again.

The communication topology of three vehicles is

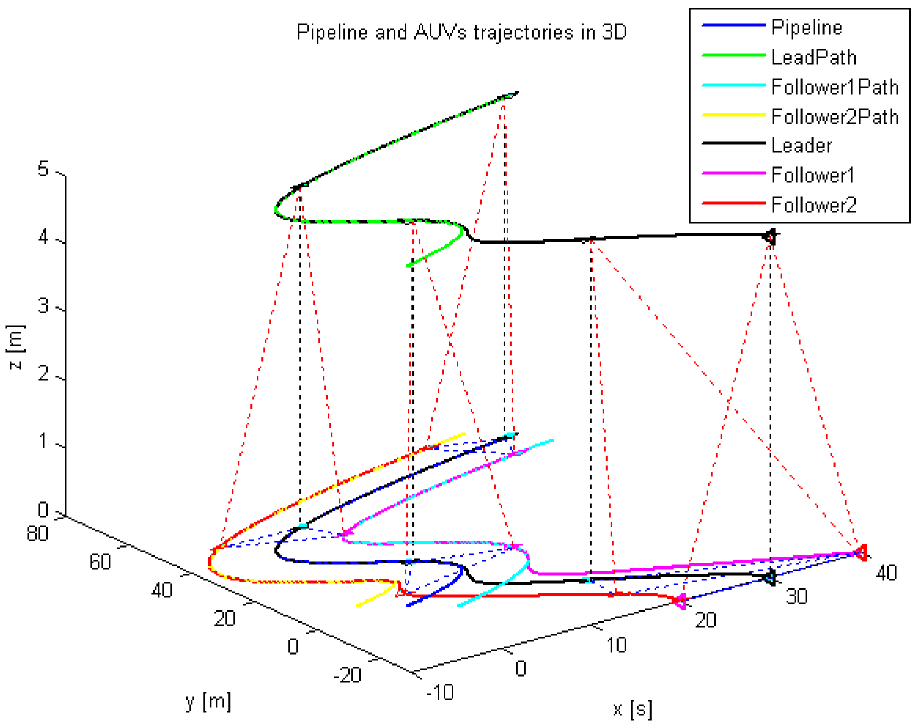

Figure 6.7 – Underwater pipeline and AUVs paths in 3D

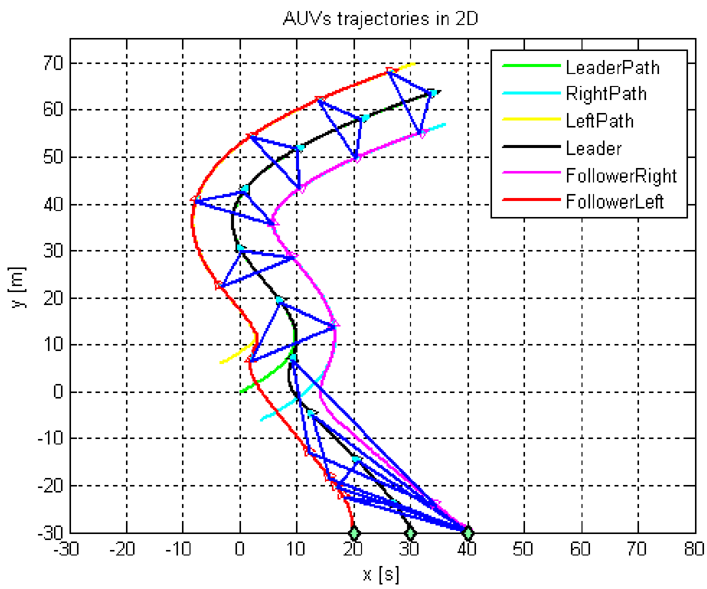

Figure 6.8 – Ledear/Followers in a triangle formation projected in 2D

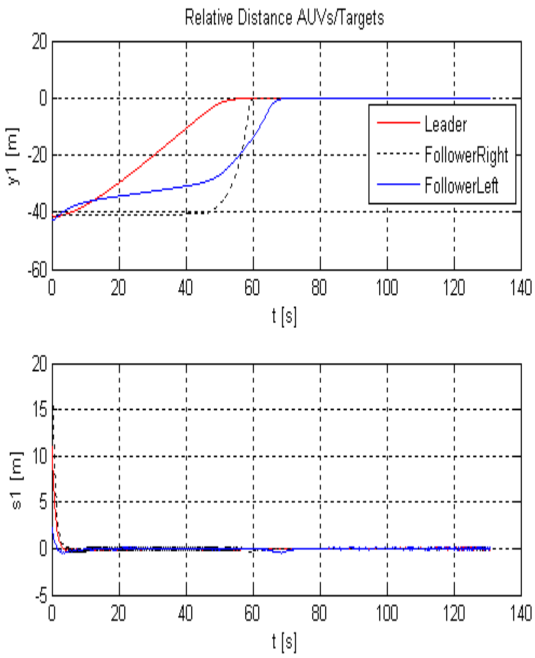

(a) Relative distances between AUVs/virtual targets

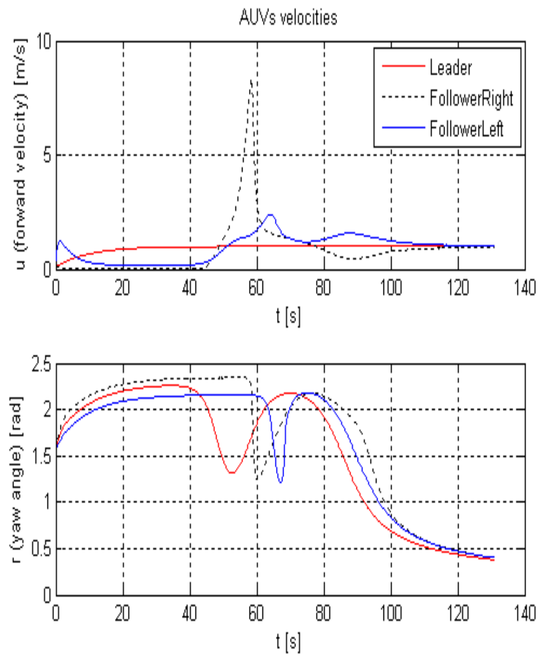

(b) AUV linear velocities and orientations

Figure 6.9 – Path follower errors and velocities of vehicles

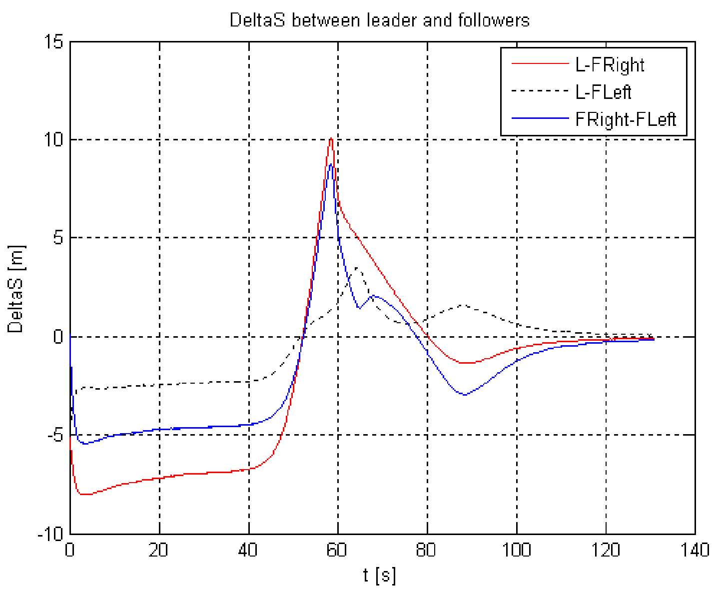

Figure 6.10 – Evolution of the relative distance between leader and followers

$$L = D - A = \begin{pmatrix} 1 & -1 & 0 \\ -1 & 2 & -1 \\ 0 & -1 & 1 \end{pmatrix}$$

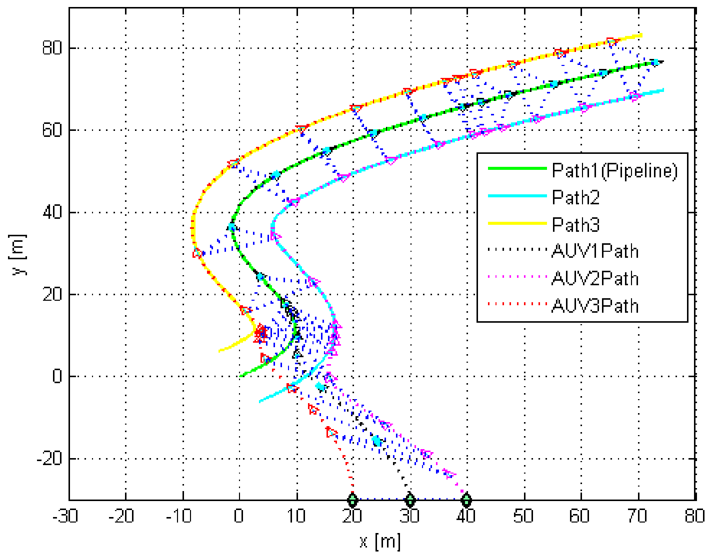

Figure 6.11 – Coordinated path following of underactuated AUVs with varied formation patterns

To implement the decentralized control strategy, the initial conditions of the AUVs are the same as described in the case of centralized control. As illustrated in Figure 6.11, the "triangle - inline - triangle" formation along the desired path has been well built via coordinated control. The tracking error for each AUV is shown in 6.12, where the along-track error and cross-track error converges to 0. The top subplot in Figure 6.13 shows that the speed profiles of AUVs converge to the desired speed $u_d = 1.0m/s$, and the bottom subplot in Figure 6.13 clearly shows that the distances between each pair of AUVs, coincide with the procedure during building "triangle - inline - triangle" varied formation, and converge to zero (l_0 is already incorporated in triangle formation) when each geometric formation pattern is achieved.

In Figure 6.9(b) of centralized control case, two followers have to adapt their surge speeds according to the leader's surge speed and achieve $u_d = 1.0m/s$. However, in the top subplot of Figure 6.13 of decentralized control case, there is no leader and all three vehicles cooperatively adapt their surge speeds depending on its neighbors's speed in the defined communication topology. Consequently, the amplitude of varied surge speeds of follower vehicles is higher than that of vehicles in decentralized control strategy, and the convergence rate in decentralized control is faster than that in centralized control strategy. Furthermore, by comparing Figure 6.9(b) and the bottom subplot of Figure 6.13, we can conclude that the convergence rate of the relative distance between vehicles in decentralized case is also faster that that in centralized leader-follower control case.

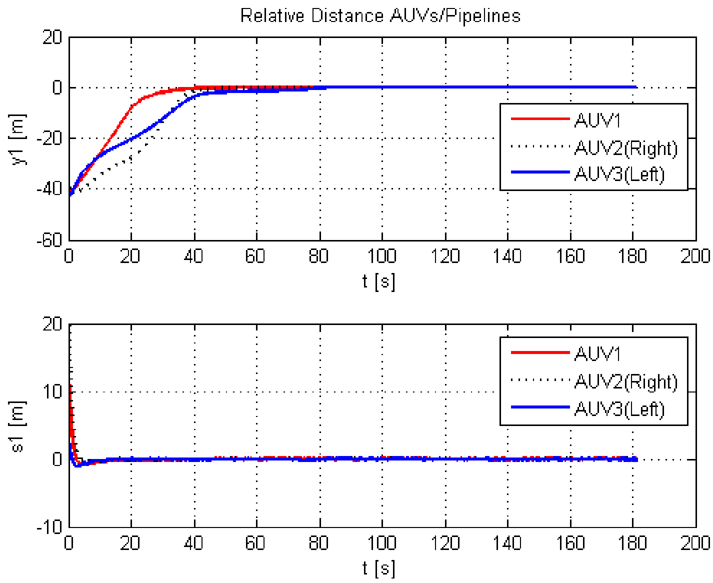

Figure 6.12 – Relative distances between AUVs/Paths

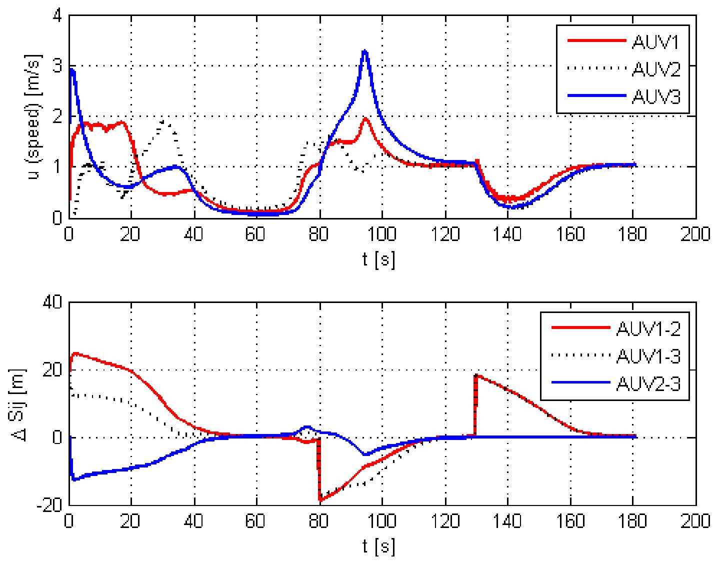

Figure 6.13 – AUV velocities and formation errors

6.3.2 Examples of coordinated paths tracking

In order to illustrate the performance of the proposed coordinated paths tracking algorithms, two cases of simulations are shown in this section.

6.3.2.1 Example 1 : triangle formation of 3 vehicles

In this example, a team of $N = 3$ identical nonholonomic unicycle-type wheeled mobile vehicles under triangle formation path tracking control, is simulated to illustrate the effectiveness of the proposed decentralized coordinated controller.

The physical parameters of the i-th vehicle ($i \in \{1, \ldots, N\}$) are taken from [Lapierre et al., 2006] :

$$\begin{bmatrix} m_i \\ I_i \end{bmatrix} = \begin{bmatrix} 9kg \\ 0.1kg\ m^2 \end{bmatrix}$$

The path parameter and of the FRP which generates the baseline for the whole formation is taken as

$$\Gamma_0(x_{r0}(\tau_0), y_{r0}(\tau_0), \psi_{r0}(\tau_0)) = \ [\tau_0, 0, 0]^T \tag{6.50}$$

which is a straight line. The timing law of path parameter sets as $\dot{\tau}_0(t) = 1.0\ m/s$, and the initial FRP and two virtual target are setting as $\tau_0 = 0, \tau_1 = 2, \tau_2 = 0$.

The offset vectors from the virtual targets to the FRP are chosen as

$$\begin{bmatrix} l_1(x_{r1}(\tau_1), y_{r1}(\tau_1)) \\ l_2(x_{r2}(\tau_2), y_{r2}(\tau_2)) \\ l_3(x_{r3}(\tau_3), y_{r3}(\tau_3)) \end{bmatrix} = \begin{bmatrix} [0, 0, 0]^T \\ [3,\ 3\cos(0.5\tau_2) + 8,\ 0]^T \\ [3,\ 3\sin(0.5\tau_3) - 8,\ 0]^T \end{bmatrix} \tag{6.51}$$

The choice for l_1 means that the virtual target on the first path coincides with the FRP, such that the first path coincides with the baseline Γ_0 which is a straightline. The other two virtual targets move on two sinusoidal paths generated from the baseline according to (6.16), (6.50) and (6.51), due to the intended setting for l_2 and l_3.

The initial position of three AUVs are $x = [-5, -5, -5]^T m$ and $y = [0, 5, -5]^T m$. The initial velocities are $u_0 = [0.2, 0.2, 0.2]^T m/s, r_0 = [0, 0, 0]^T rad/s$, and the initial orientations are $\theta_0 = [0, 0, 0]^T$. The communication topology is given as

$$L = \begin{bmatrix} 1 & -1 & 0 \\ -1 & 2 & -1 \\ 0 & -1 & 1 \end{bmatrix}$$

It means the communication network of the whole vehicle team is a chain topology, where vehicle 2 is the bridge to exchange information between vehicle 1 and vehicle 3.

In Figure 6.14, it shows 3 vehicles's positions and orientations while building and keeping the triangle formation.

In Figure 6.15, it shows that the disagreement between the FRP and 2 virtual targets in the form of $\sqrt{(\tau_0-\tau_1)^2+(\tau_0-\tau_2)^2+(\tau_1-\tau_2)^2}$, asymptotically converges to zero.

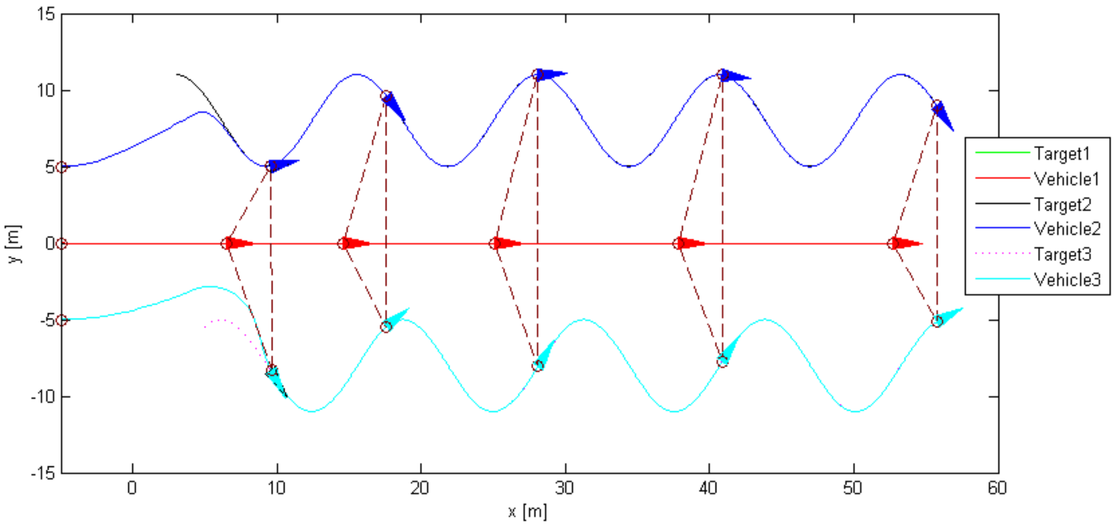

Figure 6.14 – Triangle formation based on coordinated paths tracking

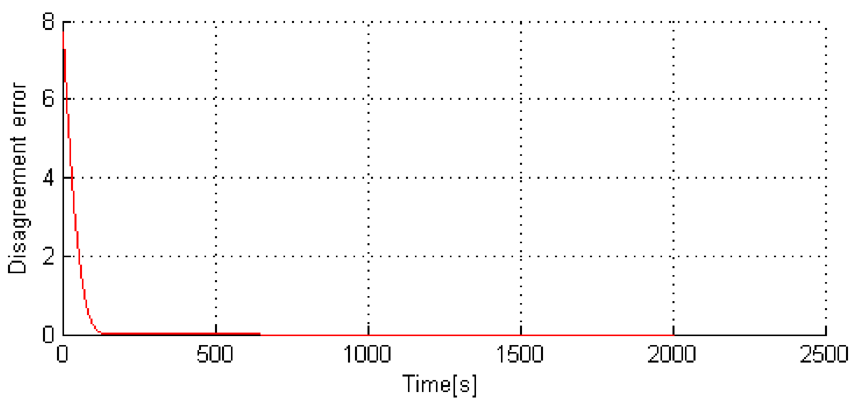

Figure 6.15 – Disagreement between the FRP and 2 virtual targets

Figure 6.16(a) illustrates how the first vehicle moves with a constant speed, while the other two vehicles move with sinusoidal-like time varying speeds, in order to maintain the rigid triangle formation of three vehicles following one straightline and two sinusoidal paths.

In Figure 6.16(b) (upper subplot), it shows the paths tracking errors (along-track error and cross-track error) of three vehicles asymptotically converge to zero. In Figure 6.16(b) (bottom suplot), it shows that the total tracking errors in the form of $\sqrt{x_{ei}^2 + y_{ei}^2 + \theta_{ei}^2}$, asymptotically converges to zero.

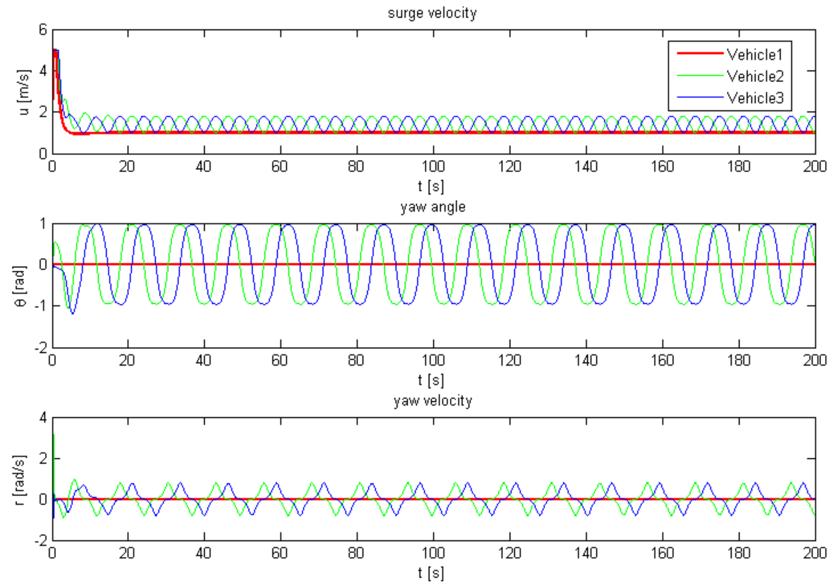

(a) Velocities and orientations of 3 vehicles

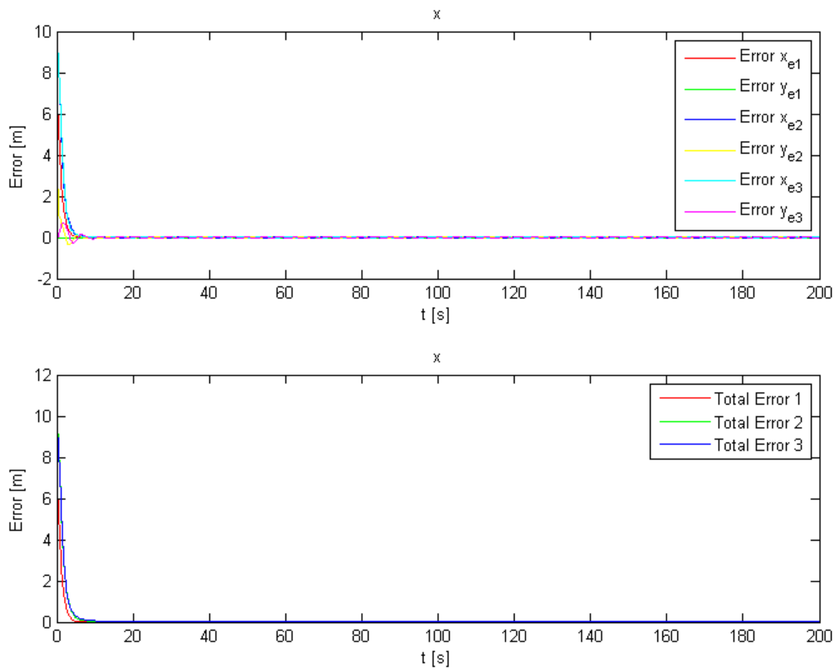

(b) Paths tracking errors

Figure 6.16 – Velocity profiles and tracking errors

6.3.2.2 Example 2 : circle formation of 10 vehicles

In this example, a team of $N = 10$ identical nonholonomic unicycle-type wheeled mobile vehicles under circle formation path tracking control, is simulated and the physical vehicle parameters are the same with the example 1.

The initial velocities are taken as $u_i = 0.2\ m/s, \omega_i = 0\ rad/s$. The initial positions and orientations of 10 vehicles are as follows :

$$\begin{bmatrix} x_i \\ y_i \\ \theta_i \end{bmatrix} = \begin{bmatrix} -5 & -5 & -5 & -10 & -10 & -10 & -15 & -15 & -15 & 0 \\ 0 & 5 & -5 & 0 & 5 & -5 & 0 & -5 & 5 & 0 \\ 0 & 0 & 0 & 0 & 0 & 0 & 0 & 0 & 0 & 0 \end{bmatrix}$$

The path parameter of the FRP which generates the baseline for the whole formation is taken as

$$\Gamma_0(x_{r0}(\tau_0), y_{r0}(\tau_0), \psi_{r0}(\tau_0)) = \ [\tau_0, 10\sin(0.1\tau_0), \arctan(\cos(0.1\tau_0))]^T \tag{6.52}$$

The timing law of path parameter sets as $\dot{\tau}_0(t) = 0.1\ m/s$, and the initial FRP and virtual targets are setting as $\tau_0 = 0, \tau_1 = 2, \tau_2 = 0, \tau_3 = 2, \tau_4 = 0, \tau_5 = 2, \tau_6 = 0, \tau_7 = 2, \tau_8 = 0, \tau_9 = 0, \tau_{10} = 8$.

The offset vector from the virtual targets to the FRP are chosen as

$$l_i((x_{ri}(\tau_i), y_{ri}(\tau_i)) = \begin{bmatrix} 10\sin(2\pi(i-1)/N) \\ 10\cos(2\pi(i-1)/N \\ 0 \end{bmatrix} \tag{6.53}$$

where $i \in \{1, 2, \ldots, N\}$.

These choices mean the baseline Γ_0 is a sinusoidal path, and the desired paths for 10 vehicles are generated from the baseline according to (6.16), (6.52) and (6.53). Moreover, the desired formation shape is a circle, as its vertices are uniformly distributed on a circle centered on the sinusoidal baseline with a radius 10m.

The control gains, the initial path parameters and the parameters involved in the path parameters updating are as follows :

$$\tau_i(0) = [0, 0, 0, 0, 0, 0, 0, 0, 0, 0]^T$$
$$\omega_0 = 0.1\ m/s, k_f = 1, W = diag(1, 1, 1)$$

Moreover, the vehicle's speed limitation $0 < u_i(t) < 1.2m/s$ and $-1.5\pi rad/s < \omega(t)_i < 1.5\pi rad/s$ are assumed in the simulation.

The communication topology is given as

$$L = \begin{bmatrix} 3 & -1 & -1 & 0 & 0 & 0 & 0 & 0 & 0 & -1 \\ -1 & 1 & 0 & 0 & 0 & 0 & 0 & 0 & 0 & 0 \\ 0 & -1 & 0 & 2 & -1 & 0 & 0 & 0 & 0 & 0 \\ 0 & 0 & -1 & 2 & -1 & 0 & 0 & 0 & 0 & 0 \\ 0 & 0 & 0 & -1 & 1 & 0 & 0 & 0 & 0 & 0 \\ 0 & 0 & 0 & 0 & 0 & 1 & -1 & 0 & 0 & 0 \\ 0 & 0 & 0 & 0 & 0 & -1 & 3 & -1 & 0 & -1 \\ 0 & 0 & 0 & 0 & 0 & 0 & -1 & 1 & 0 & 0 \\ 0 & 0 & 0 & 0 & 0 & 0 & 0 & 0 & 1 & -1 \\ -1 & 0 & 0 & 0 & 0 & 0 & -1 & 0 & -1 & 3 \end{bmatrix}$$

which means the communication topology of the whole 10 vehicles team is not all-to-all and quite sparse. The maximum communication links of one vehicle to other vehicles in the team are 3 in this communication case. Note that collision free among vehicles is not considered in this simulation, and it can be referred to the work in [Xiang et al., 2010b, Xiang et al., 2010c] and will be systemically included in the future work.

In Figure 6.17(a), all vehicles asymptotically track their reference paths while building the circle formation simultaneously, where the actual trajectory of the i-th vehicle is plotted in the thick line. The composite paths tracking errors $\sqrt{x_{ei}^2 + y_{ei}^2 + \theta_{ei}^2}, (i = 1, ..., 10)$, are plotted in Figure 6.17(b).

The evolving velocities of the virtual targets moving along the paths and the actual vehicles are shown in Figure 6.18(a) and 6.18(b) respectively.

Extension of example 2 : scaling circle formation of 10 vehicles

In this simulation, the shrunk circle formation is built according to the representation of paths rotation and scaling given in (6.21). Since the rotation of circle does not make much sense, only the scaling parameters in (6.54) are used here to build the shrunk circle formation, defined as

$$S = \begin{bmatrix} a(1 - k\frac{t}{T}) & 0 \\ 0 & b(1 - k\frac{t}{T}) \end{bmatrix} \tag{6.54}$$

where $a = b = 1; k = 0.7, T = 1000$. The formation begin to be shrunk from the time instant $t = 600$. Initial conditions are set as the same as previous example.

The simulation result is given in Figure 6.19. It shows that the circle formation is shrinking and achieve the final circle formation with $1/3$ radius of the original radius at the time instant $t = 1000$, as $a(1 - k\frac{t}{T})|_{t=1000} = b(1 - k\frac{t}{T})|_{t=1000} = 0.3$.

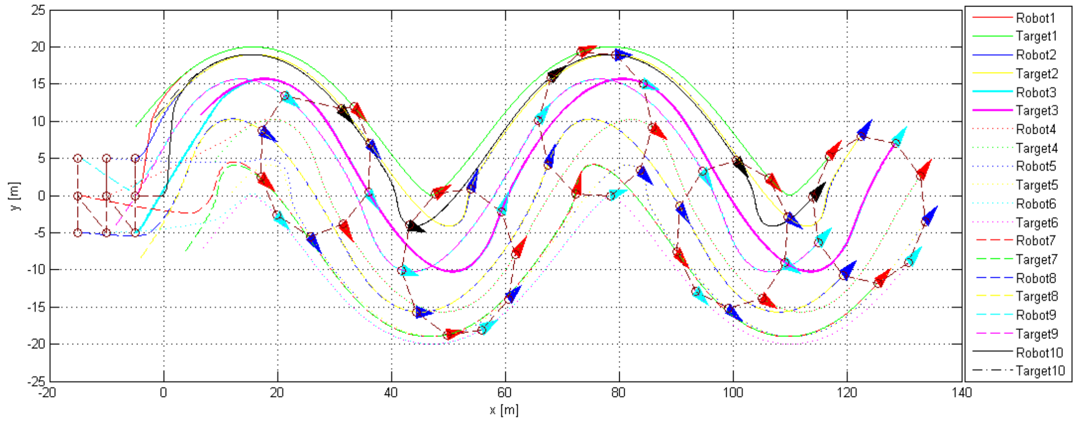

(a) Evolution of building circle formation

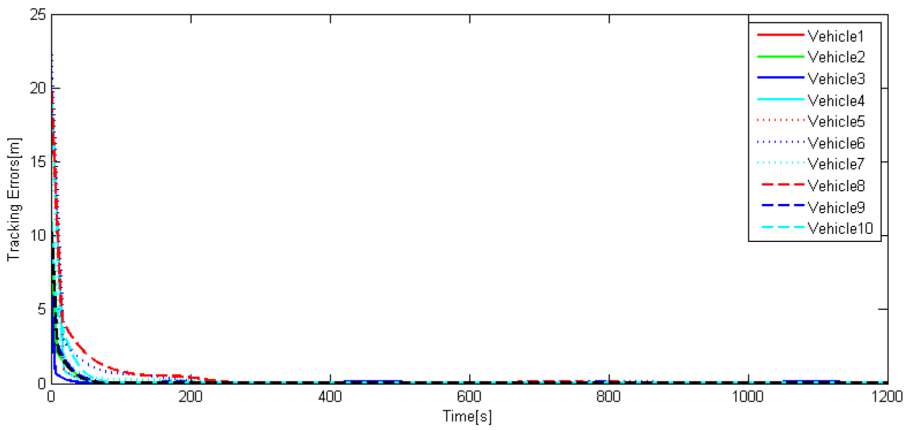

(b) Tracking errors in the form of $\sqrt{x_{ei}^2 + y_{ei}^2 + \theta_{ei}^2}$

Figure 6.17 – Circle formation based on coordinated paths tracking

6.4 Summary

In this chapter, coordinated motion control design based on paths following and paths tracking are proposed, where the control of virtual targets moving along the paths is the fundmental issue. The leader-follower and virtual structure strategies are adopted in order to build the desired formation pattern. Both the centralized and decentralized framework are implemented in the control design. Algebraic graph theory is used to represent the communication topology of multi-vehicle system, which is the instrumental tool for decentralized control design.

Through the coordinated control design, it shows that the control design for coordinated paths tracking is easily implemented, compared with that of coordinated path

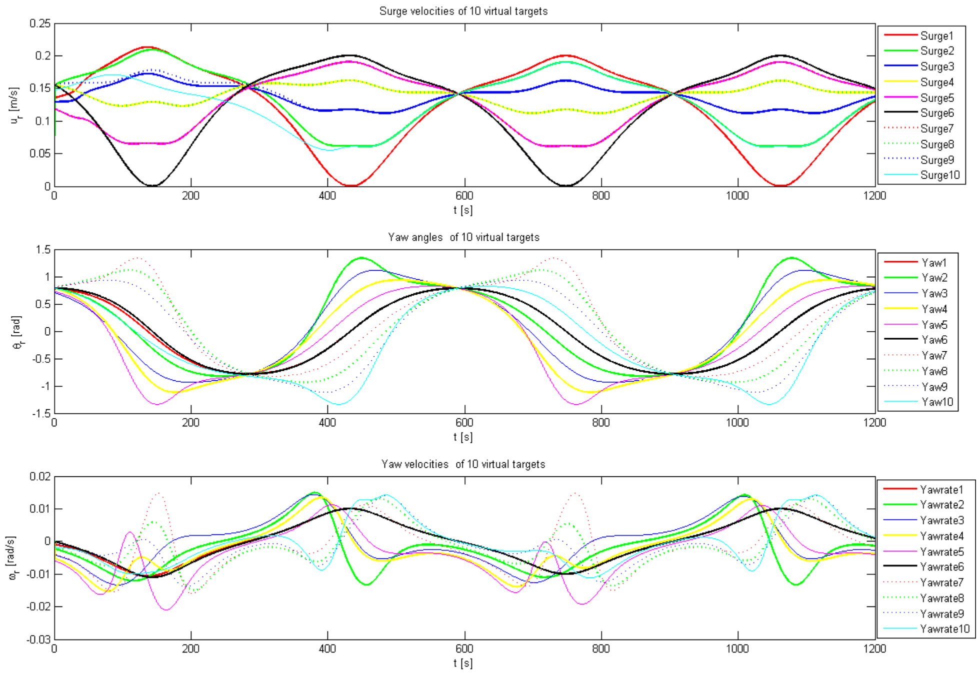

(a) Evolution of 10 virtual targets velocities during circle formation

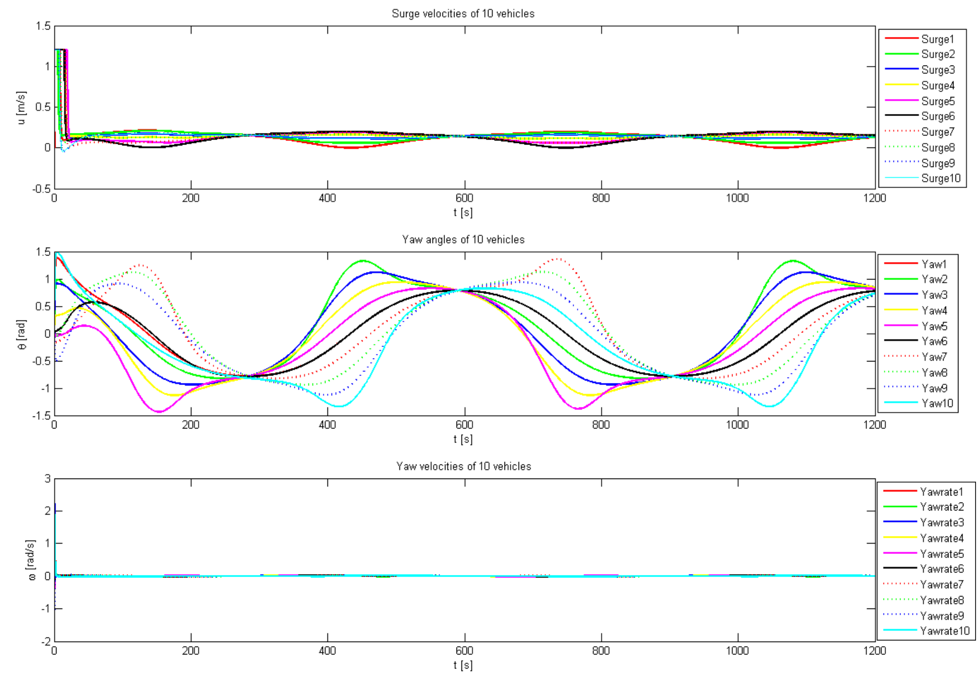

(b) Evolution of 10 vehicles velocities during circle formation

Figure 6.18 – Evolution of velocities while building circle formation

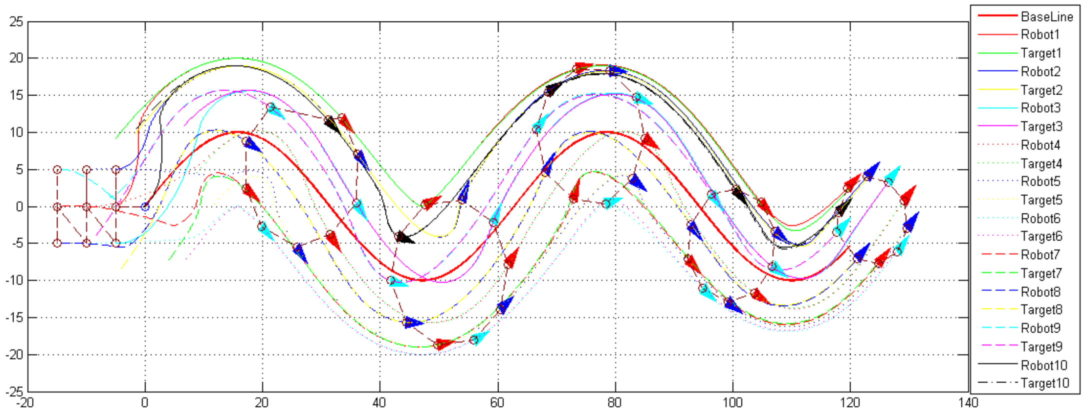

Figure 6.19 – Shrunk circle formation based on coordinated paths tracking

following, as the path parameter τ in path tracking is more flexible than the path parameter s in path following, such that complex mathematic representation is avoided to build the geometric relationship of formation pattern in coordinated path tracking.

Finally, the simulation results illustrate the performance of the proposed coordinated motion controllers.

CHAPTER 7

CONCLUSIONS

7.1 Summary of dissertation

In this dissertation, the motion control strategies and resulted control designs for autonomous vehicles are the main research interests. The motion control problem of nonholonomic unicycle-type vehicle is firstly considered, and then the control design is extended to underactuated autonomous underwater vehicles by utilizing the similarity between them. The control designs are mainly based on Lyapunov theory and backstepping technique, to derive the motion controllers in dynamics stage.

The motion control problems, trajectory tracking and path following are analyzed firstly, and the advantages and disadvantages of both kinds of motion control are illustrated through the simulation results. Sequently, the path tracking control is proposed by incorporating both the features of trajectory tracking and path following, in order to achieve the smooth spatial convergence and tight temporal convergence as well. The approaching angle guidance and adapted LOS guidance are used for nonholonomic unicycle vehicles and underactuated underwater vehicles respectively. The virtual target introduced in path following design to get an extra control degree of freedom (DOF), inspires the control strategy to introduce the path tracking target which also brings the extra DOF in path tracking design, and merges the path following and trajectory tracking behaviors into a single path tracking controller. However, due to the side-slip angle existing in underactuated vehicles, the acceleration of AUV side-slip angle should be carefully treated in order to get well-posed control computation in both the path following and path tracking cases.

After solving the problems of motion control for the individual vehicle. The coordinated formation control of multiple autonomous vehicles is posed as a team of multiple vehicles outperforms the single vehicle in effectiveness, efficiency and robustness. Two main coordinated controls strategies are proposed, i.e., coordinated path following and coordinated path tracking under both the centralized and decentralized frameworks. The leader-follower and virtual structure strategies are adopted in order to build the desired formation pattern. Algebraic graph theory is used to represent the communication topology of multi-vehicle system, which is also the instrumental tool for decentralized control design. Moreover, it shows that the control design for coordinated paths tracking is easily implemented, as the path parameterization in path tracking is more flexible than that in path following, such that complicated mathematic representation is avoided to build the geometric relationship of desired formation patter in coordinated path tracking control.

7.2 Future work

This dissertation addresses the fundmental issues of motion control of autonomous vehicles. With the control strategies and control design methods proposed herein, several extensive topics can be envisioned, namely output feedback control, 3D motion control, and comprehensive communication considerations.

- **Output feedback control**
  All results in this dissertation are based on full-state feedback from position, heading, velocity and angular rate. Since the measurement of the underwater vehicle velocities is costly and corrupted with noise, or even unmeasurable, output feedback control of vehicles is preferable to state-feedback control. In the case when only position and yaw angle measurements are available, the velocities can be estimated using passive non-linear observer or observer backstepping approach. The problem of output feedback tracking control of fully actuated vehicles, has been solved as reported in [Nijmeijer and Fossen, 1999]. However, the nonholonomic constraints of unicycle-type mobile robots, and underactuated Lagrange mechanical system make the observer based output feedback control design is much more difficult.
- **Extension from 2D to 3D motion control**
  The simplified AUV model in horizontal plane is adopted in this theis. However, it is possible to extend the 2D path following and path tracking to the corresponding 3D motion control for autonomous underwater vehicles, which can be reached by designing the 3D heading guidance laws and using similar control strategies and techniques. Definitely, the complex 3D dynamics model of AUVs leads the control design to be much more appealing, especially in the underactuated case. Furthermore, the coordinated motion control in 3D also attracts interests since there is few works on this topic.

- **Further communication issues imposed on multi-vehicle systems**
  For coordinated control of multiple AUVs, bi-directional communication between vehicles is assumed in the dissertation and the property of undirected graph is used for rigorous proof of control laws. However, this is a conservative communication situation, and unidirectional communication could happen in practical case. Unfortunately, the directed graph theory related to unidirectional topology, can not be easily and explicitly used to rigorously derive the control laws. Moreover, the problem of time delay and packet loss during transmitting coordinated communication variables, is also of interest. Although it is partially solved for undirected graph in [Ghabcheloo et al., 2009] , but for directed communication graph, there is no sound solution yet. These issues related to communication topology of multi-vehicle systems are quite challenging and warrant the future research.

Other interesting work, for instance, dealing with model parameters uncertainties of AUVs, countering unknown constant ocean current disturbances, and simultaneously path following/path tracking and obstacle avoidance in complex dynamic environments, are worthy of subsequently research efforts as well.

APPENDIX A

Preliminary

In this part, general mathematic notation and definitions are introduced. Some stability concepts are briefly reviewed, and important stability tools are summarized for stabilizing differential equations, or $systems$ as they are defined in this thesis. Some useful inequalities are also given. The chapter ends with an overview of important concepts in algebraic graph theory, which gives the theoretic foundations for coordinated control on multiple vehicles.

A.1 Mathematical preliminaries

This section introduces the some mathematic notation and definitions used throughout the thesis.

1. Lipschitz condition

   Considering the nonautonomous system described by ordinary differential equations as follows

   $$\dot{x} = f(t, x) \tag{A.1}$$

   where $f : [0, \infty) \times D \to \Re^n$ is piecewise continuous in t, and $D \in \Re^n$ is a domain that contains the origin $x = 0$. Let $f(t, x)$ satisfies the *Lipschitz condition*

   $$\|f(t, x) - f(t, y) \leq L\|x - y\| \tag{A.2}$$

   for all (t, x) and (t, y) in some neighborhood of (t_0, x_0), where $L \in \Re^+$ is called a *Lipschitz constant*.

   Definition A.1.1 *Given a piecewise continuous function $f(t, x)$, it is said to be*

   ◇ *locally Lipschitz in x on $[a, b] \times D$, if each point $x \in D$ has a neighborhood D_0 such that f satisfies (A.2) on $[a, b] \times D_0$ with some Lipschitz constant L_0.*

◇ *globally Lipschitz in x on $[a, b] \times \Re^n$, if f satisfies (A.2) for each point $x \in \Re^n$ with the same Lipschitz constant L.*

Particularly, the Lipschitz condition implies any discontinuous function $f(x) : \Re \to \Re$, is not locally Lipschitz at the point of discontinuity.

2. uniformly continuous

Definition A.1.2 *The function $f(t, x)$ is uniformly continuous in x on $[0, \infty] \times D$ if for any $\varepsilon \geq 0$, there exists $\delta \geq 0$ such that $\|f(t, x) - f(t, y)\| \leq \varepsilon$ for all $x, y \in D$ satisfying $\|x - y\| \leq \delta$ and $\forall t \geq 0$.*

It means small changes in x results in small changes in $f(t, x)$ uniformly in t.

Notice that the Lipschitz property of a function is weaker than continuous differentiability, but stronger than uniformly continuity. Hence, there is following sufficient condition for uniform continuity [Lapierre and Jouvencel, 2008].

Lemma A.1.3 *A function $f(t, x)$ is uniformly continuous, if $\dot{f}(t, x)$ exists and is bounded.*

This part introduces the notation and some definitions used in this thesis.

Definition A.1.4 *Time derivatives of a function $x(t)$ are denoted $\dot{x}, \ddot{x}, ..., x^n$. A superscript with an argument variable denote partial differentiation with respect to that argument,i.e., $\alpha^t(x, t) := \frac{\partial \alpha}{\partial t}$, $\alpha^{x^2}(x, t) := \frac{\partial \alpha}{\partial x^2}$, ..., $\alpha^{x^n}(x, t) := \frac{\partial \alpha}{\partial x^n}$.*

Definition A.1.5 *Class $\mathcal{C}^r$ function : a function $f : X \to Y$ is of class $\mathcal{C}^r$, written $f \in \mathcal{C}$, if the k-th partial differentiation with respect to argument variable x, i.e., $f^{x^k}(x), k \in \{0, 1, ..., r\}$ is defined and continuous for all $x \in X$. In addition, f is continuous if $f \in \mathcal{C}^0$, f is continuously differentiable if $f \in \mathcal{C}^1$, and f is smooth if $f \in \mathcal{C}^\infty$.*

Definition A.1.6 *The p-norm of a vector is $|x|_p := (\sum_{i=1}^n |x_i|^p)^{\frac{1}{p}}$, where the most commonly used 2-norm, or the Euclidean vector norm, simply denoted $|x| := \|x\|_2 = (x^T x)^{1/2}$. This reduces to the absolute value for a scalar.*

Definition A.1.7 *Let $\mathcal{L}_p$ denote the set of all piecewise continuous function $x : [0, \infty) \to \Re^n$ being p-integrable on $[0, \infty)$, that is*

$$\mathcal{L}_p = \{x(t) : \int_0^\infty |x(t)|^p dt < \infty\} \tag{A.3}$$

3. Comparison functions

Scalar comparison functions, known as class $\mathcal{K}$, $\mathcal{K}_\infty$ and $\mathcal{KL}$ functions, are useful mathematical tools to define stability.

Definition A.1.8 *Class $\mathcal{K}$ function : a continuous and strictly increasingly function $\alpha : [0, a) \to [0, \infty)$ with $a(0) = 0$.*

Definition A.1.9 *Class $\mathcal{K}_\infty$ function : a class $\mathcal{K}$ function which satisfies $a = \infty$ and $\alpha(r) \to \infty$ as $r \to \infty$.*

Definition A.1.10 *Class $\mathcal{KL}$ function : a continuous function $\beta : [0, a) \times [0, \infty) \to [0, \infty)$, such that for each fixed s, the mapping $\beta(r, s) \in \mathcal{K}$ with respect to r ; and for each fixed r, the mapping $\beta(r, s)$ is decreasing with respect to s and $\beta(r, s) \to 0$ as $s \to \infty$.*

A.2 Lyapunov stability

The primary requirment for control system is stability. This section give a brief review of some stability concepts and tools for stability analysis, such as Lyapunov theorem, invariance principle for both autonomous and nonautonomous system, and Input-to-state stability.

The theorems and definitions are mainly collected from [Khalil, 2002] and [Li and W., 1991]. However, the proofs are not reported here

1. Lyapunov stability for autonomous system

Consider the ***autonomous system***

$$\dot{x} = f(x) \tag{A.4}$$

where $f : D \to \Re^n$ is a locally Lipschitz map from a domain (open and connected set) $D \subset \Re^n$ into $\Re^n$. Suppose the system has an equilibrium at the origin $x = 0$, that is, $f(0) = 0$. It is no loss of generality as any equilibrium can be shifted to the origin by a change of variables.

Theorem A.2.1 (Lyapunov stability theorem)

Let $x = 0$ be an equilibrium point for autonomous system (A.4) and $D \subset \Re^n$ be a domain containing $x = 0$. Let $V : D \to \Re^n$ be a $\mathcal{C}^1$ function such that

$$V(0) = 0 \& V(x) > 0, x \in D \setminus \{0\} \tag{A.5}$$

$$\dot{V}(x) \leq 0, x \in D \tag{A.6}$$

Then, $x = 0$ is stable. Moreover, if

$$\dot{V}(x) < 0, x \in D \setminus \{0\} \tag{A.7}$$

then $x = 0$ is asymptotically stable.

Definition A.2.2 (positively invariant set)

Let $x(t)$ be a solution of (A.4). A set M is said to be a positively invariant set if

$$x(t_0) \in M \Rightarrow x(t) \in M, \forall t \geq t_0 \tag{A.8}$$

Theorem A.2.3 (LaSalle's theorem)

Let $\Omega \subset D$ be a compact (closed and bounded) subset that is positively invariant with respect to autonomous system $\dot{x} = f(x)$. Let $V : D \to \Re$ be a $\mathcal{C}^1$ function such that $\dot{V}(x) \leq 0$ in Ω. Let $E = \{x \in \Omega | \dot{V}(x) = 0\}$ and M be the largest invariant set in E. Then every solution starting in Ω approaches M as $t \to \infty$.

When we need to establish the largest invariant set in E is the origin, the special case of LaSalle's theorem (or LaSalle's invariance principle) comes up as follows

Theorem A.2.4 (Barbashin-Krasovskii theorem)

Let $x = 0$ be an equilibrium point for the autonomous system $\dot{x} = f(x)$. Let $V : R^n \to R$ be a $\mathcal{C}^1$ radially unbounded and positive definite function such that $\dot{V}(x) \leq 0$ for all $x \in \Re^n$. Let $E = \{x \in \Re^n | \dot{V}(x) = 0\}$ and suppose that no solution can stay forever in E, other than the trivial solution $x(t) \equiv 0$. Then the origin is UGES.

2. Lyapunov stability for nonautonomous system

The origin is an equilibrium point for ***nonautonomous system*** (A.1) at $x = 0$, if

$$f(t, 0) = 0, \forall t \geq 0 \tag{A.9}$$

Definition A.2.5 *The equilibrium point of (A.1) is*

Uniformly stable (US), if and only if there exist a class $\mathcal{K}$ function $\alpha(\cdot)$ and a positive constant c, independent of t_0, such that

$$\|x(t)\| < \alpha(\|x(t_0)\|), \forall t \geq t_0 \geq 0, \forall \|x(t_0)\| < c. \tag{A.10}$$

Uniformly asymptotically stable (UAS), if and only if there exist a class $\mathcal{KL}$ function $\beta(\cdot)$ and a positive constant c, independent of t_0, such that

$$\|x(t)\| < \beta(\|x(t_0)\|, t - t_0)\|, \forall t \geq t_0 \geq 0, \forall \|x(t_0)\| < c. \tag{A.11}$$

Uniformly globally asymptotically stable (UGAS), if and only if inequality (A.11) is satisfied for any initial state $x(t_0)$.

Exponentially stable (ES), if there exist positive constant k, r, c such that the class $\mathcal{KL}$ function $\beta(\cdot)$ in inequality (A.11) satisfied with

$$\beta(r, s) = kre^{-\lambda s}, \forall \|x(t_0)\| < c \tag{A.12}$$

Uniformly globally exponentially stable (UGES), if and only if inequality (A.12) is satisfied for any initial state $x(t_0)$.

Theorem A.2.6 (Lyapunov Theorem for nonautonomous system)

Let $V : [0,\infty) \times D \to \Re$ be $\mathcal{C}^1$ function such that

$$\alpha_1(\|x\|) \leq V(t,x) \leq \alpha_2(\|x\|) \tag{A.13}$$

$$\dot{V}(t,x) = \frac{\partial V}{\partial t} + \frac{\partial V}{\partial t} f(t,x) \leq -W_3(x) \tag{A.14}$$

$\forall t \geq 0, \forall x \in D$, where $\alpha_i(\cdot), i = 1,2,3$ is class $\mathcal{K}$ function defined on $[0,r) \in \Re^+$. Then equilibrium $x = 0$ is UAS, if all the assumptions hold globally with $r = +\infty$, and $\alpha_1(\cdot), \alpha_2(\cdot) \in \mathcal{K}_\infty$, then $x = 0$ is UGAS. Moreover, if $\alpha_i(\|x\|) = c_i\|x\|^r, i = 1,2,3$ where $c_i, r \in \Re^+$ and $r \geq 1$, then $x = 0$ is ES, if all assumptions hold globally, then the origin is UGES.

A function $V : [0,\infty) \times D \to \Re$ is said to be *positive definite* if $V(t,x) \geq \alpha_1(\|x\|)$ for some class $\mathcal{K}$ function $\alpha_1(\cdot)$, *radially unbounded* if $\alpha_1(\cdot)$ is class $\mathcal{K}_\infty$, and *decrescent* if $V(t,x) \leq \alpha_2(\|x\|)$ for some class $\mathcal{K}$ function $\alpha_2(\cdot)$ function.

Remark 1 : (globally) exponentially stable equals uniformly (globally) exponentially stable(UGES), and implies uniformly (globally) asymptotically stable (UGAS).

Remark 2 : it is not necessary to establish uniform convergence for time-invariant, or autonomous systems since [Hale and Lunel, 1993] (Ch.6, Lemma 1.1) show that, asymptotic stability implies uniform asymptotic stability.

Similarly, there is counterpart of invariance principle-like theorem for nonautonomous sytems, which is called Barbalat's lemma.

Lemma A.2.7 (Barbalat's lemma)

Let $f(t)$ be a uniformly continuous function on $[0,\infty)$, and assume $\lim_{t\to\infty} \int_0^t f(\tau)d\tau$ exist and is finite. Then $f(t) \to 0$ as $t \to \infty$.

By using the sufficient condition of uniform continuous function from Lemma A.1.3, there is following corollary

Corollary A.2.8 (Corollary of Barbalat's lemma)

Let $\dot{f}(t)$ be a double differentiable function on $[0,\infty)$, and assume $f(t)$ is finite such that $\ddot{f}(t)$ exists and is bounded. Then $\dot{f}(t) \to 0$ as $t \to \infty$.

A.3 Backstepping technique

Backstepping is a recursive design for systems with nonlinearities not constrained by linear bounds. This section give a brief review of the backstepping approach for control design. See [Kokotovic, 1992] and [Fossen and Strand, 1999] for details.

The key idea of backsteppping is to start with a system which is stabilizable with a known feedback law for a known Lyapunov function, and then to add an integrator to its input. For the augmented system, a new stabilizing feedback law is explicitly designed and proven to be stabilizing for a new Lyapunov function, and so on. To show how it works, a basic form of the backstepping procedure is explained with a short design example. Suppose a system to be controlled is given below :

$$\begin{cases} \dot{x}_1 = f_1(x_1) + x_2 \\ \dot{x}_2 = f_2(x_1, x_2) + u \\ y = x_1 \end{cases} \tag{A.15}$$

where x_1, x_2 are state variables and u is the control input. Let the design objective be regulate the output $y(t) \to 0$ as $t \to 0$.

The idea behind backstepping is to consider the state x_2 as a control input for x_1 making the x_1 system globally asymptotically stable. By considering the Lyapunov function $V_1 = \frac{1}{2}x_1^2$, introduce the control input $x_2 := \alpha(x_1) = -k_1x_1 - f_1(x_1)$ such that

$$\dot{V}_1 = -k_1x_1^2 < 0, x_1 \neq 0 \tag{A.16}$$

where $k_1 > 0$ is the feedback gain. Since x_2 is a virtual control variable for x_1, one defines

$$\begin{cases} z_1 = x_1 \\ z_2 = x_2 - \alpha(x_1) \end{cases} \tag{A.17}$$

The system (A.15) is then written in terms of these new variables, resulting in

$$\begin{cases} \dot{z}_1 = -k_1z_1 + z_2 \\ \dot{z}_2 = f_2(x_1, x_2) + u - \frac{\partial\alpha}{\partial x_1}\dot{x}_1 \end{cases} \tag{A.18}$$

For the system (A.18), a control Lyapunov function is constructed from V_1 by adding a quadratic term which penalizes the residual error z_2 between the virtual control input x_2 and virtual control law $\alpha(x_1)$, this suggests that we examine

$$V_2(z_1, z_2) = V_1(z_1) + \frac{1}{2}z_2^2 \tag{A.19}$$

Differentiating $V_2(z_1, z_2)$ with respect to time yields

$$\dot{V}_2 = -z_1^2 + z_2(z_1 + f_2(x_1, x_2) + u - \frac{\partial\alpha}{\partial x_1}(x_2 + f_1(x_1))) \tag{A.20}$$

To guarantee global asymptotically stability, $\dot{V}_2$ has to be negative definite. This can be achieved by choosing the control input, u as

$$u = -f_2(x_1, x_2) - z_1 - k_2z_2 + \frac{\partial\alpha}{\partial x_1}(x_2 + f_1(x_1)) \tag{A.21}$$

with $k_2 > 0$, yields :

$$\dot{V}_2 = -k_1 z_1^2 - k_2 z_2^2 < 0, \forall z_1 \neq 0, z_2 \neq 0 \tag{A.22}$$

which means that GAS is achieved at the equilibrium $(x_1, x_2) = (0, -f_1(0))$.

If u in not the actual control input but a virtual control law consisting state variables, then the system can be further augmented by proceeding the procedure again. Hence, the backstepping design can be recursively go ahead until the final actual control input arrived. This example highlights the key recursive feature of backstepping : the control Lyapunov function for step $k+1$ is constructed as

$$V_{k+1} = V_k + (x_k - \alpha_{k-1}(x_1, ..., x_{k-1}))^2 \tag{A.23}$$

where V_k is the k-th control Lyapunov function and α_{k-1} is the virtual control law which renders $\dot{V}_k < 0$ for $x_k = \alpha_{k-1}(x_1, ..., x_{k-1})$.

In order to apply backstepping technique to a system, it must have a so called *lower triangular form*. Systems which have a "strict feedback" form (A.24) is one typical example falling into this category.

$$\begin{cases} \dot{x}_1 = f(x_1) + g(x_1)x_2 \\ \dot{x}_2 = f_1(x_1, x_2) + g_1(x_1, x_2)x_3 \\ \dots \\ \dot{x}_i = f_i(x_1, x_2, ..., x_i) + g_i(x_1, x_2, ..., x_i)x_{i+1} \\ \dots \\ \dot{x}_n = f_n(x_1, x_2, ..., x_n) + g_n(x_1, x_2, ..., x_n)u \end{cases} \tag{A.24}$$

The recursive procedure is explicit for above system and the global stability can be derived. In case of more general "pure feedback" form (A.25), the stability result may not be explicit or global, but a nonvanishing region of stability is still guaranteed.

$$\begin{cases} \dot{x}_1 = f_1(x_1, x_2) \\ \dot{x}_2 = f_2(x_1, x_2, x_3) \\ \dots \\ \dot{x}_i = f_i(x_1, x_2, ..., x_{i+1}) \\ \dots \\ \dot{x}_n = f_n(x_1, x_2, ..., x_n, u) \end{cases} \tag{A.25}$$

In (A.24) or (A.25), the recursive design with the system x_1 and continuously with x_2, x_3, ..., ect. Introducing a change of coordinates during the recursive design process, $z = \phi(x)$ where $\mathbf{z} = [z_1, z_2, ..., z_n]^T, \mathbf{x} = [x_1, x_2, ..., x_n]^T$ and $\phi(x) : \Re^n \rightarrow \Re^n$ is a transformation to be interpreted later. The backstepping coordinate transformation is a *global* *diffemorphism*, if the mapping $\phi(x)$ and $\phi^{-1}(x)$ are a c^1 function on $\Re^n$, and local if the inverse transformation $\phi^{-1}(z)$ only exists on a subspace of $\Re^n$. The diffemorphism characteristics ensures the state vector **x** has the same stability property with **z**.

Backstepping technique has two flexibilities :

1) Nonlinear damping : the virtual control law α_i is only derived to produce a negative definite $\dot{V}_i$, which can keep some "useful nonlinearities" (i.e., nonlinear damping terms) rather than to cancel all system nonlinearities as feedback linearization method has to do.

2) Easily extensible : the facility with which backstepping incorporated unknown parameters and nonlinear interval uncertainties (disturbances) contributed to its instant popularity and rapid application, extended to adaptive backstepping , robust backstepping, etc.

Appendix B

Modeling of autonomous underwater vehicles

In this part, the mathematical model of the autonomous underwater vehicles is introduced for the purpose of designing the motion control system. The comprehensive description of the model, can be referred in [Fossen, 2002].

In the following parts, the standard SNAME notations in Table 3.1 are used to build the kinematic and dynamics model of underwater vehicles.

B.1 Kinematics model of AUV

The first time derivative of the position vector η_1, is related to the linear velocity vector ν_1 through the following transformation

$$\dot{\eta}_1 = J_1(\eta_2)\nu_1 \tag{B.1}$$

The transformation matrix $J_1(\eta_2)$ is the rotation matrix from $\{B\}$ to $\{I\}$ parameterized by the vector of Euler anglers, given by

$$R_B^I(\eta_2) = J_1(\eta_2) = \begin{bmatrix} \mathrm{c}\psi\mathrm{c}\theta & -\mathrm{s}\psi\mathrm{c}\phi + c\psi\mathrm{s}\theta\mathrm{s}\phi & \mathrm{s}\psi\mathrm{s}\phi + \mathrm{c}\psi\mathrm{s}\theta\mathrm{c}\phi \\ \mathrm{s}\psi\mathrm{c}\theta & \mathrm{c}\psi\mathrm{c}\phi + \mathrm{s}\psi\mathrm{s}\theta\mathrm{s}\phi & -\mathrm{c}\psi\mathrm{s}\phi + \mathrm{s}\psi\mathrm{s}\theta\mathrm{c}\phi \\ -\mathrm{s}\theta & \mathrm{c}\theta s\phi & \mathrm{c}\theta\mathrm{c}\phi \end{bmatrix} \tag{B.2}$$

where $\mathrm{s}\cdot = \sin(\cdot)$ and $\mathrm{c}\cdot = \cos(\cdot)$.

Actually, the linear velocity rotation matrix $J_1(\eta_2) := R_B^I(\eta_2)$ is usually described by three rotations about the z, y, x axes subsequently :

$$R_B^I(\eta_2) = R_{z,\psi}R_{y,\theta}R_{x,\phi} \tag{B.3}$$

And, $J_1(\eta_2)$ is an element in the special orthogonal group of order 3, denoted as $SO(3)$:

$$SO(3) = \{R|R \in \Re^{3\times 3},\ RR^T = R^T R = \text{I and det } R = 1\} \tag{B.4}$$

Hence, $J_1(\eta)$ is globally invertible and $J_1^{-1}(\eta_2) = J_1^T(\eta_2)$. Furthermore, the derivative of the rotation matrix is

$$\dot{J}_1(\eta_2) = J_1(\eta_2)S(\nu_2) \tag{B.5}$$

where $S(\nu_2)$ is skew-symmetric, that is, $S(\nu_2) = -S(\nu_2)^T$ with the expression :

$$S(\nu_2) = \begin{bmatrix} 0 & -r & q \\ r & 0 & -p \\ -q & p & 0 \end{bmatrix} \tag{B.6}$$

The first time derivative of the Euler angle vector η_2, is related to the body-fixed velocity vector ν_2 through the following transformation

$$\dot{\eta}_2 = J_2(\eta_2)\nu_2 \tag{B.7}$$

where $J_2(\eta_2)$ is given by

$$J_2(\eta_2) = \begin{bmatrix} 1 & -\mathrm{s}\phi\mathrm{t}\theta & \mathrm{c}\phi\mathrm{t}\theta \\ 0 & \mathrm{c}\phi & -\mathrm{s}\phi \\ 1 & \mathrm{s}\phi/\mathrm{c}\theta & \mathrm{c}\phi/\mathrm{c}\theta \end{bmatrix} \tag{B.8}$$

where s$\cdot = \sin(\cdot)$, c$\cdot = \cos(\cdot)$ and t $= \tan(\cdot)$.

Notice from (B.9) that $J_2(\eta_2)$ is not defined when pitch angle $\theta = \pm\pi/2$. In this case, a four-parameter method rather than Euler angles can be used instead to describe it [Fossen, 1994]. Nevertheless, most marine vehicles may not operate close to the singularity due to the physical suppression from the metacentric restoring forces.

With (B.1) and (B.7), the kinematics of the marine vehicle in the body-fixed frame can be written in compact form as

$$\begin{bmatrix} \dot{\eta}_1 \\ \dot{\eta}_2 \end{bmatrix} = \begin{bmatrix} J_1(\eta_2) & 0_{3\times 3} \\ 0_{3\times 3} & J_2(\eta_2) \end{bmatrix} \begin{bmatrix} \nu_1 \\ \nu_2 \end{bmatrix} \Longleftrightarrow \dot{\eta} = J(\eta)\nu \tag{B.9}$$

B.2 Dynamics model of AUV

Applying the Newton-Euler equation of motion of a rigid body, it results in the following 6-DOF dynamic model of a marine vehicle :

$$M_{RB}\dot{\nu} + C_{RB}(\nu)\nu = \tau_{RB} \tag{B.10}$$

where M_{RB} denote the rigid body inertia matrix, C_{RB} denote the rigid body Coriolis and Centripetal matrix, the generalized velocity vector in the body-fixed frame $\nu = [\nu_1^T, \nu_2^T]^T = [u, v, \omega, p, q, r]^T$, and the generalized external force and moment vector $\tau_{RB} = [\tau_1^T, \tau_2^T]^T = [X, Y, Z, K, M, N]^T$ can be written as the sum of four components :

$$\tau_{RB} = \tau_H + \tau_E + \tau \tag{B.11}$$

where τ_H captures the hydrodynamic force and moment resulted from added mass, restoring force (due to gravity and buoyancy), nonlinear damping and friction ; τ_E denotes the external environmental disturbance force and moment resulted from wind, waves and currents acting on the vehicle in the body-fixed frame ; τ represents the propulsion forces and moments.

Combing equations (B.10) and (B.11), with the detailed representation of each components in [Fossen, 2002] together, the 6-DOF marine vehicle dynamics is then expressed in the body-fixed frame as follows :

$$M\dot{\nu} + C(\nu)\nu + D(\nu)\nu + g(\eta) = \tau + \tau_E \tag{B.12}$$

where $g(\eta)$ is the restoring force and moment vector, $M = M_{RB} + M_A$, $C(\nu) = C_{RB}(\nu) + C_A(\nu)$, and M_A and $C_A(\nu)$ denote the added mass matrix and hydrodynamic Coriolis and Centripetal matrix, respectively.

The matrices in (B.12) have some intrinsic properties which are useful during control design.

1. For a rigid body at rest or at most is moving at low speed in ideal fluid, the matrix M is always constant and symmetric positive definite :

$$M = M^T > 0, \ \dot{M} = 0_{6\times 6} \tag{B.13}$$

2. For a rigid body moving through an ideal fluid, the $C(\nu)$ can always be parameterized such that it is skew-symmetric :

$$C(\nu) = -C^T(\nu), \ \forall \nu \in \Re^6. \tag{B.14}$$

The skew-symmetric property of $C(\nu)$ implies that

$$s^T C(\nu) s = 0, \ \forall s \in \Re^6. \tag{B.15}$$

3. For a rigid body moving in an ideal fluid, the hydrodynamic damping matrix $D(\nu)$ is real, and strictly positive definite. Furthermore, it can be assumed to be symmetric in low speed applications. That is

$$D(\nu) = D(\nu)^T > 0, \ \forall \nu \in \Re^6. \tag{B.16}$$

The marine vehicle dynamics can be expressed in the earth-fixed coordinates :

$$M_\eta(\eta)\ddot{\eta} + C_\eta(\nu,\eta)\dot{\eta} + D_\eta(\nu,\eta)\dot{\eta} + g_\eta(\eta) = J^{-T}(\eta)(\tau + \tau_E) \tag{B.17}$$

where

$$\begin{array}{ll} M_\eta(\eta) = J(\eta)^{-T} M J(\eta) & C_\eta(\nu,\eta) = J(\eta)^{-T}[C(\nu) - MJ(\eta)^{-1}\dot{J}(\eta)]J(\eta) \\ D_\eta(\nu,\eta) = J(\eta)^{-T} D(\nu) J(\eta) & g_\eta(\eta) = J(\eta)^{-T} g(\eta) \end{array} \tag{B.18}$$

with the assumption that $J(\eta)^{-1}$ exists, i.e., $\theta \neq \pm\pi/2$.

Following the same assumption used in the body-fixed representation, (B.17) has some special properties :

$$\begin{array}{ll} M_\eta(\eta) = M_\eta(\eta)^T, \forall \eta \in \Re^6, & D_\eta(\nu,\eta) > 0, \forall \eta, \nu \in \Re^6 \\ s^T[\dot{M}_\eta(\eta) - 2C_\eta(\nu,\eta)s = 0, \forall s, \eta, \nu \in \Re^6 & \end{array} \tag{B.19}$$

A vehicle is said to be underactuated if it has less number of independent control inputs than degrees of freedom to be controlled, according to the definition of underactuated system. In general, suppose that there are $m < 6$ independent actuaors are available for underactuated vehilces. If there are no actuators in certain motion components, the corresponding elements in the actutaion vector τ are set to be zero.

Hence, the dynamic motion equation of underactuated marine vehicle is different from the fully-actuated vehicle, as the control vector τ in dynamics equation (B.12) with underactuation constraints should be rewritten as

$$\tau = [\tau_1, \tau_2, ..., \tau_6]^T, \text{ where } \tau_i = 0, \forall i \in \{1, 2, ..., 6\}, \text{and } \sum_{i=1}^{m} i < \sum_{j=1}^{6} j \tag{B.20}$$

BIBLIOGRAPHY

[Aguiar, 2001] Aguiar, A. (2001). *Nonlinear Motion Control of Nonholonomic and Underactuated Systems*. PhD thesis, IST, Portugal.

[Aguiar et al., 2005a] Aguiar, A., Hespanha, J., and Pascoal, A. (2005a). Stability of switched seesaw systems with application to the stabilization of underactuated vehicles. In *Decision and Control, 2005 and 2005 European Control Conference. CDC-ECC '05. 44th IEEE Conference on*, pages 4584 – 4589.

[Aguiar and Hespanha, 2007] Aguiar, A. P. and Hespanha, J. P. (2007). Trajectory-tracking and path-following of underactuated autonomous vehicles with parametric modeling uncertainty. *Automatic Control, IEEE Transactions on*, 52(8) :1362–1379.

[Aguiar et al., 2005b] Aguiar, A. P., Hespanha, J. P., and Kokotovic, P. V. (2005b). Path-following for nonminimum phase systems removes performance limitations. *Automatic Control, IEEE Transactions on*, 50(2) :234–239.

[Aguiar et al., 2008] Aguiar, A. P., Hespanha, J. P., and Kokotovic, P. V. (2008). Performance limitations in reference tracking and path following for nonlinear systems. *Automatica*, 44(3) :598–610.

[Aguiar and Pascoal, 2007a] Aguiar, A. P. and Pascoal, A. M. (2007a). Coordinated path-following control for nonlinear systems with logic-based communication. In *Proc. 46th IEEE Conference on Decision and Control*, pages 1473–1479.

[Aguiar and Pascoal, 2007b] Aguiar, A. P. and Pascoal, A. M. (2007b). Dynamic positioning and way-point tracking of underactuated auvs in the presence of ocean currents. *International Journal of Control*, 80(7) :1092–1108.

[Aicardi et al., 1995] Aicardi, M., Casalino, G., Bicchi, A., and Balestrino, A. (1995). Closed loop steering of unicycle like vehicles via lyapunov techniques. *IEEE Robotics & Automation Magazine*, 2(1) :27–35.

[Aicardi et al., 2001] Aicardi, M., Casalino, G., Indiveri, G., Aguiar, P., Encarnacao, P., and Pascoal, A. (2001). A planar path following controller for underactuated marine vehicles. In *Proc. of MED01-9th IEEE Mediterranean Conference on Control and Automation, Dubrovnik, Croatia.*

[Al-Hiddabi and McClamroch, 2001] Al-Hiddabi, S. A. and McClamroch, N. H. (2001). Aggressive longitudinal aircraft path tracking using nonlinear control. *Asian Journal of Control*, 3(4) :280–288.

[Al-Hiddabi and McClamroch, 2002] Al-Hiddabi, S. A. and McClamroch, N. H. (2002). Aggressive longitudinal aircraft trajectory tracking using nonlinear control. *Jouranl of Guidance, Control, and Dynamics*, 25(1) :26–32.

[Almeida et al., 2007a] Almeida, J., Silvestre, C., and Pascoal, A. (2007a). Coordinated control of multiple vehicles with discrete-time periodic communications. In *Proc. 46th IEEE Conference on Decision and Control*, pages 2888–2893.

[Almeida et al., 2007b] Almeida, J., Silvestre, C., and Pascoal, A. (2007b). Path following control of fully actuated surface vessels in the presence of ocean currents. In *Proc. 2007 Conference on Control Applications in Marine Systems (CAMS07),Bol, Croatia.*

[Almeida et al., 2010] Almeida, J., Silvestre, C., and Pascoal, A. (2010). Cooperative control of multiple surface vessels in the presence of ocean currents and parametric model uncertainty. *Int. J. Robust Nonlinear Control*, 20(14) :1549–1565.

[Altafini, 2002] Altafini, C. (2002). Following a path of varying curvature as an output regulation problem. In *IEEE Trans. on Automat. Contr.*, volume 47, pages 1551–1556.

[Anderson and Robbins, 1998] Anderson, M. and Robbins, A. (1998). Formation flight as a cooperative game. volume 25, pages 244 –251.

[Antonelli et al., 2008] Antonelli, G., Fossen, T. I., and Yoerger, D. R. (2008). Underwater robotics.

[Antsaklis and Baillieul, 2007] Antsaklis, P. and Baillieul, J. (2007). Special issue on technology of networked control systems. *Proceedings of the IEEE*, 95(1) :5 –8.

[Arrichiello et al., 2006] Arrichiello, F., Chiaverini, S., and Fossen, T. I. (2006). Formation control of underactuated surface vessels using the null-space-based behavioral control. In *Proc. IEEE/RSJ International Conference on Intelligent Robots and Systems*, pages 5942–5947.

[Astolfi, 1996] Astolfi, A. (1996). Discontinuous control of nonholonomic systems. *Systems & Control Letters*, 27(1) :37–45.

[Astolfi et al., 2002] Astolfi, A., Chhabra, D., and Ortega, R. (2002). Asymptotic stabilization of some equilibria of an underactuated underwater vehicle. *Systems & Control Letters*, 45(3) :193–206.

[Bak et al., 2001] Bak, M., Poulsen, N. K., and Ravn, O. (2001). Path following mobile robot in the presence of velocity constraints. Technical Report IMM-TR-2001-7, Informatics and Mathematical Modelling, Technical University of Denmark, DTU.

[Balch and Arkin, 1998] Balch, T. and Arkin, R. C. (1998). Behavior-based formation control for multirobot teams. *Robotics and Automation, IEEE Transactions on*, 14(6) :926–939.

[Batista et al., 2009] Batista, P., Silvestre, C., and Oliveira, P. (2009). A sensor-based controller for homing of underactuated auvs. *Robotics, IEEE Transactions on*, 25(3) :701 –716.

[Beard et al., 2001a] Beard, R., Lawton, J., and Hadaegh, F. (2001a). A coordination architecture for spacecraft formation control. *Control Systems Technology, IEEE Transactions on*, 9(6) :777 –790.

[Beard et al., 2001b] Beard, R., Lawton, J., and Hadaegh, F. (2001b). A feedback architecture for formation control. In *IEEE Transactions on Control Systems Technology*, volume 9, pages 777 –790.

[Behal et al., 2002] Behal, A., Dawson, D., Dixon, W., and Fang, Y. (2002). Tracking and regulation control of an underactuated surface vessel with nonintegrable dynamics. *Automatic Control, IEEE Transactions on*, 47(3) :495 –500.

[Bertin and Branca, 2000] Bertin, D. and Branca, L. (2000). Operational and design aspects of a precision minewarfare autopilot. In *Proceedings of the Warship 2000, London, UK.*

[Bibuli et al., 2009] Bibuli, M., Bruzzone, G., Caccia, M., and Lapierre, L. (2009). Path-following algorithms and experiments for an unmanned surface vehicle. *Journal of Field Robotics*, 26(8) :669–688.

[BØrhaug, 2008] BØrhaug, E. (2008). *Nonlinear Control and Synchronization of Mechanical Systems*. PhD thesis, Norwegian University of Science and Technology, Faculty of Information Technology, Mathematics and Electrical Engineering.

[Børhaug et al., 2010] Børhaug, E., Pavlov, A., Panteley, E., and Pettersen, K. Y. (2010). Straight line path following for formations of underactuated marine surface vessels. *Control Systems Technology, IEEE Transactions on*, 18(6) :1 –14.

[Børhaug et al., 2007] Børhaug, E., Pavlov, A., and Pettersen, K. (2007). Straight line path following for formations of underactuated underwater vehicles. In *Decision and Control, 2007 46th IEEE Conference on*, pages 2905 –2912.

[Børhaug et al., 2008] Børhaug, E., Pavlov, A., and Pettersen, K. (2008). Integral los control for path following of underactuated marine surface vessels in the presence of constant ocean currents. In *Decision and Control, 2008. CDC 2008. 47th IEEE Conference on*, pages 4984 –4991.

[Breivik and Fossen, 2006] Breivik, M. and Fossen, T. (2006). A unified control concept for autonomous underwater vehicles. pages 4920–4926, Minneapolis, Minnesota, USA.

[Breivik et al., 2008] Breivik, M., Hovstein, V. E., and Fossen, T. I. (2008). Ship formation control : A guided leader-follower approach. In *IFAC World Congress, Seuol*, pages 16008–16014.

[Brockett, 1983] Brockett, R. W. (1983). Asymptotic stability and feedback stabilization. *Differential Geom. Control Theory*, pages 181–191.

[Bullo et al., 2009] Bullo, F., Cortes, J., and Piccoli, B. (2009). Special issue on control and optimization in cooperative networks. *SIAM Journal on Control and Optimization*, 48(1) :vii–vii.

[Burger et al., 2009] Burger, M., Pavlov, A., Borhaug, E., and Pettersen, K. (2009). Straight line path following for formations of underactuated surface vessels under influence of constant ocean currents. In *American Control Conference, 2009. ACC '09.*, pages 3065 –3070.

[Canudas de Wit, 1993] Canudas de Wit, C. (1993). Nonlinear control design for mobile robots. In *Recent trends in mobile robots, Yuan F. Zhang (Ed.)*, volume 11, pages 121–156. World scientific series in Robotics and Automated Systems.

[Canudas de Wit, 1998] Canudas de Wit, C. (1998). Trends in mobile robot and vehicle control. In *Control Problems in Robotics and Automation, Lecture Notes in Control and Information Sciences, Siciliano, Bruno and Valavanis, Kimon (Eds)*, volume 230, pages 151–175. Springer Berlin, Heidelberg.

[Canudes de Wit et al., 1994] Canudes de Wit, C., Berghuis, H., and Nijmeijer, H. (1994). Practical stabilization of nonlinear systems in chained form. In *Decision and Control, 1994., Proceedings of the 33rd IEEE Conference on*, volume 4, pages 3475 –3480.

[Cheah et al., 2009] Cheah, C. C., Hou, S. P., and Slotine, J. J. E. (2009). Region-based shape control for a swarm of robots. *Automatica*, 45(10) :2406–2411.

[Coron and Rosier, 1994] Coron, J.-M. and Rosier, L. (1994). A relation between continuous time-varying and discontinuous feedback stabilization. *Journal of Mathematical Systems, Estimation and Control*, 4(1) :67–48.

[Craig, 1986] Craig, J. (1986). *Introduction to Robotics Mechanics and Control*. Addison-Wesley, New York.

[Cui et al., 2010] Cui, R., Sam Ge, S., Voon Ee How, B., and Sang Choo, Y. (2010). Leader-follower formation control of underactuated autonomous underwater vehicles. *Ocean Engineering*, 37(17-18) :1491–1502.

[Curtin et al., 2005] Curtin, T. B., Crimmins, D. M., Curcio, J., Benjamin, M., and Roper, C. (2005). Autonomous underwater vehicles : Trends and transformations. *Marine Technology Society Journal*, 39 :65–75.

[De Gennaro and Jadbabaie, 2006] De Gennaro, M. and Jadbabaie, A. (2006). Formation control for a cooperative multi-agent system using decentralized navigation functions. In *American Control Conference, 2006*, pages 1346 –1351.

[Defoort et al., 2008] Defoort, M., Floquet, T., Kokosy, A., and Perruquetti, W. (2008). Sliding-mode formation control for cooperative autonomous mobile robots. *Industrial Electronics, IEEE Transactions on*, 55(11) :3944 –3953.

[Desai et al., 2001] Desai, J. P., Ostrowski, J. P., and Kumar, V. (2001). Modeling and control of formations of nonholonomic mobile robots. *Robotics and Automation, IEEE Transactions on*, 17(6) :905–908.

[Diaz del Rio et al., 2001] Diaz del Rio, F., Jimenez, G., Sevillano, J. L., Vicente, S., and Civit Balcells, A. (2001). A path following control for unicycle robots. *J. Robotic Syst.*, 18(7) :325–342.

[Diaz del Rio et al., 2002] Diaz del Rio, F., Jimenez, G., Sevillano, J. L., Vicente, S., and Civit Balcells, A. (2002). A new method for tracking memorized paths : application to unicycle robots. In *MED 2002. 10th Mediterranean Conference on Control and Automation*.

[Dierks and Jagannathan, 2007] Dierks, T. and Jagannathan, S. (2007). Asymptotic stability of nonholonomic mobile robot formations using multilayer neural networks. In *Decision and Control, 2007 46th IEEE Conference on*, pages 1944 –1950.

[Dimarogonas and Kyriakopoulos, 2008a] Dimarogonas, D. and Kyriakopoulos, K. (2008a). Connectedness preserving distributed swarm aggregation for multiple kinematic robots. *Robotics, IEEE Transactions on*, 24(5) :1213–1223.

[Dimarogonas and Kyriakopoulos, 2006] Dimarogonas, D. V. and Kyriakopoulos, K. J. (2006). A connection between formation control and flocking behavior in nonholonomic multiagent systems. In *Robotics and Automation, 2006. ICRA 2006. Proceedings 2006 IEEE International Conference on*, pages 940–945.

[Dimarogonas and Kyriakopoulos, 2008b] Dimarogonas, D. V. and Kyriakopoulos, K. J. (2008b). A connection between formation infeasibility and velocity alignment in kinematic multi-agent systems. *Automatica*, 44(10) :2648–2654.

[Dixon et al., 2000] Dixon, W., Dawson, D., Zhang, F., and Zergeroglu, E. (2000). Global exponential tracking control of a mobile robot system via a pe condition. *Systems, Man, and Cybernetics, Part B : Cybernetics, IEEE Transactions on*, 30(1) :129 –142.

[Do, 2008] Do, K. (2008). Formation tracking control of unicycle-type mobile robots with limited sensing ranges. *Control Systems Technology, IEEE Transactions on*, 16(3) :527 –538.

[Do et al., 2002a] Do, K., Jiang, Z., and Pan, J. (2002a). Underactuated ship global tracking under relaxed conditions. *Automatic Control, IEEE Transactions on*, 47(9) :1529 – 1536.

[Do and Pan, 2006] Do, K. and Pan, J. (2006). Robust path-following of underactuated ships : Theory and experiments on a model ship. *Ocean Engineering*, 33(10) :1354–1372.

[Do and Pan, 2007] Do, K. and Pan, J. (2007). Nonlinear formation control of unicycle-type mobile robots. *Robotics and Autonomous Systems*, 55(3) :191–204.

[Do et al., 2002b] Do, K. D., Jiang, Z. P., and Pan, J. (2002b). Universal controllers for stabilization and tracking of underactuated ships. *Systems & Control Letters*, 47(4) :299–317.

[Do et al., 2004a] Do, K. D., Jiang, Z. P., Pan, J., and Nijmeijer, H. (2004a). A global output-feedback controller for stabilization and tracking of underactuated odin : A spherical underwater vehicle. *Automatica*, 40(1) :117–124.

[Do et al., 2004b] Do, K. D., Pan, J., and Jiang, Z. P. (2004b). Robust and adaptive path following for underactuated autonomous underwater vehicles. *Ocean Engineering*, 31(16) :1967–1997.

[Douglas-Westwood, 2009] Douglas-Westwood (2009). Auv market to total $2.3 billion over the next decade. www.dw-1.com/files/files/514-AUV%202010%20news%20release%20-%20FINAL.pdf.

[Dunbar and Murray, 2006] Dunbar, W. B. and Murray, R. M. (2006). Distributed receding horizon control for multi-vehicle formation stabilization. *Automatica*, 42(4) :549–558.

[Egerstedt et al., 1998] Egerstedt, M., Hu, X., and Stotsky, A. (1998). Control of a car-like robot using a virtual vehicle approach. In *Decision and Control, 1998. Proceedings of the 37th IEEE Conference on*, volume 2, pages 1502 –1507 vol.2.

[Egerstedt et al., 2001] Egerstedt, M., Hu, X., and Stotsky, A. (2001). Control of mobile platforms using a virtual vehicle approach. *Automatic Control, IEEE Transactions on*, 46(11) :1777–1782.

[Egerstedt and Xiaoming, 2001] Egerstedt, M. and Xiaoming, H. (2001). Formation constrained multi-agent control. *Robotics and Automation, IEEE Transactions on*, 17(6) :947–951.

[Encarnacao et al., 2000] Encarnacao, P., Pacoal, A., and Arcak, M. (2000). Path following for autonomous marine craft. In *Proceedings of the 5th IFAC Conference on Manoeuvring and Control of Marine Craft*, pages 117–122.

[Encarnacao and Pascoal, 2000] Encarnacao, P. and Pascoal, A. (2000). 3d path following for autonomous underwater vehicle. In *Decision and Control, 2000. Proceedings of the 39th IEEE Conference on*, volume 3, pages 2977 –2982.

[Encarnacao and Pascoal, 2001] Encarnacao, P. and Pascoal, A. (2001). Combined trajectory tracking and path following : an application to the coordinated control of autonomous marine craft. In *Decision and Control, 2001. Proceedings of the 40th IEEE Conference on*, volume 1, pages 964–969.

[Erfu and Dongbing, 2007] Erfu, Y. and Dongbing, G. (2007). Nonlinear formation-keeping and mooring control of multiple autonomous underwater vehicles. *Mechatronics, IEEE/ASME Transactions on*, 12(2) :164–178.

[Fahimi, 2007] Fahimi, F. (2007). Non-linear model predictive formation control for groups of autonomous surface vessels. *International Journal of Control*, 80(8) :1248–1259.

[Fantoni and Lozano, 2002] Fantoni, I. and Lozano, R. (2002). *Non-linear Control for Underactuated Mechanical Systems*. Communications and Control Engineering, Springer, Berlin, Germany.

[Faulwasser and Findeisen, 2009] Faulwasser, T. and Findeisen, R. (2009). *Nonlinear Model Predictive Path-Following Control*, volume 384 of *Nonlinear Model Predictive Control, Lecture Notes in Control and Information Sciences*, pages 335 –343. Springer Berlin / Heidelberg.

[Fax and Murray, 2002] Fax, J. A. and Murray, R. M. (2002). Graph laplacians and stabilization of vehicle formations. In *15th Triennial World Congress of the International Federation of Automatic Control, Barcelona, 21-26 July 2002*.

[Fax and Murray, 2004] Fax, J. A. and Murray, R. M. (2004). Information flow and cooperative control of vehicle formations. *Automatic Control, IEEE Transactions on*, 49(9) :1465–1476.

[Fierro and Lewis, 1997] Fierro, R. and Lewis, F. L. (1997). Control of a nonholomic mobile robot : Backstepping kinematics into dynamics. *J. Robotic Syst.*, 14(3) :149–163.

[Fiorelli et al., 2006] Fiorelli, E., Leonard, N. E., Bhatta, P., Paley, D. A., Bachmayer, R., and Fratantoni, D. M. (2006). Multi-auv control and adaptive sampling in monterey bay. *Oceanic Engineering, IEEE Journal of*, 31(4) :935 –948.

[Fossen et al., 2003] Fossen, T., Breivik, M., and Skjetne, R. (2003). Line-of-sight path following of underactuated marine craft. In *Proceedings of the* 6^{th} *Conference on Manoeuvring and Control of Marine Craft (MCMC 2003)*, Girona, Spain.

[Fossen, 1994] Fossen, T. I. (1994). *Guidance and Control of Ocean Vehicles*. Wiley, New York.

[Fossen, 2002] Fossen, T. I. (2002). *Marine Control Systems : Guidance, Navigation and Control of Ships, Rigs and Vehicles*. Marine Cybernetics AS, Trondheim.

[Fossen and Strand, 1999] Fossen, T. I. and Strand, J. P. (1999). Tutorial on nonlinear backstepping : Applications to ship control. *Modeling, Identification and Control,* 20(2) :83–135.

[Fox et al., 1999] Fox, D., Burgard, W., Dellaert, F., and Thrun, S. (1999). Monte carlo localization : Efficient position estimation for mobile robots. In *Proceedings of the Sixteenth National Conference on Artificial Intelligence (AAAI'99)*, pages 343 –349.

[Fua et al., 2007] Fua, C.-H., Ge, S., Do, K. D., and Lim, K.-W. (2007). Multirobot formations based on the queue-formation scheme with limited communication. *Robotics, IEEE Transactions on*, 23(6) :1160 –1169.

[Gazi and Passino, 2003] Gazi, V. and Passino, K. M. (2003). Stability analysis of swarms. *Automatic Control, IEEE Transactions on*, 48(4) :692–697.

[Ge and Fua, 2005] Ge, S. and Fua, C.-H. (2005). Queues and artificial potential trenches for multirobot formations. *Robotics, IEEE Transactions on*, 21(4) :646 –656.

[Ghabcheloo et al., 2009] Ghabcheloo, R., Aguiar, A. P., Pascoal, A., Silvestre, C., Kaminer, I., and Hespanha, J. (2009). Coordinated path-following in the presence of communication losses and time delays. *SIAM Journal on Control and Optimization,* 48(1) :234–265.

[Ghabcheloo et al., 2006a] Ghabcheloo, R., Pascoal, A., Silvestre, C., and Kaminer, I. (2006a). Coordinated path-following control of multiple vehicles subject to bidirectional communication constraints. In *Group Coordination and Cooperative Control,Lecture Notes in Control and Information Sciences, Springer-Verlag, Kristin Y. Pettersen and Jan Tommy Gravdahl and Henk Nijmeijer (Eds)*.

[Ghabcheloo et al., 2006b] Ghabcheloo, R., Pascoal, A., Silvestre, C., and Kaminer, I. (2006b). Coordinated path following control of multiple wheeled robots using linearization techniques. *International Journal of Systems Science,* 37(6) :399–414.

[Ghabcheloo et al., 2007] Ghabcheloo, R., Pascoal, A., Silvestre, C., and Kaminer, I. (2007). Non-linear co-ordinated path following control of multiple wheeled robots with bidirectional communication constraints. *Int. J. Adapt. Control Signal Process.*, 21(2-3) :133–157.

[Ghommam and Mnif, 2009] Ghommam, J. and Mnif, F. (2009). Coordinated path-following control for a group of underactuated surface vessels. *Industrial Electronics, IEEE Transactions on*, 56(10) :3951–3963.

[Ghommam et al., 2008] Ghommam, J., Saad, M., and Mnif, F. (2008). Formation path following control of unicycle-type mobile robots. In *Proc. IEEE International Conference on Robotics and Automation ICRA 2008*, pages 1966–1972.

[Godsil and Royle, 2001] Godsil, C. and Royle, G. (2001). *Algebraic Graph Theory*. Springer-Verlag, Berlin, Germany.

[Goldstein, 1980] Goldstein, H. (1980). *Classical Mechanics*. Addison-Wesley, U.S.A., 2nd edition.

[Hale and Lunel, 1993] Hale, J. K. and Lunel, S. (1993). *Introduction to Functional Differential Equations*. Applied Mathematical Sciences, Springer, Berlin, Germany.

[Hauser and Hindman, 1995] Hauser, J. and Hindman, R. (1995). Maneuver regulation from trajectory tracking : Feedback linearizable systems. pages 595 –600.

[Hespanha et al., 1999] Hespanha, J. P., Liberzon, D., and Morse, A. S. (1999). Logic-based switching control of a nonholonomic system with parametric modeling uncertainty. *Systems & Control Letters*, 38(3) :167–177.

[Hindman and Hauser, 1996] Hindman, R. and Hauser, J. (1996). Maneuver modified trajectory tracking. In *Proc. of Int. Symp. Mathematical Theory Networks and Systems, St. Louis, MO, USA.*, pages 1473–1479.

[Ihle et al., 2005] Ihle, I.-A., Jouffroy, J., and Fossen, T. (2005). Formation control of marine surface craft using lagrange multipliers. In *Decision and Control, 2005 and 2005 European Control Conference. CDC-ECC '05. 44th IEEE Conference on*, pages 752–758.

[Ihle et al., 2004] Ihle, I.-A., Skjetne, R., and Fossen, T. (2004). Nonlinear formation control of marine craft with experimental results. In *Decision and Control, 2004. CDC. 43rd IEEE Conference on*, volume 1, pages 680 –685.

[Ihle, 2006] Ihle, I.-A. F. (2006). *Coordinated Control of Marine Craft*. PhD thesis, Norwegian University of Science and Technology, Faculty of Information Technology, Mathematics and Electrical Engineering.

[Ihle et al., 2007] Ihle, I. A. F., Arcak, M., and Fossen, T. I. (2007). Passivity-based designs for synchronized path-following. *Automatica*, 43(9) :1508–1518.

[Jadbabaie et al., 2003] Jadbabaie, A., Lin, J., and Morse, A. (2003). Coordination of groups of mobile autonomous agents using nearest neighbor rules. *Automatic Control, IEEE Transactions on*, 48(6) :988 – 1001.

[Jaulin, 2009a] Jaulin, L. (2009a). A nonlinear set membership approach for the localization and map building of underwater robots. *Robotics, IEEE Transactions on*, 25(1) :88 –98.

[Jaulin, 2009b] Jaulin, L. (2009b). Robust set-membership state estimation ; application to underwater robotics. *Automatica*, 45(1) :202–206.

[Jaulin et al., 2002] Jaulin, L., Kieffer, M., Walter, E., and Meizel, D. (2002). Guaranteed robust nonlinear estimation with application to robot localization. *Systems, Man, and Cybernetics, Part C : Applications and Reviews, IEEE Transactions on*, 32(4) :374 –381.

[Jaulin et al., 2000] Jaulin, L., Walter, E., Lévêque, O., and Meizel, D. (2000). Set inversion for chi-algorithms, with application to guaranteed robot localization. *Math. Comput. Simulation*, 52 :197 –210.

[Jetto et al., 1999] Jetto, L., Longhi, S., and Vitali, D. (1999). Localization of a wheeled mobile robot by sensor data fusion based on a fuzzy logic adapted kalman filter. *Control Engineering Practice*, 7(6) :763–771.

[Jiang, 2002] Jiang, Z.-P. (2002). Global tracking control of underactuated ships by lyapunov's direct method. *Automatica*, 38(2) :301–309.

[Jiang, 2011] Jiang, Z.-P. (2011). *Controlling Underactuated Mechanical Systems : A Review and Open Problems*, volume 407 of *Advances in the Theory of Control, Signals and Systems with Physical Modeling, Lecture Notes in Control and Information Sciences*, pages 77–88. Springer Berlin / Heidelberg.

[Jiang and Nijmeijer, 1997] Jiang, Z. P. and Nijmeijer, H. (1997). Tracking control of mobile robots : A case study in backstepping. *Automatica*, 33(7) :1393–1399.

[Kaminer et al., 1998] Kaminer, I., Pascoal, A., Hallberg, E., and Silvestre, C. (1998). Trajectory tracking for autonomous vehicles : An integrated approach to guidance and control. *Jouranl of Guidance, Control, and Dynamics*, 21(1) :29–38.

[Kanayama et al., 1990] Kanayama, Y., Kimura, Y., Miyazaki, F., and Noguchi, T. (1990). A stable tracking control method for an autonomous mobile robot. *Robotics and Automation, 1990. Proceedings., 1990 IEEE International Conference on*, 1 :384–389.

[Kang and Yeh, 2002] Kang, W. and Yeh, H.-H. (2002). Co-ordinated attitude control of multi-satellite systems. *Int. J. Robust Nonlinear Control*, 12(2-3) :185–205.

[Kanjanawanishkul and Zell, 2009] Kanjanawanishkul, K. and Zell, A. (2009). Path following for an omnidirectional mobile robot based on model predictive control. pages 3341 –3346.

[Khalil, 1996] Khalil, H. K. (1996). *Nonlinear Systems*. Prentice-Hall, Upper Saddle River, NJ, 2nd edition.

[Khalil, 2002] Khalil, H. K. (2002). *Nonlinear Systems*. Prentice-Hall, Upper Saddle River, NJ, 3rd edition.

[Klein et al., 2008] Klein, D. J., Bettale, P. K., Triplett, B. I., and Morgansen, K. A. (2008). Autonomous underwater multivehicle control with limited communication : theory and experiment. In *Proceedings of the Second IFAC Workshop on Navigation, Guidance and Control of Underwater Vehicles (NGCUV 2008)*, Killaloe, Ireland.

[Klein et al., 2010] Klein, D. J., Gupta, V., and Morgansen, K. A. (2010). Coordinated control of robotic fish using an underwater wireless network. In *Wireless Networking Based Control,Springer, Mazumder, Sudip K. (Ed.)*.

[Kokotovic, 1992] Kokotovic, P. (1992). The joy of feedback : nonlinear and adaptive. *Control Systems Magazine, IEEE*, 12(3) :7 –17.

[Kolmanovsky and McClamroch, 1995] Kolmanovsky, I. and McClamroch, N. (1995). Developments in nonholonomic control problems. *Control Systems Magazine, IEEE*, 15(6) :20 –36.

[Kumar et al., 2005] Kumar, V., L., E., N., and Morse, A. S. E. (2005). *Cooperative Control*, volume 309. Springer-Verlag.

[Kyrkjebø et al., 2007] Kyrkjebø, E., Pettersen, K. Y., Wondergem, M., and Nijmeijer, H. (2007). Output synchronization control of ship replenishment operations : Theory and experiments. *Control Engineering Practice*, 15(6) :741–755.

[Lapierre and Jouvencel, 2008] Lapierre, L. and Jouvencel, B. (2008). Robust nonlinear path-following control of an auv. *IEEE Journal of Oceanic Engineering*, 33(2) :89–102.

[Lapierre et al., 2006] Lapierre, L., Soetano, D., and Pascoal, A. (2006). Nonsingular path following control of a unicycle in the presence of parametric modelling uncertainties. *International Journal of Robust and Nonlinear Control*, 16(10) :485–503.

[Lapierre and Soetanto, 2003] Lapierre, L. and Soetanto, D. (2003). Coordinated motion control of marine robots. In *Proceedings of the 6^{th} Conference on Manoeuvring and Control of Marine Craft (MCMC 2003)*, Girona, Spain.

[Lapierre and Soetanto, 2007] Lapierre, L. and Soetanto, D. (2007). Nonlinear path-following control of an auv. *Ocean Engineering*, 34(11-12) :1734 –1744.

[Lapierre et al., 2003] Lapierre, L., Soetanto, D., and Pascoal, A. (2003). Nonlinear path following with applications to the control of autonomous underwater vehicles. In *Decision and Control, 2003. Proceedings. 42nd IEEE Conference on*, volume 2, pages 1256 – 1261.

[Lapierre et al., 2007] Lapierre, L., Zapata, R., and Lepinay, P. (2007). Combined path-following and obstacle avoidance control of a wheeled robot. *International Journal of Robotics Research*, 26(4) :361–375.

[Laumond, 1998] Laumond, J.-P. P. (1998). *Robot Motion Planning and Control*. Springer-Verlag New York, Inc., Secaucus, NJ, USA.

[Lawton et al., 2003] Lawton, J. R. T., Beard, R. W., and Young, B. J. (2003). A decentralized approach to formation maneuvers. *Robotics and Automation, IEEE Transactions on*, 19(6) :933–941.

[Lee et al., 2001] Lee, T.-C., Song, K.-T., Lee, C.-H., and Teng, C.-C. (2001). Tracking control of unicycle-modeled mobile robots using a saturation feedback controller. *Control Systems Technology, IEEE Transactions on*, 9(2) :305 –318.

[Lefeber, 2000] Lefeber, E. (2000). *Tracking Control of Nonlinear Mechanical Systems*. PhD thesis, University of Twente, Enschede, The Netherlands.

[Lefeber et al., 2003] Lefeber, E., Pettersen, K., and Nijmeijer, H. (2003). Tracking control of an underactuated ship. *Control Systems Technology, IEEE Transactions on*, 11(1) :52 – 61.

[Leonard, 1995] Leonard, N. (1995). Control synthesis and adaptation for an underactuated autonomous underwater vehicle. *Oceanic Engineering, IEEE Journal of*, 20(3) :211 –220.

[Leonard et al., 2007] Leonard, N., Paley, D., Lekien, F., Sepulchre, R., Fratantoni, D., and Davis, R. (2007). Collective motion, sensor networks, and ocean sampling. *Proceedings of the IEEE*, 95(1) :48 –74.

[Leonard and Fiorelli, 2001] Leonard, N. E. and Fiorelli, E. (2001). Virtual leaders, artificial potentials and coordinated control of groups. In *Decision and Control, 2001. Proceedings of the 40th IEEE Conference on*, volume 3, pages 2968–2973.

[Lewis, 1989] Lewis, E. V. (1989). *Principles of Naval Architecture*, volume III. SNAME, Jersey City, NJ., 2nd edition.

[Lewis and Tan, 1997] Lewis, M. A. and Tan, K.-H. (1997). High precision formation control of mobile robots using virtual structures. *Autonomous Robots*, 4(4) :387–403.

[Li and W., 1991] Li, J. S. and W. (1991). *Applied nonlinear control*. Prentice Hall.

[Li et al., 2009a] Li, Z., Sun, J., and Oh, S. (2009a). Design, analysis and experimental validation of a robust nonlinear path following controller for marine surface vessels. *Automatica*, 45(7) :1649–1658.

[Li et al., 2009b] Li, Z., Sun, J., and Oh, S. (2009b). Path following for marine surface vessels with rudder and roll constraints : An mpc approach. In *American Control Conference, 2009. ACC '09.*, pages 3611 –3616.

[Lin et al., 2004] Lin, Z., Broucke, M., and Francis, B. (2004). Local control strategies for groups of mobile autonomous agents. *Automatic Control, IEEE Transactions on*, 49(4) :622–629.

[Lin et al., 2005] Lin, Z., Francis, B., and Maggiore, M. (2005). Necessary and sufficient graphical conditions for formation control of unicycles. *Automatic Control, IEEE Transactions on*, 50(1) :121 – 127.

[M. Krstic and Kokotovic, 1995] M. Krstic, I. K. and Kokotovic, P. (1995). *Nonlinear and Adaptive Control Design*. Wiley, New York.

[McDowell et al., 2002] McDowell, P., Chen, J., and Bourgeois, B. (2002). Uuv teams, control from a biological perspective. In *OCEANS '02 MTS/IEEE*, volume 1, pages 331 – 337.

[M'Closkey and Murray, 1994] M'Closkey, R. and Murray, R. (1994). Exponential stabilization of driftless nonlinear control systems via time-varying, homogeneous feedback. In *Decision and Control, 1994., Proceedings of the 33rd IEEE Conference on*, volume 2, pages 1317 –1322.

[M'Closkey and Murray, 1997] M'Closkey, R. and Murray, R. (1997). Exponential stabilization of driftless nonlinear control systems using homogeneous feedback. *Automatic Control, IEEE Transactions on*, 42(5) :614 –628.

[Micaelli and Samson, 1993] Micaelli, A. and Samson, C. (1993). Trajectory tracking for unicycle-type and two-steering-wheels mobile robots. Research Report RR-2097, INRIA.

[Moreau, 2005] Moreau, L. (2005). Stability of multiagent systems with time-dependent communication links. *Automatic Control, IEEE Transactions on*, 50(2) :169–182.

[Moreira et al., 2007] Moreira, L., Fossen, T. I., and Guedes Soares, C. (2007). Path following control system for a tanker ship model. *Ocean Engineering*, 34(14-15) :2074–2085.

[Morin and Samson, 2009] Morin, P. and Samson, C. (2009). *Springer Handbook of Robotics*, chapter Motion control of wheeled mobile robots, pages 799–826. Springer.

[Murray, 2007] Murray, R. M. (2007). Recent research in cooperative control of multivehicle systems. *Journal of Dynamic Systems, Measurement, and Control*, 129(5) :571–583.

[Murray et al., 1992] Murray, R. M., Walsh, G., and Sastry, S. (1992). Stabilization and tracking for nonholonomic control systems using time- varying state feedback. In *Proc. IFAC Symp. on Nonlinear Control Systems Design*, pages 182–187, Bordeaux, France.

[Nijmeijer and Fossen, 1999] Nijmeijer, H. and Fossen, T. (1999,). *New directions in non-linear observer design, lecture notes in control and information sciences*, volume 244. Springer, Berlin.

[Oelen and van Amerongen, 1994] Oelen, W. and van Amerongen, J. (1994). Robust tracking control of two-degrees-of-freedom mobile robots. *Control Engineering Practice*, 2(2) :333–340.

[Ogren et al., 2002] Ogren, P., Egerstedt, M., and Xiaoming, H. (2002). A control lyapunov function approach to multiagent coordination. *Robotics and Automation, IEEE Transactions on*, 18(5) :847–851.

[Ogren et al., 2004] Ogren, P., Fiorelli, E., and Leonard, N. E. (2004). Cooperative control of mobile sensor networks :adaptive gradient climbing in a distributed environment. *Automatic Control, IEEE Transactions on*, 49(8) :1292–1302.

[Oh and Sun, 2010] Oh, S.-R. and Sun, J. (2010). Path following of underactuated marine surface vessels using line-of-sight based model predictive control. *Ocean Engineering*, 37d(2-3) :289–295.

[Olfati-Saber, 2006] Olfati-Saber, R. (2006). Flocking for multi-agent dynamic systems : algorithms and theory. *Automatic Control, IEEE Transactions on*, 51(3) :401–420.

[Olfati-Saber et al., 2007] Olfati-Saber, R., Fax, J., and Murray, R. (2007). Consensus and cooperation in networked multi-agent systems. *Proceedings of the IEEE*, 95(1) :215–233.

[Olfati-Saber and Murray, 2004] Olfati-Saber, R. and Murray, R. M. (2004). Consensus problems in networks of agents with switching topology and time-delays. *Automatic Control, IEEE Transactions on*, 49(9) :1520–1533.

[Oriolo and Nakamura, 1991] Oriolo, G. and Nakamura, Y. (1991). Control of mechanical systems with second-order nonholonomic constraints : underactuated manipulators. In *Decision and Control, 1991., Proceedings of the 30th IEEE Conference on*, volume 3, pages 2398 –2403.

[Papoulias, 1991] Papoulias, F. (1991). Bifurcation analysis of line of sight vehicle guidance using sliding modes. *International Journal of Bifurcation and Chaos*, 1(4) :849–865.

[Papoulias, 1992] Papoulias, F. A. (1992). Guidance and control laws for vehicle pathkeeping along curved trajectories. *Applied Ocean Research*, 14(5) :291–302.

[Pascoal et al., 2000] Pascoal, A., Oliveira, P., Silvestre, C., Sebastiao, L., Rufino, M., Barroso, V., Gomes, J., Ayela, G., Coince, P., Cardew, M., Ryan, A., Braithwaite, H., Cardew, N., Trepte, J., Seube, N., Champeau, J., Dhaussy, P., Sauce, V., Moitie, R., Santos, R., Cardigos, F., Brussieux, M., and Dando, P. (2000). Robotic ocean vehicles for marine science applications : the european asimov project. In *OCEANS 2000 MTS/IEEE Conference and Exhibition*, volume 1, pages 409 –415.

[Pavlov et al., 2007] Pavlov, A., Borhaug, E., Panteley, E., and Pettersen, K. Y. (2007). Straight line path following for formations of underactuated surface vessels. In *Seventh IFAC Symposium on Nonlinear Control Systems (2007) , South Africa*, volume 7 of *Nonlinear Control Systems*.

[Pavlov et al., 2009] Pavlov, A., Nordahl, H., and Breivik, M. (2009). Mpc-based optimal path following for underactuated vessels. In *Proceedings of the* 8^{th} *Conference on Manoeuvring and Control of Marine Craft (MCMC 2009)*, Casa Grande Hotel, Guaruja (SP), Brazil.

[Pettersen and Egeland, 1996] Pettersen, K. and Egeland, O. (1996). Position and attitude control of an underactuated autonomous underwater vehicle. In *Decision and Control, 1996., Proceedings of the 35th IEEE*, volume 1, pages 987 –991.

[Pettersen and Fossen, 2000] Pettersen, K. and Fossen, T. (2000). Underactuated dynamic positioning of a ship-experimental results. *Control Systems Technology, IEEE Transactions on*, 8(5) :856 –863.

[Pettersen and Lefeber, 2001] Pettersen, K. and Lefeber, E. (2001). Way-point tracking control of ships. volume 1, pages 940 –945.

[Pettersen, 1996] Pettersen, K. Y. (1996). *Exponential Stabilization of Underactuated Vehicles*. PhD thesis, Department of Engineering Cybernetics, Norwegian University of Science and Technology.

[Pettersen et al., 2006] Pettersen, K. Y., Gravdahl, J. T., and Nijmeijer, H. E. (2006). *Group Coordination and Cooperative Control*, volume 336. Springer.

[Pettersen and Nijmeijer, 2001] Pettersen, K. Y. and Nijmeijer, H. (2001). Underactuated ship tracking control : theory and experiments. *International Journal of Control*, 74(14) :1435 – 1446.

[Pettersen and Nijmeijer, 2002] Pettersen, K. Y. and Nijmeijer, H. (2002). Underactuated ship tracking control ; theory and experiments. *IEEE Trans. Automat. Contr.*, 40 :1759 – 1762.

[Pomet, 1992] Pomet, J.-B. (1992). Explicit design of time-varying stabilizing control laws for a class of controllable systems without drift. *Systems & Control Letters*, 18(2) :147–158.

[Porfiri et al., 2007] Porfiri, M., Roberson, D. G., and Stilwell, D. J. (2007). Tracking and formation control of multiple autonomous agents : A two-level consensus approach. *Automatica*, 43(8) :1318–1328.

[Ren, 2007] Ren, W. (2007). Consensus strategies for cooperative control of vehicle formations. *Control Theory Applications, IET*, 1(2) :505 –512.

[Ren, 2008a] Ren, W. (2008a). On consensus algorithms for double-integrator dynamics. *Automatic Control, IEEE Transactions on*, 53(6) :1503 –1509.

[Ren, 2008b] Ren, W. (2008b). Synchronization of coupled harmonic oscillators with local interaction. *Automatica*, 44(12) :3195–3200.

[Ren et al., 2004] Ren, W., Beard, R. W., and Beard, A. W. (2004). Decentralized scheme for spacecraft formation flying via the virtual structure approach. *AIAA Journal of Guidance, Control, and Dynamics*, 27 :73–82.

[Ren et al., 2005] Ren, W., Beard, R. W., and McLain, T. W. (2005). Coordination variables and consensus building in multiple vehicle systems. In Kumar, V., Leonard, N. E., and Morse, A. S., editors, *Cooperative Control*, volume 309 of *Lecture Notes in Control and Information Sciences*, pages 171–188, Berlin. Springer-Verlag.

[Ren et al., 2008] Ren, W., Chao, H., Bourgeous, W., Sorensen, N., and Chen, Y. (2008). Experimental validation of consensus algorithms for multivehicle cooperative control. *Control Systems Technology, IEEE Transactions on*, 16(4) :745 –752.

[Riedel and Healey, 1998] Riedel, J. and Healey, A. (1998). Shallow water station keeping of auvs using multi-sensor fusion for wave disturbance prediction and compensation. volume 2, pages 1064 –1068.

[Rizzi et al., 2002] Rizzi, A., Cassinis, R., and Serana, N. (2002). Neural networks for autonomous path-following with an omnidirectional image sensor. *Neural Computing &amp ; Applications*, 11(1) :45–52.

[Rosales et al., 2009] Rosales, A., Scaglia, G., Mut, V., and di Sciascio, F. (2009). Trajectory tracking of mobile robots in dynamic environments–a linear algebra approach. *Robotica*, 27(07) :981–997.

[Roumeliotis and Bekey, 2000] Roumeliotis, S. and Bekey, G. (2000). Bayesian estimation and kalman filtering : a unified framework for mobile robot localization. In *Robotics and Automation, 2000. Proceedings. ICRA '00. IEEE International Conference on*, volume 3, pages 2985 –2992 vol.3.

[Rysdyk, 2003] Rysdyk, R. (2003). Robotic ocean vehicles for marine science applications : the european asimov project. In *Proceedings of the AIAA Unmanned Unlimited Conference*.

[Samson, 1992] Samson, C. (1992). Path following and time-varying feedback stabilization of a wheeled mobile robot. In *Proc. Int. Conf, ICARCV'92, Singapore*, pages RO–13.1.

[Samson, 1995] Samson, C. (1995). Control of chained systems : Application to path following and time-varying point-stabilization of mobile robots. In *IEEE Trans. on Automat. Contr.*, volume 40, pages 64–77.

[Sanz et al., 2010] Sanz, P. J., Ridao, P., Oliver, G., Melchiorri, C., Casalino, G., Silvestre, C., Petillot, Y., and Turetta, A. (2010). Trident : A framework for autonomous underwater intervention missions with dexterous manipulation capabilities. In *Symposium on Intelligent Autonomous Vehicles 2010*.

[Schoenwald, 2000] Schoenwald, D. (2000). Auvs : In space, air, water, and on the ground. *Control Systems Magazine, IEEE*, 20(6) :15 –18.

[Shamma and Cloutier, 1993] Shamma, J. S. and Cloutier, J. R. (1993). Gain-scheduled missile autopilot design using linear parameter varying transformations. *JOURNAL OF GUIDANCE, CONTROL, AND DYNAMICS*, 16(3) :256–263.

[Silvestre, 2000] Silvestre, C. (2000). *Multi-objective optimization theory with application to the integrated design of controllers/plants for autonomous vehicle*. PhD thesis, IST, Portugal.

[Silvestre et al., 2002] Silvestre, C., Pascoal, A., and Kaminer, I. (2002). On the design of gain-scheduled trajectory tracking controllers. *Int. J. Robust Nonlinear Control*, 12(9) :797–839.

[Sira-Ramfrez, 1999] Sira-Ramfrez, H. (1999). On the control of the underactuated ship : a trajectory planning approach. In *Decision and Control, 1999. Proceedings of the 38th IEEE Conference on*, volume 3, pages 2192 –2197.

[Skjetne, 2005] Skjetne, R. (2005). *The Maneuvering Problem*. PhD thesis, Norwegian University of Science and Technology, Faculty of Information Technology, Mathematics and Electrical Engineering.

[Skjetne and Fossen, 2001] Skjetne, R. and Fossen, T. (2001). Nonlinear maneuvering and control of ships. volume 3, pages 1808 –1815.

[Skjetne et al., 2004] Skjetne, R., Fossen, T. I., and Kokotovic, P. V. (2004). Robust output maneuvering for a class of nonlinear systems. *Automatica*, 40(3) :373–383.

[Skjetne et al., 2005] Skjetne, R., Fossen, T. I., and Kokotovic, P. V. (2005). Adaptive maneuvering, with experiments, for a model ship in a marine control laboratory. *Automatica*, 41(2) :289–298.

[Skjetne et al., 2002] Skjetne, R., Moi, S., and Fossen, T. (2002). Nonlinear formation control of marine craft. volume 2, pages 1699 – 1704.

[Skjetne and Teel, 2004] Skjetne, R. and Teel, A. (2004). Maneuvering dynamical systems by sliding-mode control. volume 2, pages 1277 – 1282.

[SNAME and Engineers, 1950] SNAME, T. s. o. N. A. and Engineers, M. (1950). Nomenclature for treating the motion of a submerged body through a fluid. Number 1-5.

[Soetanto et al., 2003] Soetanto, D., Lapierre, L., and Pascoal, A. (2003). Adaptive, non-singular path-following control of dynamic wheeled robots. In *Decision and Control, 2003. Proceedings. 42nd IEEE Conference on*, volume 2, pages 1765 – 1770.

[Tanner et al., 2007] Tanner, H. G., Jadbabaie, A., and Pappas, G. J. (2007). Flocking in fixed and switching networks. *Automatic Control, IEEE Transactions on*, 52(5) :863–868.

[Thrun et al., 2001] Thrun, S., Fox, D., Burgard, W., and Dellaert, F. (2001). Robust monte carlo localization for mobile robots. *Artificial Intelligence*, 128(1-2) :99–141.

[Toussaint et al., 2000] Toussaint, G., Basar, T., and Bullo, F. (2000). H infin ;-optimal tracking control techniques for nonlinear underactuated systems. In *Decision and Control, 2000. Proceedings of the 39th IEEE Conference on*, volume 3, pages 2078 –2083.

[Walsh et al., 1994] Walsh, G., Tilbury, W., Sastry, S., Murray, R., and Laumond, J. P. (1994). Stabilization of trajectories for systems with nonholonomic constraints. *IEEE Transactions on Automatic Control*, 39 :216–222.

[Wang, 1991] Wang, P. K. C. (1991). Navigation strategies for multiple autonomous mobile robots moving in formation. *J. Robotic Syst.*, 8(2) :177–195.

[Wei and Beard, 2005] Wei, R. and Beard, R. W. (2005). Consensus seeking in multiagent systems under dynamically changing interaction topologies. *Automatic Control, IEEE Transactions on*, 50(5) :655–661.

[Whitcomb, 2000] Whitcomb, L. (2000). Underwater robotics : out of the research laboratory and into the field. In *Proceedings of Robotics and Automation, ICRA2000. IEEE International Conference on*, volume 1, pages 709 –716.

[WHOI, 2007] WHOI (2007). Woods hole oceanographic institution : Robot paints stunning map of deep-sea volcano. http ://www.whoi.edu/oceanus/viewArticle.do ?id=34926.

[Wu, 2001] Wu, C. W. (2001). Synchronization in arrays of coupled nonlinear systems : passivity, circle criterion, and observer design. *Circuits and Systems I : Fundamental Theory and Applications, IEEE Transactions on*, 48(10) :1257 –1261.

[Xiang et al., 2010a] Xiang, X., Jouvencel, B., and Parodi, O. (2010a). Coordinated formation control of multiple autonomous underwater vehicles for pipeline inspection. *International Journal of Advanced Robotic System*, (1) :75–84.

[Xiang et al., 2010b] Xiang, X., Lapierre, L., and Jouvencel, B. (2010b). Guiance based collision free and obstacle avoidance of autonomous vehicles under formation constraints. In *Symposium on Intelligent Autonomous Vehicles 2010*.

[Xiang et al., 2010c] Xiang, X., Lapierre, L., and Jouvencel, B. (2010c). Guidance based collision avoidance of coordinated nonholonomic autonomous vehicles. In *Intelligent Robots and Systems, 2010. IROS 2010. IEEE/RSJ International Conference on*, pages 4547–4552.

[Xiang et al., 2009a] Xiang, X., Lapierre, L., Jouvencel, B., and Parodi, O. (2009a). Coordinated path following control of multiple nonholonomic vehicles. In *OCEANS 2009-EUROPE, 2009. OCEANS '09.*, pages 1–7.

[Xiang et al., 2009b] Xiang, X., Lapierre, L., Jouvencel, B., and Parodi, O. (2009b). Coordinated path following control of multiple wheeled mobile robots through decentralized speed adaptation. In *Intelligent Robots and Systems, 2009. IROS 2009. IEEE/RSJ International Conference on*, pages 4547–4552.

[Yang et al., 2005] Yang, E., Gu, D., and Hu, H. (2005). Improving the formation-keeping performance of multiple autonomous underwater robotic vehicles. In *Mechatronics and Automation, 2005 IEEE International Conference*, volume 4, pages 1890 – 1895.

[Zabczyk, 1989] Zabczyk, J. (1989). Some comments on stabilizability. *Applied Mathematics & Optimization*, 19(1) :1–9.

[Zhang et al., 2000] Zhang, R., Chen, Y., Sun, Z., Sun, F., and Xu, H. (2000). Path control of a surface ship in restricted waters using sliding mode. *Control Systems Technology, IEEE Transactions on*, 8(4) :722 –732.

[Zhang and Tian, 2010] Zhang, Y. and Tian, Y.-P. (2010). Consensus of data-sampled multi-agent systems with random communication delay and packet loss. *Automatic Control, IEEE Transactions on*, 55(4) :939 –943.

RESUME en français et anglais

CONTRÔLE COORDONNÉ DE FLOTTILLE DE VÉHICULES SOUS-MARINS SOUS-ACTIONNÉS AUTONOMES

Cette thése traite de la question du contrôle du mouvement d'engins non-holonomes et sous-actionnés évoluant de manière coordonnée et autonome. Les différentes approches considérées sont le suivi de trajectoire (Trajectory Tracking - TT) et le suivi de chemin (path following - PF). Une nouvelle méthode de contrôle est proposée. Dénommée Path-Tracking (PT), elle permet de cumuler les avantages de chacune des deux précédentes méthodes, permettant de cumuler la souplesse de la convergence induite par le suivi de chemin avec le respect des contraintes temporelles du suivi de trajectoire.

L'étude et la réalisation de la commande démarre avec l'étude du cas du robot nonholonome de type 'Unicycle' et se base sur les principes de 'Lyapunov' et de 'Backstepping'. Ces premiers résultats sont ensuite étendus au cas d'un véhicule sous-marin sous-actionné de type AUV ('Autonomous Underwater Vehicle'), en analysant les similarités cinématiques entre ces deux types de véhicules. De plus, il est montré la nécessité de prendre en compte les propriétés dynamiques du système de type AUV, et la condition de 'Stern dominancy' est établie de façon à garantir que le problème est bien posé et ainsi que la commande soit aisément calculable. Dans la cas d'un système marin sur-actionné, qui peut ainsi effectuer des tâches de navigation au long cours et de positionnement désiré ('Station keeping'), une commande hybride est proposée.

Enfin, la question du contrôle coordonné d'une formation d'engins marin est abordée. Les solutions de commande pour les tâches de suivi de chemin coordonné ('coordinated path following') et de 'coordinated path tracking' sont proposées. Les principes du 'leader-follower' et la méthode des structures virtuelles sont ainsi traitées dans un cadre de contrôle centralisé, et le cas décentralisé est traité en utilisant certains principes de théorie des graphes.

Mots-clé : systéme sous-actionné, véhicule de type unicyle, véhicules autonomes sous-marins (AUVs), suivi de chemin, path tracking, design basée sur Lyapunov, principe de backstepping, contrôle coordonné de formation

---

COORDINATED MOTION CONTROL OF UNDERACTUATED AUTONOMOUS UNDERWATER VEHICLES

In this dissertation, the problems of motion control of nonholonomic and underactuated autonomous vehicles are addressed, namely trajectory tracking (TT), path following (PF), and novelly proposed path tracking (PT) which blending the PF and TT together in order to achieve smooth spatial convergence and tight temporal performance as well.

The control design is firstly started from the benchmark case of nonholonomic unicycle-type vehicles, where the Lyapunov-based design and backstepping technique are employed, and then it is extended to the underactuated AUVs based on the similarity between the control inputs of two kinds of vehicles. Moreover, dealing with acceleration of side-slip angle is highlighted, and stern-dominant property of AUVs is standing out in order to achieve well-posed control computation. Smooth transitions of motion control from underactuated to fully actuated AUVs are also proposed.

Finally, coordinated formation control of multiple autonomous vehicles are addressed in two-folds, including coordinated paths following and coordinated paths tracking, based on leader-follower and virtual structure method respectively under the centralized control framework, and then solved under decentralized control framework by resorting to the algebraic graph theory.

Keywords : underactuated system, unicyle-type vehicle, AUVs, path following, path tracking, Lyapunov-based design, backstepping technique, coordinated formation control